Investigating the roles of HMGB1 and its receptor, RAGE, in chronic lymphocytic leukaemia

Faith Norster

Submitted in partial fulfilment of the requirements of the Degree of Doctor of Philosophy

October 2018

Centre for Haemato-Oncology

Barts Cancer Institute

Barts and the London School of Medicine and Dentistry

Queen Mary University of London

Statement of Originality

I, Faith Norster, confirm that the research included within this thesis is my own work or that where it has been carried out in collaboration with, or supported by others, that this is duly acknowledged below and my contribution indicated. Previously published material is also acknowledged below.

I attest that I have exercised reasonable care to ensure that the work is original, and does not to the best of my knowledge break any UK law, infringe any third party's copyright or other Intellectual Property Right, or contain any confidential material.

I accept that the College has the right to use plagiarism detection software to check the electronic version of the thesis.

I confirm that this thesis has not been previously submitted for the award of a degree by this or any other university.

Signature: 

Date: 02/10/2018

Details of collaboration and publications:

Tissue microarrays were previously constructed by Andrew Clear and Andrew Owen

CD5 and Ki67 immunohistochemistry staining was performed by Andrew Clear

ZAP70 immunohistochemistry staining was performed by Dr Meg Ashton-Key and Professor Graham Packham at the University of Southampton

Mass spectrometry sample preparation and mass spectrometry sample runs were performed in collaboration with Dr David Britton and Dr Pedro Casado

Mass spectrometry bioinformatic analysis was performed by Dr David Britton and Dr Pedro Casado

Abstract

High plasma levels of inflammatory mediator, high mobility group box protein 1 (HMGB1), and its main receptor, receptor for advanced glycation end products (RAGE), is associated with poor prognosis for a variety of cancers, but little is known about this signalling axis in chronic lymphocytic leukaemia (CLL). We have previously determined significantly increased HMGB1 levels in the plasma of CLL patients compared to healthy controls, associated with poor clinical outcome. It is unknown whether the HMGB1-RAGE signalling axis contributes to disease progression and can directly promote CLL B-cell survival by converging with toll-like receptor 9 (TLR9) signalling. Moreover, the role of soluble RAGE (sRAGE), a free extracellular receptor fragment that functions as a decoy receptor in blood plasma, is poorly documented for CLL. The overall aim of my PhD is to (1) determine expression of HMGB1 receptors, RAGE and TLR9, in CLL B-cells and their prognostic significance in patients with CLL; (2) assess global cell-signalling network activation following exogenous HMGB1 treatment and blockade with neutralising anti-RAGE antibody; (3) study the impact of sRAGE in CLL.

Lymph node RAGE expression positively correlated with TLR9, Ki67 and ZAP70 – markers of proliferating and aggressive disease. Patients with high lymph node RAGE expression confer inferior overall survival in comparison to patients with low RAGE expression. Further risk stratification of RAGE with Ki67 and ZAP70 lymph node expression increased the prognostic power of RAGE, highlighting a significant interaction between these variables. HMGB1 induced activation and colocalization of RAGE and TLR9 in CLL B-cells. Phosphoproteomic analysis highlights activation of MAPK signalling in primary CLL cells following HMGB1 treatment *in vitro* for patients with ZAP70 expression. We confirmed increased plasma levels of HMGB1 and surprisingly of sRAGE in CLL patients compared to healthy controls, but not of other RAGE ligand, S100B. Plasma sRAGE levels did not reach a high enough concentration to inflict full HMGB1 inhibition, but RAGE shedding could be induced *in vitro* by stimulating metalloprotease termed a disintegrin and metalloproteinase domain-containing protein 10 (ADAM10) with ionomycin in RAGE-transfected HEK293 cell line and primary CLL cells, and blocked when ADAM10 was specifically inhibited with GI254023X.

In summary, this study demonstrates that overexpression of HMGB1 receptor, RAGE, in CLL lymph nodes is associated with a worse clinical outcome in patients with CLL. HMGB1 activates both RAGE and TLR9 in primary CLL B-cells. sRAGE has a protective effect in CLL by prolonging time to first treatment and sRAGE originates from ectodomain shedding, dependent on ADAM10. We therefore propose that HMGB1 and surface RAGE may play an important role in

promoting CLL cell proliferation and cell survival, and plasma sRAGE combined with HMGB1 could be markers of disease monitoring.

Dedication

To Mum, Mark and Grandad Harris – thank you for your endless support, encouragement and belief in me, always.

Acknowledgements

Firstly, I would like to express my sincere gratitude to my primary supervisor, Dr Li Jia, for her continuous support, guidance and encouragement during the time of my PhD research and in writing this thesis. She has taught me important research skills and provided the practical means for undertaking this work. I would also like to thank my second supervisor, Professor John Gribben, for his insightful knowledge and encouragement, and for motivating me to think about the wider implications of my research. I am truly grateful for both of their support.

My sincere thanks also go to all the patients who donated samples, to Sameena Iqbal and the tissue bank staff for gathering and retrieving patient samples, and to Janet Matthews who supplied the patient information. Thank you to Andrew Clear for constructing the tissue microarrays, for his expertise, support and patience regarding all things immunohistochemistry related. Thank you also to Maria Calaminici for offering her histopathology expertise. I would also like to thank David Britton and Pedro Casado for their mass spectrometry expertise and support.

I am particularly grateful to Farideh Miraki-Moud, for her unparalleled advice and support with cell culture and flow cytometry, and for her friendship and encouragement in the lab. My huge thanks also goes to Robert Petty for his wisdom and guidance when I started my PhD research.

I thank my fellow Haemato-Oncology and Barts Cancer Institute colleagues for the stimulating discussions, support, sharing of protocols and, of course, for all the fun we had over the last four years. Thank you to Emma Vilventhraraja, Sabari Vallath and Helena Church for being there at all times - my PhD would not have been the same without you. Thank you to my friends for the laughter, reassurance and care packages received while writing this thesis – your encouragement has kept me going.

Last but not least, I would like to thank my family, to Mum, Mark, Chloé and Aidan - what a journey it has been for all of us, words cannot express how grateful I am. Mum, the sacrifices you have made on my behalf over the years and your unfaltering support has shaped my career, and helped me reach this point - thank you.

Finally, to Grandad Harris, for watching over me.

Table of Contents

List of Figures

List of Tables

List of abbreviations

ADAM10	A disintegrin and metalloproteinase domain-containing protein 10
AF	Alexa Fluor
ALL	Acute lymphoblastic leukaemia
BCR	B-cell receptor
BLNK	B-cell linker protein
BM	Bone marrow
BMSC	Bone marrow stromal cells
BR	Bendamustine with rituximab
BSA	Bovine serum albumin
BTK	Bruton tyrosine kinase
CAR	Chimeric antigen receptor
CIs	Confidence intervals
CLL	Chronic lymphocytic leukaemia
Co-IP	Co-Immunoprecipitation
CTL	Cytotoxic T lymphocytes
CV	Coefficient of variation
DAB	3,3'-diaminobenzidine
DAG	Diacylglycerol
DAMPs	Damage-associated molecular patterns
DAPI	4’,6-diamidino-2-phenylindole
DAVID	Database for Annotation, Visualization and Integrated Discovery
DC	Dendritic cells
DTT	Dithiothreitol
ECL	Enhanced chemiluminescent
ELISA	Enzyme-Linked Immunosorbant Assay
EP	Ethyl pyruvate
ERK 1/2	Extracellular signal-regulated kinase 1/2
es-RAGE	Endogenous secreted-RAGE
FBS	Foetal bovine serum

FCR	Fludarabine and cyclophosphamide with rituximab
FFPE	Formalin-fixed paraffin-embedded
FL-RAGE	Full-length RAGE
GC	Germinal centre
GEO	Gene Expression Omnibus
HAG	Human anti-globulin antibody
HIER	Heat induced epitope retrieval
HMGB1	High mobility group box protein 1
HR	Hazard ratio
HRP	Horseradish peroxidase
IFM	Immuno-fluorescent microscopy
Ig	Immunoglobulin
IGHV	Immunoglobulin heavy-chain variable
IHC	Immunohistochemistry
IKK	Inhibitor of NF-κB kinase complex
IL	Interleukin
IRAKs	IL-1R associated kinases
IκB	Inhibitor of NF-κB
KSEA	Kinase Substrate Enrichment Analysis
LC MS/MS	Liquid chromatography–mass spectrometry / mass spectrometry
LN	Lymph node
LPS	Lipopolysaccharide
MAPK	Mitogen-activated protein kinase
M-CLL	Mutated CLL
MDSC	Myeloid derived suppressor cell
MFI	Median fluorescence intensity
mTORC1	Mechanistic target of rapamycin complex 1
MyD88	Myeloid differentiation primary response protein
MZ	Mantle zone
NKs	Natural killer cells

NLCs	Nurse-like cells
NLS	Nuclear localisation signals
NSAIDs	Non-steroidal anti-inflammatory
ODN	Oligodeoxynucleotide
OS	Overall survival
PAGE	Polyacrylamide gel electrophoresis
PAMPs	Pathogen-associated molecular patterns
PB	Peripheral blood
PBMC	Peripheral blood mononuclear cells
PBS	Phosphate buffered saline
PC	Proliferation centre
PI	Propidium iodide
PI3k	Phosphoinositide 3-kinase
PKC	Protein kinase C
PLC-γ2	Phospholipase Cγ2
PRR	Pattern-recognition receptor
PS	Phosphatidylserine
PVP	Polyvinylpyrolidine
R	Pearson's correlation coefficient
RA	Reactive
RAGE / AGER	Receptor for advanced glycation end products
Rb	Retinoblastoma
ROS	Reactive oxygen species
SBDS	Similarity Bright Detail Score
SD	Standard deviation
SDS	Sodium dodecyl sulphate
SEC	Similarity Eroded Score
SHM	Somatic hypermutation
SLE	Systemic lupus erythematosus
sRAGE	Soluble receptor for advanced glycation end products

TAMs	Tumour-associated macrophages
TAMs	Tumour-associated macrophage subsets
TBST	Tris-Buffered Saline with 0.1% Tween-20
T-helper cells	T_H
Ti02	Titanium dioxide
TIR	Toll/IL-IR receptor domains
TLR	Toll-like receptor
TLR9	Toll-like receptor 9
TMA	Tissue microarray
TMB	3, 3',5,5'-tetramethylbenzidine
TNF	Tumour necrosis factor
TRAF6	Tumour-necrosis-factor-receptor associated factor 6
T-regulatory cells	T_{REGS}
U-CLL	Unmutated CLL
VEGF	Vascular endothelial growth factor
α-RAGE	Anti-RAGE

Chapter I

Introduction

1.1 Inflammation

1.1.1 The inflammatory response

In its simplest form, inflammation is a molecular and cellular immune response to host damage and homeostatic imbalance. Triggers of inflammation can range from a variety of exogenous and/or endogenous inducers, leading to different physiological responses to restore homeostasis. Injury and infection were early known activators of the inflammatory response,[1,2] where controlled, acute inflammation to such inducers is beneficial to regain tissue homeostasis and limit host damage. The initiating causes of systemic chronic dysregulated inflammation are not clear, and frequently results in harm to the host.[1] Although acute inflammation in response to infection and injury is more aggressive than chronic in the short term, systemic chronic inflammation is associated with the pathogenesis of a wide variety of life-threatening diseases (such as sepsis, cardiovascular disease, diabetes, cancer and autoimmune disease).[3]

Inflammation is a complex interplay of regulatory networks. The adaptive response can broadly separate into 4 categories – inducers, sensors of innate immunity, mediators and effectors (Table 1).[3,4] Each stage contributes to a different type of inflammatory response to maximise effective regain of homeostasis. Different types of inducers are surveyed by a variety of sensors, the sensors relay the correct message via secreted cytokines, chemokines and inflammatory signalling pathways, to recruit the suitable effector leukocytes.

For example, the presence of lipopolysaccharide (LPS) sensed by pattern recognition receptor (PRR) toll-like receptor 4 (TLR4) on tissue resident macrophages is indicative of bacterial infection.[5] This leads to the secretion of TNF-α and IL-6 to recruit neutrophil to the site of infection, that release the contents of their toxic granules to eliminate the pathogen.[6,7] The pro-inflammatory microenvironment progresses to anti-inflammatory, to facilitate recruitment of tissue-repair monocytes and phagocytic macrophages.[8] In response to trauma and injury, endogenous stress signals or damage-associated molecular patterns (DAMPs) alert the tissue remodelling and repair arms of the immune system via TGF-α/β, IL-4, IL-10 and IL-13 mediators, to eliminate damaged cells and regenerate tissues.[9] In both settings, chronic inflammation is established when infection persists or host damage continues to occur, and results in the addition of other effector cell subsets; the polarization of the chronic inflammatory state is largely dependent on the type of effector T-cell and macrophage subset (Table 1).[3] Although acute inflammation follows a clear set of mechanisms, systemic chronic inflammation initiation and maintenance in pathological conditions are poorly understood.

Table 1 The components involved in an inflammatory response

Stage	Effect	Components involved
Inducer	Inducers are a group of specific conserved molecules that are found on micro-organisms or host-molecules that are not usually localised in the extracellular environment. They alert the immune system to danger.	Can be from exogenous or endogenous origin - Exogenous: pathogen-associated molecular patterns (PAMPs), virulence factors, allergens, irritable chemicals. - Endogenous: Sequestered or compartmentalised under normal conditions but are released during stress or trauma. Include ATP, HMGB1, S100, RNA/DNA and potassium ions.
Sensor	Sensors recognise inducers of inflammation and are mostly membrane bound receptors. Activation of these receptors initiates cell activation and the beginning of an immune response.	Involves PRRs: - Toll-like receptors (TLRs), nod-like receptors, C-type lectin receptors, scavenge receptors, RIG-like helicases, receptor for advanced glycation end-products (RAGE) expressed in immunocompetent cells, epithelium, endothelium and stromal cells (i.e. localised at barriers or tissue surveillance) - Other foreign bodies, not encompassed under the host PAMP recognition, are sensed by 'missing self' (lack of MHC-I expression) by natural killer cells.
Mediator	Act as messengers between sensing danger and the immune response. Mediators act on a variety of target cells and tissues, allowing the host to adapt to potential damaging conditions.	Mediators originate from various sources including cell secretion, inactive plasma precursors or preformed granules. This results in variable inflammatory outcomes such as vasodilation, vasoconstriction, leukocyte recruitment, chemotaxis, cell differentiation. - Cytokines (TNF-α, IL-1, IL-6 IFN-γ,TGF-β) , chemokines, complement proteins, lipid mediators (prostaglandins), vasoactive amines (histamine).
Effector	Regain and maintain tissue homeostasis. Clear infection, cell-death debris and repair tissue damage.	Different cell types mediate different responses. Cell-mediated killing: - T-helper 1 cells (T_H1) elicit cell-mediated killing to clear infection via activation of CD8+ cytotoxic T cells and natural killer cells. - M1 macrophages support T_H1 cells by phagocytosis and antigen presentation. Antibody-mediated immunity: - T_H2 cells activate the humoral antibody-mediated immunity to allergens. - M2 macrophages promote T_H2 responses by tissue remodelling/repair and immunoregulation.

1.1.2 Inflammation and cancer

The ability of a host cell to transform into a successful malignant cell requires various acquired capabilities. With increasing research, 10 hallmarks of cancer are reported as the key functional characteristics of cancer development that differentiates malignant cells from normal-functioning healthy cells (Figure 1-1).[10]

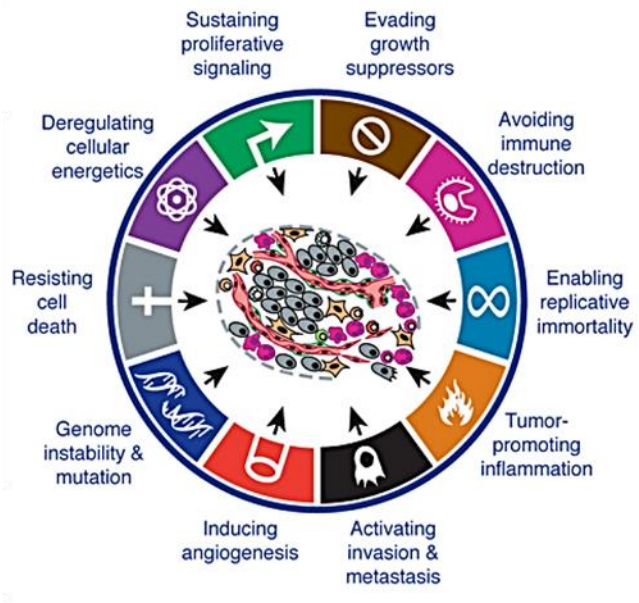

Figure 1-1 The 10 Hallmarks of Cancer
Over the last 15 years, research has expanded our understanding and knowledge of cancer pathogenesis from the original 6 hallmarks, to 10 capabilities acquired for cells to transform. These new hallmarks include deregulating cellular energetics, avoiding immune destruction, genome instability and mutations, and tumour promoting inflammation.[10]

As an established hallmark of cancer, a chronic inflammatory microenvironment plays an important role in the progression of the neoplastic process, contributing to the survival and migration of cancers, including chronic lymphocytic leukaemia.[10-14] A normal inflammatory response is regulated by release of anti-inflammatory cytokines, the action of T-regulatory cells and myeloid suppressor cells.[15] Whereas dysregulated chronic inflammation contributes to immune evasion, tumour promotion, invasion, metastasis, and proliferative signalling – 4 hallmarks of cancer. The presence of immune cells in neoplastic tissues was noted by Virchow in the 19th century, but it's only in the last few decades that our understanding of tumour-associated inflammation has supported Virchow's hypothesis.[16] Tumour infiltrating immune cells are able to engage with malignant cells and mediate dynamic molecular crosstalk with malignant cells and surrounding stroma to engineer a niche pro-tumour environment. Immune cells communicate with malignant cells by direct contact and through production of reactive

nitrogen and oxygen species, cytokines, chemokines, prostaglandins and growth factors which signal in a paracrine and autocrine manner to facilitate a positive pro-inflammatory pro-survival feedback loop.[17] In fact, inflammation is involved in every step of tumourigenesis.

Peyton Rous demonstrated cancers arise from 'initiated cells'.[18] Environmental and chemical carcinogens, autoimmune damage, chronic inflammatory exposure, genotoxic stress or a failure in DNA repair mechanisms induce DNA alterations giving rise to initiating genetic events that are reversible. To establish a malignant status, these initiated cells require promoter events. Promoter events support cell growth, recruit inflammatory cells and increase production of reactive nitrogen and oxygen species resulting in further DNA damage and establishment of a "wounds that do not heal". This simplified cycle continues due to persistent initiator events and irresolvable tissue damage. Although smouldering inflammation is present in tumours with a relationship to chronic inflammatory initiating events, this type of inflammation is also observed in tumours irrespective of the trigger for tumour development, or that do not display an inflammatory-link (i.e. breast cancer).[12] Therefore, a chronic inflammatory microenvironment is a vital component of tumour development and one of the hallmarks of cancer.

1.1.3 The origin of inflammation in cancer

The origin of chronic smouldering inflammation supporting promotion of cancer cells arises from intrinsic and extrinsic pathways. Intrinsic inflammatory activation occurs due to genetic events that lead to the upregulation of oncogenes (such as RAS, RET and MYC), or tumour suppressor gene inactivation (such as PTEN and TGF-β).[12] The RET/PTC chromosome rearrangement in human papillary thyroid cancer is sufficient to induce development of this cancer by activating protein tyrosine kinase, RET, and downstream inflammatory response.[19] Oncogene activation results in the activation of the inflammatory transcriptome and production of pro-inflammatory cytokines, chemokines and prostaglandins which in turn, promote establishment of pro-tumour paracrine and autocrine signalling.[20] The intrinsic pathway is responsible for the inflammatory involvement in tumours that have no underlying inflammatory conditions.

In the extrinsic pathway, underlying localised inflammation from inflammatory or infectious conditions increase the risk of cancer development. It is estimated around 20% of cancers are caused by chronic infection and autoimmunity.[21] For example, individuals with Crohn's disease have an increased risk of colon cancer, and Hepatitis C infection is associated with increased risk of liver cancer, highlighting the input of underlying chronic inflammation in tumour development.[22,23] Moreover, environmental carcinogens such as tobacco smoke and UV light are highly mutagenic and irritable, promoting the development of lung cancer and skin cancer, respectively.[24] The culmination of pro-inflammatory cytokines, chemokines, prostaglandins and

DAMPs established by underlying inflammation/infection activates pro-inflammatory transcription factors in tumour cells, i.e. NF-κB, STAT3 and HIF1α.[12] The intrinsic and extrinsic pathways converge at this stage and maintain tumour-associated inflammation by positive feedback signalling.

Regarding inflammatory maintenance, tumours are often referred to as "wounds that do not heal".[25] NF-κB, STAT3 and HIF1α activated tumour cells release pro-inflammatory cytokines and growth factors (IFN-γ, IL-1, IL-4, IL-6, IL-10, TGF-β, TNF, VEGF, CSF), as well as chemokines (CXCL13, CXCL1, CXCL8, CXCL10, CCL22). Cytokines are directly linked to malignant progression, and chemokines facilitate leukocyte recruitment, particularly cells of the polarised myeloid lineage and T-helper cells.[26] Alike to wound healing, tumours secrete vascular endothelial growth factor (VEGF) which acts on the tumour stroma to persistently generate extracellular matrix. However, where wound healing is self-limiting, the components of the extracellular matrix (fibroblasts, platelets and adipocytes) are a rich source of cytokines and growth factors (particularly TGF-β and VEGF) contributing to angiogenesis, metastasis and tumour progression.[27] As tumour development progresses, the centre of tumour masses are commonly hypoxic, and undergo necrosis, causing release of DAMPs and pro-inflammatory cytokines such as HMGB1, TNF, IL-1 and IL-6 – this smouldering inflammatory cycle persists.[28] Moreover, radio- and chemotherapy induce tissue damage and cell death, causing further release of DAMPs and pro-inflammatory cytokines; the wound-healing response following cancer therapy can exhibit pro- and anti-tumour effects.[21]

1.1.4 Pro- and anti-tumour inflammation

Within the same tumour, pro- and anti-tumour inflammation coexist. Innate and adaptive immune cells, surrounding stroma and malignant cells communicate via direct cell-cell contact or through production of cytokines and chemokines. The combinatorial cytokine, chemokine, DAMP profile of the microenvironment will decide the activation state of these different cell types and dictate the balance between pro-tumour and anti-tumour inflammation (Table 2).[29] The polarised inflammatory microenvironment is sustained by autocrine and paracrine signalling. Although malignant cells are constantly assessed by immune surveillance mechanisms, once immune evasion is achieved and if tumours are left untreated, they rarely regress; highlighting pro-tumour inflammation usually exceeds anti-tumour immunity.[30]

The driving anti-tumour mechanisms involve immune cell-subsets that mediate cell-killing. Infiltration of CD4+ T_H1 cells secretes IFN-γ and activate CD8+ cytotoxic T lymphocytes (CTL) and natural killer cells (NKs).[31,32] Tumour-antigen presentation by M1 polarized macrophages and dendritic cells prime the cytotoxic mechanisms towards tumour cells to perform cell killing.[8] On

the other hand, wound healing immune mechanisms comprise the major components of pro-tumour responses. M2 polarized tumour-associated macrophages (TAMs) are important players of pro-tumour inflammation, promoting tissue remodelling and angiogenesis compared to cell-killing.[26] This requires the action of CD4+ T_H2 and T_H17 cells compared to T_H1 and CTL responses. The smouldering wound healing response supports further DNA damage and genomic instability in tumour cells and tumour promoting properties. The action of T-regulatory cells (T_{REGS}) encompasses both anti- and pro-tumour responses by suppressing inflammation through IL-10 production.[33]

Table 2 Pro-tumour inflammation and anti-tumour immunity cellular responses

	Anti-tumour immunity	**Pro-tumour inflammation**
Macrophage	IL-12, IFN-γ - M1 phagocytosis and antigen-presenting macrophages, inhibit T_{REGS} and activate T_H1 response	IL-4/6/10/13 - M2 tumour-associated macrophages for wound healing, provides growth factors and cytokines for tumour growth
Dendritic Cell (DC)	Antigen presenting cells – activate T_H1 and cell mediated-killing response	Antigen presentation for T_H2 cells and B-cells – humoral response instead of cytotoxic response
CD4+ T cell	T_H1 response – produce IFN-γ, help cytotoxic T-lymphocyte response	T_H2 and T_H17 response – wound healing (IL-4, IL-5, IL-10). Induce differentiation of macrophages, myeloid derived suppressor cells and activates the B-cell humoral response instead of cell-mediated killing
CD8+ T cell	Cell-mediated tumour cell killing (granzymes, perforin; IFN-γ secretion)	-
T-regulatory cell	Immune suppression	Immune suppression – IL-10, TGF-β inhibit CD8+ cytotoxic T-lymphocytes
Natural killer (NK) cell	Cell-mediated tumour cell killing	-
B-cell	Produce tumour-specific antibodies	Humoral response – production of cytokines and antibodies, does not mediate tumour cell death. Activate mast cells
Myeloid derived suppressor cell (MDSC)	-	Inhibit DCs, NKs and CD4+ T_H1 cells. Produce cytokines, chemokines, proteases.

1.1.5 Targeting cancer-associated inflammation

The clinical manifestations of tumour-associated inflammation are associated with worse clinical outcomes for patients with cancer and are included in disease diagnosis/staging, particularly in haematological malignancies.[34] B symptoms, such as high fever (over 38°C), night sweats and weight loss are indicative of high circulating levels of inflammatory cytokines such as TNF-α, IL-1 and IL-6 and confer a poor prognosis in CLL.[35] As our understanding of cancer-associated inflammation improves, particularly the mechanisms linked to pro- and anti-tumour immunity, therapies harnessing and manipulating aspects of the inflammatory response are of increasing interest.

Methods to target tumour-associated inflammation include non-selective strategies that affect systemic inflammation, or selective mechanisms to manipulate specific arms of the inflammatory/immune response. Non-steroidal anti-inflammatory drugs (NSAIDs) and aspirin are widely known preventive agents.[11] NSAIDs inhibit cyclooxygenase 1 and 2, that are expressed in inflammatory conditions, preventing production of prostaglandins and angiogenesis;[36] risk of colon cancer was reduced in people who had taken NSAIDs.[37] However, long term use of NSAIDs as a cancer preventing strategy is not advised due to non-selectivity and other side effects, unless individuals are at high-risk of cancer development.[38]

Targeted strategies manipulate specific pathways of the inflammatory response to dampen pro-tumour signalling and amplify anti-tumour immunity. Non-tumour components of the tumour microenvironment pose as a stable target compared to malignant cells directly, where acquired chemotherapy resistance results in the failure of anti-cancer agents.[34] Selective targets include cytokines, chemokines, integrins, inflammatory transcription factors, tumour antigens for immune-cell directed therapies and manipulation of T-cell functions. For example, anti-IL-6 antibody, siltuximab, has been evaluated in prostate cancer and platinum-resistant ovarian cancer.[39] Targeting CCL2 chemokine produced by breast cancer cells with neutralising antibodies, abrogates recruitment of CCR2-positive monocytes, reducing metastasis.[40] The roles of pro-inflammatory transcription factors, STAT3, NF-κB and HIF1α as central regulators of pro-tumour signalling and angiogenesis place them as ideal microenvironment targets. Transcription factors are inferior drug targets, due to their nuclear localisation and lack of suitable small molecule binding sites,[41] but targeting downstream targets such as JAK1 and JAK2 have shown promise for STAT3-mediated pathways in cancer.[42] Finally, therapies that redirect cell-mediated immunity towards malignant cells are proving successful in clinic. Anti-CD20 monoclonal antibody, Rituximab, targets CD20 expressed on the surface of malignant cells in B-cell malignancies (including CLL) and promotes antibody-dependent cell cytotoxicity.[43] Moreover,

interfering with immune checkpoints can restore T-cell function. Pembrolizumab, is FDA approved for the treatment of a variety of cancers including melanoma, Hodgkin's lymphoma, lung cancer and is of current intense interest in CLL.[44,45]

1.2 Chronic Lymphocytic Leukaemia

CLL is currently an incurable disease of malignant, antigen-stimulated, mature B-lymphocytes (expressing CD5, CD19 and CD23) present in peripheral blood and lymphoid organs. The disease heavily relies on the microenvironment milieu for external survival signals,[13,14,46-48] as well as B-cell receptor signalling via surface IgM, and a variety of genetic aberrations contributing to CLL pathogenesis.[49] CLL is a highly diverse and heterogeneous disease, reflected in variations in clinical manifestations, prognostic biomarkers and need and type of therapeutic management. Clinical translation of the molecular mechanisms driving CLL progression is aiding in identifying high-risk patients and development of targeted therapeutic approaches.

1.2.1 CLL development

Two landmark studies identified the cellular origin and 2 main subsets of CLL disease, where patients display different disease progression and outcome rates.[50,51] Gene expression profiling and genetic studies identified 2 origins of CLL-cell development based on the point of exit from B-cell maturation (Figure 1-2).[52] Cells from unmutated-CLL (U-CLL) origin are pre-germinal centre, surface immunoglobulin-M (IgM) expressing, mature naïve B-cells that have encountered antigen, but have not yet undergone somatic hypermutation (SHM) of the immunoglobulin heavy-chain variable (IGHV) gene region. Mutated-CLL (M-CLL) derive from post-germinal centre B-cells that have undergone SHM of the IGHV gene region; this gives rise to higher affinity surface B-cell receptors (IgM and IgD) for specific antigens. M-CLL cells tend to display an anergic B-cell phenotype and do not retain B-cell receptor (BCR) signalling responsiveness compared to U-CLL cells.[53] Patients with CLL cells that express unmutated IGHV genes generally have a more aggressive disease compared to patients with M-CLL.[49]

The expression levels of surface BCRs are lower, and the Ig repertoire is limited, in CLL patients compared to B-cells from a healthy individual; this emphasises biased IGHV gene usage, and limited somatic hypermutation and combinatorial diversity.[54,55] Sections of the variable region in Ig molecules are matched across a third of CLL patients, referred to as Ig 'stereotypes'.[56] This combination highlights the importance of BCR signalling in selecting and driving CLL cell survival, based on receptor binding activity, and the limited antigen repertoire which must select for these stereotyped B-cells.[57] Therefore, as BCR signalling plays an important role in CLL development, this signalling pathway is an attractive therapeutic target.

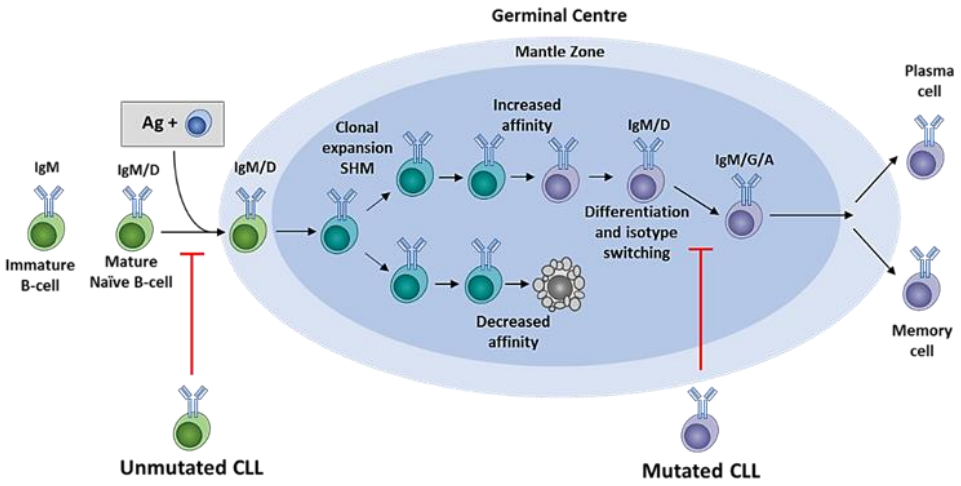

Figure 1-2 CLL B-cell development
2 main subsets of CLL exist. The first subset, U-CLL, develop from pre-germinal centre, mature B-cells encountering antigen in secondary lymphoid organs. The second subset are post-germinal centre B-cells that have undergone clonal expansion and somatic hypermutation (SHM) of their IGHV genes that give rise to higher affinity surface IgM/IgD (B-cells receptors). M-CLL arise before BCRs undergo isotype switching to different classes of Ig molecules. Figure adapted from [53].

1.2.2 The molecular pathogenesis of CLL

The difference in CLL disease severity and outcome between U-CLL and M-CLL subsets are not solely due to differences in IGHV mutational status. Disease molecular pathogenesis is also attributed to chromosomal alterations, somatic mutations, epigenetic modifications, activated signalling pathways and molecular crosstalk with the inflammatory microenvironment within the CLL lymph nodes and bone marrow.[58]

1.2.2.1 Genetics

A variety of genetic lesions contribute to disease initiation and clinical progression. Although chromosome translocations are highly common in haematological malignancies, they are rare in CLL. Instead, 80% of CLL patients harbour a chromosomal alteration – deletion in 13q14.3 (del(13q)), deletion in 11q22-23 (del(11q)), deletion in 17p13 (del(17p)), and trisomy 12.[59] Del(13q) is observed in 50-60% of patients and occurs more frequently in patients with M-CLL. This chromosomal alteration is associated with a favourable prognosis, due to deletion of the *DLEU2-mir-15-16* cluster that regulates expression of anti-apoptotic proteins.[60] Both del(11q) and del(17p) are associated with an unfavourable outcome; del(11q) is observed in ~20% of CLL patients and encompasses the loss of tumour suppressor gene ATM (involved in DNA damage repair), whereas del(17p) is found in <10% of CLL patients and harbours loss of tumour suppressor gene *TP53.*[61] Finally, an extra copy of chromosome 12 is observed in <15% of patients

and is associated with intermediate CLL disease risk – although, there is high co-occurrence of this chromosome abnormality and *NOTCH1* mutations.[62]

Somatic mutations have clear pathogenic impact on the course of CLL disease and contribute to genetic heterogeneity. Whole genome and exome sequencing studies revealed a small number of recurrent somatic mutations that are putative drivers of CLL development and can be assigned to common biological pathways.[61,63,64] For example, *TP53, ATM* and *POT1* mutations affect DNA damage and protection of telomeres,[65] *SF3B1* and *XPO1* mutations result in aberrant RNA splicing,[65] and *CHD2* and *ZMYM3* mutations disrupt genome/chromatin structure.[65] In terms of cell signalling, *BRAF, BIRC3, MyD88* and *PAX5* mutations affect BCR-TLR-NF-κB signalling pathways and activation,[65] while mutations in *NOTCH1* result in the constitutive activation of Notch signalling.[65] The relative frequencies of these mutations are variable between the U-CLL and M-CLL cohorts, but overall, mutations with notable frequency in CLL patients include *SF3B1* (21% of patients), *ATM* (15%), *TP53* (7%), *NOTCH1* (6%), *BIRC3* (4%), and *MyD88* (3%).[64,66]

Alterations in the expression of specific miRNAs contributes to CLL disease pathogenesis. Del(13q) encompasses deletion of mir-15a and mir-16-1 in 50-60% of CLL patients. Loss of these tumour suppressor miRNAs results in the upregulation of anti-apoptotic genes *BCL2* and *MCL1*.[67] Moreover, intense interest in understanding the CLL epigenome revealed high intra-tumour methylation heterogeneity and suggests a role for transcription-mediated epigenetic programming in CLL.[68]

1.2.2.2 BCR signalling

Functional BCR signalling is vital for the maturation and survival of B-cells, including mature malignant B-cells such as CLL. Alike to normal B-cells, CLL cells require continuous microenvironment support for survival, regardless of initiating cytogenetic and genomic events.[69] The outcome of BCR signalling is heterogeneous in CLL; antigen engagement results in B-cell activation/proliferation, or anergy – an unresponsive state of cell lethargy where a secondary co-signal (i.e. T-cell help) was not received.[70] The signalling pathway resulting in anergy is not well-defined, but is more common in patients with M-CLL largely giving rise to indolent disease.[53]

BCR signalling is driven by autoantigens in CLL, supported by the restricted Ig repertoire and surface Ig stereotypes (Figure 1-3).[47,70,71] The BCR is comprised of surface IgM or IgD complexed with the signalling CD79A and CD79B heterodimer. Antigen engagement induces formation of the signalosome, where crosslinking of surface Ig molecules triggers phosphorylation of immunoreceptor tyrosine-based activation motifs in CD79A and CD79B by Lyn.[53] This induces the recruitment of Syk through tandem SH2 domains and Src-family kinase-dependent

phosphorylation or autophosphorylation. Lyn-mediated phosphorylation of CD19 and activation of Syk leads to the recruitment of B-cell linker protein (BLNK), Bruton tyrosine kinase (BTK), phospholipase Cγ2 (PLC-γ2), phosphoinositide 3-kinase (PI3K) and Akt.[69] After formation of the signalosome, downstream signalling is initiated. PLC-γ2 generates inositol-1,4,5-triphosphate ($Ins(1,4,5)P_3$) and diacylglycerol (DAG) triggering release of Ca^{2+} from the endoplasmic reticulum and activation of RAS and protein kinase C (PKC). Syk and RAS/RAF1 signalling pathways activate mitogen-activated protein kinase signalling pathway (MAPK), including extracellular signal-regulated kinase 1/2 (ERK1/2), leading to the activation of NF-κB and the pro-inflammatory transcriptome.[53] PI3K produces phosphatidylinositol 3,4,5-triphosphate required for full activation of BTK and AKT, and downstream activation of mechanistic target of rapamycin complex 1 (mTORC1). The activation of kinase cascades and downstream transcription factors including NFAT, MYC, JUN, ATF2 and NF-κB links BCR signalling to biological responses such as cell survival, proliferation, migration or apoptosis.[70]

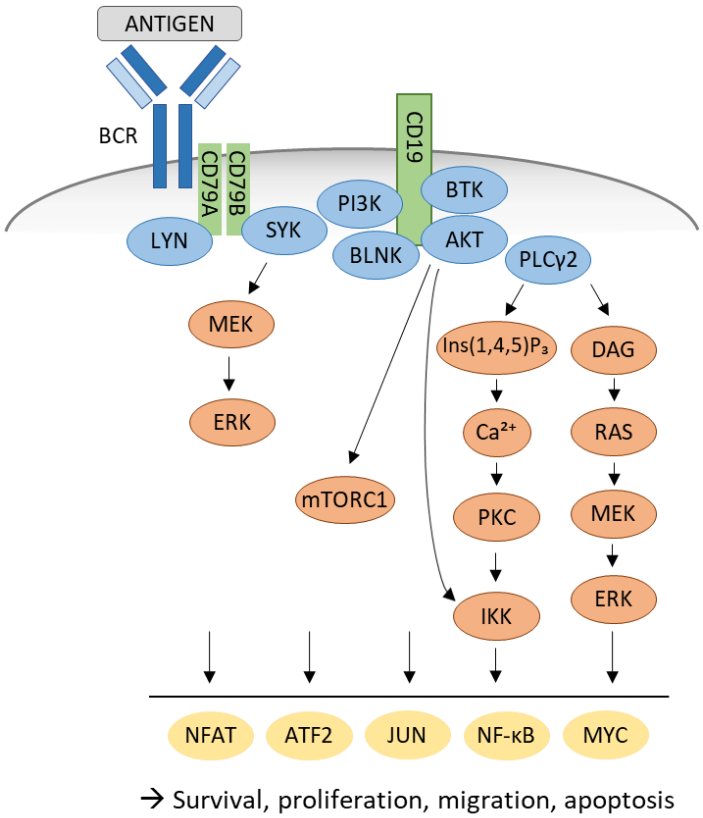

Figure 1-3 B-cell receptor signalling in CLL
Following antigen crosslinking and BCR activation, the signalosome is formed, comprised of LYN, SYK, BLNK, BTK, PLC-γ2, PI3K and AKT. The production of BCR mediators DAG, $Ins(1,4,5)P_3$ and Ca^{2+} release from the endoplasmic reticulum triggers activation of downstream signalling pathways. RAS/RAF, MAPK/ERK and mTORC1 are activated, leading to the activation of transcription factors NFAT, ATF2, JUN, NF-κB and Myc. Ultimately, BCR signalling results in B-cell activation/proliferation predominately in U-CLL, and anergy in M-CLL - indicative of constitutive ERK and NF-κB stimulation. Adapted from [58].

1.2.2.3 CLL inflammatory microenvironment

CLL is a model system for inflammatory-driven progression of cancer. Although CLL cells circulate in peripheral blood, the lymph node harbours the proliferative CLL fraction in specialised structures called proliferation centres.[46] A powerful gene expression analysis of matched CLL cells from peripheral blood, bone marrow and lymph nodes identified enhanced activation of BCR-associated signalling pathways and NF-κB activation in CLL lymph nodes; this was significantly higher in U-CLL.[47] Further assessment of CLL-cell proliferation by expression of c-MYC, E2F, and immunohistochemical and flow-based staining of Ki67, demonstrated CLL cells follow chemokine gradients into lymph nodes, and proliferate in 'proliferation centres'.[47]

The CLL lymph node is a niche site rich in tumour-associated non-neoplastic cells and inflammatory cytokines, chemokines, integrins, autoantigen and growth factors. Within such proliferation centres, various key microenvironment-CLL interactions occur (Figure 1-4).[72] Only a fraction of CLL cells actively proliferate at a given time, while other cells remain in a quiescent unstimulated or anergic state. First, surrounded by antigen presenting nurse-like cells (NLC; CD68+/CD163+ macrophage) or free autoantigens with available T-cell help, BCR stimulation can occur.[53,73] Other pro-survival signalling pathways mediated by NLCs include secretion and release of TNF, BAFF and APRIL leading to the activation of NF-κB in CLL cells, and production of CXCL12 which moderates CLL-cell CXCR4 surface expression and LN homing.[74,75] Moreover, our group identified increased levels of extracellular HMGB1 in the plasma of CLL patients, which triggers activation of STAT3 and NF-κB in NLCs – HMGB1-mediated NLC differentiation and activation in turn, maintains CLL cell survival.[76] T-cells mediate direct and indirect pro-survival contact with CLL-cells through the CD40L-CD40 axis, and production of pro-survival cytokines, such as IL-4 which upregulates surface IgM.[77] The immune checkpoint interaction, PDL1 on CLL cells and PD1 strongly expressed by CLL CD4+ T-cells, favours immune evasion; targeting this interaction is of current therapeutic interest for the treatment of CLL.[78] In addition, other microenvironmental interactions that support CLL-cell proliferation include the Wnt5a-ROR1 signalling axis,[79] contact with mesenchymal stromal cells via VCAM1-α4β1 integrin interaction,[80] (the action of several chemokines in CLL-cell migration to lymphoid tissues (CXCL12, CCL19, CCL21) and recruitment of further tumour-associated inflammatory cells (CCL3, CCL4, CCL12, CCL22) to the proliferation centre microenvironment.[81]

The central coordinators of the inflammatory response, and end-point activation for many cytokines and chemokines upregulated in CLL, is NF-κB and STAT3 transcription factor activation.[20] These transcription factors provide a survival advantage for CLL cells by, in turn, inducing production and release of inflammatory cytokines and chemokines in a positive

feedback loop; a smouldering pro-tumour inflammatory microenvironment is established, sustaining CLL-cell survival.[82]

Our group previously demonstrated for the first time the importance of HMGB1 in CLL-NLC differentiation

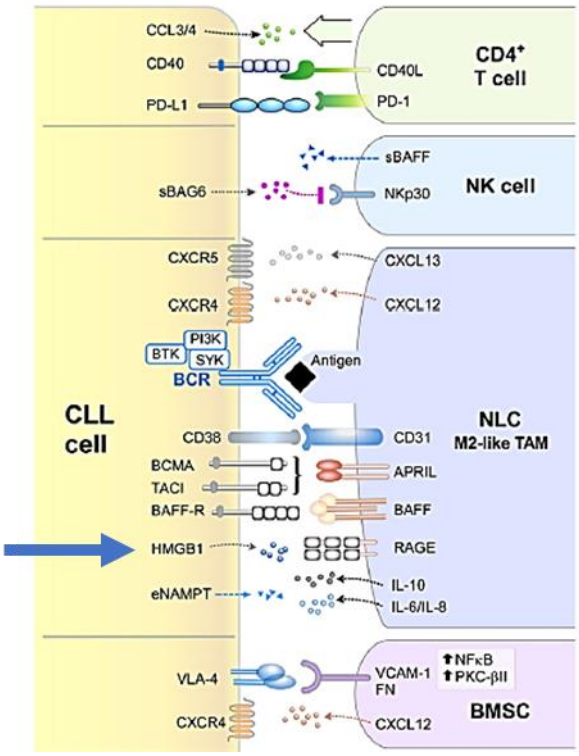

Figure 1-4 The CLL lymph node microenvironment
The LN is a rich source of cellular and molecular interactions. Pro-tumour interactions occur between CLL with CD4+ T-cells, natural killer cells, nurse-like macrophages (NLC; an M2-like macrophage) and bone marrow stromal cells (BMSC). Figure adapted from [72].

1.2.3 Clinical disease staging

The median onset of age for CLL is 71 years of age, and >75% of patients are 65 years or over at the time of diagnosis (www.cancer.org).[83] Patients are usually asymptomatic at the time of diagnosis but can present with a wide range of clinical features including B-symptoms (fatigue, weight loss and excessive night sweats), enlarged lymph nodes, splenomegaly, increased risk of infection with hypogammaglobulinemia and autoimmune cytopenia.[58] Diagnosis of CLL is usually made with a full blood cell count and flow cytometry; patients are diagnosed with CLL when they present with >5000 clonal B-cells per µl of blood that are positive for CD5, CD19 and CD23 by flow cytometry, express low levels of CD20 and lack CD10.[35] Blood tests and blood smears are usually adequate to make a CLL diagnosis, but in some cases a bone marrow or lymph node biopsies are performed to assess lymphocytic infiltration in the bone marrow and rule out suspected lymphoma.[58]

The Rai and Binet staging criteria are classical systems to categorise CLL disease (low to high risk is 0-III and A-C, respectively) based on clinical features such as thrombocytopenia,

lymphadenopathy and lymphocytosis.[84,85] The Binet system is more popular in UK clinical practice and separates patients into 3 groups. Patients with low risk CLL are assigned Binet stage A if palpable enlarged lymph nodes are found at less than 3 sites and the patient does not have cytopenia. Patients have Binet stage B disease if palpable enlarged lymph nodes are observed at 3 or more sites (lymphoid organ sites – cervical, axillary and inguinal nodes, the spleen and liver), without cytopenia. High risk CLL is assigned Binet stage C if patients have cytopenia, characterised by a haemoglobin level lower than 10g/dl; these patients have a predicted median survival of 2 years.[85]

1.2.4 Cytogenetic and molecular prognostic markers for CLL

Following a diagnosis, a patient's clinical course is highly variable – some patients do not require treatment for years, if at all, whereas other patients rapidly develop high risk disease and require treatment immediately. A wealth of prognostic factors aids CLL disease management – the use of multivariable models helps to identify patients that require therapy, or certain types of therapy, based on clinical, genetic and molecular prognostic features.[86,87]

Clinical features associated with a poor disease outcome include Binet stage C disease, >65 years of age and male gender.[86] Poor prognostic cytogenetic alterations assessed clinically at disease presentation include del(17p) and del(11q), where inactivating *TP53* mutations are associated with del(17p).[88] Other prognostic factors include patients with a complex karyotype, high levels of serum β2-microglobulin (>3.5mg per L) and a very high absolute lymphocyte count of (>50,000 cells per μl).[89,90]

The association between IGHV mutational status and clinical outcome for CLL was a huge breakthrough in understanding the molecular basis of CLL disease pathogenesis.[50,51] Approximately 35% of patients carry U-CLL, associated with worse prognosis and aggressive disease (predicted median survival of 8 years). Conversely, 65% of patients carry somatic mutations in the IGHV gene region and possess more indolent disease, with a predicted survival of 24 years. Both U- and M-CLL share a similar gene expression profile but are differentiated by the upregulation of ZAP70 and CD38 in U-CLL.[91,92] CLL B-cell ZAP70 expression is a common surrogate prognostic factor for IGHV mutation status, due to the cost and complexity in performing IGHV gene sequencing. The prognostic expression cut off point for ZAP70 is >20% of CLL peripheral B-cells by flow cytometry, and >30% for CD38.[93]

The molecular basis underlying the association with ZAP70 CLL B-cell expression and poor prognosis was an area of speculation; as a T-cell specific tyrosine kinase, expression in B-cells is not common.[94] However, ZAP70 expression in U-CLL increases BCR signalling capacity, reduces

surface IgM internalisation (allowing strong BCR activation) and crosslinks TLR9 signalling with the BCR pathway - this is independent of ZAP70 kinase activity.[95,96] Therefore ZAP70 has a hypothesised function as an adaptor/scaffold protein.[93]

1.2.5 CLL therapy

CLL risk stratification and signs of disease progression direct the decision to initiate therapy. The therapeutic landscape of CLL is changing, with new targeted agents increasing survival times for patients with high risk disease. As such, the presence or absence of prognostic markers described above help define therapy eligibility. Patients with Binet stage A/B disease and who are asymptomatic, do not require therapy and are assessed under 'watch and wait' for signs of disease progression.[35] Indications to initiate treatment include symptomatic disease, Binet stage C disease, palpable lymphadenopathy, cytopenia and a lymphocyte doubling count in <1 year.[35] Then, the choice of therapy is largely dependent on the presence of del(17p) and *TP53* mutations, the IGHV mutational status (if available), and the patient's clinical fitness and age.

1.2.5.1 Chemotherapy/ chemoimmunotherapy

Chemotherapeutic agents have conventionally been used for the treatment of CLL; classical agents include purine analogues such as fludarabine, and alkylating agents such as cyclophosphamide, chlorambucil and bendamustine. Three phase III clinical trials (including CLL8 and CLL11 trials) demonstrated the clinical efficacy and prolonged progression-free survival from combining chlorambucil with anti-CD20 monoclonal antibodies rituximab, obinutuzumab or ofatumumab,[97,98] and the combination of fludarabine and cyclophosphamide with rituximab (FCR).[43] Consequently, patients with symptomatic disease, without del(17p) or *TP53* mutations, are eligible for bendamustine with rituximab (BR) and patients with these treatment indication criteria and M-CLL disease, are eligible for FCR.[99,100] However, chemoimmunotherapy does not yield a sustainable response in patients with del(17p) or *TP53* mutations, so these patients are better suited for upfront targeted therapy.[101]

1.2.5.2 Targeted agents

Novel agents targeting specific pro-tumour factors are revolutionising CLL therapy;[102] Ibrutinib and Idelalisib target BTK and PI3K respectively, involved in the BCR signalling pathway.[88] Other novel targeted therapies under clinical development include higher specificity BCR inhibitors targeting SYK, BTK and PI3K; checkpoint inhibitors targeting PDL1-PD1 T-cell interactions; BCL2 antagonists targeting anti-apoptotic responses; and chimeric antigen receptor (CAR) T-cells directing cell-mediated leukaemic killing towards CD19 antigen.[103]

Ibrutinib is a suitable therapy for patients without del(17p)/*TP53* mutations that do not meet the fitness criteria to withstand chemoimmunotherapy. Moreover, Ibrutinib is approved in the US and Europe for front-line therapy for symptomatic patients with del(17p)/*TP53* mutations (RESONATE-2 trial), as well as in patients with relapsed disease (RESONATE-1 trial), owing to higher response rates compared to ofatumumab alone.[104,105] Other targeted agents not yet approved for front-line therapy, but approved for relapsed/refractory CLL include Idelalisib (targeting PI3K) and Venetoclax (targeting BCL2).[106,107] Trials investigating combinatorial targeted therapies are providing higher response rates due to synergistic activity, but treatment related complications and toxicity is still a huge issue and accounts for a high proportion of treatment dropout.[108,109] Although many targeted agents are still under investigation and not yet approved, many CLL patients can access these agents through clinical trials, upon meeting clinical trial criteria.

Therapies modulating the immune system and cell transplantation are under clinical development. Targeting immune checkpoints restores T-cell recognition and cancer cell destruction, avoiding immune evasion. Inhibitors of proteins that act as co-stimulatory or co-inhibitory signals to molecules expressed on T-cells is currently under clinical investigation in CLL.[110] CLL cells express high levels of PD-L1 that bind to PD-1 receptor on T-cells, dampening cytotoxic T-cell responses and partly contributing to the CLL exhausted T-cell phenotype. Although PD-L1 blockade yielded positive responses with *in vivo* models, this has yet to be recapitulated in phase I/II clinical trials for patients with relapsed CLL.[78] Allogeneic stem cell transplant is not a suitable or a desirable therapeutic option for many CLL patients, even though it has high curative potential. Patient age and fitness, adverse effects of immune suppression, donor availability, graft versus host disease and risk of infection renders this therapy inappropriate and ill-tolerated in many patients with CLL.[111] An emerging cellular immunotherapy with therapeutic potential in CLL is T-cell therapy with CARs. T-cells from patients are modified *ex vivo* to express CARs directed to CD19 antigen expressed on malignant B-cells. CAR-T-cells reintroduced into the patient restore the cytotoxic T-cell response and specifically target malignant CLL cells. Although early trials demonstrated the clinical ability to reach complete remission for patients with relapsed/refractory CLL, the efficacy of this therapy has yielded lower responses compared to acute lymphoblastic leukaemia (ALL).[112] Future studies looking at overcoming the exhausted T-cell phenotype to yield better CAR-T-cell responses could improve the clinical activity of this therapy.[113]

1.2.6 Current status of CLL

CLL is still an incurable disease and relapse is common for high-risk patients. Inflammatory dysregulation, acquired immune deficiency (through the action of immunosuppressive IL-10 and PDL1 expression) and treatment-related complications leave patients susceptible to infection and clinical complications.[114] Patients with immune deficiency and infection-related or treatment-related complications/inflammation, account for a high proportion of CLL death.[58] As such, chronic-inflammatory symptoms worsen with disease progression, but there are no inflammatory markers for prognosis.[82] Current targeted therapies lead to high overall response rates but complete responses are not common.[115] There is a real need for combinatorial therapies targeting many different aspects of CLL biology, particularly immuno-restorative agents, to improve complete response rates; these strategies also need to avoid acquired immune deficiency and treatment toxicity. Improved understanding of molecular mechanisms contributing to disease pathogenesis will lead to identification of therapeutic targets and better risk stratification for patients with CLL.

1.3 High Mobility Group Box 1 Protein (HMGB1)

HMGB1 has an established role in many types of solid cancer as an inflammatory mediator, associated with poor prognosis and increased mortality.[116] Despite its established important role, HMGB1 is not a well-known inflammatory mediator and is overlooked in many areas of cancer pathogenesis, including in CLL disease pathogenesis.

HMGB1 is a member of the HMG-super family and is an evolutionary ancient and highly conserved protein found in metazoans and mainly localised in the nuclei of all eukaryotic cells.[117] The protein was first discovered in 1978 as a non-histone DNA binding protein.[118] Preferentially bound to bent or kinked DNA, HMGB1 promotes formation of nucleosomes and loading of regulatory complexes to DNA, facilitating recombination, DNA replication, transcription regulation and maintenance of genome stability. For this reason, HMGB1 deleted mice pups die within 24 hours of hypoglycaemia, due to impaired transcriptional control.[119] It was not until 20 years later, a secondary role for HMGB1 was discovered as an intercellular inflammatory mediator released by macrophages and other cell types.[120] Once present in the extracellular milieu, HMGB1 acts on variety of cell types through cell-surface receptor engagement and has roles in various cellular processes – wound healing, autophagy, cell death, cell proliferation, inflammatory activation and disease pathogenesis.[121-123]

1.3.1 HMGB1 protein structure

The HMGB1 gene sequence is located on chromosome 13q12 and translates into a 25kDa protein. The proximal A-box and B-box folded helical domains bind DNA in a non-sequence dependent manner (Figure 1-5). Considered as a chromatin structural protein, HMGB1 binds with high affinity to the minor groove of kinked/bent DNA, particularly bent linker DNA between nucleosomes.[124,125] HMGB1 contains 2 nuclear localisation signals (NLS), 1 is located in the A-box (NLS1; amino acids 28-44) and 1 in the B-box (NLS2; amino acids 179-185).[126] These motifs are rich in lysine residues, 4 in NLS1 and 5 in NLS2, which undergo acetylation modification regulating the nuclear localisation of HMGB1, particularly in macrophages.[127] Interactions with nuclear proteins is mediated by the acidic C-terminal tail, comprised of a string of glutamic and aspartic acid residues.[128] Conserved cysteine residues located at positions 23, 45 and 106 are susceptible to redox modification; this regulates extracellular HMGB1 activity. Regulation of HMGB1 functional activity is strictly mediated by a combination of post-translational modifications including acetylation, oxidisation, phosphorylation, glycation, methylation and ADP ribosylation.

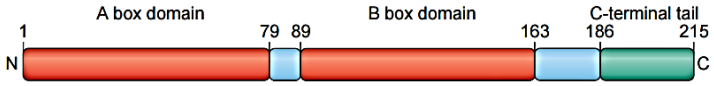

Figure 1-5 HMGB1 protein structure
HMGB1 consists of 2 DNA binding boxes (A and B), nuclear localisation signals and a negatively charged C-terminal tail that facilitates histone/nucleosome binding. Figure adapted from.[126]

1.3.2 Extracellular HMGB1

HMGB1 has an established extracellular role as a DAMP.[9,129] The extracellular role of HMGB1 was first identified as a delayed inflammatory mediator secreted by macrophages, following TNF-α and IL-1 release.[120] This was confirmed by observation of increased serum HMGB1 levels in mice, 12 hours after lipopolysaccharide (LPS) stimulation.[130] Passively released by damaged/dying cells and actively by immunocompetent cells, HMGB1 acts as a powerful danger signal and adjuvant (Figure 1-6).[126,131-133]

During necrotic cell death, HMGB1 is released as a free molecule, in a fully reduced state with immunogenic potential.[134] Apoptosis is classically regarded as non-immunogenic cell death to maintain healthy homeostasis. Early studies failed to observe free-molecule HMGB1 release during apoptosis compared to necrosis.[134] However, a recent study demonstrated the release of HMGB1 bound to nucleosome DNA fragments during apoptosis, by a mitochondrial ROS-dependent mechanism (Figure 1-6).[135] In addition, the high levels of reactive oxygen species (ROS) produced during apoptosis results in the release of fully oxidised HMGB1, compared to the all-thiol state during necrosis. Active release of HMGB1 is mediated by immunocompetent cells such as monocytes, macrophages, dendritic cells and natural killer cells following cell activation.[136] HMGB1 frequently shuttles between the cytoplasm and nucleus;[127,137] hyperacetylation of the 4 lysine residues in NLS1 and 5 lysine residues in NLS2 block re-entry into the nucleus and initiates extracellular release via a non-classical vesicle mediated secretory pathway that is specific to haematopoietic cells.[127,138]

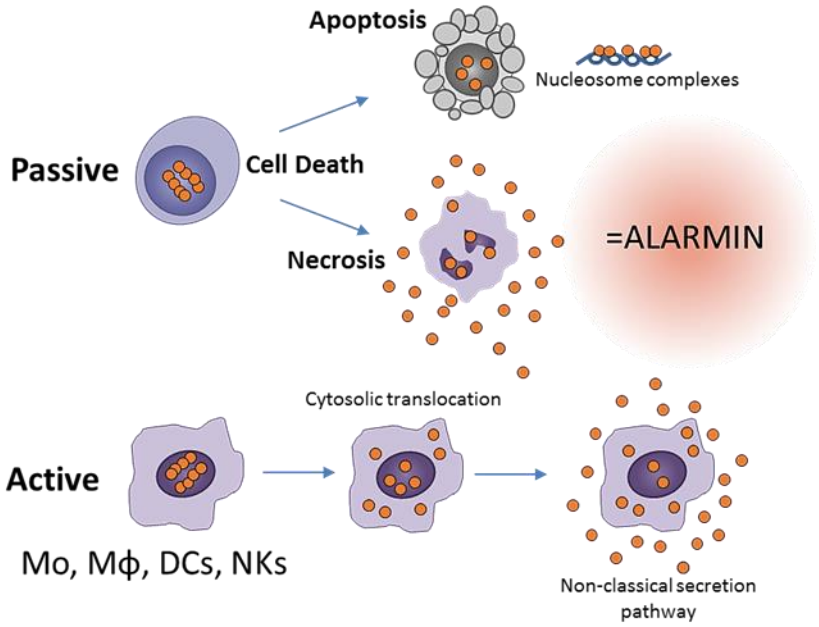

Figure 1-6 HMGB1 release
All cell types possess the ability to release HMGB1 passively: 1) Bound to nucleosome complexes during apoptosis; 2) Released as a free molecule during necrosis. Active release by immunocompetent cells is achieved via the non-classical secretory pathway. Monocytes (Mo), macrophages (Mϕ), dendritic cells (DC), natural killer cells (NKs).

Complex post-translational modifications regulate the extracellular function of HMGB1, dependent on the mode of cell death, metabolism and HMGB1 biology. As well as acetylation modifications regulating the release of HMGB1, the redox status of the 3 cysteine residues is specifically linked to HMGB1 cytokine or chemokine activity.[139] The B-box domain of HMGB1 is vital for cytokine activity; substitution of cysteine 106 abrogates the HMGB1-TLR4 interaction, and the B-box domain alone can induce TNF secretion in macrophages.[140] Disulphide bond formation between C23 and C45 residues are necessary for HMGB1 cytokine activity.[141] Therefore, reduction of C106 and a disulphide bond between C23 and C45 is critical for cytokine activity. To exert a chemotactic function, fully reduced HMGB1 at all 3 cysteines is required to mediate interactions with CXCL12. This chemotactic heterocomplex signals via CXCR4 on leukocytes, regulating inflammatory cell recruitment.[139] Finally, fully oxidised HMGB1 lacks both cytokine and chemokine activity, and this inactivity enhances cell death responses to anticancer agents compared to reduced HMGB1.[121]

Extracellular HMGB1 released by necrosis, apoptosis and active secretion harbour different acetylation and redox post-translational modifications that shape the course of the inflammatory response and microenvironment. Further, HMGB1 redox state is reversible, and a shift in the redox status of the inflammatory microenvironment acts as a point of feedback control for extracellular HMGB1 activity. For example, damage incurred by infection leading to

necrosis, induces release of fully reduced HMGB1.[142] With chemotactic activity, fully reduced HMGB1 promotes leukocyte recruitment to the localised site of damage. Activation of cells of the innate immune system by pro-inflammatory and pathogenic factors results in the acetylation of HMGB1 NLS and active secretion. Dynamic changes in the microenvironment redox state in response to infection and cytotoxic inflammatory responses leads to the accumulation of acetylated or disulphide-bond HMGB1 with cytokine activity.[141] Finally, fully oxidised extracellular HMGB1 accumulates due to ROS-dependent cytotoxic responses to eliminate pathogens, and/or induction of apoptosis;[141] oxidised and inactive HMGB1 regulates and limits further cytokine/chemokine HMGB1 activity.[142]

1.3.3 HMGB1 receptors

Identified receptors for HMGB1 include several pattern-recognition receptors, such as RAGE and TLR2, 4 and 9, TIM3 and CXCR4.[123,143] HMGB1 biology is complex; receptor usage is cell and tissue-type specific, and largely dependent on the HMGB1 redox status. Moreover, ligand synergism adds another level of complexity.[144,145]

HMGB1 primarily signals via TLRs in myeloid cells. The HMGB1-TLR signalling axis is involved in the differentiation and maturation of dendritic cells, monocytes and macrophages.[146] TLRs are a structurally conserved set of proteins that recognise PAMPs and endogenous stress signals, including HMGB1. TLR2 and 4 are located on the surface of innate immune cells, while TLR9 is located in endosomal and lysosomal compartments to sense internalised CpG DNA. Following receptor activation with disulphide-cytokine HMGB1, TRIF and/or MyD88 are recruited to the Toll/IL-IR (TIR) intracellular domain, initiating a signalling cascade. Activation of IRAK1,2,4, TRAF6, IKKα or IKKβ leads to NF-κB, IRF3 and IRF7 transcription factor activation and upregulation of the interferon (IFN) response and pro-inflammatory cytokines. This drives DC maturation and the activation of macrophages. RAGE predominates HMGB1-mediated somatic cell activation and is expressed by cells of myeloid and lymphoid lineage, endothelial cells and strongly expressed by lung epithelial cells.[146] As an endogenous stress signal receptor, RAGE recognises a variety of DAMP ligands, but the exact RAGE signalling pathway is not fully deciphered. HMGB1-RAGE mediated cell activation is dependent on cell type and ligand synergism, but frequently results in the activation of MAPK, RAS pathways and NF-κB.[147] As such, NF-κB binding-motifs are located in the promoter region of RAGE gene sequence, establishing a positive inflammatory feedback loop.

HMGB1 can function synergistically with other cytokines, enhancing the immunogenicity of many ligands.[148] The combination of functionally distinct HMGB1 isoforms and ligand synergism means HMGB1 targets various arms of immunological responses, and can be considered as a

central cytokine for myeloid and lymphoid cells.[131] For example, fully reduced-chemotactic HMGB1 binds to CXCL12 dimers, facilitating inflammatory cell recruitment by acting through CXCR4.[122] Bound to LPS, HMGB1 enhances TLR4 activation, encouraging anti-microbial responses.[131] Moreover, as a DNA binding protein, HMGB1 bound to extracellular CpG DNA and circulating immune complexes are responsible for the activation of TLR9 and BCR in B-cells, respectively.[149] Therefore, HMGB1 can amplify inflammation and the pathophysiology of ligands in inflammatory/immunogenic disease.

Finally, to successfully fulfil its role as a DAMP, HMGB1 must not initiate signalling cascades under homeostatic conditions. Ubiquitous HMGB1 shuttles between the nuclei and cytoplasm of every cell, regulated by methylation of lysine at position 42.[127] Acetylation of HMGB1 (mediated by the JAK/STAT1 pathway) is required to block nuclear re-entry, and stimulate active release in DCs, monocytes and macrophages.[147] To prevent stimulation of stress responses by inside out signalling, HMGB1 is actively released in secretory lysosomes via the non-classical pathway.[138] Moreover, receptors (TLR2/4/9, RAGE, CXCR4, TIM3) are either located on the cell surface, or compartmentalised in endosomes.[147] This ensures extracellular HMGB1, released through cell death and stress-induced secretion has access to HMGB1 receptors.

1.3.4 Dual roles of HMGB1 in cancer

As outlined earlier, many inflammatory inducers and mediators demonstrate both pro- and anti-tumour functions, including HMGB1 (Figure 1-7). In this respect, HMGB1 is considered a double-edged sword that contributes to smouldering chronic tumour-associated inflammation, and immunogenic malignant-cell death. As an alert signal for inflammatory sensors, HMGB1 initiates immune responses by acting primarily on several cells including antigen-presenting cells, lymphoid cells, endothelial and epithelial cells.

On the one hand, HMGB1 has anti-tumour activity by recruiting and activating dendritic cells - professional antigen presenting cells that augment malignant cell death via T_H1 and CD8+ CTL responses. Moreover, HMGB1 functions as a tumour suppressor in breast cancer by interacting with retinoblastoma (RB), repressing transcription and inducing apoptosis. [150]. HMGB1 plays a demonstrated role in immunogenic cell death following anticancer therapy.[151] Therapy-mediated destruction of tumour cells releases HMGB1 and tumour-antigens, which stimulate anti-tumour immune activity through the uptake and action of antigen presenting cells. As such, increased serum levels of HMGB1 have been reported *in vitro* following 4 and 24 hours chemotherapeutic treatment of glioma, melanoma and lung cancer cells, particularly with alkylating agents.[152-154]

In pro-tumour inflammation, HMGB1 can activate the surrounding stroma and endothelial cells through cell-surface receptor engagement, facilitating to the extravasation and increased infiltration of inflammatory cells.[155] As a potent activator of monocytes, disulphide-cytokine HMGB1 stimulates the differentiation of M2-macrophages and tumour-associated macrophage subsets (TAMs), including NLCs in CLL.[76] The action of M2 macrophage subsets further promote a T_H2 and T_H17 non-cytotoxic response, contributing to smouldering wound-healing inflammation. HMGB1 can also inhibit anti-tumour immunity by inducing the differentiation of myeloid derived suppressor cells – these cells block CD8+ CTL responses and promote the accumulation of T_{REGS}.[156]

Finally, HMGB1 can signal in a paracrine and autocrine fashion, establishing a positive feedback loop.[116] Passively released by stressed/damaged or dying tumour cells, the consequent activation of immune-cell subsets initiates active HMGB1 secretion. Within the same tumour, the 3 functional isoforms of HMGB1 may coexist, fully reduced (chemokine), disulphide or acetylated HMGB1 (cytokine), and fully oxidised (inactive), resulting in the infiltration of further inflammatory cells and broad-scale inflammatory activation. Thus, HMGB1 likely contributes to both pro- and anti-tumour responses within the same malignant spatial vicinity. However, the overall molecular and cellular components of the tumour microenvironment will largely decide the polarisation of the HMGB1 response; where HMGB1 will have an additive effect on chronic smouldering or anti-tumour inflammation.

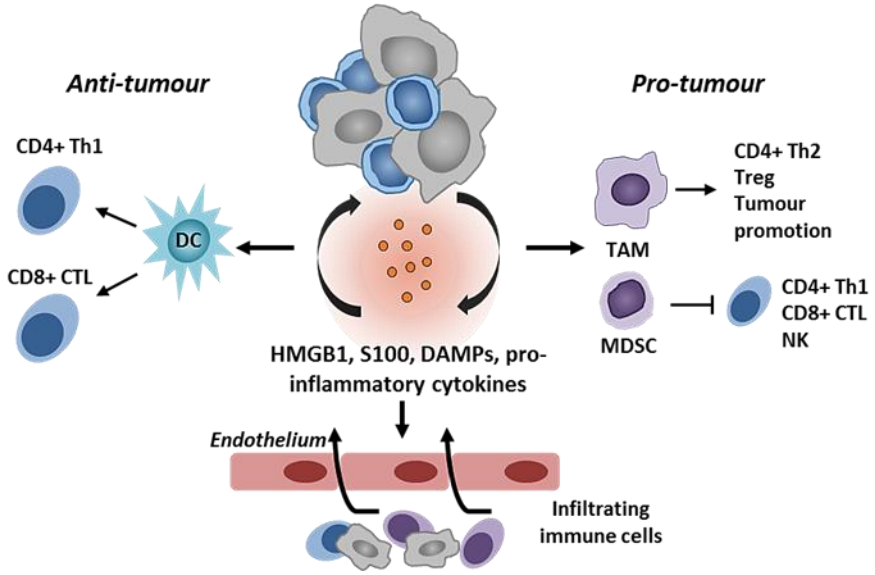

Figure 1-7 Anti- and pro-tumour roles of HMGB1
HMGB1 can increase immunogenic cell death by activating dendritic cells and Th1-mediated killing. HMGB1 also increases cellular extravasation into the tumour microenvironment and support tumour promotion by activating a T_H2 and M2 macrophage response. Finally, HMGB1 can signal in an autocrine fashion leading to an inflammatory positive feedback loop.

1.3.5 HMGB1 and disease

Extracellular HMGB1 is implicated in a growing body of malignant and non-malignant diseases (Table 3). In most cases, higher plasma HMGB1 levels are associated with poor disease outcome.[128] An increased understanding of the role of HMGB1 in disease pathogenesis is demonstrating the current clinical relevance of this signalling axis.

Table 3 Increased plasma HMGB1 levels in various diseases [76,120,157-162]

Diseases	HMGB1 concentration (median)	Reference
Normal	0-10 ng/ml	
Sepsis	Non-survival 84 ng/ml Survival 25 ng/ml	Wang 1999
Mechanical trauma	526 ng/ml 2-6 hours post injury	Peltz 2009
Systemic Lupus Erythematosus	27 ng/ml 0 ng/ml	Ma 2012/ Li 2010
Ovarian cancer	Patient 78 ng/ml Healthy Control 26 ng/ml	Li 2014
Lung cancer	Patient 76 ng/ml Healthy Control 7.7 ng/ml Large tumour>small tumour	Shang 2009
Hepatocellar carcinoma	Patient 84 ng/ml Healthy Control 7.0 ng/ml	Cheng 2008
CLL	Untreated 59 ng/ml Relapsed 168 ng/ml Remission 38 ng/ml Healthy Control 10 ng/ml	Jia 2014

i. Non-malignant disease:

Owing to the immunomodulatory functions of HMGB1, it is involved in autoimmune and acute inflammatory disease pathogenesis. Elevated HMGB1 serum levels are reported in patients with systemic lupus erythematosus (SLE) and rheumatoid arthritis, associated with increased immunogenicity of nucleosome complexes in SLE and release of TNF-α in rheumatoid arthritis.[145,163] Acting as a DAMP, higher levels of serum HMGB1 are implicated and associated with worse prognosis in severe sepsis,[120] and increased expression has been demonstrated following burn trauma and haemorrhagic shock.[164]

ii. Cancer:

Each of the 10 hallmarks of cancer are associated with alterations in HMGB1 function, expression and localisation.[116,151] For example, extracellular HMGB1 is involved in proliferative

signalling, tumour-associated inflammation and immune evasion, explained earlier. HMGB1 is a key regulator of autophagy, and prevents induction of apoptosis – therefore resisting malignant cell death. Moreover, nuclear HMGB1 is involved in the maintenance of chromatin stability, contributing to replicative immortality.[119,165] A nuclear interaction between HMGB1 and Rb is required to exert the tumour-suppressing transcriptional repressor activity of Rb in breast cancer.[150] Finally, the HMGB1-RAGE signalling axis in endothelial cells results in the upregulation of integrins and VEGF, contributing to angiogenesis.[166,167] As such, overexpression and increased serum levels of HMGB1 is associated with worse survival for a variety of cancers – colon, ovarian, prostate, breast, cervical, gastric, lung and liver.[116] Although the clinical relevance of HMGB1 serum levels have been determined, the functional mechanism associated with poor prognosis has not been fully studied.

iii. CLL

Our group have recently reported for the first time that HMGB1 is present at a higher concentration in the plasma of CLL patients and is associated with poor clinical outcome (Table 3).[76] We previously found that extracellular HMGB1, from passive HMGB1 release (indicative of high levels of extracellular DNA), induces differentiation of NLCs via RAGE and TLR9 receptors, which in turn promote proliferation and survival of CLL B-cells.[76] Whether extracellular HMGB1 could directly stimulate CLL B-cells and which receptor(s) binds and elicits the activation of signalling pathways are currently unknown.

1.3.6 Anti-HMGB1 therapeutic agents

Anti-HMGB1 agents have been promising at ameliorating the inflammatory-modulating effects of HMGB1 in experimental models of sepsis, arthritis, and murine models of cancer (glioma and lung). [130,163,168] Current antagonistic therapeutic agents include anti-HMGB1 antibodies, HMGB1 recombinant A-box, soluble RAGE decoy receptor and ethyl pyruvate (EP).[126] Anti-HMGB1 antibodies neutralise extracellular HMGB1 to ameliorate its cytokine and chemokine ability without affecting the nuclear function of the protein. Treatment with anti-HMGB1 antibodies improved survival in mouse models of haemorrhagic shock and can suppress inflammation *in vitro* from studies on autoimmune conditions.[130,169,170] Recombinant HMGB1 A-box (1 DNA-binding domain) competes with HMGB1 for binding sites on HMGB1 receptors, and preclinical studies have demonstrated anti-inflammatory potential.[130,170] EP is a potent inhibitor of HMGB1 active release, by preventing HMGB1 phosphorylation through calcium chelation[171] and preventing HMGB1 acetylation.[172] It exerts successful anti-tumour effects in experimental mouse models of lung and gastric cancer.[173,174] Moreover, EP was studied in a phase II clinical trial for the anti-inflammatory effect of EP for high-risk patients undergoing cardiac surgery.

Although not effective in this disease setting, the drug was safe and non-toxic in humans.[175] Overall, it's important to consider that completely blocking HMGB1 activity using these anti-HMGB1 agents may also target beneficial responses, particularly following anti-cancer therapy.

1.4 Receptor for Advanced Glycation End Products (RAGE or AGER)

Among all HMGB1 receptors, RAGE is the only receptor demonstrating a link with HMGB1 in cancer.[176]

RAGE is a multi-ligand transmembrane protein of the immunoglobulin superfamily expressed on the cell surface of all leukocytes, endothelial and epithelial cells.[177,178] It was the first HMGB1 receptor identified in neurites, and later confirmed in other cell types.[179-181] To fulfil the role as a PRR, a wide range of endogenous stress signals, including HMGB1, S100 proteins and AGEs, are detected by RAGE. Due to expression on all leukocytes, RAGE links innate and adaptive immune responses. Perpetuation of RAGE signalling establishes inflammatory loops and is implicated in several chronic inflammatory disorders.[182-185]

1.4.1 RAGE protein structure

RAGE gene sequence is located on chromosome 6 within the MHC class III region, composed of 11 exons. At the protein level, RAGE is a 404 amino acid type I transmembrane protein and is composed of an extracellular domain, a single transmembrane helix and a short intracellular cytoplasmic tail (Figure 1-8).[186] The extracellular domain is composed of 3 Ig-like molecules, 1 V-type and 2 C-type as structural subunits. The V- and C1- domains both carry a positive surface charge and primarily mediate ligand interactions, while the C2 domain carries a negative charge;[187] HMGB1 interacts with the V-type subunit. RAGE ligands are structurally diverse, but share a common negative surface charge. A strong electrostatic ligand-RAGE interaction initiates receptor activation and sustained ligand-RAGE signalling.[187] The 42 amino acid RAGE cytoplasmic tail is unstructured and lacks enzymatic activity or known signalling motifs. Despite this, the cytoplasmic tail is still essential for cell signalling capability.[188]

1.4.1.1 Ligand binding

Ligand binding is regulated by post-translational modifications and receptor complex pre-assembly. RAGE undergoes N-glycosylation at Asn25 and Asn81, regulating ligand binding and subsequent signalling.[189] Unlike many type I transmembrane proteins, RAGE pre-assembles in the plasma membrane of at least 4 RAGE molecules prior to ligand engagement.[190] This process is favoured by a higher surface concentration of RAGE, and ligand engagement induces cytoplasmic domain conformational changes, initiating various signalling cascades.

1.4.1.2 Splice variants

RAGE undergoes extensive alternative splicing, producing 20 different RAGE isoforms. 12 are fully translated to protein level characterized by N- or C-terminus truncations (hRAGEsec, sRAGE1, sRAGE2, sRAGE3, N-truncated and secretory, Δ8-RAGE, RAGEΔ, NtRAGEΔ, sRAGEΔ,

RAGE_v4 and RAGE_v13), while the other splice variants are targeted to the nonsense-mediated mRNA degradation pathway.[191,192] Signalling competent full-length membrane bound RAGE (FL-RAGE) is the main isoform expressed.[186] Other splice variants of RAGE are not signalling-competent, but one isoform in particular abrogates membrane-RAGE signalling. Endogenous secreted RAGE (esRAGE; sRAGE1) is the predominant splice variant with notable expression in humans, and lacks transmembrane and cytoplasmic domains.[193] All other splice variants are expressed at very low protein levels.[191]

1.4.2 RAGE signalling pathway

Defining RAGE signalling is complex. The receptor engages numerous ligands, with 3 extracellular subunits capable of ligand binding, and is expressed in many cell types with different intracellular pathways. Moreover, HMGB1-ligand synergism offers RAGE-independent signalling pathways for cell activation.

In response to HMGB1 engagement via the RAGE V-domain, conformational changes in the pre-assembled RAGE multimer complex induce conformational changes in the cytoplasmic domain, or induces receptor-ligand internalisation.[145,194] RAGE lacks established intracellular signalling motifs or enzyme activity, but is hypothesised to act as an adaptor protein.[195] Conformational changes in the cytoplasmic domain facilitates activation of downstream signalling (i.e. MAPK and PI3K pathways), but the precise intracellular binding partners or signalling mediators linking RAGE to well-known signalling pathways are unknown. The main role of receptor internalisation is to dampen HMGB1-mediated signalling activation by reducing ligand-activated RAGE on the cell surface, but receptor endocytosis presents another pathway linking extracellular ligands to intracellular receptors – i.e. HMGB1 with endosomal TLR9.[128]

Evidence for the activation of signalling cascades in a variety of cell types include the MAPK pathway (via ERK1/2, p38 activation), PI3K and AKT, the JAK-STAT pathway, and activation of MyD88 via TLR9 (HMGB1 binds to TLR2 and TLR4 directly).[145,196,197] Activation of RAGE in endothelial cells leads to the activation of PI3K and MAPK signalling.[186] Downstream activation of NF-κB induces upregulation of the inflammatory transcriptome, including expression of leukocyte adhesion molecular VCAM-1 and ICAM-1.[198] RAGE signalling recruits mDia1 to the cytoplasmic domain and the activation of Src, Rac and the PI3K pathway in smooth muscle cells, while the full signalling pathway in monocytes, dendritic cells and lymphocytes is only partially resolved.[186] RAGE activation is reported to activate MAPK signalling via ERK1/2 in immune cells, resulting in the activation of NF-κB. Pro-inflammatory RAGE signalling induces production and release of TNF-α, IL-1β, CCL3, CCL5 and CXCL12 from macrophages,[199] and TNF-α, IL-6 and CXCR4 from dendritic cells;[200] although the exact cytokine/chemokine profile is dependent on the

overall inflammatory microenvironment polarisation. In B-cells, RAGE augments the proliferation of AM14 B-cells response by delivery of CpG-ODN ligand to intracellular TLR9 (ligand-synergism).[145,149] Well established transcription factor activation downstream of RAGE signalling include NF-κB and SP-1, highlighting an important role in inflammation.[178] These pathways are key mediators of the stress response, cell activation, migration and proliferation.

1.4.2.1 Regulation of RAGE signalling

Regulation of RAGE signalling is a vital step in preventing chronic inflammatory dysregulation, owing to the role of RAGE as a linker between innate and adaptive inflammatory responses. The first level of regulation is implicated at the transcription level. The promoter region of RAGE contains 2 binding sites for NF-κB inflammatory transcription factor, propagating pro-inflammatory signalling.[201,202] Although the regulation and functionality of RAGE alternative splicing is less well understood, FL-RAGE and es-RAGE are the only RAGE isoforms with notable protein expression. Extracellular sRAGE functions as a decoy receptor, dampening RAGE signalling, but also originates from membrane receptor proteolytic cleavage.

Post-translational levels of receptor regulation include i. glycosylation (at Asn25 and Asn81);[189] ii. surface RAGE pre-assembly; iii. ligand-induced receptor internalisation and exocytosis (receptor shuttling); iv. RAGE shedding. RAGE pre-assembles into multimers, independent of ligand availability/ligand levels.[190] This regulates the amount of signalling-competent RAGE at the cell surface, regardless of FL-RAGE surface concentration. However, multimer formation is disrupted by the inclusion of spliced RAGE isoforms, producing non-functional receptor hetero-multimers that are signalling incompetent.[186] Upon receptor activation, the strength of RAGE signalling is controlled by RAGE endocytosis and exocytosis. RAGE receptor can be internalised via lipid rafts into vesicular structures, cutting off downstream signalling - a negative feedback mechanism utilised by various cell-surface receptors.[203] This is observed *in vitro* following S100B stimulation.[204] Conversely, receptor exocytosis following ligand-induced activation increases RAGE cell-surface receptor availability. Fusion of RAGE-containing vesicles with the plasma membrane, observed a few minutes after pro-inflammatory stimulation, perpetuates rapid inflammatory responses.[205] Finally, ligand-induced receptor shedding also switches off RAGE-signalling, and sequesters circulating extracellular RAGE ligands. ADAM10-mediated RAGE ectodomain proteolysis is regulated by Ca^{2+} signalling, protein kinase C (PKC), G-protein coupled receptors following receptor activation.[206,207]

1.4.3 Soluble RAGE

sRAGE functions as an antagonistic decoy receptor of plasma HMGB1, limiting chronic inflammation. The pool of plasma sRAGE originates from 2 main sources - alternative splicing to

produce esRAGE, or surface FL-RAGE ectodomain proteolytic cleavage. Both extracellular sRAGE isoforms are structurally similar, formed of the 3 extracellular domains (V, C1 and C2) with full RAGE ligand-binding capacity (Figure 1-8).[208] In a healthy setting, HMGB1 and sRAGE plasma levels are inversely associated; healthy individuals with high plasma sRAGE levels exhibit low extracellular HMGB1 levels in a given population.[209] Although this inverse relationship ensures inflammatory responses are regulated in healthy individuals, the concentration of plasma sRAGE does not exceed extracellular HMGB1 concentrations (mean± standard deviation for 640 healthy individuals: plasma HMGB1 1.65± 0.04ng/ml; sRAGE 0.45± 0.01ng/ml).[209] In chronic disease, the HMGB1-sRAGE inverse relationship is frequently reversed,[128] and the underlying mechanisms responsible for this observation is currently an active area of inflammatory research.

1.4.3.1 Alternatively spliced endogenous secreted RAGE

Alternatively spliced esRAGE (or sRAGE variant 1) is characterised by inclusion of the 5' end of intron 9 and exclusion of exons 10 and 11 (the transmembrane domain encoding sequence). This results in a sequence frame shift and a premature UGA stop codon in intron 9.[210] Expression of the esRAGE splice variant produces a 347-amino acid protein, with a distinct 16-amino acid C-terminal tail (encoded by part of intron 9) and lacks the transmembrane domain.[211] esRAGE packaged into endosomes fuses with the plasma membrane where the receptor is secreted into the extracellular environment.[191]

Regulation of RAGE splicing is still not fully understood. *In vitro* studies and *in vivo* mouse models revealed tissue-specific RAGE splice variant expression patterns, although the gene expression levels are not reflected at the protein level.[212] Therefore, RAGE alternative splicing must be regulated by upstream unknown extracellular triggers and signalling pathways that are tissue-specific.

1.4.3.2 RAGE ectodomain shedding

Alternatively spliced esRAGE constitutes ~20% of extracellular sRAGE.[213] Proteolytic cleavage of membrane-bound FL-RAGE, releasing the extracellular domain, makes up the remainder of the pool of sRAGE. The stability of FL-RAGE at the cell surface is controlled by metalloproteinase, ADAM10.[214,215] Cleavage of the extracellular domain (V, C1 and C2 subunits) catalysed by ADAM10, occurs following ligand-induced cell activation. This firstly disconnects surface-RAGE with the cytoplasmic RAGE domain and downstream signalling pathways; secondly, the free sRAGE fragment sequesters extracellular RAGE ligands, dampening inflammatory positive feedback loops.[214,215]

ADAM10

ADAM10 (a disintegrin and metalloproteinase) is a member of the zinc metalloprotease family located at the plasma membrane and was originally identified as an α-secretase for myelin basic protein.[216] Formed of multiple domains, ADAM10 undergoes various steps of post-translational processing and cleavage to produce a fully functional α-secretase.[217] The catalytic domain of ADAM10 contains a zinc-binding and various glycosylation motifs, and is responsible for cleaving an estimated 40 proteins.[218] The majority of ADAM10 substrates are type I transmembrane proteins (such as RAGE), some are type II transmembrane proteins (i.e. Fas ligand) and few ligands are glycosylphosphatidylinositol anchored proteins. ADAM10 cleaves RAGE ~12 amino acids upstream of the transmembrane domain. RAGE cleavage is inducible in a dose-dependent manner following 1-hour treatment *in vitro* with RAGE ligand, S100B, in comparison to positive controls (ADAM10 activators) ionomycin and PMA.[219] Mechanisms to regulate ADAM10 activity and substrate cleavage include ADAM10 maturation by proteolytic processing, GPCR-mediated signalling, signalling via Ca^{2+}, PKC, and PI3K in response to ligand binding.[206,207,220] Moreover, increased levels of receptor shedding and sRAGE may also be attributed to increased expression or activity of ADAM10. I.e. ADAM10 is one of the α-secretases responsible for NOTCH1 cleavage in CLL B-cells.[221] Therefore patients with NOTCH1 mutations may produce higher levels sRAGE as a by-product, but this has not yet been studied.

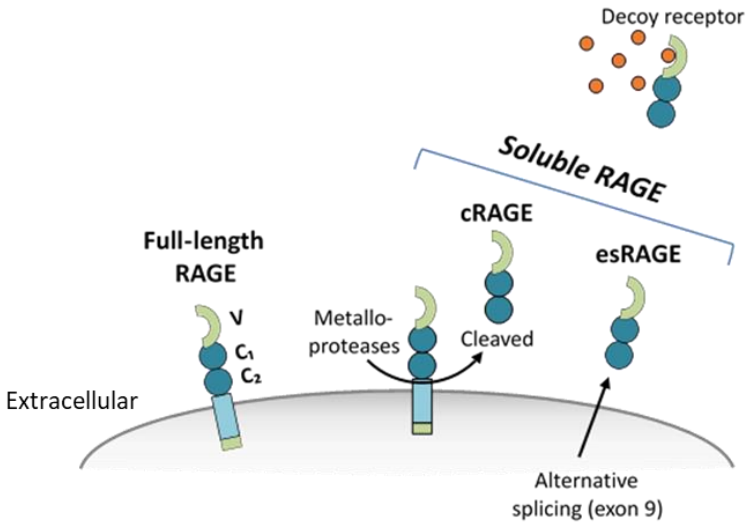

Figure 1-8 RAGE alternative splicing and receptor shedding
Full-length membrane bound RAGE is the predominant isoform. Soluble RAGE can act as a decoy receptor, sequestering ligands in the extracellular space and dampening membrane-RAGE activation. Origins of soluble RAGE include alternative splicing (endogenous secreted RAGE – esRAGE) and cell-surface proteolytic cleavage (cleaved – cRAGE).

1.4.4 RAGE and disease

Both FL-RAGE and sRAGE are implicated in the pathogenesis of a variety of chronic inflammatory conditions including acute inflammation, infectious and malignant diseases.

i. Autoimmunity:

Acting as a receptor for HMGB1, FL-RAGE is involved in non-malignant inflammatory conditions such as systemic lupus erythematosus (SLE), diabetes, Alzheimer's, multiple sclerosis and hepatic disorders.[182,185,222] HMGB1-RAGE signalling in endothelial cells mediates SLE vasculitis, while RAGE and mDia1 intracellular interactions are involved in the pathogenesis of macrovascular complications in diabetic hyperglycaemia.[223]

On the other hand, extracellular sRAGE has clinical significance as an antagonist and regulator of RAGE signalling. Decreased sRAGE plasma levels were observed in SLE, rheumatoid arthritis and Kawasaki disease, failing to act as a decoy receptor and regulate inflammatory activation.[128] Whereas elevated extracellular sRAGE levels were reported following severe trauma, acute renal failure and systemic inflammatory response syndrome, due to release of RAGE DAMP ligands during stress.[128]

ii. Cancer:

Activation and elevated expression of FL-RAGE has been demonstrated in a variety of cancers.[123,224] *In vitro* and *in vivo* studies support a direct role for RAGE in the migration and invasion of tumour cells, owing to RAGE-mediated activation of tumour-associated cells and demonstrated roles in chemotaxis.[225] RAGE expression in macrophages is necessary for angiogenesis in glioma,[226] while RAGE blockade *in vivo* decreased tumour growth and metastasis in mice implanted with Lewis lung carcinoma cells.[168] Moreover, the HMGB1-RAGE axis plays a key role in regulating mitochondrial bioenergetics in pancreatic cancer cells.[227]

Serum levels of sRAGE are easily attainable and powerful circulating disease biomarkers.[228,229] A meta-analysis assessing circulating extracellular sRAGE levels with cancer risks (breast, lung, pancreas, liver, colorectal), demonstrated the protective role of increased serum sRAGE levels in cancer development.[230,231] However, in other studies decreased serum sRAGE levels were detected in breast and pancreas cancer compared to healthy controls - but this response is parallel to disease progression.[232,233]. Overexpression of spliced esRAGE in C6 glioma cells suppressed JNK signalling, inhibiting tumorigenesis; tumour burden was significantly decreased in immunodeficient severe combined immunodeficient (SCID) mice transfected with the esRAGE-overexpressed C6 glioma cells compared to mock transfected mice.[234] Whether this response was specifically due to extracellular esRAGE decoy receptor ability, or disruption of surface RAGE pre-assembly was not fully investigated.

iii. CLL:

Despite our current understanding of RAGE/sRAGE in solid cancer, plasma levels of sRAGE and RAGE expression in CLL B-cells, function, and association with CLL disease progression is not known. So far, previous work in our laboratory demonstrated a functional role for RAGE in the differentiation of NLCs, important for the maintenance and proliferation of CLL cells.[76]

1.4.4.1 Anti-RAGE therapeutic agents

RAGE signalling can be blocked by various antagonists to inhibit RAGE-mediated disease pathogenesis. Using a ligand-based drug design approach, small molecule inhibitors of RAGE directly bind to the RAGE V-domain, blocking RAGE-Aβ interactions and Alzheimer's disease progression.[235-237] Azeliragon (TTP488) is currently under investigation in a multicentre phase III clinical trial to evaluate the safety and efficacy of Azeliragon in patients with mild Alzheimer's disease (STEADFAST study; NCT02080364). Other therapeutic options include blocking membrane-RAGE with a monoclonal antibody. This ameliorated sepsis and tumour progression in animal models.[168,238] Finally, induction of FL-RAGE proteolytic cleavage could provide an intrinsic alternative mechanism to ameliorate RAGE-inflammatory responses.[239,240] RAGE shedding can be induced *In vitro* with the use of calcium ionophores, ionomycin and phorbol 12-myristate 13-acetate (PMA), to raise intracellular Ca^{2+} levels and activate PKC-dependent RAGE cleavage. However, these agents are not suitable for *in vivo* use. Physiological strategies include reducing cholesterol content using statins to increase RAGE shedding.[241] It is important to note though, that statins interfere with rituximab efficacy for the treatment of CLL by inducing conformational changes in CD20.[242]

1.5 Toll-like Receptor 9 (TLR9)

TLR9 is an intracellular receptor for HMGB1 located in endosomal membranes.[243] Classified as a PRR, TLR9 has important roles in host defence, innate and adaptive immunity.[244] The classical bacterial ligand for TLR9, unmethylated CpG (cytosine followed by guanine nucleotide), was identified in TLR9 deficient mice.[245] Compared to bacterial genomes, CpG occurrence is rare and highly methylated in mammalian genomes.

1.5.1 TLR9 protein structure

All identified 11 TLRs are type 1 membrane glycoproteins, with up to 25 leucine rich repeat motifs in the extracellular domain. These motifs form a β-strand and an α-helix giving an overall horseshoe structure.[246] Even though the leucine-rich repeat extracellular domain is highly conserved, each TLR recognises different PAMPs.[5] The gene sequence for TLR9 is located on chromosome 3 (3p21.2). The transcribed TLR9 protein is located in endosomal compartments, suited for recognition of nucleic acids following scavenging phagocytosis.[247] Unmethylated single strand CpG-DNA binds to TLR9 with high affinity compared to methylated or double-strand CpG-DNA.[248] Although the molecular basis of CpG-DNA-TLR9 agonistic binding has not been elucidated, recent structural studies demonstrate a symmetric CpG-DNA-TLR9 dimer complex is formed.[249] Three types of CpG ligand have been identified based on the different elicited responses in plasmacytoid dendritic cells – CpG-A, CpG-B (mainly responsible for B-cell activation) and CpG-C.[250] The intracellular domain of TLR9 shares homology with interleukin receptor (Toll/IL-1 receptor domains (TIR)). Composed of three conserved boxes, boxes 1 and 2 are structurally positioned to reveal their side chains to mediate interactions with adaptor molecules.[251] Important intracellular mediators of TLR9 activation include myeloid differentiation primary response protein (MyD88), IL-1R associated kinases (IRAKs) and tumour-necrosis-factor-receptor associated factor 6 (TRAF6).[252]

1.5.2 TLR9 signalling pathway

TLR signalling pathways are well defined and facilitate rapid host immune responses to harmful pathogens. Following CpG ligand engagement, TLR9 undergoes dimerisation inducing conformational changes in the cytoplasmic TIR domains (Figure 1-9).[246] This poises the receptor for adaptor interactions, particularly with MyD88.[246] Originally identified following IL-6 induction in macrophages, MyD88 also contains TIR and death domains that are essential for coupling receptor-downstream signalling mediators.[253] The C-terminus of MyD88 homodimers are recruited to the cytoplasmic TIR domain of TLR9, and associate with serine/threonine kinase, IRAK4, via death domain-death domain interactions. Once this triad is formed a kinase cascade

is initiated.[253] Activation of IRAK4 phosphorylates IRAK1; IRAK1 auto-phosphorylates, recruiting TRAF6 to the receptor complex; TRAF6 mediates activation of the inhibitor of NF-κB (IκB) kinase complex (IKK). Inactive NF-κB subunits (p65, Rel-B, Rel-C, p50 and p52) are sequestered in the cytoplasm by IκB, blocking transcription factor activation.[244] Activation of IKK complex phosphorylates IκB, targeting the inhibitors for polyubiquitination and proteasomal-degradation. Free NF-κB subunits translocate to the nucleus, inducing expression of pro-inflammatory cytokines such as type-I IFNs.[254]

1.5.2.1 Regulation of TLR9 signalling

Regulation of TLR signalling is essential to avoid over production of excess inflammatory cytokines. TLR9 and CpG-ODN responses are negatively regulated by IRAK-M, SOCS1 and Triad3A. IRAK-M expression is induced in macrophages and monocytes following TLR activation. IRAK-M lacks enzyme activity and prevents formation of IRAK-1-TRAF6 complex and downstream signalling.[255] The precise mechanism by which SOCS1 downregulates TLR signalling is not clear, but CpG-ODN stimulation in macrophages induced expression of SOCS1.[256] Finally, polyubiquitination of TLR9 by E3 ubiquitin ligase, Triad3A, targets TLR9 for proteolytic degradation.[257] The combination of pro-inflammatory phosphorylation cascades and negative regulators limit excess innate inflammatory responses and harm to the host.

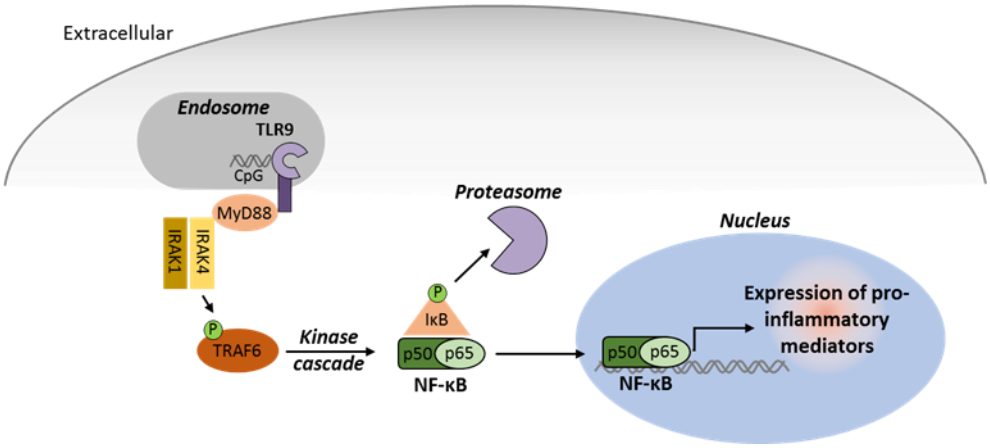

Figure 1-9 TLR9 signalling
CpG-TLR9 engagement in the endosome initiates interactions with MyD88, IRAK4, and IRAK1. Activation of a kinase cascade results in the activation of TRAF6, IKK and degradation of IκB. NF-κB subunits translocate to the nucleus following IκB release and upregulate expression of pro-inflammatory cytokines.

1.5.3 TLR9 and disease

TLR9 contributes to the pathogenesis of inflammatory and immune diseases due to the intrinsic ability to recognise host-derived ligands that become available during disease progression (i.e host CpG-DNA and immune complexes).

i. Autoimmunity:

Firstly, TLR9 plays a big role in autoimmunity, particularly in SLE and rheumatoid arthritis. SLE pathogenesis is mediated by autoantibodies to self-DNA. SLE B-cells are activated by chromatin immune-complexes by dual engagement of the BCR, internalisation of this receptor complex and interaction with intracellular TLR9.[144,258-260] Host CpG motifs are contained in the auto-reactive IgG complexes. Moreover, dual engagement BCR and intracellular TLR9 is observed in rheumatoid arthritis.[261] IG2a-chromatin complexes stimulate TLR9 and production of rheumatoid factor.

ii. Cancer:

TLR9 has opposing functions in cancer. Receptor expression is linked to tumour invasion and angiogenesis in squamous carcinoma, lung cancer and bladder cancer, but TLR9 agonists are clinically promising as anti-tumour adjuvants for melanoma, renal cell carcinoma and glioblastoma.[262-267]

iii. CLL:

TLR9 activation is more complex in CLL. Originally, CpG-oligonucleotides (ODNs) were viewed as potential therapeutic agents for the treatment of CLL.[268] Consequent studies reported opposing responses to CpG-ODN-TLR9 engagement in CLL B-cells, based on unmutated or mutated IGHV gene status.[269-271] U-CLL TLR9 stimulation drives cell proliferation, whereas induction of apoptosis occurred in M-CLL. The link between TLR9 signalling dichotic responses in CLL cells was identified to be dependent on the expression and activity of ZAP70.[96] TLR9 is sufficient to fully engage BCR-signalling in ZAP70 positive CLL cells, protecting malignant cells from apoptosis.[96] Here, ZAP70 acts as an adaptor between BCR signalling and TLR9. Following TLR9 activation, Src is phosphorylated in both U- and M-CLL cells. Activated Src phosphorylates Syk, dependent on ZAP70 expression, at tyrosine-352 and tyrosine-525/526 (required for full Syk kinase activation). BCR signalling is propagated, resulting in the production and release of auto-reactive IgM, and engagement of surface BCR in an autocrine manner.[96,272,273]

1.5.3.1 TLR9 immunomodulatory agents

TLR9 agonists represent promising anti-cancer therapeutics, due to TLR9-mediated activation of T-cell immunity, antigen presentation, DC maturation, NK cell activation and type-I IFN response.[264] CpG-ODNs have shown promising clinical activity for melanoma, and as an adjuvant therapy for some B-cell lymphomas.[263,274,275] On the other hand, TLR9 antagonists have not been investigated in cancer, but a phase II clinical trial on the efficacy of IMO-8400 demonstrated a reduction in psoriasis severity.[276] As there is a clear distinction in TLR9-mediated CLL B-cell proliferation or induction of apoptosis (dependent on IGHV mutational status and ZAP70 expression), the use of TLR9 agonists or TLR9 antagonists could have potential as immunotherapeutic strategies for the treatment of CLL.

1.6 Crosstalk between HMGB1, RAGE and TLR9

Studies on RAGE and TLR9 expression in solid cancers highlight their separate pro-tumorigenic roles.[277-279] Few studies have assessed the co-linked functions of these receptors.[280] In non-malignant disease, interactions between HMGB1, TLRs and RAGE form an inflammatory triad, activating NF-κB following hyperglycaemia in diabetes.[281] Moreover, HMGB1 is an established CpG-ODN binding partner.[149] In autoreactive SLE B-cells, HMGB1 is an essential component of DNA-containing immune complexes that stimulate RAGE internalisation and TLR9 activation.[145,260] This represents a separate pathway for DNA ligands to undergo internalisation, aside from BCR endocytosis.

Consistent with this, our group previously reported HMGB1-mediated activation of RAGE/TLR9 in NLCs in CLL. HMGB1 binds to RAGE on the cell surface of NLCs, inducing receptor internalisation and colocalization with intracellular TLR9 (Figure 1-10).[76] This results in the activation of STAT3 and NF-κB. HMGB1 signalling induces differentiation of NLCs, which was blocked with anti-HMGB1 neutralising antibodies.[76] It is currently unknown whether HMGB1/RAGE/TLR9 signalling axis can directly promote CLL B-cell survival and contribute to disease progression.

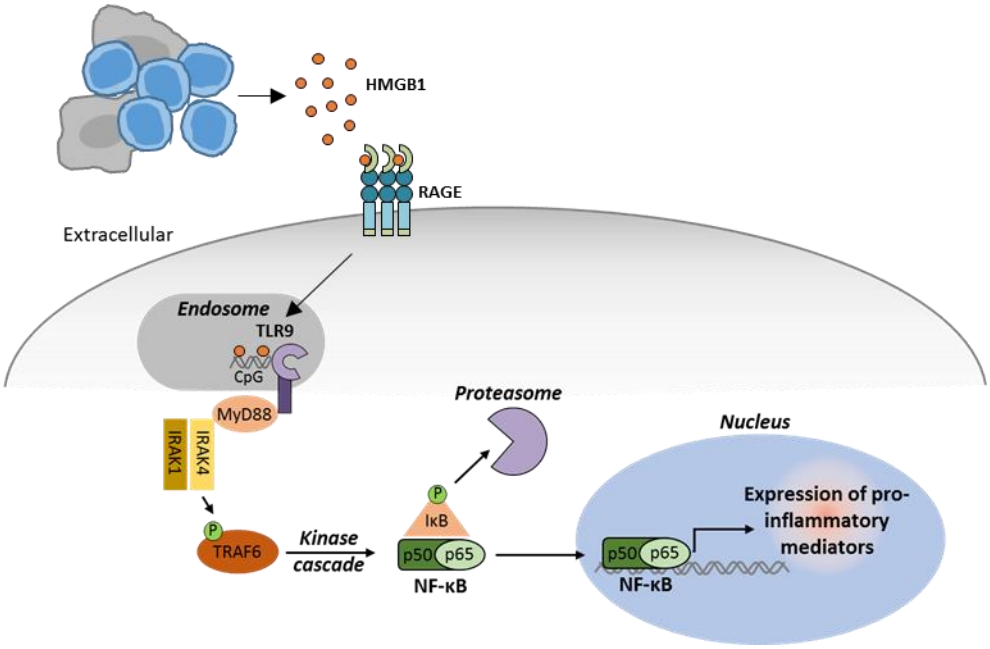

Figure 1-10 RAGE and TLR9 signalling in resposne to HMGB1 engagement in CLL NLCs
Active or passive release of HMGB1 results in the accumulation of HMGB1 in blood plasma. Following HMGB1 engagement at the cell surface, RAGE is internalised and colocalises with TLR9 at the endosome. CpG-HMGB1 delivery to TLR9 results in the activation of with MyD88, IRAK4, and IRAK1. The kinase cascade results in the activation of TRAF6, IKK and degradation of IκB. NF-κB subunits translocate to the nucleus following IκB release and upregulate expression of pro-inflammatory cytokines.

1.7 Aims

While the role of HMGB1 is well established in solid cancer, the involvement of HMGB1 in CLL disease pathogenesis has not been fully elucidated. We hypothesise that increased levels of extracellular HMGB1 in CLL patients, may promote CLL cell survival by activating CLL cells directly via RAGE and/or TLR9, as reported in autoreactive B-cells and CLL NLCs. Therefore, the main aims of this study are:

1.7.1 Assess the prognostic impact of HMGB1 receptors RAGE and TLR9 and their effects on CLL overall survival

We aim to determine the expression of HMGB1 receptors, RAGE and TLR9, in CLL lymph nodes, and if HMGB1 receptor expression could be used as a clinical prognostic marker for CLL. Using IHC and TMA technology we will determine CLL lymph node expression levels of these proteins and compare to clinical data to determine their prognostic significance in CLL.

1.7.2 Determine the clinical relevance of the HMGB1-RAGE signalling axis

Previous work in our laboratory identified increased levels of HMGB1 in CLL patient plasma, but the main receptor for HMGB1, RAGE, is expressed on various cell types and is multiligand. To infer a direct effect on CLL B-cells, the work in this chapter will assess RAGE and TLR9 expression on CLL B-cells and the survival outcome of HMGB1 signalling in primary CLL cells. Moreover, we will compare levels of extracellular HMGB1, S100B and soluble RAGE decoy receptor to assess the clinical likelihood of HMGB1 as the main RAGE ligand in CLL.

1.7.3 Determine HMGB1-mediated cell signalling activation

The full HMGB1 and RAGE cell signalling network in B-cells is unknown. To determine if RAGE and TLR9 function cooperatively in response to HMGB1 engagement, we will use 2 imaging systems to assess HMGB1-mediated colocalization of RAGE and TLR9. Further, we will use an unbiased phosphoproteomic approach to assess whole cell signalling network activation following treatment with RAGE agonist, HMGB1, and TLR9 agonist, CpG-ODN (B-class).

1.7.4 Determine the origin of soluble RAGE in CLL

Soluble RAGE has potential anti-HMGB1 antagonistic activity and is a promising clinical plasma marker for inflammatory disorders. To assess the role of sRAGE in CLL, the work in this chapter will determine the origin of sRAGE in CLL and further assess the activity of ADAM10 as the main RAGE sheddase.

Chapter II

Materials and Methods

2.1 Cell Lines and Cell Culture

Cell lines were used to optimise cell-based treatments and experiments due to their ease of growth, uniform genotype, phenotype and immortality.[282] The human B-CLL cell line, Mec1, was used for *in vitro* studies as a stable prolymphocytoid transformed CLL (CLL-Pro) cell model system with unlimited growth potential.[283] HEK293 cell line was used as a vehicle for the expression of FL-RAGE and es-RAGE pcDNA3 plasmids due to the ease of transfection.[284] Cells were cultured in RPMI-1640 growth complete media with 10% heat inactivated foetal bovine serum (FBS), 2.0mM L-glutamine, 100U/ml Penicillin and 100µg/ml Streptomycin at 37°C in a humidified 5% CO_2 incubator (Appendix I, 1.1). Cell line density was maintained between 0.5-2x10^6 cells/ml using a Luna-II™ Automated Cell Counter (Logos Biosystems; Appendix I, 1.2) and passaged every 2-3 days. Cell stimulations were either performed in complete growth media, serum-starved media (complete growth media with 0.5% FBS), or serum-free media (complete growth media without FBS). Serum-starved and serum-free media were used in cell-signalling experiments to better assess the physiological response to exogenous stimulating agents and limit prior cell-signalling activation from growth factors in FBS.[285]

2.2 Patient Samples

2.2.1 Ethical consideration

Ethical approval for the use of peripheral blood mononuclear cells (PBMC), lymph node (LN) biopsies and plasma from CLL patients and healthy donors was obtained from the East London and the City Health Authority Local Research Ethics Committee. Biological material was obtained and stored with written informed consent from patients and volunteers in accordance with the Human Tissue Act (2004). All human tissue and cells were identified by patient vial ID and hospital number. Clinical information was provided courtesy of the clinical database manager Mrs. Janet Matthews.

2.2.2 Patient sample selection

Primary patient cells and LN biopsies were used *in vitro* as a more biologically and clinically relevant tool than cell line models. 64 CLL patients with a lymphocyte count of greater than 20×10^9/L were enrolled in this study to ensure samples included enough CLL cells for our *in vitro* studies. Selection criteria for CLL patients include cases that were either untreated or had not received treatment or steroids for over 6 months, to limit the interference of treatment with our *in vitro* assays. Fresh blood samples for this work were obtained from patients with consent via the Barts Cancer Institute Tissue Acquisition Officers in lithium-heparin vacutainer blood collection tubes, to avoid calcium chelation by EDTA. Cryopreserved CLL PBMCs were acquired

from the Barts Cancer Institute Tissue Bank upon request. All patient PBMC samples were collected from 2011-2017. LN biopsies were incorporated in tissue microarrays (TMAs) from 42 reactive (RA) LN and 91 CLL patients where quality formalin-fixed paraffin-embedded (FFPE) tissue and clinical follow up data were available.[76] CLL LN sections were sourced from pre-treated, post-treated and relapsed biopsies that were excised at St Bartholomew's Hospital between the years 1990-2011. RA LNs were taken from patients undergoing further testing for LN malignancy, but diagnosed with follicular hyperplasia that was non-malignant. These RA controls represent an activated B-cell non-malignant comparison. 15 healthy volunteers were enrolled for control plasma donation with informed consent. Healthy plasma samples were collected in March 2016 and were not age or sex-matched due to availability of donors.

2.2.3 Isolation of plasma and PBMCs from fresh CLL blood

Fresh plasma and PBMCs were removed from whole blood, received directly from clinic in lithium-heparin vacutainers, to isolate CLL cells for *in vitro* cell culture. First, plasma was separated by centrifugation of whole blood at 1500rpm for 5 minutes, followed by removal of the top plasma layer. Plasma aliquots were stored immediately at -80°C in cryovials. Fresh PBMCs were separated from whole blood by density gradient centrifugation over Lymphoprep (Axis-Shield; Appendix I, 2.0). Whole blood was diluted 1:1 in RPMI 1640 complete medium and 10ml gently layered on top of 3ml Lymphoprep solution. Blood was centrifuged at 2000rpm for 20 minutes with slow acceleration and deceleration settings. The PBMC monolayer was isolated using a Pasteur pipette and resuspended in RPMI complete medium followed by measurement of cell count and viability using a Luna-II™ automated cell counter (Logos Biosystems). Cells were washed with RPMI complete medium to remove remaining Lymphoprep and re-suspended at $5x10^6$ cells/ml. Cells were cultured at 37°C in a humidified 5% CO_2 incubator overnight for no longer than 15 hours before initiating *in vitro* experiments. CLL cells left longer in culture rapidly undergo apoptosis due to removal from supportive microenvironment interactions and soluble growth factors.[47]

2.2.4 CD19+ positive selection and CLL negative selection

The percentage of CLL B-cell purity is highly heterogeneous among CLL patient PBMC samples due to the presence of other myeloid and lymphoid cells in peripheral blood. For downstream studies on CLL B-cells alone, CLL B-cells were enriched from patient PBMCs using MACS CD19 positive selection or B-CLL negative selection kits (Appendix I, 2.0; Miltenyi Biotech).

CD19+ B-cells were isolated by incubating $40x10^6$ CLL PBMCs with magnetic microbeads conjugated to human monoclonal anti-CD19 human antibody. After a 15-minute incubation, to ensure all CD19+ B-cells were bound to microbeads, the CD19+ microbead cell suspension was loaded onto a MACS LS column held in a magnetic MACS separator. The MACS LS column is composed of a matrix of ferromagnetic spheres that amplify the magnetic field, and capture flowing microbeads. CD19+ microbead labelled cells were retained in the column by binding to the magnetic matrix, while unlabelled non B-cells were eluted by washing the column with 4ml ice-cold 0.5% bovine serum albumin (BSA) phosphate-buffered saline (PBS) (Appendix I, 2.1). The wash buffer flows through the LS column by gravity, to prevent disruption of the CD19+ cell-microbead to column interaction. After 3 washes, CD19+ cells were eluted by removing the MACS LS column from the magnetic field and collecting CD19+ cells in 5ml ice-cold wash buffer (0.5% BSA in PBS) by applying force on the MACS LS column with a plunger. CD19+ cells remain bound to microbeads for downstream experiments.

CD19 cross-linking induced by anti-CD19 microbead binding may influence CLL B-cell viability and activation status. Negative B-CLL isolation depletes PBMCs of numerous cell types leaving B-cells unbound; this method was used as a non-manipulated B-cell comparison. $40x10^6$ CLL PBMCs were incubated with biotin-conjugated monoclonal antibodies against CD2, CD3, CD4, CD14, CD15, CD16, CD34, CD61, CD235a and FceRIa before incubation with anti-biotin microbeads. The microbead-cell suspension was applied to a MACS LS column held in a magnetic field. The cell suspension passed through the MACS LS column by gravity-flow, allowing labelled cells to bind to the magnetic matrix while unlabelled CLL B-cells remain unbound. Unlabelled CLL B-cells were eluted in the first wash with 5ml ice-cold 0.5% BSA PBS wash buffer by gravity-flow. Labelled cells were not eluted from the column. Both CD19+ selection and B-CLL cell negative selection recovered at least $20x10^6$ cells, half of the input cell count. After elution using either kit, cell count was measured and cells were washed once in RPMI 1640 complete medium prior to downstream experiments.

2.3 Immunohistochemistry

Immunohistochemistry (IHC) is a well-established method to detect protein expression in tissue sections, utilised widely in disease diagnosis.[286,287] The method is based on specific antigen-antibody binding in tissue sections. However, due to the nature of tissue preservation and fixation, the tissue section needs to undergo various processing steps prior to antibody-antigen binding visualisation.[288] Antigen retrieval, by enzyme or heat based methods, is necessary to remove protein cross links and structural modifications formed during formalin tissue fixation to unmask epitopes for antibody binding. Following antibody-antigen reactions, a labelled detection system is used to visualise the immune reaction. Most detection systems utilise secondary antibodies conjugated to enzymes (peroxidase, alkaline phosphatase) that catalyse formation of a coloured precipitate when a chromogen is applied (Figure 2-1).

In the last decade, this method has greatly improved due to advances in tissue fixation, antigen retrieval and sensitive antibody detection systems. TMA technology allows simultaneous high throughput examination of hundreds of samples on a single microscope slide, saving reagents, reducing technical time and variability in results.[289]

2.3.1 Tissue Microarray construction

For this study, formalin-fixed paraffin embedded (FFPE) TMAs were prepared from LN biopsies from 91 CLL patients and 42 RA samples by our in-house histopathologist, Andrew Clear. Representative malignant areas were identified by Professor Maria Calaminici following haematoxylin and eosin staining and triplicate 1-mm² LN cores were taken from each LN using an automated arraying system (TMA Booster-Alphelys). Cores were arrayed onto a recipient empty paraffin block, cut to 3µm thick sections using a Leica RM2232 microtome and transferred onto Superfrost™ glass slides by Andrew Clear.[76,290,291]

2.3.2 IHC Staining

Slides were prepared for immunostaining by complete removal of paraffin wax using xylene and re-hydration in 100% alcohol (IMS) and running tap water (Appendix I, 3.0). Endogenous peroxidase activity was blocked by incubating slides in 2% H_2O_2 IMS for 2 rounds of 5 minutes to quench enzyme activity and ensure only applied exogenous horseradish peroxidase (HRP) produced coloured precipitate during the antibody reaction detection step (Appendix I, 3.1). Formalin fixation preserves tissue integrity but modifies the tertiary structure of proteins; heat induced epitope retrieval (HIER) reverses formalin-protein cross links and restores the original epitope conformation and electrostatic charges for antibody recognition.[292] HIER was performed

for 10 minutes in antibody specific batches using a pressure cooker (400°C) with antigen unmasking solution (Appendix I, 3.2; Vector Laboratories). Slides were immediately immersed in wash buffer to prevent tissue sections drying out, and slides were prepared for immunostaining by creating a hydrophobic barrier around tissue sections with a hydrophobic pen (Appendix I, 3.3). Optimal primary antibody dilutions (monoclonal anti-RAGE or monoclonal anti-TLR9 antibody in Zytomed antibody diluent) were determined by titration, using a fixed incubation time of 40 minutes (Appendix I, 3.4; Table A). Tissue sections were stained using the Dako autostainer (Appendix I, 3.5; Table B). Antibody reactions were visualised using a peroxidase-labelled polymer amplification 3,3'-diaminobenzidine (DAB) system (Appendix I, 3.6; Super Sensitive Polymer-Horseradish Peroxidase (HRP) IHC Detection System; BioGenex) compared to traditional avidin-biotin method which produces high levels of background from endogenous biotin. A secondary antibody conjugated to HRP-polymer detects bound primary antibody. Multiple HRP enzymes conjugated to the bound polymer amplifies the signal from one distinct epitope location. In the presence of H_2O_2 and electron donor, DAB, HRP catalyses oxidation of DAB and formation of a coloured precipitate that is insoluble in alcohol:

$$H_2O_2 + \text{DAB} \rightarrow \text{DAB precipitate and } H_2O$$

Tissue sections were washed in acid alcohol and counterstained in Mayer Haematoxylin (Appendix I, 3.1; 3.7) to identify nuclear areas. Stained slides were dehydrated in IMS and xylene before mounting with DPX xylene based mountant to ensure brown DAB precipitate remained insoluble (Appendix I, 3.8).

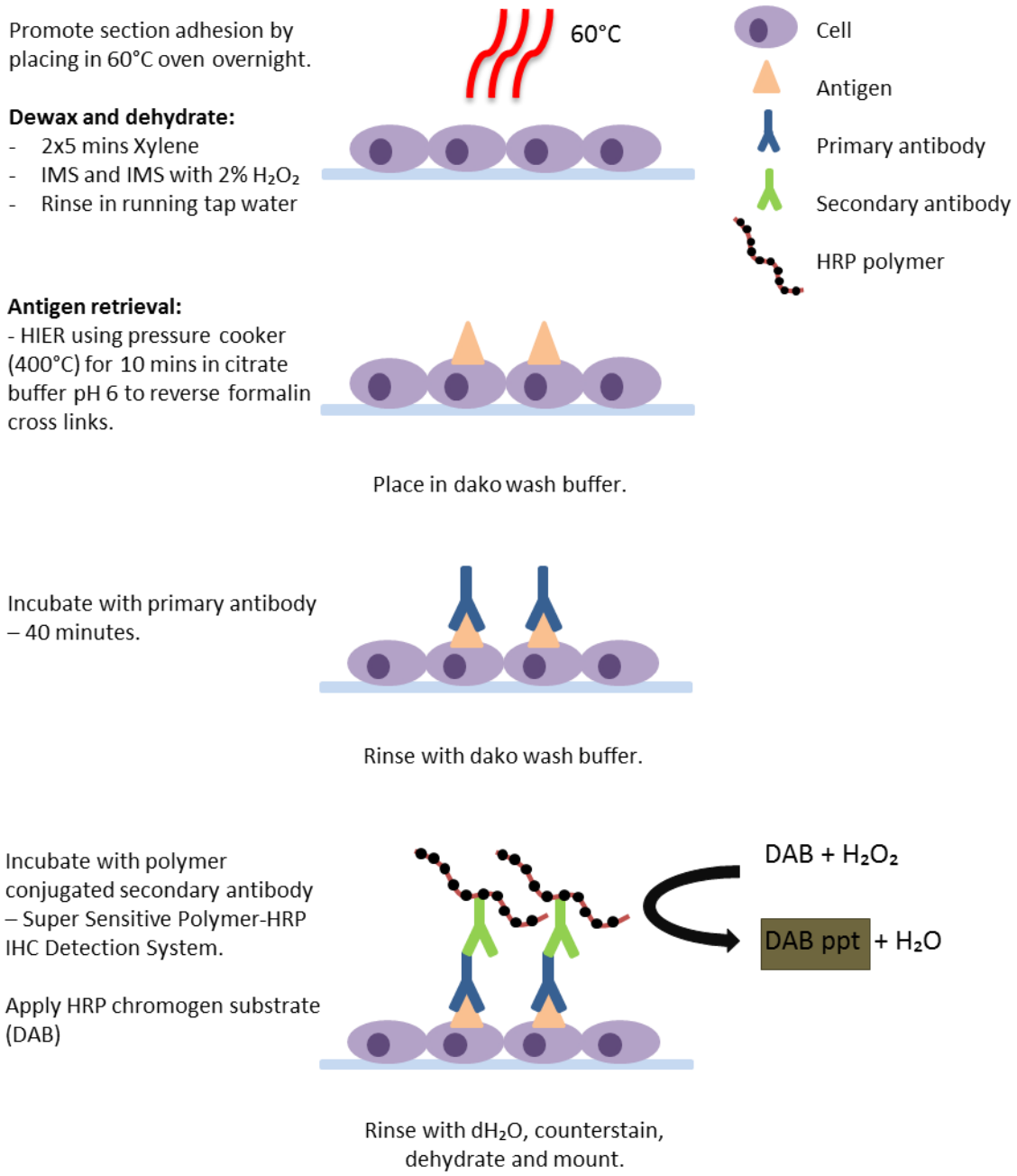

Figure 2-1. Principles of Immunohistochemistry. Adapted from Ramos JA.[293]

2.3.3 Image Analysis

Slides were scanned using the Olympus BX61 microscope and image analysis performed using the Ariol imaging system to quantify levels of anti-TLR9 or anti-RAGE antibody staining. Representative CD5 positive areas in CLL-LNs, and germinal centres of RA-LNs were selected for image analysis training. From these training areas, an automated algorithm to quantify RAGE and TLR9 staining was developed. Shape and colour image classifiers were used to measure the intensity of brown staining per cell. Cell shape was determined using blue haematoxylin-stained nuclei to identify cell number in LN cores. Colour classifier was trained based on saturation, hue and intensity of brown pixels. Minimum thresholds were set that excluded brown background

staining to ensure only positive brown pixel/protein expression was measured. Once the training algorithm was optimised per antibody stain, it was applied to all TMAs. Protein levels are expressed as the percentage of cells positive for brown staining in the LN core. Mean percent-positive staining was calculated for each stain per patient. Incomplete or damaged LN cores were excluded from analysis. Data for the levels of Ki67 and ZAP70 LN expression were from the tissue bank databases and performed by Mr Andrew Clear from Barts Cancer Institute and Dr Meg Ashton-Key from the University of Southampton, respectively.

2.4 Flow Cytometry

Flow cytometry is a widely used assay that utilises multi-parameter analysis of single cells in suspension to determine cell-population purities and cell-surface/intracellular protein/molecule expression.[294,295] A flow cytometer measures forward and side scatter from cells that pass through a laser beam to differentiate cell populations, and fluorescence intensity from fluorescent-labelled antibodies or dyes that bind to protein or ligand targets.[296]

Cell suspensions are hydrodynamically focused into a stream of single cells in sheath fluid. Single cells passing through the laser beam scatter light, detected by a forward-scatter detector and various side scatter detectors. Forward scatter measures cell size and helps exclude doublet-cells from analysis; side scatter correlates with the granularity of cells and is useful in distinguishing different cell populations based on these parameters. Cells fluorescently stained with labelled antibodies or dyes result in photon excitation and emission at specific wavelengths of light. Photomultiplying tubes detect emitted wavelengths of light from multiple fluorescent antibodies in the same cell. However, when designing multi-colour flow cytometry assays, fluorochromes from distal spectral emission wavelengths should be selected to limit spectral overlap and production of false positive results (Figure 2-2).[297] Spectral compensation by using single stained cells was adopted in this work to limit spectral overlap. For all flow cytometry experiments included in this work, data acquisition was performed using an LSR Fortessa Cell Analyzer (BD Biosciences) for 10,000 events and data files analysed with FlowJo Version 10 software.

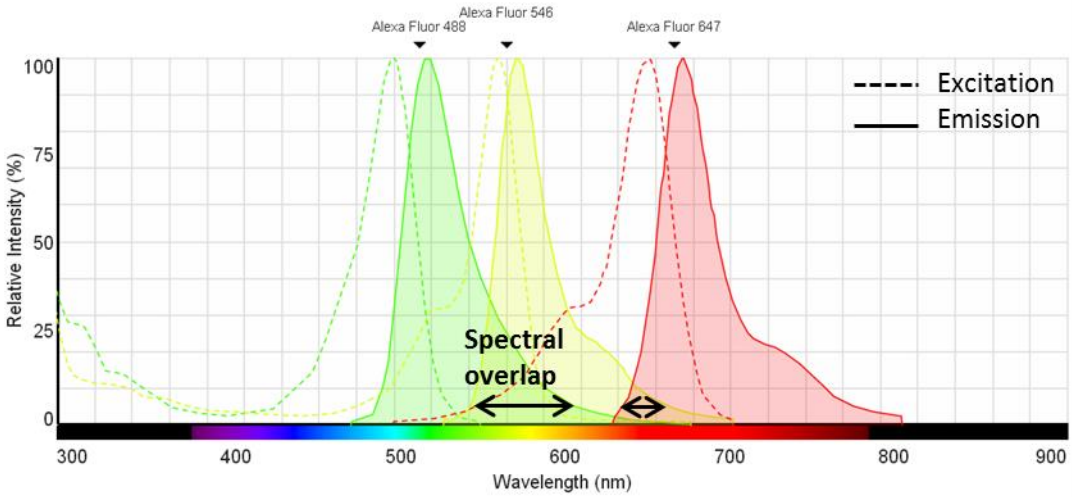

Figure 2-2. Excitation and emission spectra for AF-488, AF-546 and AF-647. Arrows indicate spectral overlap (Interactive graph from Life Technologies).

Fluorochromes and lasers used throughout experiments:

Laser	Bandpass Filter	Fluorochrome use
Violet (405nm)	450/50	DAPI
	525/50	
	610/20	
	660/20	
	710/50	
	780/60	
Blue (488nm)	530/30	AF-488; Annexin V-FITC
	695/40	Propidium iodide
Yellow/Green (561nm)	582/15	
	610/20	
	670/30	PE/Cy5
	710/50	
	780/60	PE/Cy7
Red (641nm)	670/14	AF-647; APC
	730/45	
	780/60	APC/Cy7

2.4.1 Evaluation of RAGE and TLR9 expression in CLL PBMCs

Surface/intracellular RAGE and intracellular TLR9 expression in different PB cell types was assessed by flow cytometry to determine the main cell types in CLL that express RAGE and TLR9. By using flow cytometry, PBMCs are easily co-stained with cell markers, instead of performing cell-separation to isolate homogeneous cell types. Cryopreserved mononuclear CLL cells from 6 CLL patients were incubated at 37°C in RPMI complete growth medium to recover for 2 hours prior to staining. Non-specific binding was blocked by incubating with 50µl 2% human anti-globulin antibody (HAG) blocking buffer (Appendix I, 4.1; Sigma) for 20 minutes. After washing with 2% FBS wash buffer (Appendix I, 4.2), $1x10^6$ cells per flow tube were co-stained with anti-CD14-PE/Cy5, anti-CD19-PE/Cy7, anti-CD3-FITC antibodies (Appendix I, 4.3; Table C) for 30 minutes at room temperature. For intracellular staining, cells were washed with 2% FBS wash buffer and permeabilised and fixed with 50µl CytoFix/CytoPerm (Appendix I, 4.1; BD Biosciences) for 20 minutes at room temperature; while for RAGE surface staining, cells remained non-permeabilised. Intracellular non-specific binding was blocked with 50µl 2% HAG for 20 minutes and cells were stained with primary antibodies for RAGE or TLR9 for 1 hour (Appendix I, 4.3; Table C). Cells were washed with 2% FBS wash buffer and primary RAGE and TLR9 antibody binding was detected using Alexa Fluor (AF) 488 or 647 conjugated IgG secondary antibodies for 30 minutes at room temperature in 50µl 2% HAG blocking buffer (Appendix I, 4.3; Table C). Cells were washed with 2% FBS containing PBS wash buffer and the nuclei of all non-permeabilised cells were stained with 50ng/ml DAPI in 300µl 2% FBS containing wash buffer (Appendix I, 4.4-4.5) to distinguish live/dead cells during data acquisition. Data acquisition was performed using

a LSR Fortessa Cell Analyser. FITC and AF-488 signals were measured using the blue laser (488nm) at bandpass B530/30; AF-647 signal was measured under the red laser (641nm) at bandpass R670/14; DAPI signal was measured using the violet laser (405nm) at bandpass V450/50; PE/Cy5 and PE/Cy7 signals were measured using the yellow-green laser (560nm) at bandpass YG670/30 and YG780/60, respectively. Lymphocytes, single cells and live cells (for non-permeabilised cells) were gated for analysis. Values for mean fluorescence intensity (MFI) and percentage of cells positive for RAGE/TLR9 compared to unstained controls were exported from FlowJo Version 10 software for statistical analysis.

2.4.2 Determination of ZAP70 expression in CLL cells

ZAP70 positivity is determined in CLL by flow cytometry. However, there is currently no standardised flow cytometric procedure to measure ZAP70 expression.[298] All published methods were reviewed, and herein describes the isotype corrected T/B-CLL ratio method where ZAP70 MFI in CLL CD19+/CD5+ B-cells is compared to the ZAP70 MFI from CD3+ T-cells.[299] Cryopreserved mononuclear CLL cells from 50 patients with matched plasma for ELISA, were incubated with 0.5mg/ml DNase (Appendix I, 4.6) for 5 minutes at room temperature to digest extracellular DNA. DNase was removed by washing cells in RPMI 1640 complete medium, centrifugation at 1500rpm for 5 minutes and resuspending cells at $1x10^6$ cells/ml fresh RPMI 1640 complete growth medium. Cells were left to rest at 37°C for 2 hours prior to staining. Cell viability was measured using the Luna-II™ automated cell counter and cells with viability <80% after resting was not taken forward for ZAP70 flow cytometry analysis. Non-specific binding was blocked by incubating with 50µl 2% HAG blocking buffer for 20 minutes, followed by cell surface co-staining with anti-CD3-APC, anti-CD5-APC/Cy7 and anti-CD19 PE/Cy7 for 30 minutes in the dark (Appendix I, 4.3; Table C) for all patient test samples and fluorescence-minus-one (FMO) control tubes. Isotype controls were included and stained with mouse anti-IgG1κ conjugated to either APC, APC/Cy7 or PE/Cy7 (Appendix I, 4.3; Table C). Cells were washed with 2% FBS wash buffer and then permeabilised and fixed with 50µl CytoFix/CytoPerm for 20 minutes. Non-specific binding in permeabilised cells was blocked with 50µl 2% HAG blocking buffer, followed by intracellular staining with anti-ZAP70-AF-488 clone IE7.2 for patient test samples, or mouse anti-IgG1κ AF488 for FMO and isotype controls (Appendix I, 4.3; Table C). Cells were washed with 2% FBS wash buffer and resuspended in 300µl flow wash buffer for flow cytometry data acquisition. AF-488 signal measured using the blue laser (488nm) at bandpass B530/30; APC and APC/Cy7 signals were measured under the red laser (641nm) at bandpass R670/14 and R780/60, respectively; PE/Cy7 signal was measured using the yellow-green laser (560nm) at bandpass YG780/60. Data was recorded for 10,000 events and lymphocytes and single cells were gated

for analysis. ZAP70 positive gates were set subject to isotype controls and FMO sample gates. Values for ZAP70 MFI from CD5+/CD19+ CLL cells, CD3+ T-cells and isotype control MFI values were exported from FlowJo Version 10 software for statistical analysis.

2.4.3 Evaluation of CLL cell death by Annexin V/PI assay

Cell death can be assessed by a flow cytometric procedure called Annexin V assay. Annexin V conjugated to FITC binds to the phospholipid phosphatidylserine (PS) that is exposed from the cytoplasmic side of the plasma membrane to the extracellular side during early apoptosis.[300] Propidium iodide (PI) was included in this assay as a marker for dead cells, by intercalating between DNA bases in a sequence independent manner. DNA is exposed to PI in necrotic and secondary necrotic dead cells that have lost membrane integrity, but not in viable cells with normal plasma membranes. Therefore, this assay allows determination of viable cells (Annexin V-/PI-), early apoptotic events (Annexin V-FITC+/PI-) and late apoptotic (secondary necrotic)/dead/necrotic cells (Annexin V-FITC+/PI+).[301] Fresh primary CLL cells were resuspended at a cell density of $2x10^6$/ml in RPMI 1640 complete growth medium. Cells were treated with 10µl sterile PBS, 200ng/ml HMGB1, 500ng/ml HMGB1 or 10µg/ml neutralising anti-RAGE antibody (Appendix I, 13.1-13.2) for 48 and 120 hours at 37°C in a humidified 5% CO_2 incubator to assess the effect of these treatments on CLL cell death *in vitro*. After treatment, cells were washed in 4ml ice-cold PBS to quench cell signalling and resuspended at $1x10^6$ cells per flow tube in 100µl 1x Annexin V Binding Buffer (Appendix I, 4.7; BD Pharmingen FITC Annexin V Apoptosis Detection Kit I). Cells were co-stained with 5µl FITC Annexin V and 5µl PI for 15 minutes in the dark (Appendix I, 4.7; BD Pharmigen FITC Annexin V Apoptosis Detection Kit I). Stain was removed by washing with 4ml ice-cold PBS and resuspension in 300µl 1x Annexin V Binding Buffer. Data for CLL cell death was acquired immediately after staining using a LSR Fortessa Cell Analyser. Annexin V-FITC and PI signals were measured using the blue laser (488nm) at bandpass B530/30 and B695/40, respectively. Compensation was included to limit spectral overlap. Values for the percentage of viable cells (Annexin V-/PI-), early apoptotic cells (Annexin V+/PI-) and necrotic/dead cells (Annexin V-/PI-) per treatment compared to unstained controls were exported for statistical analysis.

2.4.4 Evaluation of CLL cell purity in PBMCs

CLL cell purity is highly heterogenous among CLL patient PB. It was important to assess CLL purity to factor in the presence of supportive cell types for cell death assays; and for mass spectrometry sample inclusion criteria to ensure phosphoproteomic signals originate from CLL cells. Standard CLL cell identification by flow cytometry is performed by assessing CD5 and CD19 antigen double

positive expression in whole PBMCs, with gating set in comparison to isotype controls.[302] Freshly isolated CLL PBMCs were incubated at 5x10^6 cells/ml at 37°C in RPMI complete growth medium overnight prior to staining. Non-specific binding was blocked for 1x10^6 cells/flow tube by incubating with 50µl 2% HAG blocking buffer for 20 minutes, followed by cell surface co-staining with anti-CD5-PE/Cy7 and anti-CD19-APC for 30 minutes in the dark (Appendix I, 4.3; Table C). Isotype controls were included and patient cells were stained with mouse anti-IgG1κ PE/Cy7 and APC (Appendix I, 4.3; Table C). Cells were washed with 4ml 2% FBS containing wash buffer, and resuspended in 300µl 2% FBS containing wash buffer with 50ng/ml DAPI prior to flow cytometry to distinguish live/dead cells during data acquisition. CD19-APC and CD5-PE/Cy7 signals were measured using the red laser (641nm) at bandpass R670/14, and the yellow-green laser (560nm) at bandpass YG780/60, respectively. Values for the percentage of CLL cells (CD5+/CD19+) compared to isotype control gates were exported for statistical analysis.

2.4.5 Evaluation of membrane RAGE shedding

HMGB1 receptor, RAGE, can undergo membrane shedding from the surface of cells into cell culture medium under stimulatory conditions. Membrane RAGE cleavage is catalysed by ADAM10 as an inflammatory dampening response; ADAM10 activity can be induced by ionophore, ionomycin, or selectively inhibited by GI25423X without targeting other ADAM proteases. In this work, cell surface RAGE and ADAM10 expression was assessed by flow cytometry following stimulation or inhibition of ADAM10 activity. 2x10^6/ml Mec1 cells and 1x10^6/ml HEK293 FL-RAGE transfected cells were cultured in 6-well plates in 2ml serum-free RPMI medium 1 hour before stimulations. ADAM10 sheddase activity was blocked, prior to other stimulations with ADAM10 inhibitor GI254023X 5µM, 10µM or 20µM for 1 hour (Appendix I, 13.4). ADAM10 inhibited cells were washed in sterile PBS and resuspended in 2ml RPMI serum-free medium. Cells were then treated with PBS, HMGB1 50ng/ml, HMGB1 200ng/ml, HMGB1 500ng/ml, DMSO, ionomycin 500nM or GI254023X 5µM, 10µM and 20µM again combined with ADAM10 stimulator, ionomycin 500nM (Appendix I, 13.1; 13.4; 13.5). All treatments were performed for 1 hour at 37°C in a humidified 5% CO_2 incubator. Following treatments, conditioned medium from cell lines was collected by centrifugation at 1500rpm for 5 minutes to pellet cells and removal of conditioned medium supernatant; supernatant aliquots were stored in -20°C for ELISA. Live cells were harvested for flow cytometry by spinning 1x10^6 cells/flow cytometry tube at 1500rpm for 5 minutes. Non-specific binding was blocked by incubating cell lines with 50µl 2% HAG blocking buffer for 20 minutes, followed by separate cell surface staining with primary antibodies for rabbit anti-RAGE and rabbit anti-ADAM10-N-terminal for 30 minutes (Appendix I, 4.3; Table C). Cells were washed in 2% FBS containing wash buffer and primary

antibody binding was detected using AF-488 or AF-647 conjugated goat anti-rabbit IgG secondary antibodies for 30 minutes at room temperature in 50µl 2% HAG blocking buffer. Cells were washed in 2% FBS containing wash buffer and resuspended in 300µl 2% FBS wash buffer with 50ng/ml DAPI prior to flow cytometry to distinguish live/dead cells during data acquisition. RAGE and ADAM10 signals were measured using the blue laser (488nm) at bandpass B530/30, and the red laser (641nm) at bandpass R670/14, respectively. Values for RAGE and ADAM10 MFI in viable FL-transfected HEK293 and Mec1 cells were exported from FlowJo Version 10 software for statistical analysis.

2.5 Enzyme-Linked Immunosorbant Assay (ELISA)

The plasma concentrations of HMGB1, S100B and soluble RAGE were determined in 54 CLL patients and 15 healthy controls using HMGB1, S100B and sRAGE sandwich ELISA kits (Appendix I, 5.0; Merck Millipore, Abcam and Cambridge Bioscience, respectively). This quantitative method is a powerful tool to measure protein concentration in solution, particularly for human plasma and cell culture supernatants. The antigen of interest is 'sandwiched' between a capture antibody immobilised on the plate base and a detection antibody. The detection antibody is either directly conjugated to an enzyme reporter system, or indirectly using a secondary antibody. ELISAs used in this study utilised a biotin-streptavidin HRP direct detection system. Anti-HMGB1, S100B and RAGE biotinylated detection antibodies bind to HRP-conjugated streptavidin; this reporter enzyme catalyses production of coloured product in proportion to the amount of HMGB1/S100B/RAGE bound to the capture antibodies (Figure 2-3). The use of 96-well polystyrene plates makes this method high-throughput and easy to perform.

Fresh plasma was obtained by centrifugation of whole CLL and healthy blood at 1500rpm 5 minutes. The top plasma layer was removed and contaminating cells and insoluble material were removed from plasma by centrifugation again at 4000×g at 4°C for 10 minutes. Plasma aliquots were stored at -80°C prior to ELISA. Appropriate protein standards and reagents were included in all ELISA kits and standard curves were generated while CLL and healthy plasma concentration was assayed. The ELISA assay procedure was similar for all ELISA kits. All ELISA plates were manufactured with pre-bound capture antibodies specific for the human antigen of choice – HMGB1, S100B and sRAGE. ELISA kit reagents and protein standards were prepared prior to running the assay with the materials provided (Appendix I, 5.1-5.3). ELISA plates were washed with provided 1X Tris-Buffered Saline with 0.1% Tween-20 (TBST) wash buffer to ensure wells were clear of contaminants and to pre-wet the capture-antibodies at the base of each well before incubating with plasma/cell culture supernatant. Fixed volumes of CLL plasma, healthy control plasma, cell culture supernatant and protein standards were incubated in ELISA wells with immobilised antibodies for fixed time points, dependent on the ELISA kit (2-24 hours). Wells were washed 3-5 times with provided 1X TBST wash buffer to remove unbound plasma analytes. Antigen-immobilised antibody reactions were detected by incubating with anti-S100B, anti-RAGE or anti-HMGB1 biotinylated detection antibodies for fixed incubation time points (2-24 hours dependent on ELISA kit). Unbound biotinylated antibodies were rinsed from wells with 1X TBST wash buffer 3-5 times. Immobilised-biotinylated antibodies were then conjugated to HRP detection enzyme via streptavidin for 2 hours. ELISA wells were washed 3-5 times with 1X TBST to remove unbound HRP-conjugate. HRP substrate, 3, 3',5,5'-tetramethylbenzidine (TMB), was added to each well with H_2O_2 for 5-30 minutes (dependent on ELISA kit) to catalyse oxidation of

TMB, production of water and a solution colour change to blue. Stop solution (0.3M HCl or 0.35M H_2SO_4) was added to the ELISA plates to quench further activity of HRP and formation of blue-product. The colour change induced by HRP activity was measured by absorbance at 450nm using POLARstar Optima plate reader; the absorbency is directly proportional to the amount of HMGB1/S100B/sRAGE captured in wells. The concentration of each analyte per patient were derived by interpolation from the standard curve generated in the same assay from ELISA kit-specific protein standard readouts.

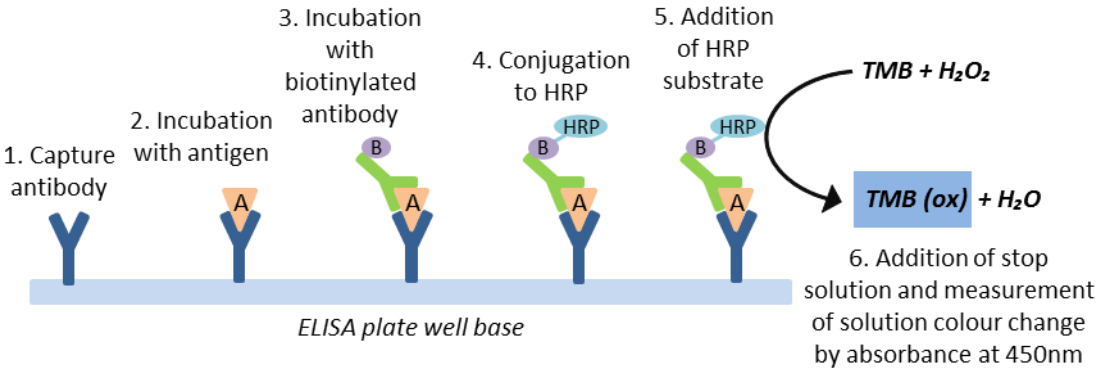

Figure 2-3. Principles of sandwich ELISA. Adapted from http://www.abcam.com/protocols/sandwich-elisa-protocol-1. ELISAs were purchased with pre-coated capture antibodies at the base of ELISA wells. ELISA plates were incubated with primary CLL or healthy plasma, cell culture supernatant and ELISA kit protein standards. Antigen-antibody reactions were visualised by addition of a biotinylated secondary antibody to the antigen of interest. HRP was conjugated to the sandwich antibody complex via biotin-streptavidin reaction. HRP catalysed the oxidation of TMB to produce a blue colour solution change. Stop solution was added (0.3M HCl or 0.35M H_2SO_4) to quench HRP enzyme activity. Absorbance measured at 450nm is directly proportional to the amount of antigen captured in ELISA wells.

2.6 Immuno-fluorescent Microscopy

Immuno-fluorescent microscopy (IFM) is a qualitative technique used to investigate protein expression with additional spatial localisation information and can reveal protein-protein interactions.[303] Proteins are fluorescently labelled with primary antibodies and fluorochrome-conjugated secondary antibodies. For this study, AF-488 (excitation/emission wavelengths: 495nm/519nm) and AF-546 conjugated secondary antibodies (excitation/emission wavelengths: 556nm/573nm) were used that have limited spectral overlap on the Nikon eclipse fluorescence microscope (Figure 2-2). By targeting specific proteins with fluorescent tagged antibodies and imaging cells are 100x magnification, immunofluorescent microscopy provides a window to assess physiological processes at a molecular level which is lacking from expression-based assays.

Fresh primary CLL cells were isolated from whole blood outlined in section 2.2.3. CLL cells were resuspended at a density of $5x10^6$/ml in fresh RPMI 1640 complete growth medium in a 12-well plate and left to rest for 2 hours prior to treatments. CLL cells were stimulated with 200ng/ml HMGB1 (Appendix I, 13.1) with or without anti-RAGE neutralising antibody (Appendix I, 13.2) for 2 and 4 hours. Where anti-RAGE antibody was used, cells were pre-treated with anti-RAGE antibody for 30 minutes to allow inhibition of surface RAGE, before addition of HMGB1 for 2 and 4 hours. Control samples were treated with PBS vehicle control at the same volume used for HMGB1 treatments. Following treatments, cells were pelleted by centrifugation for 5 minutes at 1500rpm and then washed with PBS. Cells were pelleted and mixed with 10µl RPMI 1640 complete growth medium to give a concentrated cell suspension. Superfrost™ slides were divided into 4 sections using a hydrophobic barrier pen (Appendix I, 3.0); 3µl of concentrated cell suspension was spread onto the surface of the Superfrost™ slide in each section and left to air-dry for 5 minutes. Once bone-dry, cells in each section were fixed and permeabilised with 50µl CytoFix/CytoPerm solution (Appendix I, 6.0) for 30 minutes at room temperature for intracellular protein staining. Slides were rinsed in a beaker of TBST (Appendix I, 6.1) and non-specific binding was blocked by incubating each slide section with 50µl TBS blocking buffer (pH 7.4) containing 2.5% goat serum and 2.5% donkey serum and 0.1% saponin for 30 minutes (Appendix I, 6.2). Cells were co-stained for TLR9 and RAGE, MyD88 and TLR9, or separately for NF-κB and STAT3-P^{Y705} with primary antibodies (Appendix I, 6.3; Table D) in 50µl 2.5% goat and 2.5% donkey blocking buffer in a humidified opaque box. Slides were rinsed in TBST for 3 rounds of 5 minutes before primary antibodies were detected with donkey anti-mouse IgG or goat anti-rabbit IgG secondary antibodies conjugated to AF-488 or AF-546 (Appendix I, 6.3; Table D) in 50µl blocking buffer for 1 hour in a humidified opaque box. Unbound antibody was removed by 3 washes with TBST. The nuclei of cells stained for NF-κB and STAT3 were counterstained with

DAPI (Appendix I, 6.4) in TBST for 5 minutes in a humidified opaque box. Background DAPI was removed by rinsing slides in TBST before leaving slides to air-dry completely. Slides were mounted with ProLong Gold anti-fade reagent to prevent fluorochome quenching and stain-bleed and slides were imaged on the same day.

Immunofluorescence was observed at 100x magnification using the Nikon eclipse Ci-E fluorescence microscope using the green, blue and red channels.[76] Protein colocalisation and protein nuclear translocation using DAPI nuclear stain were analysed by WCIF ImageJ software. The intensive correlation analysis method was used for protein colocalisation analysis.

2.7 ImageStream X Mark II Flow Cytometry

The introduction of Imagestream X Mark II (ISS) instrument and IDEAS analysis software has advanced flow cytometry and imaging technology. This system integrates features of high throughput flow cytometry with fluorescence microscopy allowing multiparameter analysis. This effective combination allows for acquisition of statistically powerful data and detailed morphological fluorescence information that is used for various applications.[304] For this study, ImageStream X Mark II flow cytometry was used to measure protein colocalisation and nuclear localisation as a quantitative comparison to qualitative-based fluorescence microscopy.

Like flow cytometry, immuno-labelled cells in suspension are focused into a core stream and illuminated by brightfield light, 488nm blue, 405nm violet and 633nm red lasers (Figure 2-4). The instrument objective lens detects scattered light, transmitted light and up to 4 independent fluorescence signals for up to 10^4 events. Signals are decomposed into 6 defined wavelength ranges (4 fluorescence images, 1 brightfield and 1 darkfield image) and collected using a charge-coupled device camera.[305] Compared to standard photomultiplier tubes in flow cytometry, the charge-coupled device camera converts photons into photocharges in an array of pixels, correlating fluorescence and brightfield signals to distinct morphometric locations in an image. Spectral compensation is performed using separate stained samples for every fluorochrome used to limit fluorescence emission spill over.

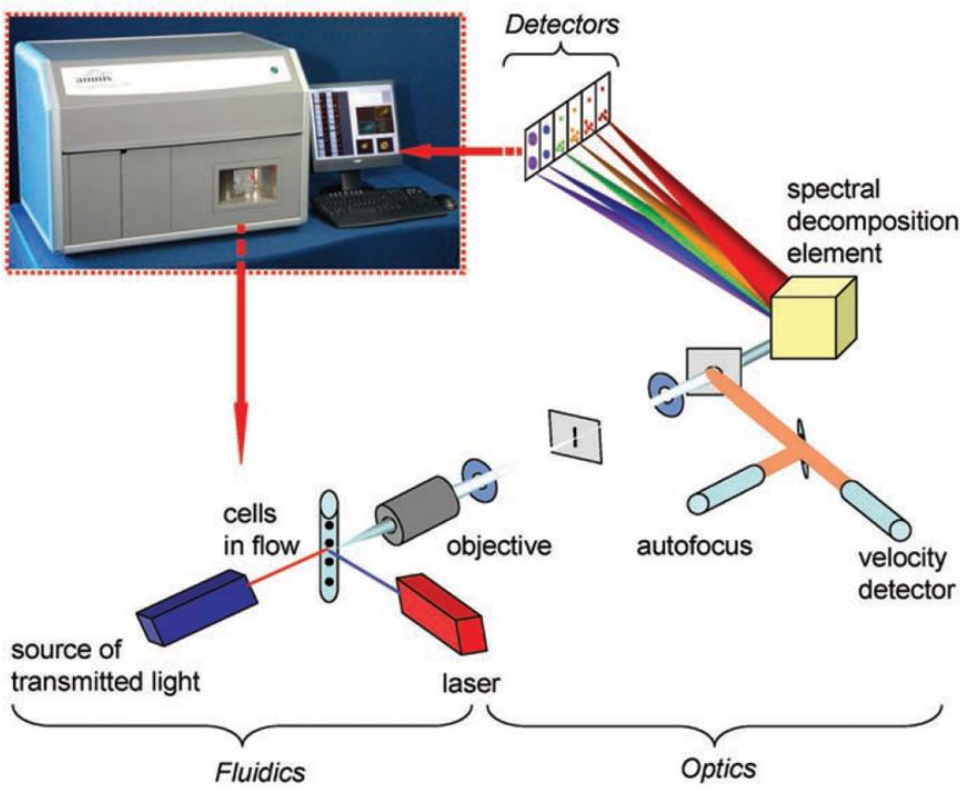

Figure 2-4. The ImageStream X Mark II flow cytometer. Adapted from Zuba-Surma et al.[306]

2.7.1 Immunostaining procedure

Fresh primary CLL cells were isolated from whole blood outlined in section 2.2.3. CLL cells were resuspended at a density of $5x10^6$/ml in 2ml fresh RPMI 1640 complete growth medium in 6-well plates and left to rest for 2 hours prior to treatments. CLL cells were stimulated with 200ng/ml HMGB1 (Appendix I, 13.1) with or without anti-RAGE neutralising antibody (Appendix I, 13.2) for 2 and 4 hours. Where anti-RAGE antibody was used, cells were pre-treated with anti-RAGE antibody for 30 minutes to allow inhibition of surface RAGE, before addition of HMGB1 for 2 and 4 hours. Control samples were treated with PBS vehicle control at the same volume used for HMGB1 treatments. Following treatments, cell suspension was collected in Eppendorf tubes and centrifuged for 5 minutes at 1500rpm. Cell culture medium supernatant was removed and cell pellets washed in PBS, before centrifugation again. All samples were fixed and permeabilised with CytoFix/CytoPerm for 30 minutes on ice to allow for intracellular staining. Cells were washed with TBST (Appendix I, 6.1). Non-specific binding was blocked by incubating with 50µl TBS (pH 7.4) containing 5% goat serum, 5% donkey serum and 0.1% saponin for 30 minutes (Appendix I, 6.2). Cells were co-stained for TLR9 and RAGE, MyD88 and TLR9, or separately for NF-κB and STAT3-P^{Y705} with primary antibodies (Appendix I, 7.1; Table F) in 50µl 5% goat and 5% donkey blocking buffer. Cells in Eppendorf tubes were washed in TBST and primary antibodies were detected with donkey anti-mouse IgG or goat anti-rabbit IgG secondary

antibodies conjugated to AF-488 or AF-647 for 1 hour in the dark (Appendix I, 7.1; Table F). Unbound antibody was removed by 2 washes with TBST and centrifugation at 1500rpm for 5 minutes. The nuclei of cells stained for NF-κB and STAT3 were stained with DAPI 1:1000 in TBST for 10 minutes in the dark. Background DAPI was removed by washing in TBST and all stained cell pellets were resuspended in 50µl TBST in Eppendorf tubes for ImageStream Mark II flow cytometry. Single stained cells for fluorochromes AF-488, AF-647 and DAPI were included to perform compensation. Unstained samples are not needed for ImageStream flow cytometry data acquisition due to the use of brightfield light to set gating parameters. Data was collected for 5000 single cells in focus at 40x or 60x magnification where stated.

2.7.2 ImageStream data analysis – IDEAS software

The IDEAS analysis software package calculates over 200 photometric and morphometric parameters for each individual cell collected, in addition to gating percentages and fluorescence images, allowing a huge range of applications from one experiment.[304] In this study, the ImageStream was used to measure protein colocalisation and transcription factor nuclear translocation.

The colocalisation coefficient, Similarity Bright Detail Score (SBDS), was used to test if 2 probes were localised in the same region of a cell. The SBDS was calculated on a pixel by pixel basis between 2 fluorescent channels; i.e. RAGE detected by AF-488 secondary antibody and TLR9 detected by AF-647 secondary antibody. The IDEAS software calculates optimal background fluorescence erosion from original images to concentrate bright spots. Next, the Pearson's correlation coefficient measured the spatial location similarity of bright spots in the AF-488 and AF-647 image pair. This coefficient is log transformed to give the SBDS; cells with a higher SBDS have higher levels of bright spots in the same spatial location between an image pair. Nuclear translocation of NF-κB and STAT3 transcription factors were measured using the Similarity Eroded Score (SEC). Measured by a similar algorithm to SBDS, the spatial correlation between nuclear fluorescence from DAPI staining, and NF-κB and STAT3 was an indication of nuclear translocation. The Pearson's correlation coefficient was log-transformed to give SEC; a higher SEC reflects increased nuclear translocation and transcription factor activation. 5000 events were recorded and single cells in focus were gated for analysis; the mean SBDS or SEC was measured for every cell per treatment group and raw data was exported for statistical analysis.

2.8 Western Blotting

Western blotting is a routine gold standard procedure for protein expression analysis introduced nearly 40 years ago.[307] Proteins extracted from cells are denatured, made linear and negatively charged with sodium dodecyl sulphate (SDS) before separation by polyacrylamide gel electrophoresis (PAGE) based solely on protein mass. Proteins of smaller molecular weight migrate through the gel faster than larger proteins to the anode. Separated proteins bands are transferred from the gel to a nitrocellulose or PVDF membrane for subsequent detection. Target antigens are identified from the complex mixture of separated proteins by specific antigen-antibody reactions and visualised using a chemiluminescent detection system.

2.8.1 Preparation of cell lysates

Cells were stimulated at a density of $2x10^6$ cells/ml for $15x10^6$ Mec1 total cells and $5x10^6$ cells/ml for $30x10^6$ total primary CLL cells. After treatment, cells were pelleted by centrifugation at 1300rpm for 5 minutes at 4°C, followed by washing with PBS. PBS wash supernatant was removed and primary CLL cell pellets incubated with 0.5mg/ml DNase (Appendix I, 4.6) for 5 minutes at room temperature to decrease sample viscosity. DNase was removed by washing with PBST and centrifuged at 8000rpm for 2 minutes at 4°C. PBST supernatant was removed and cell pellets lysed with 50µl cell lysis buffer containing protease and phosphate inhibitors (Appendix I, 8.1). Cell lysates were incubated on ice for 20 minutes with intermittent vortexing followed by centrifugation at 13000rpm for 15 minutes at 4°C to remove cellular debris; protein containing cell lysate supernatant was removed and stored at -80°C. Patient plasma samples were centrifuged at 13000rpm for 15 mins for cell debris clearing and stored at -80°C before measuring protein concentration.

2.8.2 Determination of protein concentration – Bradford Assay

The protein concentration of cell lysates and patient plasma was measured using the Bradford assay. This assay utilises the binding of acidic Coomassie Blue G-250 to positive amine groups of amino acids. Protein binding induces an absorbance shift from 465nm to 595nm and a solution colour change from red/brown to blue.[308] The absorbance at 595nm can be measured with a spectrometer and the protein concentration of cell lysates extrapolated from a standard curve generated by a set of BSA protein standards with increasing known protein concentration.

A 96-well flat-bottom plate was prepared by adding 100µl of 1X Bio-Rad protein assay dye reagent to the appropriate number of wells (Appendix I, 8.2); protein standards and test samples were assayed in triplicate. Increasing concentrations of BSA protein standard were prepared by

diluting different volumes 0.5mg/ml BSA stock solution (Appendix I, 8.3) in 100µl Bio-Rad protein assay dye reagent to generate a standard curve (Table 4). Test protein lysates were diluted 1:10 and patient plasma 1:100 in deionised water to ensure spectrometer readings were within a measurable range. 1µl of diluted cell lysate was mixed with 100µl 1X Bio-Rad reagent. The absorbance was measured at 595nm on a spectrophotometer and protein concentrations calculated by linear regression using the equation y=mx+c, where y is the average sample absorbance at 595nm and x is protein concentration (µg/µl).

Table 4. BSA standard curve for Bradford assay.

0.5mg/ml BSA (µl)	BSA Concentration (µg)
0	0
0.5	2.5
1	5
2	10
4	20

2.8.3 Western blotting procedure

After determination of cell lysate protein concentration, 50µg protein containing cell lysate was made up to a final volume of 24µl in cell lysis buffer with 6µl 4X LDS loading buffer (to give a final 1X LDS buffer concentration). Plasma samples were incubated with 0.5mg/ml DNase for 5 minutes at room temperature, before diluting in 30µl cell lysis buffer and 10µl 4X LDS loading buffer. Samples were boiled for 10 minutes at 90°C to ensure full protein denaturation. The wells of a 12-well NuPAGE 4-12% Bis-Tris gel were rinsed with 1X MOPS running buffer (Appendix I, 8.4) before loading 20µl of denatured sample lysate per well. 4µl of MagicMark Western blotting molecular weight ladder was diluted in 20µl LDS sample loading buffer and loaded onto the first well. Where reducing SDS-PAGE was used, 2.4µl of 10X NuPAGE® reducing agent was added to LDS sample buffer and NuPAGE antioxidant included in MOPS running buffer (Appendix I, 8.5). Proteins were separated by gel electrophoresis at 200V for 50 minutes in 1X MOPS running buffer and transferred by semi-dry method onto pre-methanol soaked and transfer buffer pre-balanced PVDF membranes for 1 hour at 20V (Appendix I, 8.6). Non-specific binding was blocked by incubating in polyvinylpyrolidine (PVP) blocking buffer (Appendix I, 8.7) with rocking for 1 hour at room temperature. Membranes were incubated with primary antibody in 10ml PVP blocking buffer for 1 hour at room temperature with rocking (Appendix I, 8.8; Table H), or overnight at 4°C in PVP blocking buffer with 10% azide to limit bacterial growth (Appendix I, 8.9).

Membranes were washed in 3 rounds of 10 minutes in TBST to remove unbound primary antibody and incubated with HRP-conjugated anti-rabbit or anti-mouse secondary antibodies in PVP blocking buffer (Appendix I, 8.7; Table H); azide inhibits HRP so was not included in this incubation. Membranes were washed for 3x10 minutes again with TBST and visualised by chemiluminescence. Enhanced chemiluminescent (ECL) HRP substrate was prepared immediately before use and 1ml applied to membranes for 5 minutes with rocking (Appendix I, 8.10). Luminol is oxidised in the presence of HRP and peroxide, producing chemiluminescene at specific antigen spatial locations. Protein bands were visualised using a FujiFulm LAS 4000 developer following 2-5 minute exposures. ECL was removed by washing membranes for 5 minutes with TBST and antibodies stripped using Western blot stripping buffer for 5 minutes, before re-blocking and re-probing as described earlier; GAPDH was used as a loading control for all Western blots.

2.9 Co-Immunoprecipitation (Co-IP)

Co-IP is a pull-down assay used to assess stable protein complexes in cell lysate or serum. In this study, co-IP was used to pull-down TLR9 from primary CLL cells and assess protein-protein interactions with MyD88 and RAGE in response to a variety of CLL-cell stimulations.[76] Primary antibody against a primary protein target is incubated with Dynabeads™ Protein A that bind with high affinity to IgG. The Dynabead-antibody complex is mixed with cell lysate to pull-down protein target complexes and removed from cell lysate by magnetic separation. The antibody-protein complexes are eluted form the Dynabeads™ Protein A solid support by denaturation and separated by SDS gel electrophoresis. Anti-IgG primary antibody is used as a negative pull-down control and non-precipitated whole cell lysate analysed on the same blot to assess target protein whole cell expression. The primary protein target is probed first (i.e. TLR9) to verify co-IP success, followed by re-probing for interacting proteins of interest (i.e. MyD88 and RAGE).

Procedure

5µg of mouse anti-TLR9 or anti-mouse IgG primary antibodies diluted in 200µl PBS with 0.02% Tween-20 (PBST; Appendix I, 9.1) were incubated with 1.5mg (50µl) of Dynabeads™ Protein A per treatment for 20 minutes at room temperature, with rotation. Dynabead-antibody complexes were washed with 1ml PBST followed by magnetic separation. 500µg protein-containing CLL cell lysate (procedure outlined in section 2.8.1) in 500µl cell lysis buffer (Appendix I, 8.2) was mixed with the Dynabeads™-antibody complex and incubated for 30 minutes at room temperature, with rotation. Following antigen incubation, Dynabeads™-protein complexes were removed from unbound cell lysate by magnetic separation and washed 3 times with 500µl PBST. During the final wash, Dynabeads™-protein complex mix was transferred to fresh Eppendorf tubes to prevent co-elution of non-specific proteins bound to the tube wall. Target protein and associated protein complex was eluted from Dynabeads™ by mixing with 20µl elution buffer (Appendix I, 9.2) and boiling samples at 100°C for 10 minutes to denature proteins. Dynabeads™ were separated from the denatured antibody and target protein complex mix by placing samples in the magnetic rack and 20µl of eluted protein supernatant loaded onto a 4-12% NuPAGE® Bis-Tris gel. Blots were probed with anti-TLR9, anti-MyD88 and anti-RAGE antibodies (Appendix I, 9.3; Table J, Table K) by Western blotting (outlined in section 2.8).

2.10 LC MS/Mass Spectrometry

LC MS/mass spectrometry is an analytical technique that combines the physical separation capabilities of liquid chromatography with the mass analysis capabilities of mass spectrometry. Measuring protein expression, using antibody-based methods gives a good indication of protein levels, but protein concentration does not always correlate with enzyme activity. LC-MS/MS phosphoproteomics can measure tens of thousands of phosphorylation sites per sample, whereas antibody technologies can only measure 10s-100s of phosphorylation sites per sample analysis. Therefore, we are able measure the markers of kinase activity directly (i.e. substrate phosphorylation). In this study, we will treat fresh CLL B-cells with HMGB1 and/or CpG-ODN (B class) and/or anti-RAGE neutralising antibody to identify the major signalling pathway(s) up- or down-regulated.

Cell pellets are prepared for LC MS/MS by a specific lysing buffer, containing non-detergent components with protease and phosphatase inhibitors to minimise degradation or artefactual modification of enzymes. Proteins will be reduced and alkylated with dithiothreitol and iodoacetamide, respectively, to irreversibly prevent free sulfhydryl's from reforming disulphide bonds. Proteins are then fragmented to peptides with trypsin, and samples de-salted to remove non-peptide ions that would be detected by mass spectrometry. Finally, peptide samples are enriched for phospho-peptides by titanium dioxide (Ti02) pull-down method, prior to LC-MS/MS, and bioinformatics analyses as in previous publications.[309,310]

2.10.1 Preparation of cell lysates

Freshly isolated CLL cells with a CD19+/CD5+ purity >90%, were left to rest *in vitro* for 2 hours in complete medium prior to cell stimulation. Following 2 hours rest, cells were seeded at a density of $10x10^6$ cells/ml for $30x10^6$ total primary CLL cells in FBS-free medium to limit cell signalling activation. Cells were then treated for 15 minutes and 2 hours with 10µl PBS, 200ng/ml HMGB1, 1µM CpG-ODN, 200ng/ml HMGB1 and 1µM CpG-ODN combined, and 2 hours only for 10µg/ml anti-RAGE neutralising antibody with 200ng/ml HMGB1. Where anti-RAGE antibody was used, cells were pre-blocked for 30 minutes with 10µg/ml anti-RAGE, before addition of HMGB1 for 2 hours.

To obtain protein from whole cells, cells were immediately placed on ice for 5 minutes to limit continuation and activation of further cell signalling. 500µl 1mg DNase (Sigma) was added to prevent cell clumping for 5 minutes before centrifugation at 1300rpm at 4°C for 5 minutes. Next, cells were carefully resuspended in 10ml PBS with phosphatase inhibitors (Appendix I; 10.1) (1mM Na3VO4 and 1mM NaF) and centrifuged at 1300rpm at 4°C for 5 minutes; this was

repeated twice. Samples were then lysed in 500µL ice-cold denaturing lysis buffer (8M urea with phosphatase inhibitors) (Appendix I; 10.2) for 15 minutes before being sonicated (40 cycles; 30 seconds on; 30 seconds off; high intensity at 4°C). Following sonication, samples were left on ice for 5 minutes before being centrifuged at 16,400rpm for 15 minutes at 4°C. Protein concentration was measured using the Pierce Bicinchonic (BCA) Protein Assay Kit (Thermo Scientific). A standard curve was created using the provided Albumin Standard Ampules. The protein sample aliquots were dispensed in triplicates onto a 96-well plate. BCA working reagent was prepared by mixing Reagent A and Reagent B 50:1 and was added to each well as per the manufacturer's protocol. Following incubation at 37°C for 30 minutes, absorbance was measured using a spectrophotometer set at 562m. The protein concentrations of each sample were calculated from the mean values of the technical triplicates. Lysates were then normalised to 350µg/300µl urea (Appendix I, 10.2).

2.10.2 Trypsin digest

First, 3µl 1M Dithiothreitol (DTT) was added to each sample and left on a shaker at 24°C at 1200rpm for 30 minutes in the dark. Next, 12 µl 415mM iodoacetimide (IAM) was added to each sample and left on a shaker at 24°C at 1200rpm for 30 minutes in the dark. Samples were then diluted with 1250 µl HEPES (pH 8.0).

During the IAM incubation, trypsin beads were conditioned as follows. The appropriate volume of mobilised trypsin beads was aliquoted into a 1.5ml LoBind Eppendorf tube and centrifuged at 2000Xg at 4°C for 5 minutes. After the supernatant was removed, the volume of remaining beads was calculated and washed by adding an equal volume of HEPES (Appendix I; 10.3) and centrifuging the beads at 2000Xg at 4°C for 5 minutes. The wash step was repeated 3 times before the final addition of an equal volume of HEPES. 100 µl trypsin beads were added to each lysate sample and left overnight with agitation at 37°C in the dark.

2.10.3 De-salting for phosphoenrichment

A vacuum manifold block was first set to ~5 inHg and the necessary number of OASIS 1cc HLB (10mg) cartridges were inserted into the manifold. Waste containers were positioned underneath each cartridge. The cartridges were first conditioned with 1ml 100% Acetonitrile (ACN). Next, cartridges were incubated with 1mL 99% H_2O; 1% ACN; 0.1% Trifluoroacetic acid (TFA), followed by 0.5ml of the same solution. The samples were then loaded into the cartridges and the flow rate was kept as low as possible. The cartridges were then washed with 0.75ml 99% H_2O; 1% ACN; 0.1% TFA. The taps and cartridges were then completely purged, and the waste

containers were replaced with fresh 2ml LoBind Eppendorf tubes. Finally, the samples were eluted with 0.25 mL 1M glycolic acid (80% ACN; 5% TFA).

2.10.4 Phosphopeptide-enrichment

For each sample, 50µg of TiO_2 beads were used per 1µg protein. First, the OASIS eluted fraction volumes were all normalised to 500µl with 1M Glycolic acid (80% ACN; 5% TFA). 17.5mg of re-suspended TiO_2 beads were added to each eluted fraction and samples were incubated for 5 minutes with rotation.

During this time, the Glygen EMPTY (TF2EMT) tips were equilibrated. The Glygen EMPTY SpinTips were placed in 2ml Eppendorf tubes 200µl 100% ACN was applied. The SpinTips were centrifuged for 3 minutes at 1500Xg and the flow-through was discarded.

After the samples had been incubated with TiO_2 for 5 minutes, samples were centrifuged for 30 seconds at 2000rpm. 400µl of the remaining supernatant was removed and transferred to a fresh 1.5ml LoBind Eppendorf tube and placed on ice. The TiO_2 beads were then resuspended in the remaining solution and 100µL of the re-suspended sample was transferred to the empty SpinTips and centrifuged for 2 minutes at 1500Xg. 100µl of 1M Glycolic acid (80% ACN; 5% TFA) was added to the sample tube to re-suspend the remaining TiO_2 beads before being transferred once again to the SpinTips and centrifuged for 2 minutes at 1500Xg. The flow-through was discarded and the remaining 400µl previously aliquoted samples were transferred to the TiO2-filled SpinTips (2x200µl batches) and centrifuged for 3 minutes at 1500Xg. Next the SpinTips were washed with 100µl 1M Glycolic acid (80% ACN; 5% TFA), 100µl 100 mM Ammonium Acetate (25% ACN) and 100µl 90/10 H_2O/ACN each time being centrifuged for 2 minutes at 1500rpm. The final wash step with100µl 90/10 H_2O/ACN was repeated a total of three times to ensure complete removal of non-phosphorylated peptides.

SpinTips were then transferred to fresh 2ml LoBind Eppendorf tubes and 50 µL 5% NH4OH (10% ACN) was applied to each SpinTip. Spintips were centrifuged for 2 minutes at 1500g and the flow-through was retained. This step was repeated three times to elute phosphopeptides from the TiO_2 layer. The pooled elute from each sample was then snap-frozen in dry ice and placed in speed-vac to dry overnight. Finally, samples were stored at -80°C and were reconstituted before being analysed by liquid chromatography tandem mass spectrometry.

2.10.5 Bioinformatic analysis

Mass spectrometry data is interpreted by matching the mass to charge ratios of fragment ions in mass spectrometry spectra, to peptide fragments of all proteins. The MASCOT search engine is used to compare peptide sequences against those in the UNITPROT database.[311] Once the peptides have been derived, the localisation of phosphorylation sites is determined using the MASCOT delta score, which compares scores for both the probability of correct peptide sequence identification and phosphosite localisation.[311] As LC-MS/MS phosphoproteomics measures the markers of kinase activity directly (i.e. substrate phosphorylation), enzyme activity can be inferred using algorithms such as Kinase Substrate Enrichment Analysis (KSEA).[310] A single mass spectrometry experiment can measure thousands of phosphosites, which can be analysed using the PhosphoSitePlus database. All phosphorylation sites are targeted by a given kinase, meaning they can be grouped together in a substrate set. For KSEA, the log2- fold change of the abundance of a phosphosite between the initial and treated samples is compared.[310] Therefore, KSEA activity scores describe the activity of a kinase in one condition relative to another.

2.11 Molecular Biology Techniques

Soluble RAGE is not commercially available, so to assess the *in vitro* effects of sRAGE, endogenous-secreted RAGE (esRAGE) containing conditioned media was produced by transfecting HEK293 cells with esRAGE plasmid. HEK293 cells express low levels of full-length RAGE (FL-RAGE), so FL-RAGE transfected HEK293 cells were used as a positive control for membrane RAGE shedding assays.

2.11.1 Plasmid Selection

20µg of plasmid DNA for FL-RAGE and es-RAGE on a pcDNA3 backbone were purchased from HMGBiotech via IBL International (Appendix I, 11.1); inserted FL-RAGE and es-RAGE sequences were not given. Dried plasmid DNA was reconstituted to 1.4µg/µl and 0.768µg/µl in RNase-free water for FL-RAGE and es-RAGE, respectively, and stored at -20°C. The pcDNA3 vector includes a CMV promoter for mammalian expression and genes for ampicillin bacterial resistance and neomycin selectable marker.

2.11.2 Bacterial Inoculation

Prior to transfection, plasmid DNA is expanded by transformed competent bacteria and subsequently purified for downstream transfections. For this study, Subcloning Efficiency™ DH5α™ Competent Cells were used, a chemically altered strain of E. coli that provides higher transformation efficiencies. Competent cells were thawed on ice and 50µl of DH5α cells mixed with 10ng of FL-RAGE and es-RAGE pcDNA3 plasmids, and 250pg of provided pUC19 empty vector control; competent cells were incubated on ice for 30 minutes. Cells were then heat shocked at 42°C for 20 seconds in a heat block to promote plasmid uptake and placed back on ice for 2 minutes to recover. After transformation, 950µl of pre-warmed luria broth (LB; Appendix I, 11.2) was added to tubes and incubated at 37°C for 1 hour with shaking to allow plasmid expression and ampicillin resistance. LB-agar 10cm plates with 100µg/ml ampicillin were prepared in a sterile environment with a working flame (Appendix I, 11.3) and stored at 4°C before use. 50µl and 200µl of FL-RAGE, es-RAGE and pUC19 transformed cells were streaked onto ampicillin-agar plates and left to incubate overnight at 37°C; different volumes of transformed cells were plated to ensure well-spaced colonies were produced. Following overnight incubation, single colonies were picked using a sterile filtered tip and inoculated into 4ml pre-warmed LB media with 100µg/ml ampicillin. Bacterial inoculation was incubated at 37°C for 8 hours with shaking (300rpm); then 2.5ml diluted in 25ml pre-warmed LB media and incubated at 37°C for 8 hours with shaking (300rpm) to promote logarithmic growth of bacteria before harvesting. Glycerol stocks of bacterial inoculation were stored by mixing 500µl of

overnight culture with 500µl 50% glycerol in a cryovial at -80°C (Appendix I, 11.4); this method stabilises alive transformed frozen bacteria for many years. When used, a sterile filtered tip was used to scrape some frozen bacteria which were then spread onto pre-warmed ampicillin-agar plates.

2.11.3 Plasmid Purification

Following overnight bacteria culture, plasmid DNA was isolated by alkaline lysis and isopropanol precipitation using the QIAGEN midiprep purification kit; all buffers used were included in the kit. Bacteria were harvested by centrifugation at 6000xg for 15 minutes at 4°C and the bacteria pellet was resuspended in 4ml resuspension buffer (50mM Tris-Cl, 10mM EDTA; pH 8.0) with 100µg/ml RNase. Bacteria were lysed with 4ml lysis buffer (200mM NaOH and 1% SDS) at room temperature for 5 minutes. Cell lysis was stopped by addition of 4ml ice-cold neutralisation buffer (3M potassium acetate; pH 5.5), mixed and incubated on ice for 15 minutes to enhance formation of genomic DNA, protein and cell debris precipitate. Bacterial lysate was centrifuged at 20,000xg for 30 minutes at 4°C and the supernatant containing plasmid DNA was removed immediately; the lysate was cleared again by centrifugation at 20,000xg for 15 minutes at 4°C and supernatant removed. A QIAGEN-tip 100 was equilibrated with 4ml equilibration buffer (750mM NaCl, 50mM MOPS, 15% isopropanol and 0.15% Triton X-100) and drained by gravity-flow, before loading all the cleared plasmid DNA supernatant from the previous step. Unbound plasmid DNA was washed from the QIAGEN-tip 100 column with 2x 10ml wash buffer (1M NaCl, 50mM MOPS, 15% isopropanol; pH 7.0) and drained by gravity-flow. Plasmid DNA was eluted and collected in 5ml elution buffer (1.25M NaCl, 50mM Tris-Cl, 15% isopropanol; pH 8.5). DNA precipitation was performed addition of 3.5ml isopropanol to eluted DNA at room temperature to avoid salt precipitation, mixed and centrifuged at 15,000xg for 30 minutes at 4°C. Supernatant was removed and the DNA-isopropanol pellet washed with 2ml 70% ethanol to remove precipitated salt. DNA was centrifuged again at 15,000xg for 10 minutes at 4°C. Isopropanol and ethanol supernatant was removed and plasmid DNA pellets air-dried for 10 minutes. Plasmid DNA was dissolved in 500µl TE buffer (10mM Tris-Cl; pH 8.0; Appendix I, 11.5) and DNA yield and purity assessed with a NanoDrop 2000 spectrophotometer.

2.11.4 DNA Quantification – NanoDrop Spectrophotometer

Purified plasmid DNA concentration and purity was assessed by measuring absorbance at 260nm using a NanoDrop 2000 spectrophotometer. The NanoDrop was blanked with 1µl TE buffer, then 1µl of each sample measured in duplicate at 260nm. DNA purity was assessed by measuring the 260nm/280nm nucleic acid to protein ratio. Es-RAGE plasmid concentration was 702ng/µl; FL-

RAGE plasmid concentration was 475ng/µl; pUC19 plasmid concentration was 78ng/µl. 50µl aliquots were stored at -20°C.

2.11.5 Restriction Digest

A diagnostic restriction digest was performed to verify purification of the correct plasmid by analysing plasmid DNA fragments separated by gel electrophoresis. FL-RAGE and es-RAGE plasmids were cut into fragments using BamHI and Sma1 restriction enzymes; these enzymes were chosen based on known restriction sites in the pcDNA3 backbone and different cut sites in FL-RAGE and es-RAGE sequences, and restriction enzyme availability (Appendix I, 11.6). 1µg of FL-RAGE and es-RAGE plasmid DNA was mixed with 2µl fast digest green buffer and 12µl nuclease free water. Plasmid DNA was either left uncut, subject to single digest or subject to double digest by addition of 1µl nuclease free water, 1µl of BamHI or Sma1, or with 1µl of both BamHI and Sma1, respectively. Samples were heated to 37°C for 5 minutes in a heat block to activate enzyme activity, then heated to 80°C for 5 minutes to inactivate restriction enzymes. Digest products were separated by gel electrophoresis using a 1% agarose gel in Tris-base, boric acid and EDTA (TBE) buffer containing GelRed nucleic acid stain, at 50V for 1 hour (Appendix I, 11.7). Digested nucleic acid products were imaged using the Gene Flash Syngene Bio Imager.

2.11.6 HEK293 Cell Line Transfection

HEK293 adherent cell line was used as a vehicle for the expression of FL-RAGE and es-RAGE pcDNA3 plasmids due to the ease of transfection and production of conditioned media. Polymer based jetPRIME® reagent was used for transient DNA transfection based on high transfection efficiency and very low cytotoxicity. $1x10^6$ HEK293 cells were cultured in 10ml RPMI complete growth medium in $75cm^2$ flasks and cultured at 37°C in a humidified 5% CO_2 incubator until cells were 60-80% confluent. At the time of transfection, 5µg of FL-RAGE, es-RAGE and empty pUC19 plasmid DNA were mixed with 500µl jetPRIME® buffer and 10µl jetPRIME® reagent (Appendix I, 11.8) and incubated for 10 minutes at room temperature to promote formation of plasmid-polymer complexes. 500µl of transfection mix was added to the medium of cells in a dropwise manner and left for 4 hours at 37°C in a humidified 5% CO_2 incubator with gentle rocking. After 4 hours, HEK293 cells transfected for conditioned medium were washed with sterile PBS and resuspended in serum-free RPMI medium for 24 hours. Then, conditioned medium was collected by centrifugation at 2000rpm for 5 minutes and passed through a 0.22µM filter; conditioned medium was stored at 4°C and used for *in vitro* assays within 24 hours. HEK293 cells transfected for FL-RAGE or es-RAGE HEK293 cell expression were resuspended in fresh RPMI complete growth medium after 4 hours of transfection and left for 24 hours before harvesting.

After 24 hours, cells were pelleted by centrifugation at 1500rpm for 5 minutes, washed with ice cold PBS and used for western blot cell lysates or flow cytometry analysis. A pLenti6-GFP expressing plasmid was included in the transfection step as a control to evaluate transfection efficiency after 24 hours using a Nikon inverted wide-field microscope.

2.12 Statistical Analysis

2.12.1 General statistical Analysis

IBM SPSS 22 and GraphPad Prism 5.03 statistical software were used for data analysis. Data are shown as either mean ± standard deviation (SD) or median with interquartile range when variation was high. All pairwise comparisons were analysed using the Mann-Whitney U test between groups with unequal size and the student's t test for equal sized groups. For comparisons of more than 2 groups, One-Way ANOVA was used. Correlations were analysed by Pearson product-moment correlation to assess the linear correlation between 2 groups. Statistical significance for all tests was set at 0.05. *, ** and *** indicate P value < 0.05, 0.01, or 0.001., respectively.

2.12.2 Obtain cut off point using X-tile

Continuous data, generated from LN TMA RAGE, TLR9 and Ki67 expression, was categorised into subgroups based on the levels of biomarker expression and patient overall survival outcome using X-tile software.[312,313] Categorising variable expression into subsets is a clinically relevant method, but there is currently no standardised statistical method to determine optimal data cut points for expression variables that don't have prior defined subsets. X-tile software avoids the statistically invalid method of hunting for the best P-value (outcome-oriented) or dividing the cohort 1:1 (data-oriented) by dividing continuous data into 1:2 test/validation sets.[313] Different data divisions are assessed in the 'test' cohort and then applied to the 'validation' cohort. The software then produces the optimal number of cut points with associated P-values based on applying the test-defined cut points to the validation dataset. Using X-tile helps to identify sub-populations of expression biomarkers rooted with unknown biology which would otherwise be left unnoticed.

2.12.3 Survival Analysis

The association between protein expression and overall survival (OS) was analysed by uni-and multivariate Cox regression analysis on both continuous and categorical variables to increase statistical robustness. OS, meaning death from any cause was used to measure outcome from the date of diagnosis, to event occurring, or date of last follow up. Variables assessed as continuous data was used to determine the prognostic impact of each variable by the Cox proportional hazards model. Hazard ratios (HR) with 95% confidence intervals for OS outcome were generated using this method for continuous RAGE, TLR9, Ki67 biomarkers and age. Continuous data were divided into categories based on levels of biomarker expression using X-

tile described earlier. Chi-square test was used to analyse the frequency of distribution between 2 categorical variables. P-values and HR with 95% confidence intervals for categorical data defined by these cut points were measured by Cox regression analysis, and Kaplan-Meier survival curve analysis using a log-rank test.

Chapter III

Assess the prognostic impact of HMGB1 receptors RAGE and TLR9 and their effects on CLL overall survival

3.1 Introduction

CLL is a highly diverse and heterogeneous disease, reflected in variations in prognostic biomarkers and genetic aberrations in patients. The disease heavily relies on microenvironmental interactions for external survival signals, densely located in the CLL LN.[47] Although increased CLL cell proliferation is highly observed CLL LNs compared to quiescent cells in CLL PB, CLL LN biopsies are not routinely removed and examined to aid in CLL diagnosis or disease staging. Correlation of PB markers with CLL LN biology would give deeper insight into CLL pathogenesis and more accurate disease staging.

The Rai and Binet staging criteria are routine classical systems to classify CLL disease based on clinical features such as thrombocytopenia, lymphadenopathy and lymphocytosis (low to high risk is A-C and 0-III, respectively).[84,85] However, these staging systems do not provide an understanding of the underlying molecular biology that could be used to classify disease. CLL patients can be stratified into aggressive and indolent subsets based on IGHV gene region mutation status.[50] Approximately 35% of patients carry unmutated IGHV gene regions in CLL (U-CLL) and have a worse prognosis (predicted mean survival of 8 years), compared to patients with mutated IGHV genes (M-CLL; predicted mean survival of 24 years).[51] Both CLL subsets share a similar gene expression profile except for a marked increase in ZAP70 and CD38 expression in U-CLL.[93] Other risk factors associated with poor disease outcome include cytogenetic aberrations del(17p), del(11q), trisomy 12, and genetic lesions in NOTCH1, SF3B1, TP53, ATM, PAX5, MYD88 contributing to disease pathogenesis.[49,314,315]

The CLL LN harbours the proliferative CLL fraction, indicated by enhanced activation of BCR signalling pathways, NF-κB activation, c-MYC, E2F and Ki67 expression.[47] The CLL LN is a niche site, rich in tumour-associated cells and inflammatory cytokines, chemokines and mediators that sustain CLL cell survival. This molecular and cellular understanding is translating into emerging therapies to target CLL such as Ibrutinib and PDL1 blockade. One established CLL microenvironment interaction includes HMGB1; our group identified increased levels of HMGB1 in the plasma of CLL patients, inducing the differentiation of NLCs and associated with poorer clinical outcome.[76] The main HMGB1 receptors include TLR2, TLR4, TLR9 and RAGE, but expression levels of these receptors and usage in CLL cells in sites of active proliferation is unknown. HMGB1 has dual roles in cancer, capable of both pro- and anti-tumour responses by activating various immune cell subsets. Although increased plasma HMGB1 levels are associated with poorer clinical outcomes in CLL, it is yet to be established if the HMGB1-receptor signalling axis results in pro- or anti-tumour responses in CLL. Assessing receptor expression and

determining the prognostic significance of these receptors in the CLL LN will give an indication of the outcome response.

With increasing development of signalling inhibitors and therapies that target and shape the CLL microenvironment, easily attainable biomarkers that correlate with LN biology would give deeper insight into disease pathogenesis and therapy choice, i.e. plasma HMGB1 and LN HMGB1 receptor expression. Moreover, better biomarkers of inflammation could be used as feasible monitors in a clinical setting to assess microenvironment polarisation and predict disease outcome.

The work in this chapter will determine i) the main HMGB1 receptors in CLL; ii) if HMGB1-receptor signalling is pro- or anti-tumour; and iii) if HMGB1 receptor expression could be used as a clinical prognostic marker for CLL.

3.2 Results

3.2.1 RAGE and TLR9 expression is heterogeneous among CLL patients and lower compared to RA-LN tissue

Using available gene expression datasets,[316] we first determined gene expression of HMGB1 receptors RAGE, TLR2, TLR4 and TLR9, and of all other TLRs in CLL patient peripheral blood samples compared to age-matched healthy controls.[316] RAGE and TLR9 gene expression is significantly increased in CLL patients compared to age-matched controls (P<0.01 and P<0.001, respectively; Figure 3-1). Whereas, TLR2 and TLR4 have significantly lower gene expression. Although mRNA levels are not accurate indicators of protein levels, this data combined with reports of low TLR4 protein expression in CLL suggests RAGE and TLR9 are the most likely candidate receptors for HMGB1 in CLL cells.[76,317]

For other non-HMGB1 receptor TLRs, TLR7 gene expression was significantly increased compared to controls (P<0.001), owing to a mature B-cell phenotype and a similar TLR expression profile as memory B-cells.[317-319] TLR8 expression was significantly decreased (P<0.001).

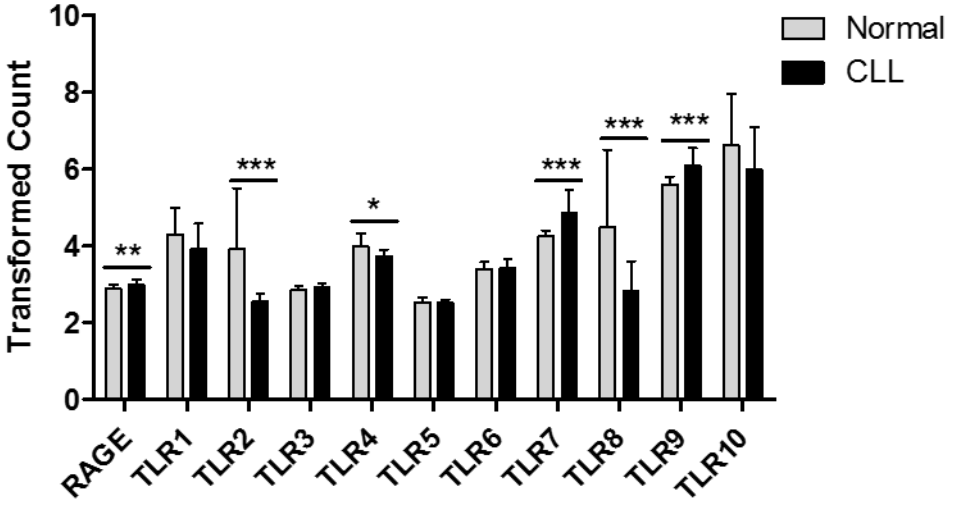

Figure 3-1 RAGE and TLR gene expression in CLL patient PB B-cells and age-matched healthy control PB B-cells
Comparison of RAGE and TLR1-10 mRNA expression in CLL PB B-cell to normal PB B-cells; n=41 and n=11, respectively. Levels of mRNA expression were obtained from an available GEO dataset assessing gene expression profiles of untreated CLL patient samples.[316] Transformed count represents log2 transformed and RMA normalised mRNA expression data. Data are presented as mean ± SD and differences compared with an unpaired Mann Whitney U test; P<0.05*, P<0.01*; P<0.001*.

To establish HMGB1 receptor expression in the LN of CLL patients, a key site of microenvironment CLL pathogenesis, we performed IHC on LN tissue biopsies arrayed onto TMAs from a cohort of 91 CLL patients and compared to RA-LN TMAs from 42 healthy controls.[47]

CLL LN biopsies were sourced from CLL patients who were either untreated or post-treatment, where tissue biopsies were removed to aid in diagnosis or assess disease progression; RA-LN biopsies were sourced from non-malignant patients.

TMA slides were stained for RAGE and TLR9 in antibody-specific batches, for accurate comparison, and protein expression image analysis performed using the Ariol automated digital analysis software. CD5 positive areas in CLL LN cores were selected for analysis to maximise malignant CLL cell-only expression measurements (Appendix Figure 5), and germinal centres of RA-LNs were selected to represent an activated B-cell control comparison (Figure 3-2A and C). RAGE protein expression, i.e. the intensity of brown DAB staining in LN cores, was measured using the Ariol shape and colour image classifiers. First, LN core cell number was determined using blue haematoxylin-stained nuclei to train the cell shape classifier. Second, the intensity of brown staining for each cell was measured using colour classifier, trained based on saturation, hue and intensity of brown pixels. Minimum thresholds were set that excluded brown background staining to ensure only strong positive brown pixel/protein expression was measured (Figure 3-2). Once the training algorithm was optimised by combining these 2 image classifiers per antibody stain, it was applied to all TMAs; the use of automated image analysis limits error, bias and variability between TMAs.

RAGE and TLR9 protein levels are expressed as the percentage of positive cells for brown staining in the LN core. Mean percent-positive staining was calculated for each stain per patient. Incomplete or damaged LN cores were excluded from analysis and patients with less than 2 full intact LNs were discarded to limit LN bias; 17 patients were discarded from analysis leaving 91 CLL patients in total.

Comparing LN protein expression, RAGE expression is localised to cell cytoplasm and cell membranes in CLL LNs, and highly expressed in the LN proliferation centre (Figure 3-3B; indicated by white arrow and assessed by our in-house histopathologist, Andrew Clear). In RA-LNs, RAGE is highly expressed in the germinal centre where B-cells proliferate and mature, but not in the mantle zone where small naïve B-cells are packed (Figure 3-3A). TLR9 is localised to the cytoplasm of nearly all cells in CLL-LNs and expressed strongly in mantle zone B-cells, and to a weaker extent in the germinal centre of RA-LNs (Figure 3-3C and D).

Overall RAGE and TLR9 expression in CLL-LNs were significantly lower when compared with the germinal centre in RA-LNs ($P<0.0001$; Figure 3-4). The vast range in RAGE and TLR9 CLL-LN expression levels (0.8-100% and 3.4-90.7%, respectively) indicate HMGB1 receptor expression is highly heterogeneous among CLL patients, and the levels of these receptors are lower compared with areas of inflamed tissue.

This data may reflect the clinical heterogeneity in CLL disease and the variability in microenvironment dependence among CLL patients. The RA-LN data highlights the routine role of RAGE in a healthy setting as an endogenous stress-response receptor and the involvement of TLR9 signalling. Our findings suggest that CLL patients do express RAGE and TLR9 proteins in niche microenvironment sites of CLL-cell proliferation, in line with the gene expression data, and provides us with rationale to further investigate the clinical significance of receptor LN expression.

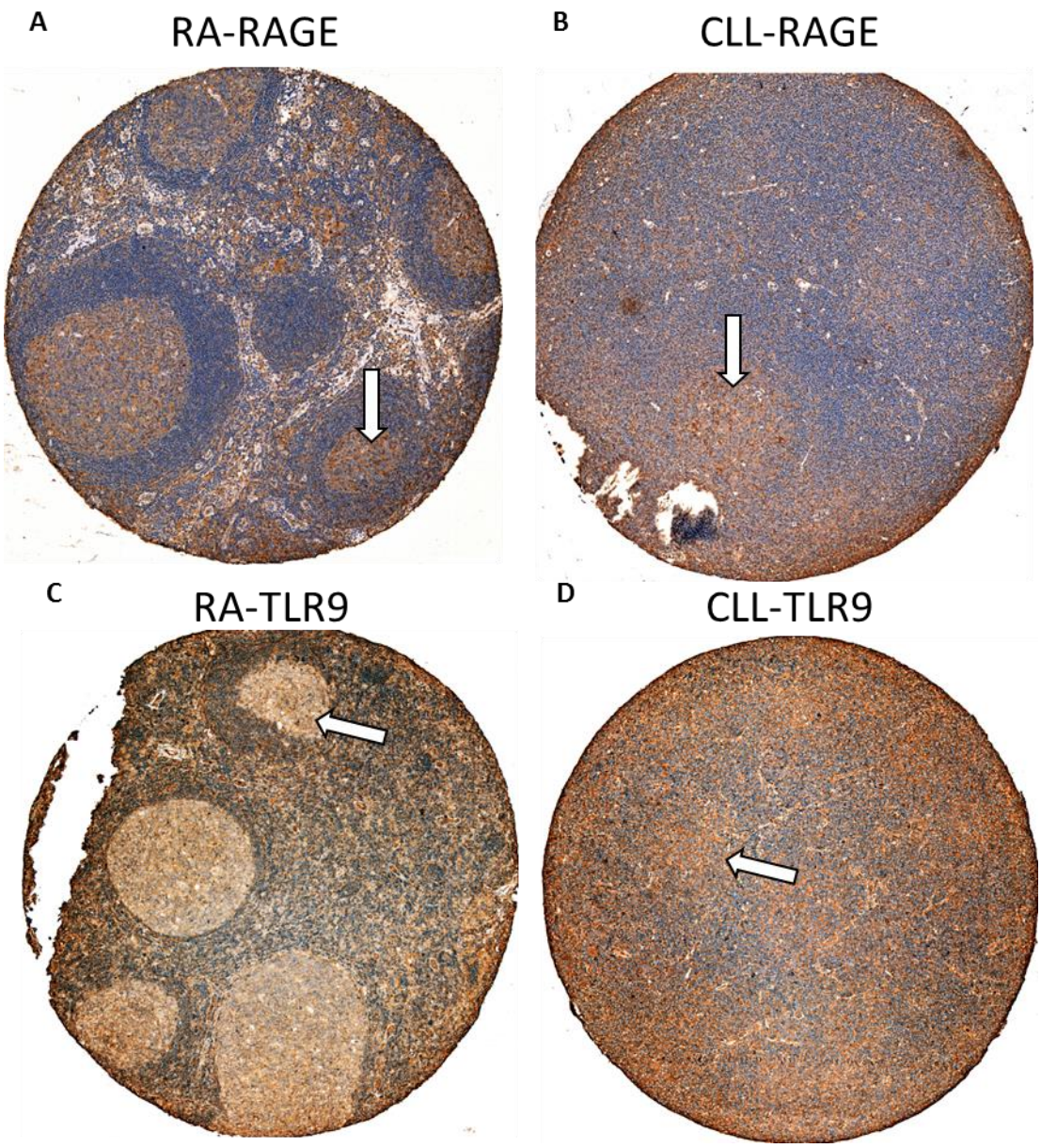

Figure 3-2 Representative images of immunohistochemical staining of RAGE and TLR9 in primary CLL and RA-LN tissue

Representative 5x magnified images of RAGE and TLR9 staining in primary CLL and RA LN tissue biopsies (A-D). CLL and RA TMAs were constructed by Andrew Clear and stained with monoclonal mouse anti-RAGE (A and B) and mouse anti-TLR9 antibodies (C and D) under optimal conditions; nuclei were visualised in blue by staining with haematoxylin. Antibody-antigen interactions were visualised using a peroxidase-labelled system with 3,3'-diaminobenzidine (DAB) chromogen to give brown staining (Super-Sensitive Polymer-HRP IHC Detection System). Weak background brown staining was excluded by selecting strong, high intensity brown pixels during image analysis training. Germinal centres of RA-LN were selected for image analysis, highlighted by white arrows (A and C), and CD5+ areas (Appendix Figure 5) for CLL LN whole cores (B and D).

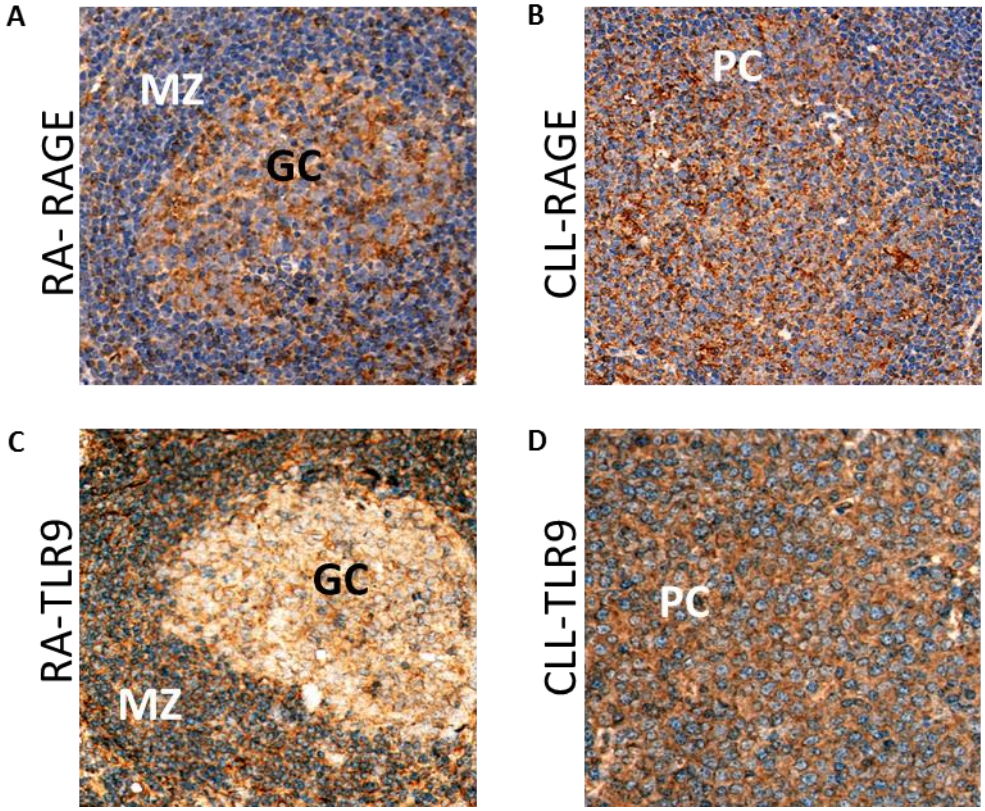

Figure 3-3 RAGE and TLR9 expression in CLL-LN and RA-LN
20x representative immunohistochemical staining images for RAGE and TLR9 in RA-LN (A and C) and CLL-LN (B and D). Proteins were stained with either mouse anti-RAGE antibody or mouse anti-TLR9 antibody and visualised in brown with DAB chromogen; nuclei of cells are stained blue with haematoxylin. 'GC', 'MZ' and 'PC' indicates germinal centres, mantle zone and proliferation centre (determined by KI67 IHC staining), respectively assessed by Andrew Clear and Professor Maria Calaminici. Magnification x20.

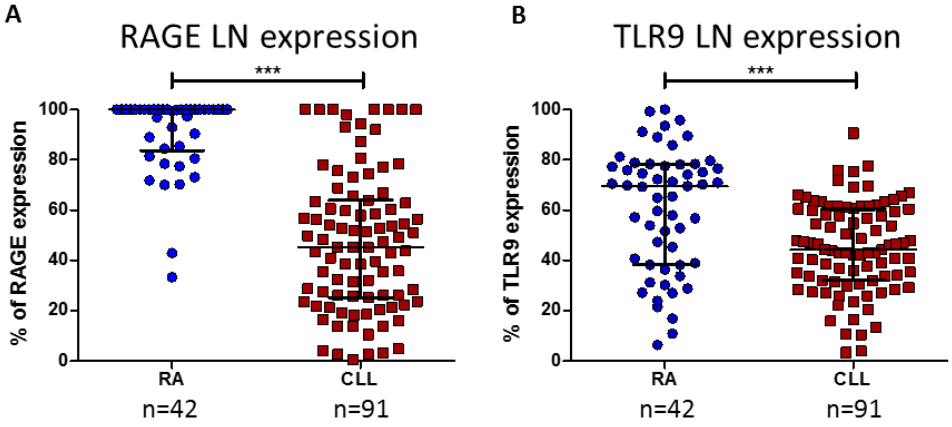

Figure 3-4 Comparison of RAGE and TLR9 expression in whole CLL-LN core with RA-LN germinal centres
Expression levels of RAGE and TLR9 previously stained by IHC and were quantified using the ARIOL digital imaging analysis software. Protein expression were calculated as the % of cells positive for brown staining in the LN core based on colour and shape image classifiers. Positive high intensity brown staining was selected based on hue, saturation and pixel intensity to remove background staining, and cell number determined by blue nuclear staining. Non-viable tissue was removed from image analysis. Statistical differences in % of protein expression between germinal centres of RA LN (n=42) and CD5+ areas of CLL LN (n=91) for RAGE (A) and TLR9 (B) was analysed by an unpaired Mann Whitney U test. Data are presented as medians with interquartile range; $P<0.0001$***.

3.2.2 RAGE expression is associated with cell proliferation and worse prognosis

Next, we determined the correlation between RAGE and TLR9 LN protein expression to infer a possible relationship between these 2 proteins in CLL disease pathogenesis. Then, we determined the strength of linkage between RAGE and TLR9 LN expression with established cell cycle proliferation marker, Ki67, and poor prognostic and aggressive disease marker, ZAP70, assessed by IHC for the same CLL LN TMA patient cohort.

Using Pearson's multiple correlation analysis, the levels of RAGE and TLR9 had a significant positive correlation (*P*<0.0001; R=0.416; Figure 3-5). This observation suggests the proteins could function in a co-linked manner, facilitating delivery of CpG-ODN to TLR9 via interaction with HMGB1, and internalisation by RAGE. However, TLR9 has other reported roles in CLL; TLR9 stimulation results in dichotic cell proliferation or cell death responses, dependent on IGHV mutational status.[96,318] The correlation coefficient between RAGE and TLR9 was R=0.416. RAGE expression is further positively correlated with ZAP70 (P<0.05; R=0.263; Figure 3-5) and strongly with Ki67 (P<0.0001; R=0.573; Figure 3-5). TLR9 LN expression also exhibited a significant positive correlation with Ki67 (P<0.0001; R=0.488; Figure 3-5), but not with ZAP70 expression. Although ZAP70 expression data used in this study originated from LN, expression scoring correlates with ZAP70 PB expression score (Appendix Figure 7).

Ki67 expression is strictly associated with cell proliferation and is present in the nuclei of cells during active phases of the cell cycle (G1, S, G2, and M phases) and absent during resting phase (G0).[320] For these reasons, Ki67 is used as an established cell proliferation marker. Correlation of both RAGE and TLR9 with Ki67 in CLL LNs, highlights an active role in mediating CLL microenvironmental interactions to induce and sustain CLL cell survival. The association between RAGE and ZAP70 does imply RAGE expression is more prevalent in aggressive CLL subsets, as ZAP70+ expression is highly restricted to unmutated CLL,[92] but this will require further investigation to fully define CLL subset specificity. The lack of correlation between TLR9 and ZAP70 could be explained by the opposing cell death/proliferation responses following TLR9 stimulation in either unmutated or mutated CLL.[96] However, further separation of this cohort of patients into ZAP70+ and ZAP70- did not reveal a significant difference in TLR9 LN expression for this cohort or patients (Appendix Figure 6).

Following a significant positive correlation with Ki67, we assessed the association between RAGE and TLR9 LN expression with proliferation centre size (assessed by expert histopathologist Maria Calaminici) and CLL disease Binet staging available on our clinical database. RAGE expression was significantly higher in LN cores with large proliferation centres (P<0.05; Figure 3-6A) compared to no association for TLR9. This result strengthens a proliferation role for RAGE, in

combination with previous data. Again, the lack of association for TLR9 is due to the opposing cell death/cell proliferation functions of receptor stimulation in CLL. No association between Binet staging and RAGE or TLR9 expression was observed for this cohort of patients (Figure 3-6B and D), and only a positive correlation between trisomy 12 and % RAGE LN expression ($P<0.05$; Appendix Figure 8B).

These results suggest RAGE could have a pro-tumour role in CLL as RAGE is predominately expressed in proliferating CLL cells and associated with more aggressive disease. The positive correlation between RAGE and TLR9 suggests these proteins could function in a co-linked manner but also maintain separate roles in CLL, as have been demonstrated before for TLR9. Further investigating the effect of RAGE expression on CLL patient outcome will indicate a predominate pro- or anti-tumour role.

A

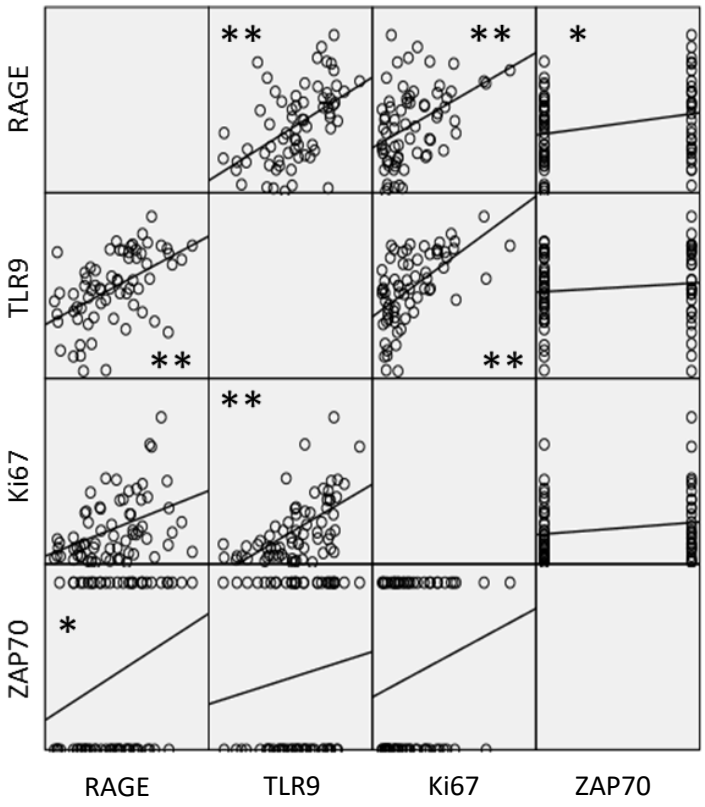

B

Correlations

		RAGE	TLR9	Ki67	ZAP70
RAGE	Pearson Correlation	1	.416**	.572**	.263*
	Sig. (2-tailed)		.000	.000	.030
	N	91	91	91	68
TLR9	Pearson Correlation	.416**	1	.488**	.120
	Sig. (2-tailed)	.000		.000	.331
	N	91	91	91	68
Ki67	Pearson Correlation	.572**	.488**	1	.181
	Sig. (2-tailed)	.000	.000		.140
	N	91	91	91	68
ZAP70	Pearson Correlation	.263*	.120	.181	1
	Sig. (2-tailed)	.030	.331	.140	
	N	68	68	68	68

**. Correlation is significant at the 0.01 level (2-tailed).

*. Correlation is significant at the 0.05 level (2-tailed).

Figure 3-5 Evaluation of correlation between RAGE and TLR9 CLL-LN expression with Ki67 and ZAP70 LN expression

LN expression levels of RAGE and TLR9 were determined by IHC and analysed with ARIOL image analysis software (Figure 3-4); LN expression levels of Ki67 and ZAP70 were previously stained on the same CLL TMAs by Andrew Clear and Dr Meg Ashton, respectively, and visualised with DAB chromogen. Ki67 protein expression levels were calculated as the % of cells positive for brown staining using the ARIOL colour and shape image classifiers. ZAP70 LN protein expression was classified as positive (2) if the % of cells positive for ZAP70 was >20 in the LN core, and negative (1) if less than <20%. Linear correlations between RAGE, TLR9, Ki67 and ZAP70 CLL expression were assessed by Pearson product-moment multiple correlation method (A). Detailed statistical data (B) are presented as R=Pearson correlation coefficient, *P*-value and sample size (N); $P<0.05$*, $P<0.01$**.

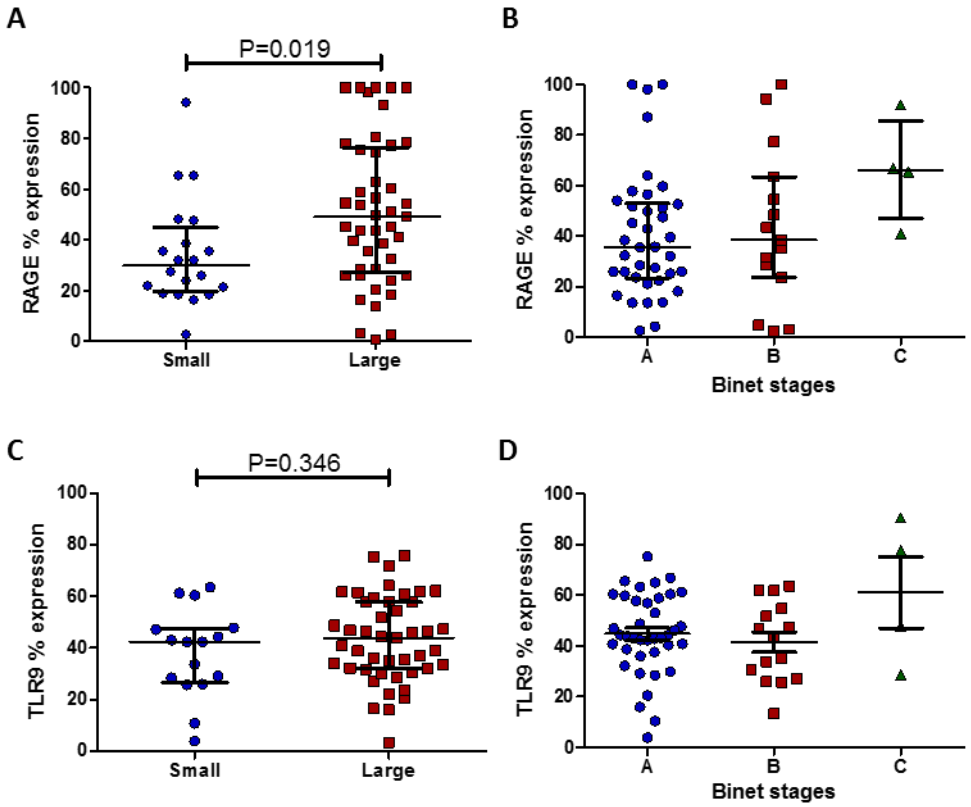

Figure 3-6 Evaluation of RAGE and TLR9 expression association with LN proliferation centre size and CLL disease Binet stage

LN protein expression levels were compared to LN proliferation centre size and CLL disease Binet staging for RAGE (A and B) and TLR9 (C and D). Proliferation centre size was previously assessed in whole LN biopsies by histopathologist, Professor Maria Calaminici, and Binet staging performed at diagnosis; clinical data was extracted from our tissue bank clinical database. Expression levels of RAGE and TLR9 were determined by IHC (Figure 3-4). Data are presented as median ± interquartile range. Statistical differences assessed by an unpaired Mann Whitney U test for proliferation centre size (A and C) and Kruskal-Wallis one-way ANOVA for Binet staging (B and D); $P<0.05$*.

3.2.3 CLL patients with high RAGE expression have a poor overall survival

We have shown RAGE expression is positively correlated with levels of ZAP70 and Ki67. ZAP70 is an established independent prognostic marker for CLL.[321] Investigating the association of HMGB1 receptor expression on CLL patient outcome will indicate a predominate pro- or anti-tumour role, and if expression of these proteins could be used to predict CLL patient outcome.

We determined the association of RAGE and TLR9 with clinical outcome by Kaplan Meier analysis. Expression levels of all continuous variables were categorised into subgroups using X-tile software, to statistically define optimal data cut points for variables that lack accepted established data ranges. This method limits the loss of biologically relevant subgroups commonly performed by dividing datasets using the median value, and prevents P-value driven cut point generation. The software separates expression data into test-validation cohorts in a 1:2 ratio. All possible cut points are rigorously investigated in the test cohort, before being applied to the validation cohort. X-tile software generated 2 cut points for RAGE, TLR9 and Ki67, separating these continuous variables into low, medium and high expression for CLL patients (Table 5); ZAP70 LN expression was previously scored as either positive or negative.

Kaplan-Meier curves were generated by the log rank test based on X-tile expression data cut points to compare differences in outcome between expression subgroups. OS, meaning death from any cause was used to measure outcome from the date of diagnosis, to event occurring, or date of last follow up for this cohort of patients. Differences in patient OS based on subgroup expression were tested using the log-rank test (Mantel-Cox), generating *P*-values, hazard ratios (HR) and 95% confidence intervals (CIs). For this analysis, HR represents the risk of death occurring by a certain time point. A HR of 2 indicates death by any cause, is 2x more likely to occur in the high expression subgroup compared to the low expression subgroup.

Separation of variables and association with OS was visualised by Kaplan-Meier curves (Figure 3-7; Figure 3-8). CLL patients with $RAGE^{HIGH}$ expression confer inferior OS (median OS =3 years; HR=2.4; n=13) compared to patients with medium/low RAGE expression (n=29 and 48, respectively; median OS =7.5 years; log rank test $P<0.05$; Figure 3-7A). This indicates that RAGE exhibits a pro-tumour function in CLL, and patients with high levels of LN RAGE have a 2.4x increased likelihood of death compared to patients with low RAGE expression. Although patients $TLR9^{HIGH}$ expression have a 1.6x higher risk of death compared to patients with $TLR9^{LOW}$, this separation was not significant by log rank test (Figure 3-7B).

Table 5. X-tile generated cut points for RAGE, TLR9 and Ki67

	RAGE	TLR9	Ki67
Low	<48.34	<39.08	<5.00
Medium	48.34–78.07	39.08–61.60	5.00–11.69
High	>78.07	>61.60	>11.69

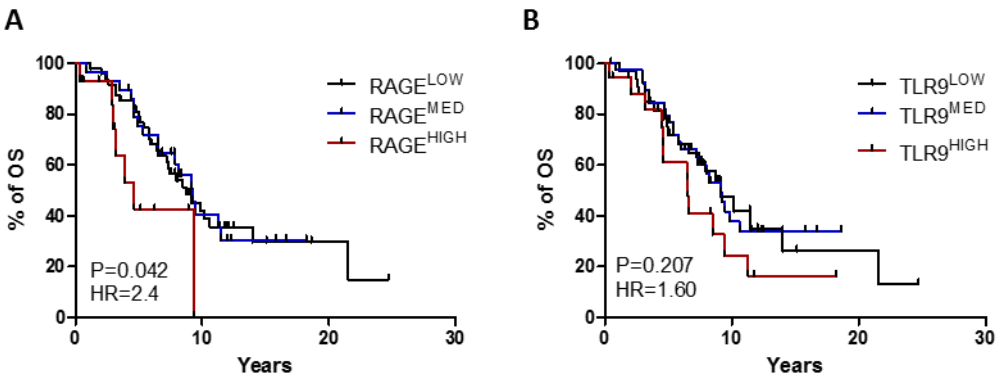

Figure 3-7 Higher expression of RAGE is associated with a poor clinical outcome for patients with CLL
Evaluation of low, medium and high RAGE (A) and TLR9 (B) LN expression on CLL patient OS. Cut-off points for each variable were obtained by X-tile statistical software (Table 5). Kaplan-Meier survival curves were generated using these data cut points and *P*-values, HR and 95% CIs were generated using a log-rank test in GraphPad Prism software. HR were produced by comparing the high expression group to the low expression group. OS= overall survival, HR= hazard ratio. The P-vale compares the low expression subgroup to the high expression subgroup.

Next, we assessed the impact of Ki67 and ZAP70 on patient OS, to test our cohort of CLL patients have phenotypic characteristics indicative of the wider CLL population. Although patients with $Ki67^{HIGH}$ and ZAP70+ expression have a shorter OS (Ki67 median OS =4.7 years; ZAP70+ median OS =5.6 years; Figure 3-8), this association was not significant for this cohort of patients. The HR for these variables were >1, suggesting higher expression of these proteins is associated with shorter OS.

All variables were compared by Chi-Square analysis using RAGE-defined cut points (Table 6). This test was used to analyse the frequency of distribution between 2 categorical variables. As RAGE expression increases, Ki67, TLR9, ZAP70 and age biomarkers increase, alongside a negative correlation with median OS rates (Chi-Square analysis; $P<0.0001$), highlighting the inferior effect of overexpression of RAGE on disease outcome. This data indicates that higher expression of RAGE, but not TLR9, is associated with a poorer clinical outcome in patients with CLL. This data suggests a functional role for RAGE in CLL disease pathogenesis, and further investigation of

RAGE prognostic significance could establish RAGE as a newly reported predictive marker of CLL disease outcome.

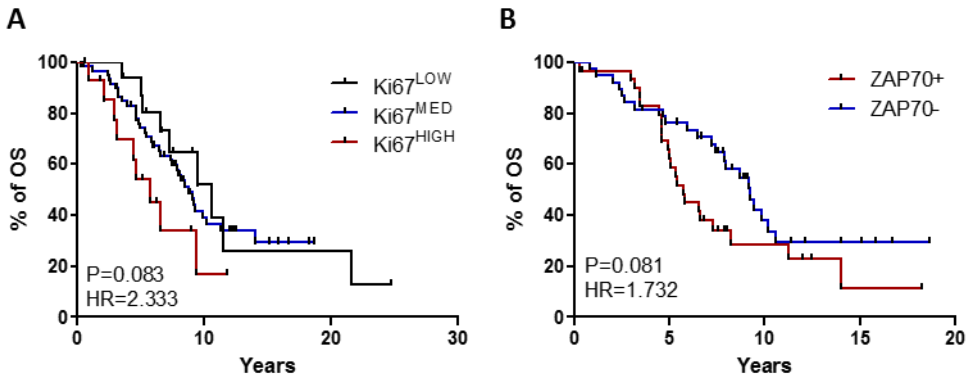

Figure 3-8 Ki67 and ZAP70 LN expression does not predict a shorter OS for this cohort of CLL patients
Evaluation of low, medium and high Ki67 (A) and positive or negative ZAP70 (B) LN expression on CLL patient OS. Cut-off points for Ki67 were obtained by X-tile statistical software (Table 5) and ZAP70 scored positive if staining >20% of cells were positive for ZAP70. Kaplan-Meier survival curves were generated using these data cut points and *P*-values, HR and 95% CIs were generated using a log-rank test in GraphPad Prism software. HR were produced by comparing the high expression group to the low expression group. OS= overall survival, HR= hazard ratio, CI= confidence intervals.

Table 6. Chi-Square analysis for all variables

	$RAGE^{LOW}$	$RAGE^{MEDIUM}$	$RAGE^{HIGH}$
RAGE (median ± SD)	25.99 ± 10.83	58.59 ± 7.12	99.07 ± 5.92
Overall Survival - Years (median ± SD)	7.49 ± 3.53	7.87 ± 3.18	3.13 ± 2.18
Ki67 (median ± SD)	2.53 ± 3.24	6.99 ± 4.41	14.24 ± 8.57
TLR9 (median ± SD)	40.60 ± 12.92	57.78 ± 12.86	55.68 ± 13.84
CD3 (median ± SD)	16.90 ± 4.54	19.17 ± 8.19	24.47 ± 9.24
Age (median ± SD)	57.00 ± 9.47	58.50 ± 6.79	64.50 ± 13.82
ZAP-70 expression	37%	52%	75%

Note: the cut points of RAGE were generated by X-tile. All other variables were separated according to the categories of RAGE. P<0.0001

3.2.4 Higher RAGE expression combined with ZAP70 and Ki67 predict a worse clinical outcome in CLL

To further evaluate the association between RAGE and TLR9 LN expression and OS for CLL patients, we conducted a Cox regression analysis on both continuous and categorical variables and compared this with other available risk factors.

The Cox regression proportional hazards analysis generates HRs with 95% CIs, by measuring the association between continuous or categorical variables, and an end-point event occurring – death by any cause in this study. In a continuous univariate analysis, the HR is a measure of the increase in risk of death occurring, per unit increase in variable expression. A HR>1 indicates higher variable expression confers worse clinical outcome and the opposite, higher variable expression confers better outcome, if the HR<1. For categorical Cox regression analysis, RAGE, TLR9 and Ki67 variable expression was separated into 3 subgroups based on X-tile-generated data cut points. ZAP70 and age variables were separated into 2 subgroups based on previously established data ranges (positive or negative ZAP70 expression, and >60 or <60 years of age, respectively). HRs were calculated by comparing the high expression subgroup to the low expression subgroup for RAGE, TLR9, and Ki67, and direct comparison between the 2 subgroups for ZAP70 and age. Both continuous and categorical Cox regression analysis was performed to increase statistical robustness in a cohort of 91 CLL patients with available survival data. A prognostic significant threshold was set to $P<0.05$ with a HR either >1 or <1 for biomarkers in this study.

Continuous variable data (RAGE, TLR9, Ki67 and age) was used to determine the prognostic impact of each variable by the Cox proportional hazards model. We confirmed age was a prognosticator for this cohort of CLL patients ($P<0.05$; HR = 1.03; n=91; Table 7) when comparing to patient OS outcome. As CLL is a disease of the elderly, higher age is already established as an indicator of disease outcome and for all disease in general, not just CLL-specific. RAGE, TLR9 and Ki67 did not show significant prognostic significance for this cohort of patients. HRs for all variables were >1 suggesting higher biomarker expression confers inferior OS, except for RAGE where the HR=1. However, use of continuous data can result in the loss of statistical robustness and underlying biology.

Table 7. Univariate Cox regression analysis for continuous variables

Variable	Overall survival	
	HR (95% CI)	***P***
RAGE	1.00 (0.99-1.02)	0.492
TLR9	1.05 (0.98-1.07)	0.270
Ki67	1.02 (0.99-1.02)	0.524
Age	1.03 (1.01-1.06)	0.018

***Note*:** Data shown were analysed by Cox proportional hazard model (n=91). Abbreviations: HR, hazard ratio; 95% CI, 95% confidence interval; *P*, P-value.

In a clinically applicable method, biomarker expression levels were categorised by cut points defined using X-tile software (Table 5) and assessed by uni- and multivariate Cox regression analysis. Univariate categorical analysis revealed patients with either high RAGE expression and/or higher age (>60 years old) had an increased risk of death ($RAGE^{HIGH}$ HR=2.41, *P*=0.042; Age^{HIGH} HR=1.74, *P*=0.05; Table 8). Other categorical variables (TLR9, Ki67, and ZAP70) did not show prognostic significance. Separating patient biomarker expression into groups is i) easier to score and assess in clinic; ii) reveals a statistical association that is overlooked when using continuous data.

To assess the prognostic interaction or confounding effects between different biomarkers we performed backward selection multivariate analysis on categorical variables (Table 8). To tease apart any prognostic relationship between RAGE and TLR9 with other covariates, these variables were first included in pairwise multivariate Cox regression analysis, before inclusion of additional covariates, to infer any changes on the HRs. Prognostic interaction between covariates was measured by calculating the magnitude of difference between univariate HR to multivariate HR value: ($HR_{adjusted}$-$HR_{univariate}$)/$HR_{adjusted}$ X 100%). Finally, all categorical variables were included in a full backward wald multivariate analysis to identify biomarkers that retained prognostic significance. This method removes variables at each step that lack prognostic significance, recalculates HRs and prognostic significance, and repeats the backward selection process until the final model results in biomarkers that retain strong prognostic significance throughout the selection process even when combined with different interacting covariates. This final model identifies robust predictors of disease outcome.

Combining ZAP70 and RAGE categorical variables greatly increased the prognostic significance of high RAGE ($RAGE^{HIGH}$ HR = 8.45, *P* =0.001; Table 8). ZAP70 and RAGE have a prognostic interaction effect of 71.5%, indicating the biological correlation between these 2 variables is

causal. Inclusion of Ki67 to RAGE and ZAP70 interacting variables further increases the prognostic significance of high RAGE and high Ki67 ($RAGE^{HIGH}$ HR = 14.2, *P*<0.0001; Table 8) with an interaction effect of 83.1%. This result, combined with a significant positive correlation between RAGE/ZAP70 and RAGE/Ki67 (Figure 3-5), indicates a causal relationship among RAGE with ZAP70 and Ki67.

TLR9 was not an independent prognostic marker and failed to gain prognostic significance when combined with other covariates (Table 8). The dual roles of TLR9 in CLL make it a difficult predictor of CLL outcome, as the opposing TLR9 responses heavily rely on the status of other variables in CLL disease pathogenesis (i.e. IGHV mutation status and BCR signalling capacity) and has only recently undergone functional investigation.[96] There was also a significant prognostic interaction between age and ZAP70 (Age^{HIGH} HR =2.50, *P*=0.006; ZAP70 HR =2.27, *P*=0.015*).* When the prognostic effect of Ki67 was stratified by ZAP70, the prognostic significance of high Ki67 increased, but had a confounding effect on ZAP70 (Table 8).

Finally, all variables were included in a full backward selection multivariate Cox regression analysis (Appendix II; Table M). In the final model, high RAGE, high Ki67 and higher age retained significance as prognostic factors for OS. These results indicate that higher expression of RAGE has important and robust prognostic value, especially when combined with ZAP70 and Ki67 variables. This study gives us rationale to further investigate the functional impact of the HMGB1-RAGE signalling axis in CLL and potential RAGE blockade.

Table 8 Uni- and multivariate Cox regression analysis on categorical variables

Univariate			**Multivariate**		
Covariates	**OS**		**Covariates**	**OS**	
	HR (95% CI)	***P***		**HR (95% CI)**	***P***
			ZAP70	0.53 (0.30-0.92)	0.062
RAGE^{MED}	0.97 (0.53-1.78)	0.930	**RAGE^{MED}**	0.88 (0.46-1.68)	0.702
RAGE^{HIGH}	2.41 (1.03-5.61)	0.042	**RAGE^{HIGH}**	8.45 (2.31-30.90)	0.001
			ZAP70	1.60 (0.85-3.01)	0.144
TLR9^{MED}		0.913	**TLR9^{MED}**	1.05 (0.54-2.04)	0.894
TLR9^{HIGH}	0.97 (0.52-1.80)	0.207	**TLR9^{HIGH}**	1.35 (0.56-3.27)	0.508
	1.60 (0.77-3.33)				
			ZAP70	1.41 (0.75-2.68)	0.290
Ki67^{MED}	0.89 (0.47-1.72)	0.735	**Ki67^{MED}**	0.79 (0.34-1.59)	0.504
Ki67^{HIGH}	1.90 (0.89-4.04)	0.094	**Ki67^{HIGH}**	3.64 (1.36-9.76)	0.010
ZAP70	1.69 (0.93-3.08)	0.084	**ZAP70**	1.47 (0.77-2.80)	0.242
			RAGE^{MED}	0.85 (0.44-1.66)	0.626
			RAGE^{HIGH}	14.2 (3.35-60.07)	<0.0001
			Ki67^{MED}	0.63 (2.29-1.39)	0.257
			Ki67^{HIGH}	4.22 (1.52-11.72)	0.006
			ZAP70	2.27 (1.17-4.39)	0.015
Age	1.74 (0.99-3.04)	0.050	**Age**	2.50 (1.29-4.84)	0.006

Note: The cut-off points for RAGE, TLR9 and Ki67 were generated by the X-tile software and listed in Table 5; RAGE^{MED} = medium subgroup; RAGE^{HIGH} = high expression subgroup. ZAP70 was classified by positive and negative populations. Age >60 years old is defined as Age^{HIGH}. The estimated measures of association before (HR_{crude}) and after adjusting ($HR_{adjusted}$) for interaction were calculated as: magnitude of interaction = ($HR_{adjusted}$-HR_{crude})/$HR_{adjusted}$ X 100%. The interaction effect of ZAP-70 on RAGE is 71.48% without Ki67 and is 83.10% with Ki67; the effect of ZAP-70 on Ki67 is 47.80% without RAGE and 54.98% with RAGE.

3.3 Discussion

In this chapter, we have shown that HMGB1 receptors, RAGE and TLR9 are heterogeneously expressed in CLL patients. Increased RAGE expression in CLL LNs positively correlated with established proliferation marker, Ki67, and aggressive disease marker, ZAP70. Moreover, high RAGE expression is associated with shorter OS and prognostic significance increased when stratified with ZAP70 and Ki67 categorical variables for patients with CLL. This data demonstrates for the first time that high RAGE expression in CLL LNs in patients with CLL, confer inferior clinical outcome.

The main HMGB1 receptors involved in initiating DAMP-associated inflammatory responses include TLR2, TLR4, TLR9 and RAGE.[123,131,143] RAGE and TLR9 were the only HMGB1 receptors with increased mRNA expression in CLL peripheral blood compared to healthy age matched controls.[316] The TLR gene expression profile in CLL PB was similar to that of memory B-cells, owing to a mature CLL B-cell phenotype.[322] Increased expression of TLR7 and TLR9 in CLL are likely due to prior activation *in vivo* with endogenous TLR7 ligands (single strand RNA) and dichotic responses following TLR9 stimulation with Class B-CpG-ODN previously documented in CLL.[96,318] Growing evidence highlights CLL LNs as a key site of CLL pathogenesis and host-tumour interactions.[47] From our results, RAGE and TLR9 LN expression is highly heterogeneous among patients, reflecting the biological and clinical diversity of CLL disease. RAGE is predominately expressed in large proliferation centres in CLL LNs; a niche site associated with the proliferation and survival of CLL cells, infiltration of T-cells and macrophages, activation of inflammatory pathways, aggressive disease and inferior survival.[323-325] RAGE and TLR9 expression in CLL LNs is overall lower compared to germinal centres in RA-LN. As sites of acute B-cell proliferation, high RAGE and TLR9 expression in reactive germinal centres highlight their routine roles in the activation and proliferation of healthy B-cells, as well as in CLL.[326,327]

An increased understanding of CLL biology is enhancing our capacity to identify patients with high risk disease, by using a wealth of risk factors.[328,329] The most powerful molecular prognostic marker utilised clinically is the IGHV mutational status. The two main subsets differ markedly, patients with no somatic hypermutations in the IGHV gene region (unmutated-CLL) generally have a more aggressive disease.[50] However, IGHV sequencing is not routinely available for all patients at diagnosis, owing to the difficulty and cost in performing this procedure as a clinical test.[330] Gene expression profiling studies identified high expression of ZAP70 and CD38 in U-CLL subsets, and ZAP70 expression can distinguish the U-CLL/M-CLL subsets with high significance.[51,92,331] Del(17p) and del(11q) are associated with U-CLL and used in disease management algorithms.[332] Although Ki67 expression is not a CLL prognostic marker, tumour

proliferation can be quantified by measuring levels of Ki67, an antigen that is strictly associated and expressed during active phases of the cell cycle (G1, S, G2 and M).[47,320] The current prognostic markers used clinically have greatly improved patient stratification and disease management, but no molecular markers to date truly reflect the microenvironmental-biology occurring in CLL LNs and contributing to disease pathogenesis. Our results show RAGE expression in CLL LNs highly correlates with levels of Ki67 and ZAP70, and poor disease outcome, indicating a predominate association with proliferative and aggressive disease.

Our group have previously shown that increased levels of extracellular HMGB1 in CLL plasma are associated with poorer clinical outcomes in these patients, but the prognostic impact of HMGB1 receptors and pathway remains elusive.[76] Previous reports demonstrate RAGE blockade supresses tumour growth in models of solid cancer,[168] but whether HMGB1 signals in a pro- or anti-tumour manner in CLL is unknown. Although RAGE expression is highly heterogeneous among CLL patients, we have shown that patients with high RAGE expression confer inferior OS. The use of X-tile software to statistically define optimal data cut points for RAGE and TLR9 that lack accepted established data ranges, limits p-value driven cut point generation.[313] Confirmed by Chi-Square analysis, RAGE-defined cut points positively correlated with levels of Ki67, TLR9, ZAP70 and age and negatively with OS rates. This suggests the HMGB1-RAGE signalling axis has a predominate pro-tumour role in CLL, and highlights this signalling axis as an important survival pathway to investigate in CLL. Using Cox regression univariate analysis, Ki67, RAGE and TLR9 continuous variables and ZAP70 categorical variable are not significant. The age of the patient has prognostic significance, but worse disease outcome is due to older age, not underlying biology. However, when we categorically divide variable expression, as would be applied clinically, $RAGE^{HIGH}$ gains independent prognostic significance for this cohort of patients. ZAP70 and Ki67 do not have independent prognostic significance, highlighting the need to combine with other data cohorts, or assess larger sample sizes, to ensure our results are indicative of the wider CLL population. The hazard ratio and prognostic significance of $RAGE^{HIGH}$ increases when stratified with ZAP70 and Ki67, indicating an interacting relationship between RAGE and these variables. Moreover, TLR9 signalling results in opposing anti- or pro- apoptotic signalling associated with unmutated or mutated IGHV gene status respectively and ZAP70 positivity.[96]

In summary, these results possible demonstrate RAGE plays an important microenvironmental role in CLL LNs. Increased CLL LN RAGE expression predicts shorter OS and is associated with expression other poor CLL disease markers. Validation of our findings with independent data cohorts will strengthen our hypothesis, and further functional validation will give insight into the precise role of RAGE and contribution to CLL disease pathogenesis.

Chapter IV

Determine the clinical relevance of the HMGB1-RAGE signalling axis

4.1 Introduction

RAGE is a multifunctional receptor, heavily involved in initiating and sustaining inflammatory signalling in response to a multitude of stress-related ligands such as HMGB1, S100 proteins and AGEs.[186] Our results in the previous chapter support a pro-tumour role for RAGE in CLL-LNs, but other RAGE ligands and receptor expression on other LN infiltrating cell subsets, may also drive this response in CLL. Further investigation of extracellular HMGB1 ligand levels with other RAGE ligands associated with cancer, their correlation with clinical data, and quantifying expression of HMGB1 receptors in different cell populations, will strengthen the clinical relevance of the HMGB1-RAGE signalling axis in CLL.

Increased expression of HMGB1 receptor, RAGE, is detected in various solid cancers, although molecular details linking RAGE expression to neoplastic transformation is limited. Few studies focus on the mechanistic link between RAGE ligands and pro- or anti-tumour cell signalling, owing to varied downstream RAGE signalling in a manner that is cell-type specific. Extracellular HMGB1 and S100B are the only RAGE ligands with reported extracellular roles in cancer, linked to a poor clinical outcome for CLL and melanoma patients, respectively.[76,333] Moreover, the interplay between membrane-bound RAGE and its isoforms, particularly the pool of extracellular soluble RAGE, are pivotal in regulating chronic inflammation through 'decoy' receptor ability.[334] In a healthy setting, extracellular HMGB1 and sRAGE levels are inversely correlated, highlighting circulating sRAGE captures and eliminates HMGB1 to limit inflammatory responses.[209] The relationship between extracellular HMGB1 or other RAGE ligand S100B, and antagonistic sRAGE in CLL is currently unknown.

Association between molecular markers and CLL clinical data provides a link to disease severity. CLL disease staging based on clinical/symptomatic features under the Rai and Binet classification systems, and assessment of chromosome aberrations, aids in disease management. However, determination of the IGHV mutational status is the gold standard molecular prognostic factor for CLL patients, guiding individualised therapy.[50,51] IGHV gene sequencing is not routinely available for patients at diagnosis in UK clinical practice, owing to the difficulty and cost in performing this procedure as a clinical test.[330] ZAP70 is one of the few genes with differential expression between the CLL subsets, with high expression associated with unmutated IGHV mutational status; therefore, ZAP70 expression serves as an alternative method for prognostic grading.[92,335] Currently, ZAP70 expression is assessed by flow cytometry using patient PB CLL B-cells, but there is no standardised method to allow reliable and reproducible testing between diagnostic laboratories.[336] A few main methods have been developed, rigorously tested and used in clinic as a surrogate for IGHV gene sequencing.[298] Our previous results showed RAGE LN

expression is associated with ZAP70 LN expression; further comparison of plasma HMGB1 with PB ZAP70 expression will give an indication of CLL subset specificity.

In the CLL disease setting, plasma HMGB1 levels are significantly increased in untreated and relapsed patients compared to healthy controls and HMGB1 induces the differentiation of NLCs that harbour CLL cell survival.[76] We have shown LN RAGE expression confers inferior OS, but whether HMGB1 drives pro-survival signalling responses directly in CLL B-cells is unknown. Assessing HMGB1-induced CLL cell proliferation *in vitro* is near impossible without co-culture with stromal cells and supporting growth factors, making it difficult to tease apart direct functional signalling outcomes.[337] Circulating CLL cells undergo cell cycle arrest in the G0 or G1 phase of the cell cycle until they re-enter the CLL LN/BM niche sites for regulatory signals. CLL cells spontaneously undergo apoptosis when cultured *in vitro*, compared to uncontrolled necrotic cell death.[338] Therefore, assessing if HMGB1 could rescue or prolong CLL cells from spontaneous cell death *in vitro,* may be a better measure of HMGB1-RAGE signalling outcome directly in CLL B-cells than measuring cell proliferation.

The work in this chapter will determine if i) RAGE and TLR9 are mainly expressed in CLL B-cells; ii) HMGB1 is the main RAGE ligand and association with CLL disease markers; iii) the outcome of HMGB1 signalling in primary CLL cells.

4.2 Results

4.2.1 RAGE and TLR9 are predominantly expressed in CLL B-cells

Our group previously demonstrated increased plasma HMGB1 levels in CLL compared to healthy controls,[76] and high RAGE LN expression confers inferior OS, highlighting a pro-tumour role for this signalling axis in CLL. However, HMGB1 receptors are expressed by numerous immune cell subsets, notably macrophages, dendritic cells, B-cells and stromal cells that comprise the CLL LN microenvironment.[72,131] In this study, we determined the cell types that mainly express RAGE and TLR9 in CLL PB, to further decipher a role for HMGB1 and its receptors, RAGE and TLR9 on CLL B-cell activation and strengthen the clinical relevance of the HMGB1-RAGE signalling axis in CLL.

RAGE and TLR9 expression was determined in T-cells, B-cells and monocytes from CLL PBMCs by flow cytometry for 6 patients. CD3, CD14 and CD19 surface staining was performed prior to permeabilisation/fixation and intracellular staining for RAGE and TLR9; surface RAGE was stained in non-permeabilised cells at the same time as CD3, CD14 and CD19 surface staining. Dead cells were excluded from flow cytometry analysis by staining with viable dye, and RAGE and TLR9 positive staining in CD3+ T cells, CD14+ monocytes and CD19+ B-cells were compared to isotype-matched controls (Figure 4-1 and Figure 4-2).

7.7% of the whole PBMC population express surface RAGE on CD19+ B-cells, compared to <1% of the PBMC population expressing surface RAGE on CD14+ monocytes, and significantly higher compared to CD3+ T-cells (P<0.0001; Figure 4-3A). When cells are permeabilised, 56.6% of the PBMC population is positive for intracellular RAGE and CD19, significantly higher than intracellular RAGE expressed in CD3+ T-cells (P<0.0001; Figure 4-3B). This expression pattern was similar for intracellular TLR9; 65.8% of the PBMC population was positive for TLR9 and CD19, compared to 5.4% TLR9+ and CD3+ (P<0.0001; Figure 4-3C).

When we consider the expression levels of RAGE and TLR9 within individual cell populations, 17.7% of CD14+ cells express RAGE on the cell surface, whereas only 8.4% of all CD19+ B-cells express surface RAGE, and 3% of CD3+ T-cells (Figure 4-3D). Although a higher proportion of CD14+ monocytes expressed RAGE on the cell surface, 60.4% of all CD19+ B-cells expressed intracellular RAGE, indicating RAGE internalisation. This was significantly higher than CD3+ T-cells (P<0.01; Figure 4-3E). Nearly all CD3+ T-cells, CD14+ monocytes and CD19+ B-cells expressed intracellular TLR9 (81.7%, 72.1% and 81.2%, respectively; Figure 4-3F).

The MFI was higher for surface RAGE expression in CD14+ monocytes compared to CD3+ T-cells and CD19+ B-cells (Figure 4-3G), but we observed significantly increased intracellular RAGE MFI

for CD19+ B-cells compared to CD3+ T-cells (P<0.01; Figure 4-3H). TLR9 MFI was similar for all cell subsets (Figure 4-3I).

Taking these data together, as CD19+ B-cells predominate CLL PB, RAGE and TLR9 expression is largely expressed in B-cells compared to T-cells and monocytes. Interestingly, RAGE MFI is lower on the surface of B-cells but much higher intracellularly. This could reflect ligand-induced internalisation and recycling to the plasma membrane. Therefore, RAGE and TLR9 are predominately expressed in circulating CD19+ B-cells and these results support our hypothesis that HMGB1 ligand could drive pro-tumour signalling via RAGE on CD19+ B-cells.

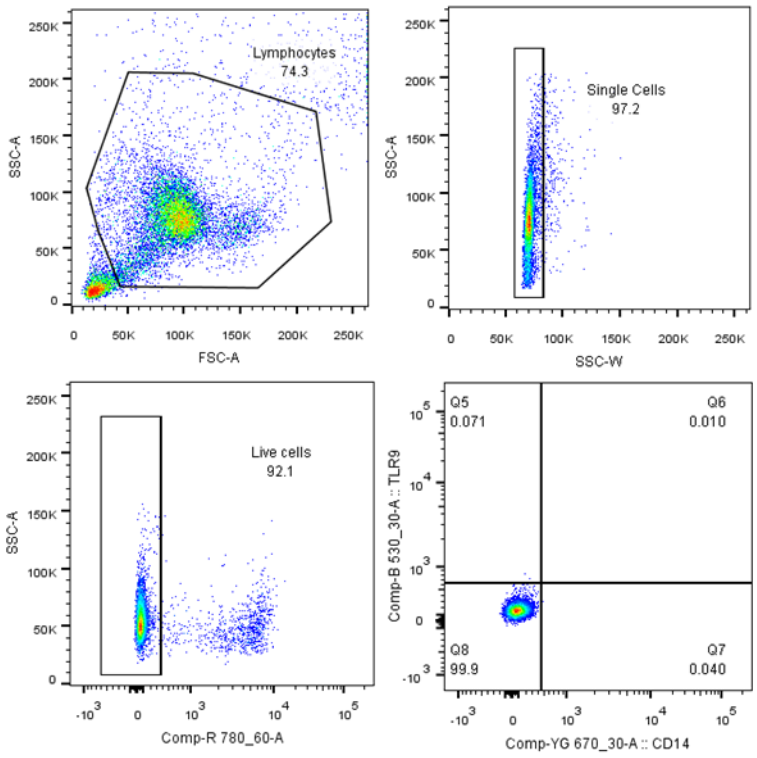

Figure 4-1 Flow cytometry gating procedure using FACS Diva software
RAGE and TLR9 staining was assessed using the Fortessa Flow Cytometer and FACS Diva software. Lymphocytes and single cells were gates, and dead cells excluded from data acquisition and analysis using viability dye. Positive fluorescence gates were set by using appropriate isotype controls for CD3, CD14, CD19, TLR9 and RAGE conjugated fluorochromes and secondary antibodies.

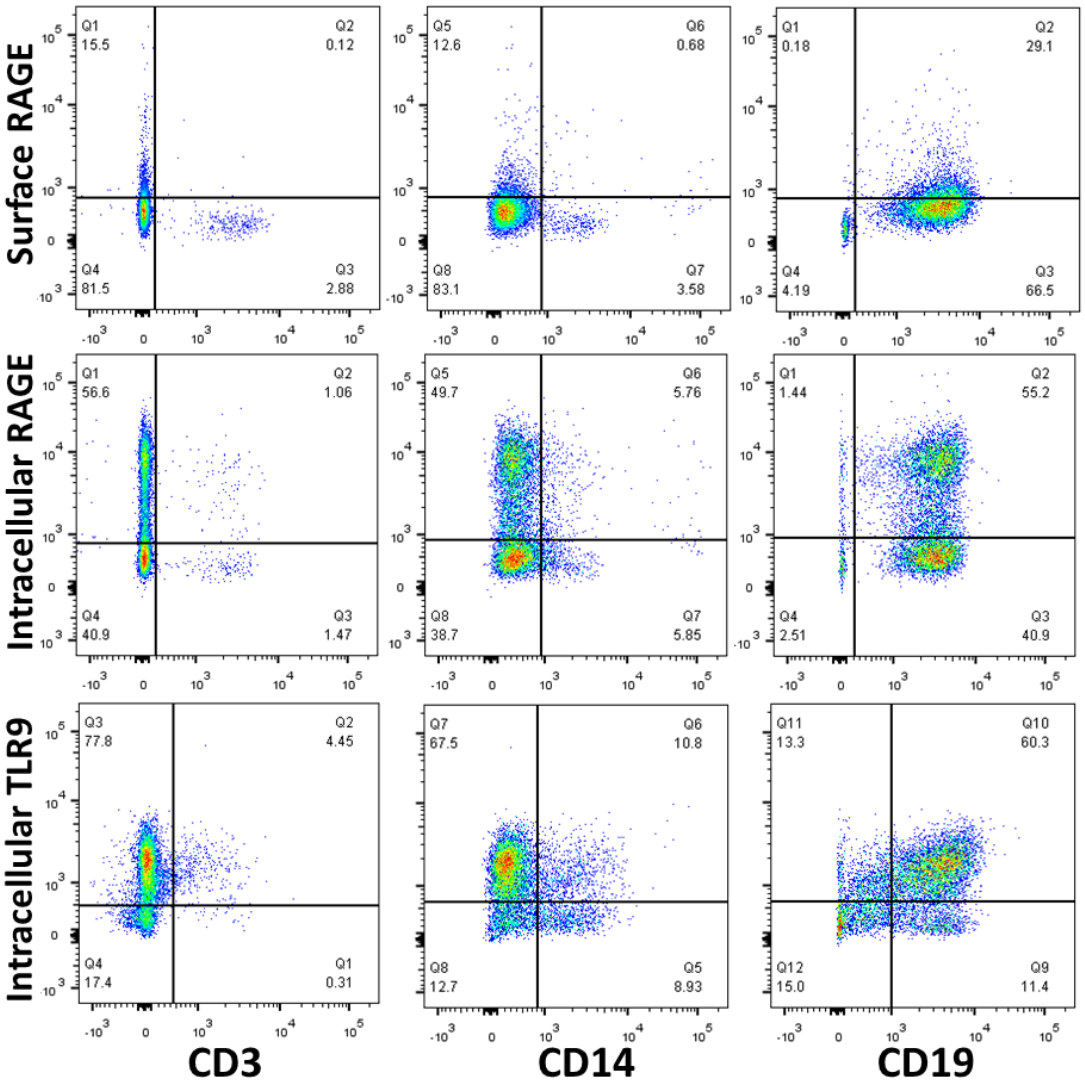

Figure 4-2 Representative flow plots for RAGE and TLR9 staining in CLL PBMCs
Cryopreserved CLL mononuclear cells from 6 patients with cell viability >90% were used for immune-staining. Cells were stained for surface markers CD3, CD14 and CD19 before permeabilization/fixation and intracellular staining for RAGE and TLR9. Surface RAGE expression was stained in non-permeabilised cells. Positive fluorescence was gated by comparing to isotype-matched controls and the expression of surface RAGE, intracellular RAGE and intracellular TLR9 compared in CD3+ T-cells, CD14+ monocytes and CD19+ B-cells.

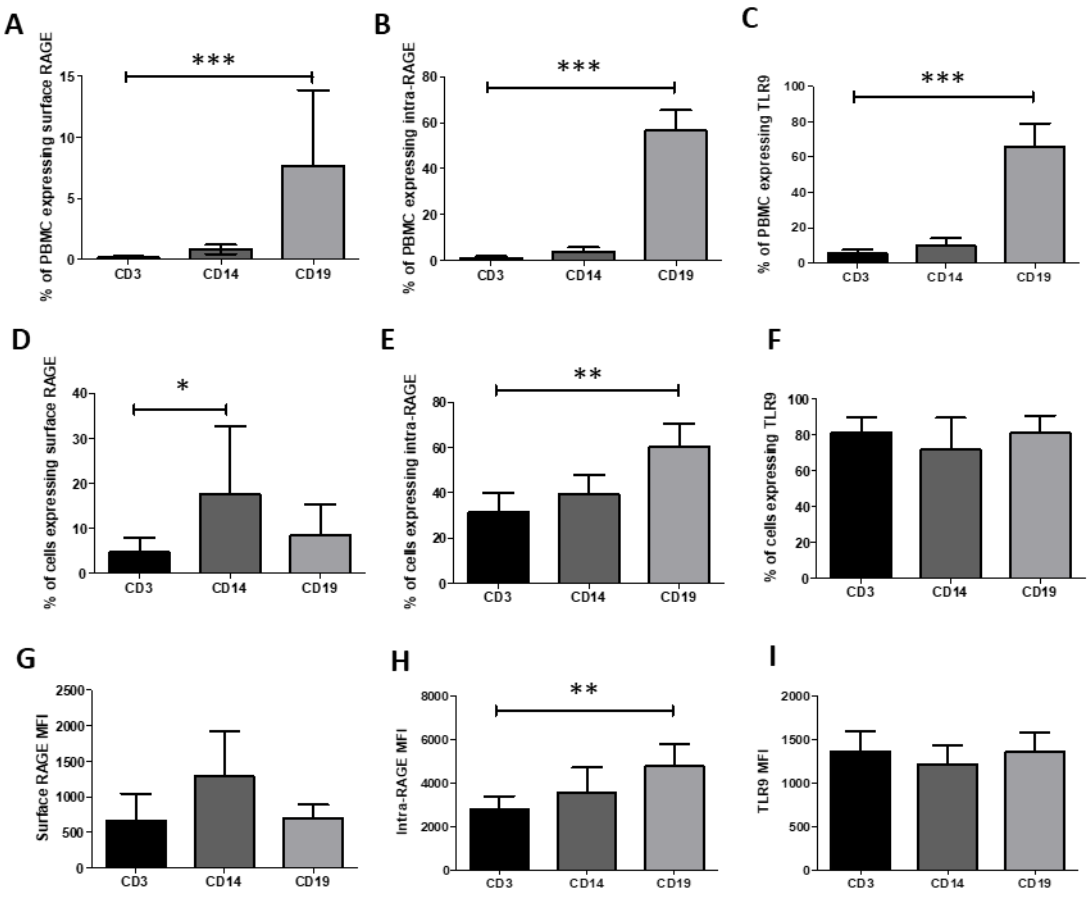

Figure 4-3 Statistical analysis of RAGE and TLR9 expression in T-cells, monocytes and B-cells
Surface RAGE (A, D, G), intracellular RAGE (B, E, H) and intracellular TLR9 (C, F, I) expression was assessed in CD3+ T-cells, CD14+ monocytes and CD19+ B-cells. Expression levels were compared by assessing the % of the whole PBMC population positive for RAGE and specific cell surface marker (A-C), the % of specific cell population RAGE or TLR9 positive, (D-F) and the MFI of surface RAGE, intracellular RAGE or TLR9 (G-I). Data are presented as the mean ± SD for 6 patients and statistical differences was analysed by a non-parametric One-way ANOVA; $P<0.05$*, $P<0.01$**, $P<0.001$***.

4.2.2 Extracellular HMGB1 is significantly higher in CLL compared to healthy controls, but not S100B

We have demonstrated RAGE is expressed in circulating PB CD19+ CLL cells and CLL LNs, but whether a different RAGE ligand outcompetes HMGB1 in CLL is unknown. Plasma levels of HMGB1 and S100B were assessed by ELISA in the same cohort of 54 CLL patients and compared to 15 healthy volunteers (Figure 4-4). Plasma was isolated from fresh whole blood by centrifugation at 1500rpm for 5 minutes at room temperature, and removal of the top plasma layer; plasma aliquots were stored at -80°C. S100B was chosen as a RAGE ligand comparison, as this plasma-derived RAGE ligand is the only S100 protein used clinically as a diagnostic marker for melanoma, with high levels of S100B associated with poor prognosis.[333] Although other S100 proteins have reported roles in cancer, particularly stress responses, these studies are focused on cellular expression of S100 proteins rather than extracellular ligand clinical relevance.[339]

HMGB1 plasma levels were significantly increased compared to healthy controls (median 72.2ng/ml and 3.4ng/ml, respectively; $P<0.0001$; Figure 4-4A), consistent with our previous published work in a smaller cohort of CLL patients.[76] Whereas, levels of plasma S100B were unaltered between CLL and healthy controls (median 0.0pg/ml for both CLL and healthy controls; Figure 4-4B).

Following a significant increase in HMGB1 plasma levels in CLL patients, we assessed the association between HMGB1 plasma levels and available clinical data (Figure 4-5). There was no association between HMGB1 plasma levels and poor cytogenetic risk factors, del(17p), del(11q) and trisomy 12, or good cytogenetic risk factor, del(13q) (Figure 4-5A), compared to CLL patients with a normal karyotype. Nor were HMGB1 levels associated with disease Binet staging (Figure 4-5B). CLL patients with untreated or relapsed disease had significantly higher extracellular HMGB1 levels compared to healthy controls (Figure 4-5C), and the statistical difference was higher between healthy controls and patients with relapsed disease. However, HMGB1 plasma levels do not correlate with time to first treatment (Figure 4-5D).

These results indicate HMGB1 is the main RAGE ligand in CLL, and S100B, the only other RAGE ligand with a documented clinical extracellular role in cancer, does not have altered levels in CLL patients compared to healthy controls. Therefore HMGB1-RAGE signalling will dominate RAGE-associated biology in CLL.

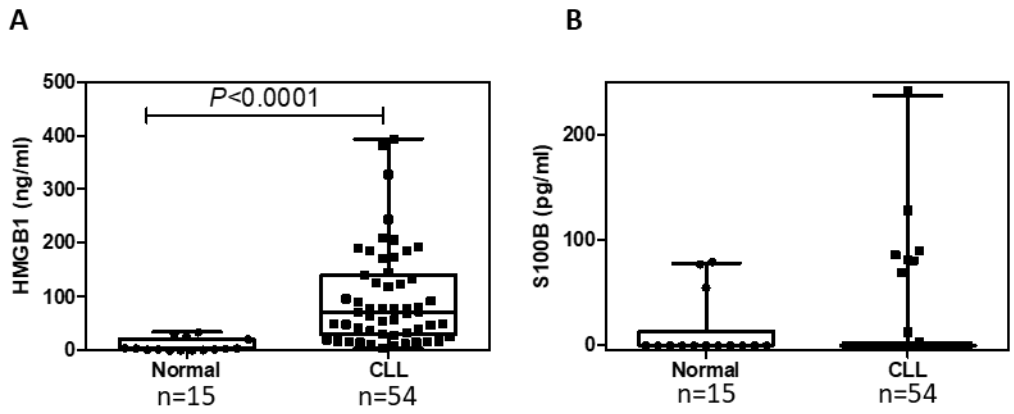

Figure 4-4 Detection of extracellular HMGB1 and S100B in healthy controls and CLL plasma

Comparison of HMGB1 (A) and S100B (B) plasma levels in primary CLL patient samples and healthy controls; n=54 and n=15, respectively. Plasma concentrations of HMGB1 and S100B were determined by sandwich ELISA. All samples were tested on the same plate with known protein concentration standards, and the concentration of test samples were extrapolated from the generated standard curve. Data are presented as median with interquartile range and analysed by a Mann Whitney U-test; *P*<0.0001***.

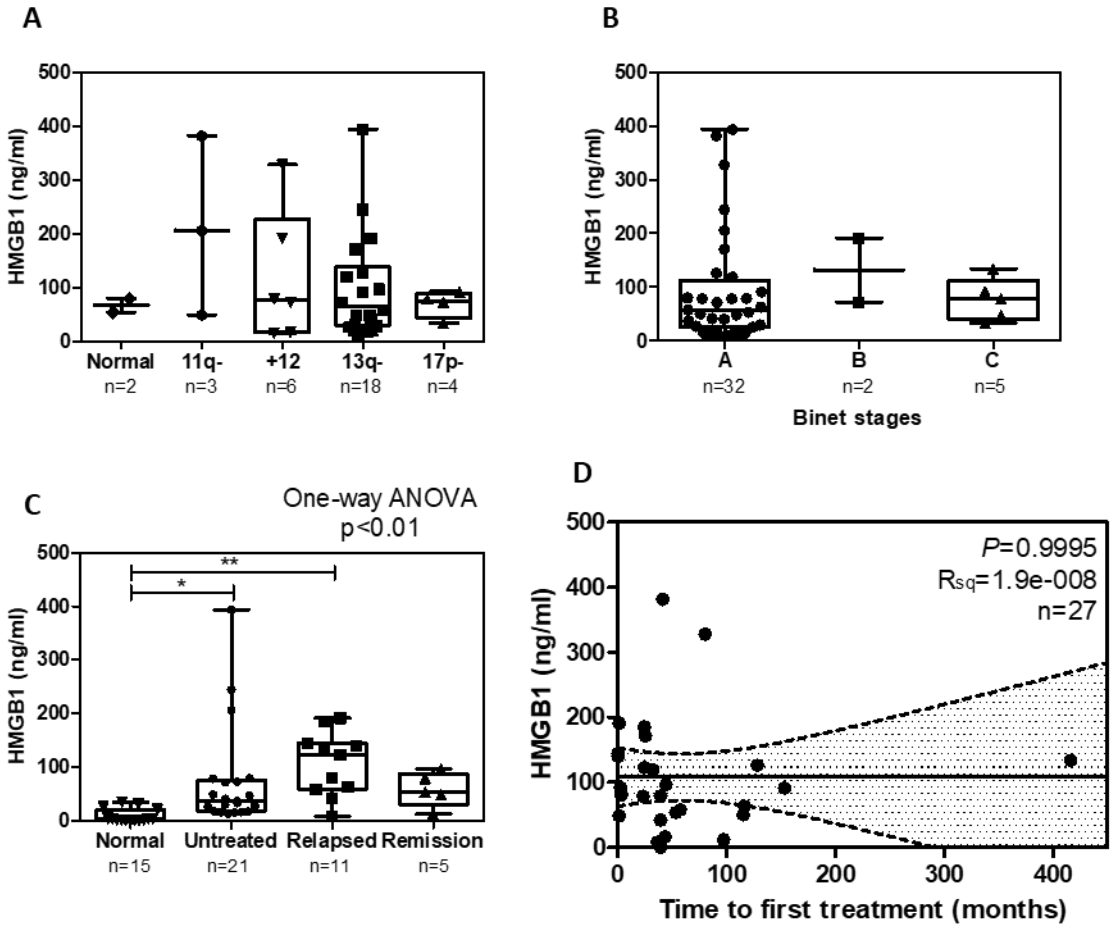

Figure 4-5 Evaluation of extracellular HMGB1 levels association with CLL cytogenetic aberrations, CLL disease Binet stage, disease clinical outcome and time to first treatment

HMGB1 plasma levels were compared with CLL patient (A) cytogenetic aberrations, (B) CLL patient Binet staging, (C) treatment and treatment outcome, and (D) time to first treatment. Fresh plasma was collected from 54 CLL patients and stored at -80°C before measuring HMGB1 concentration by ELISA. Clinical data was extracted from our tissue bank clinical database. Data presented (A-C) are median ± interquartile range and statistical differences assessed by One-way ANOVA. HMGB1 plasma levels and time to first treatment was assessed by Linear Regression. Samples sizes (n) are stated in graphs, P= *P*-value, P<0.05*, P<0.01**, R_{sq}= coefficient of determination.

4.2.3 Soluble RAGE levels are significantly higher in CLL compared to healthy controls and correlate with time to first treatment

Next, we assessed the plasma concentration of sRAGE in the same cohort of CLL patients and healthy controls, and compared this to extracellular HMGB1 levels. High plasma levels of HMGB1 in CLL may be signalling-incompetent if the RAGE ligand is sequestered by similar levels of 'decoy receptor' sRAGE. Diminished levels of sRAGE are associated with progression in different types of solid cancer, but many HMGB1-RAGE cancer studies fail to consider the extracellular role of sRAGE.[128] Moreover, as sRAGE displays decoy receptor ability, we also investigated whether extracellular sRAGE levels confer a protective effect in CLL.

In this study, sRAGE was significantly higher in the plasma of CLL patients compared to healthy controls (median 60.0pg/ml and 31.0pg/ml, respectively; *P*<0.01; Figure 4-6A). This result was surprising, but sRAGE plasma concentration was 3 orders of magnitude lower than plasma HMGB1 in CLL, so unlikely to fully inhibit HMGB1 and down-modulate HMGB1-RAGE signalling. Moreover, healthy controls were not age-matched due to availability – repeating this with a cohort of age-matched controls will confirm our findings and constitute a better comparison for CLL patients. We further investigated the strength of linkage between HMGB1, S100B and sRAGE in CLL patients and healthy controls using Pearson product-moment multiple correlation method (Figure 4-7B). In a healthy setting, HMGB1 and sRAGE plasma levels are inversely correlated, with increased levels of sRAGE limiting inflammatory responses. The classical negative inverse trend was observed for the healthy controls in this study, although this result was not significant (R=-0.112; P=0.692; Figure 4-7). In CLL, HMGB1 and S100B significantly positively correlated, owing to their stress-DAMP related roles (R=0.427; *P*<0.001; Figure 4-6B). S100B demonstrated a negative correlation with sRAGE (R=-0.041; *P*=0.766; Figure 4-6B), and HMGB1 had a positive correlation with sRAGE (R=0.084; *P*=0.547; Figure 4-6B), but these correlations were not significant for this cohort of CLL patients.

Next, we compared extracellular sRAGE levels with available clinical data to decipher any impact on patient outcome. Patients with poor prognostic karyotypes, del(17p), del(11q) and trisomy 12 had lower sRAGE levels than CLL patients with a normal karyotype or good prognostic marker del(13q); although specific comparisons were not significant (Figure 4-8A). Most of the patients included in this study were assigned a CLL disease Binet stage of A at diagnosis (n=32) i.e. less aggressive clinical characteristics, compared to Binet stage B (n=2) or Binet stage C (n=5). Again, specific comparisons between Binet staging were not significant, but the overall One-way ANOVA was significant owing to higher levels of sRAGE for patients with Binet stage A compared to B and C (P<0.05; Figure 4-8B). Although we observed significantly higher levels of sRAGE in

CLL patients compared to healthy controls, when we split the CLL patients into untreated, relapsed and partial remission subgroups, all subgroups share similar levels of extracellular sRAGE (Figure 4-8C); and these are not significantly increased compared to the healthy controls. Finally, to assess if levels of sRAGE associate with patient outcome we compared extracellular sRAGE levels to patients' time to first treatment. Patients with higher levels of extracellular sRAGE had a longer time to first treatment ($P<0.05$; Figure 4-8D).

These results demonstrate sRAGE is increased in CLL compared to healthy controls, but fell below levels capable of full HMGB1 inhibition for the same patient cohort. Absence of a negative correlation between HMGB1 and sRAGE suggested a breakdown in the negative feedback loop in CLL. Moreover, sRAGE does confer a protective effect by prolonging time to first treatment and highlights HMGB1-RAGE signalling as a clinically relevant pathway to investigate in CLL.

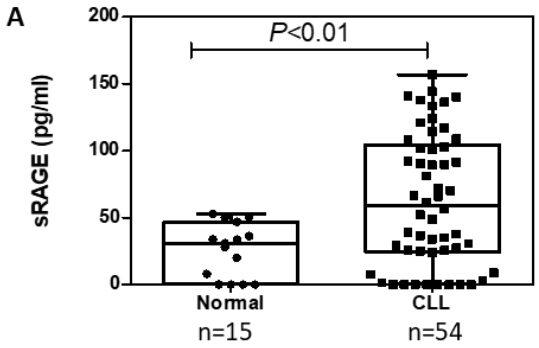

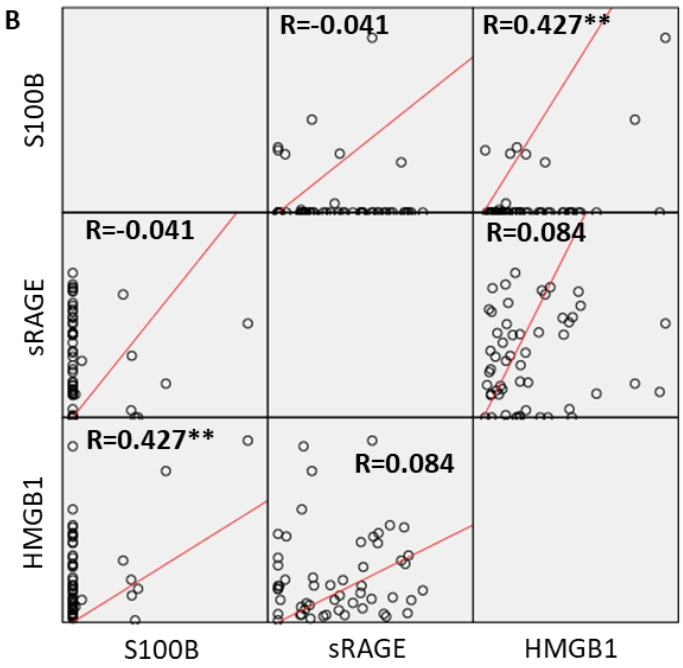

C

Correlations

		S100 pg/ml	sRAGE pg/ml	HMGB1 ng/ml
S100 pg/ml	Pearson Correlation	1	-.041	.427**
	Sig. (2-tailed)		.766	.001
	N	54	54	54
sRAGE pg/ml	Pearson Correlation	-.041	1	.084
	Sig. (2-tailed)	.766		.547
	N	54	54	54
HMGB1 ng/ml	Pearson Correlation	.427**	.084	1
	Sig. (2-tailed)	.001	.547	
	N	54	54	54

**. Correlation is significant at the 0.01 level (2-tailed).

Figure 4-6 Detection of extracellular sRAGE in CLL and healthy plasma, and correlation with plasma HMGB1 and S100B levels in CLL

Comparison of sRAGE plasma levels in primary CLL patient samples and healthy controls (A); n=54 and n=15, respectively. Plasma concentrations of sRAGE were determined by sandwich ELISA. All samples were tested on the same plate with known protein concentration standards, and the concentration of test samples were extrapolated from the generated standard curve. Data are presented as median with interquartile range and analysed by a Mann Whitney U-test. Linear correlations between plasma S100B, sRAGE and HMGB1 levels were assessed by Pearson product-moment multiple correlation method (B). Detailed statistical data (C) are presented as R=Pearson correlation coefficient, *P*-value and n=sample size; *P*<0.001**.

A

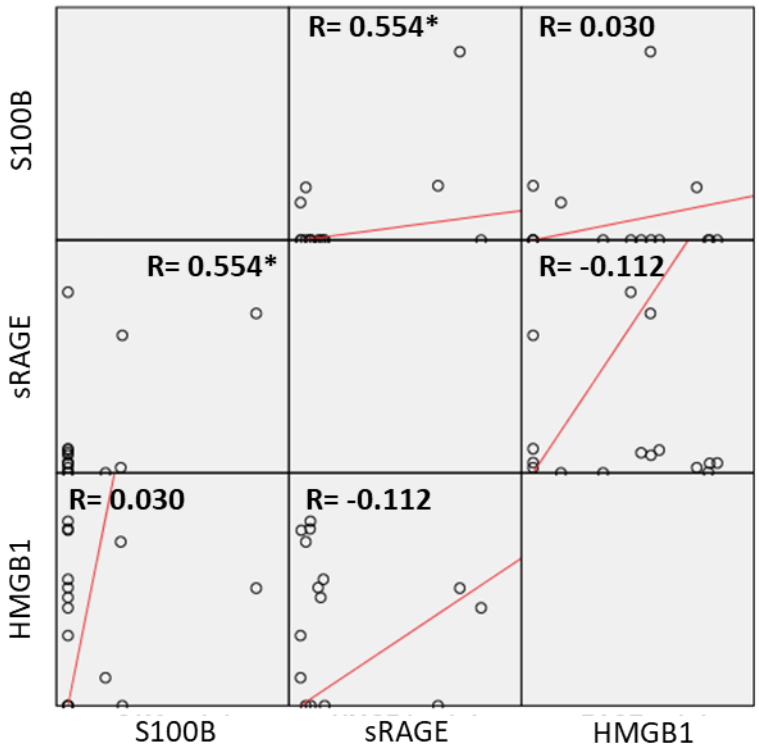

B

Correlations

		S100 pg/ml	HMGB1 ng/ml	sRAGE pg/ml
S100 pg/ml	Pearson Correlation	1	.554*	.030
	Sig. (2-tailed)		.032	.914
	N	15	15	15
HMGB1 ng/ml	Pearson Correlation	.554*	1	-.112
	Sig. (2-tailed)	.032		.692
	N	15	15	15
sRAGE pg/ml	Pearson Correlation	.030	-.112	1
	Sig. (2-tailed)	.914	.692	
	N	15	15	15

*. Correlation is significant at the 0.05 level (2-tailed).

Figure 4-7 Pearson multiple correlation analysis of extracellular HMGB1, S100B and sRAGE levels in healthy controls

Linear correlations between plasma S100B, sRAGE and HMGB1 levels were assessed by Pearson product-moment multiple correlation method (A). Plasma concentrations of HMGB1, S100B and sRAGE were determined by sandwich ELISA on the same plate as known protein standards and healthy controls. Detailed statistical data (B) are presented as R=Pearson correlation coefficient, *P*-value and n=sample size; *P*<0.05*.

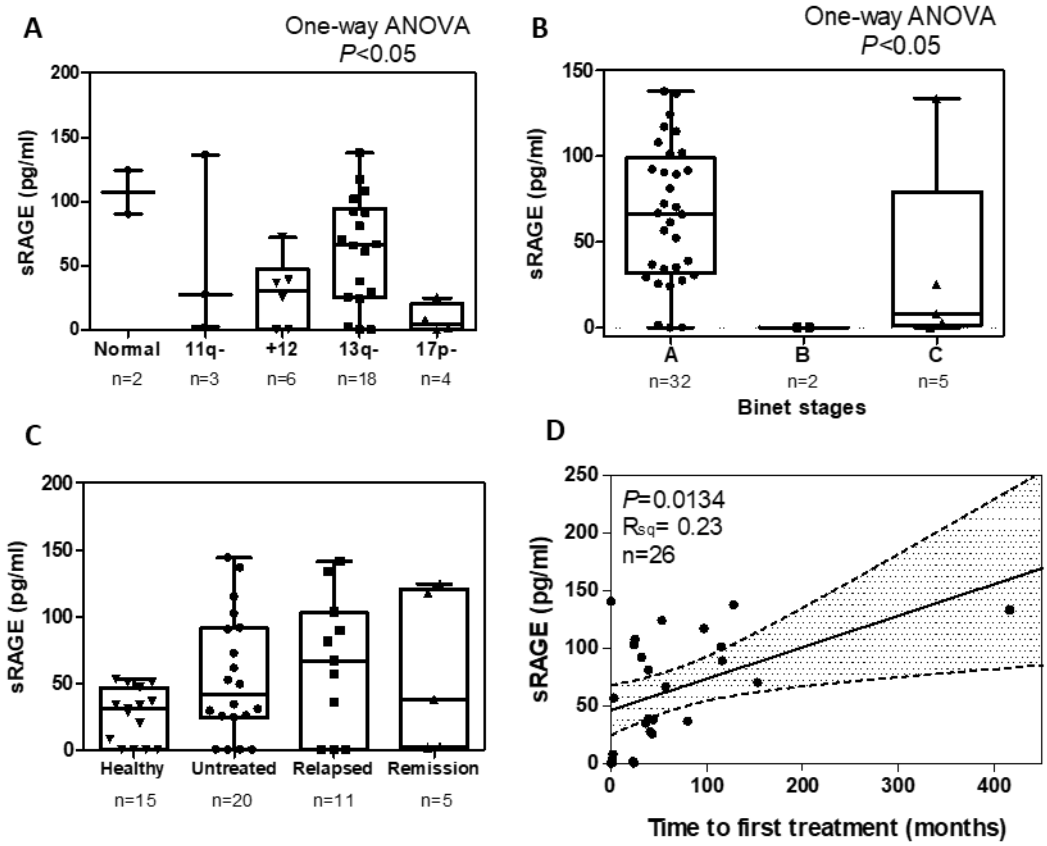

Figure 4-8 Evalulation of extracellular sRAGE association with clinical data
sRAGE plasma levels were compared with CLL patients' cytogenetic aberrations (A), CLL disease Binet staging (B), treatment and treatment outcome (C) and time to first treatment (D). Fresh plasma was collected from 54 CLL patients and stored at -80°C before measuring sRAGE concentration by ELISA. Clinical data was extracted from our tissue bank clinical database. Data presented are median ± interquartile range (A-C) and statistical differences assessed by One-way ANOVA. sRAGE plasma levels and time to first treatment was assessed by Linear regression. Samples sizes (n) are stated in graphs, P=*P*-value, *P*<0.05*, R_{sq}=coefficient of determination.

4.2.4 HMGB1 and sRAGE extracellular levels do not vary with CLL ZAP70 expression

For the patients included in this study, IGHV mutational status or ZAP70 expression was not measured at diagnosis. To further explore an association between HMGB1 and sRAGE plasma levels and CLL disease subsets, patient ZAP70 expression was determined in-house to define aggressive and indolent CLL disease subsets.

ZAP70 expression is determined by flow cytometry in comparison to a setting control. However, the type of control used, impacts the threshold set between positive and negative ZAP70 expression. The advantage of flow-based methodology compared to other expression assays (i.e. Western blotting, IHC, gene expression) is the ability to co-stain and analyse CLL cell-only populations (CD5+/CD19+ cells) compared to other cells in PB that also express ZAP70 (i.e. CD56+ NK and CD3+ T-cells).[336] The 4 main methods utilised in clinic include (Figure 4-9): 1) assessing ZAP70 positivity by comparing to a negative control isotype-matched antibody;[340] 2) assessing ZAP70 positivity by comparing to patient internal positive controls, NK and T-cells;[341] 3) assessing ZAP70 positivity by comparing to a ZAP70 antibody block negative control;[342] 4) assessing ZAP70 positivity by comparing CLL-cell ZAP70 MFI values to internal positive control T-cell MFI values.[343,344]

Using the first 3 methods described above, ZAP70 expression is determined as positive if the percentage of CLL-cell ZAP70 signal is above a threshold of 20% compared to the specific control used. For example, using the first method a patient is defined as ZAP70+ if at least 20% of CD19+/CD5+ CLL cells stain positive for ZAP70 and exceed the signal from the isotype-matched antibody control.[340] However, these 3 methods are highly subjective on user-gating, rendering the results difficult to reproduce. Other caveats of these methods include the use of NK cells as an internal positive control, in which ZAP70 protein is less stable compared to B-cells/T-cells, and the reliability of the unconjugated ZAP70-antibody block method.[336]

In a bid to standardise the method, the European Research Initiative on CLL (ERIC) conducted a harmonisation study across 20 centres in 2006, comparing ZAP70 flow-based methods and different conjugated-ZAP70 antibodies. The most reproducible method, with lower interlaboratory variation, was the T-cell/CLL-cell ZAP70 expression ratio.[298,343] This method relies on ZAP70 expression from T-cells as an internal positive control, so accounts for similar ZAP70 degradation rates as observed in B-cells, limits variation observed from different ZAP70 commercial antibodies, and avoids user variability in gating cursor placement. Previous studies recommend establishing a laboratory determined range of ZAP70 T-cell/CLL-cell ratios, and then dividing this patient cohort in half, giving ZAP70+ and ZAP70- expression.[343] A consequent larger study established a ZAP70 MFI T-cell/CLL-cell cut-off ratio of 3.0 in a test set of 173 patients, and

validated this in an independent cohort of 341 patients.[344] Observed ZAP70 ratios were unaffected by choice of ZAP70 commercial antibody (1E7.2-PE, 1E7.2-AF488, 2F3.2-FITC) compared to high interlaboratory variability when analysing ZAP70 positivity using traditional 20% threshold based methods.[298,345]

For these reasons, the ZAP70 MFI T-cell/CLL-cell ratio method was used in this study with ZAP70 1E7.2-AF488 antibody, and a cut-off ratio value of 3.0.

1) ZAP70 relative to isotype control	2) ZAP70 relative to patients NK and T cells
Threshold: ZAP70+ when 20% CLL cells exceed that of the isotype-matched negative control signal. 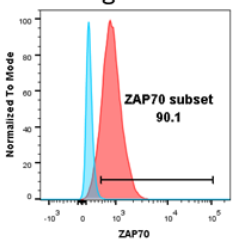 **Issues:** Highly subjective on gating.	**Threshold**: ZAP70+ when 20% CLL cells express ZAP70 comparable to NK and T-cells (positive internal control). 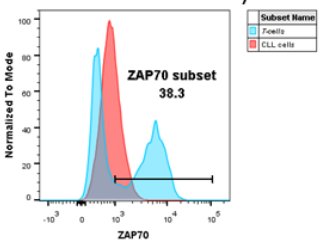 **Issues**: Highly subjective on gating and ZAP70 degrades faster in NK cells compared to B and T-cells.
3) ZAP70 non-conjugated antibody block method	**4) ZAP70 MFI T-cell/CLL-cell ratio**
Threshold: ZAP70+ when 20% CLL cells exceed that of the ZAP70 block CLL cell MFI (negative control). **Issues:** Variability in antibody block.	**Threshold:** CLL-cell ZAP70 MFI compared to T-cell internal positive control ZAP70 MFI. 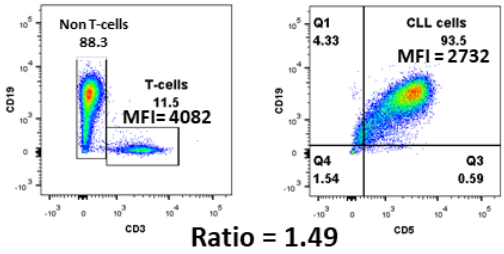 **Ratio = 1.49** **Issues:** ZAP70 positivity is dependent on previously determined range in laboratory rather than percentage.

Figure 4-9 The four main methods of ZAP70 expression assessment by flow cytometry for CLL prognostic stratification

CLL ZAP70 expression is determined by flow cytometry using patient PB CLL B-cells. Currently, there is no standardised procedure, but four main methods are utilised in clinic. 1) ZAP70 expression is positive when 20% of the signal from CD19+/CD5+ CLL B-cells exceeds the signal from an isotype-matched negative control. 2) ZAP70 expression is positive when 20% of the ZAP70 signal from CD19+/CD5+ CLL B-cells are comparable to ZAP70 signals from T-cells and NK-cells patient intrinsic positive controls. 3) ZAP70 expression is positive when 20% of the ZAP70 signal exceeds that from a ZAP70 antibody block matched patient sample negative control. 4) ZAP70 expression is positive when the ratio of ZAP70 MFI from T-cells to CD19+/CD5+ CLL B-cells is <3.0.

ZAP70 expression was assessed for the same cohort of CLL patients included in the HMGB1, S100B and sRAGE ELISAs, using matched PBMCs that were previously cryo-stored at the time of plasma isolation; all PBMCs were stored within 24 hours of isolation to limit ZAP70 degradation. 9/54 patients with a cell viability <80% after thawing, were excluded from this study, leaving 45 patients for ZAP70 analysis. Surface CD19, CD5 and CD3 were co-stained prior to permeabilisation and fixation, and intracellular ZAP70 stained with anti-ZAP70 1E7.2-AF488 conjugated antibody. ZAP70 expression was measured as the ratio of ZAP70 MFI from CD3+ T-cells to CD19+/CD5+ CLL cells; patients with a ratio >3.0 were ZAP70- and patients with a ratio <3.0 were ZAP70+.[344]

Using this method, 16 patients were ZAP70- and 29 patients were ZAP70+ for this cohort of patients. The normality of our calculated ZAP70 ratios was significant using the Shapiro-Wilk test (*P*=0.023; Figure 4-10A), revealing a non-normal data distribution with skewing towards MFI ratios <3.0, i.e. ZAP70+ expression (Figure 4-10B). We did not observe an association between extracellular HMGB1 levels and cytogenetic risk factors or Binet staging (Figure 4-5), and HMGB1 was not significantly altered between ZAP70+/- subsets (ZAP70- mean HMGB1=105.1ng/ml and ZAP70+ mean HMGB1=93.9ng/ml; *P*=0.43; Figure 4-11A). Moreover, there was no association between ZAP70+/- expression and extracellular sRAGE levels (ZAP70- mean sRAGE=61.6pg/ml and ZAP70+ mean sRAGE=59.9pg/ml; *P*=0.43; Figure 4-11B). These results demonstrate HMGB1 and sRAGE release are not CLL-subset specific.

A

Shapiro-Wilk		
Statistic	df	Sig.
.941	45	.023

B

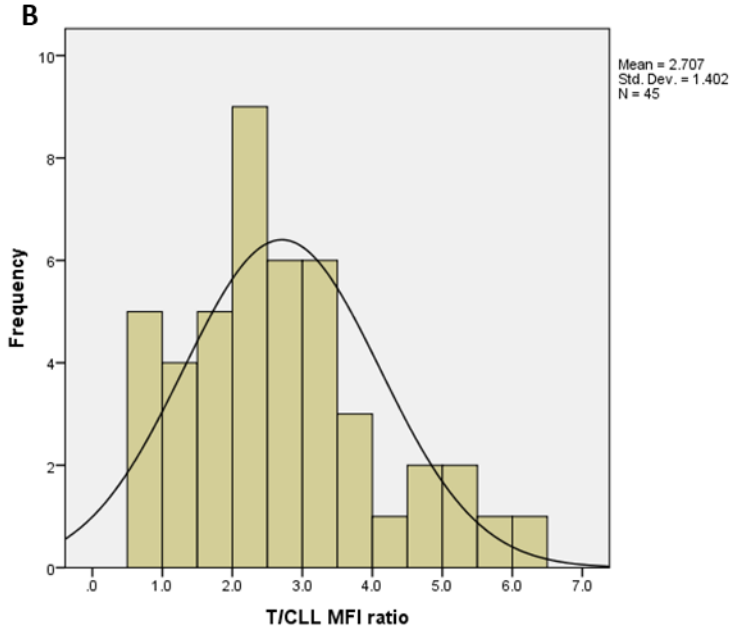

Figure 4-10 ZAP70 T-cell/CLL-cell MFI ratio data test of normaility and data distribution plot
The Shapiro-Wilk test was used to measure data normality (A); a significant result indicates a non-normal data distribution. Data are presented in a histogram plot (B) to show data spread; data are skewed towards ratios <3.0, i.e. ZAP70 positive expression.

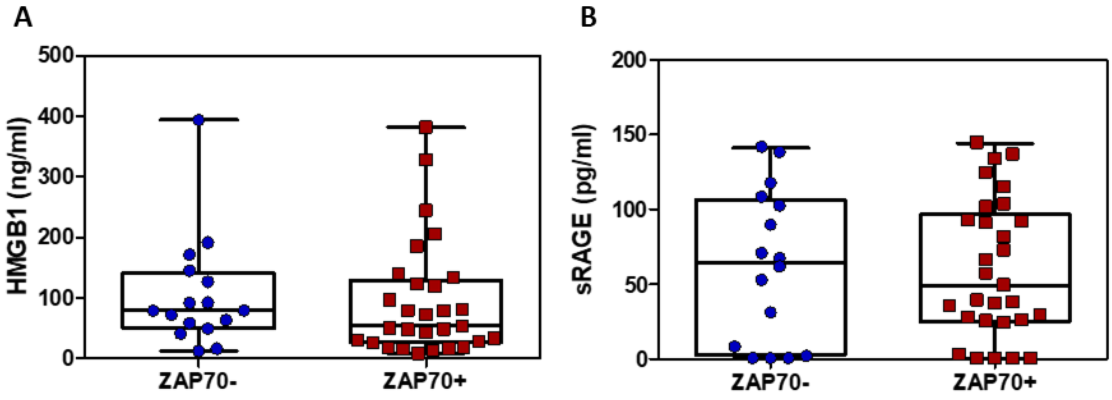

Figure 4-11 Evaluation of CLL patient HMGB1 and sRAGE plasma levels in ZAP70 positive or negative subsets
Plasma levels of CLL HMGB1 (A) and sRAGE (B) were determined by ELISA and compared to PB CLL cell ZAP70 positive or negative expression subsets determined by flow cytometry. Data are presented as medians with interquartile ranges, ZAP70+ n=29 and ZAP70- n=16; statistical difference between samples was analysed by Mann-Whitney U test.

4.2.5 Blocking HMGB1 receptor, RAGE, does not induce cell death *in vitro*

Extracellular HMGB1 has reported dual roles in cancer, driving pro-tumour or anti-tumour responses that are partly dependent on the microenvironment 'make-up' in the same spatial location.[131] To investigate the functional significance of increased HMGB1 plasma levels in CLL patients (aside from NLC differentiation), we assessed if exogenous HMGB1 stimulation prolongs CLL cell survival *in vitro* and if blockade of HMGB1 receptor, RAGE, can block survival signals.

A cell survival assay was used compared to a cell proliferation assay, due to the quiescent *in vitro* CLL-cell phenotype that is observed when primary cells are grown in culture. This phenomenon renders cell proliferation assays difficult to successfully perform *in vitro*. Cell death was assessed by the Annexin V assay in 11 freshly isolated PBMCs from CLL patients. Freshly isolated PBMCs were cultured at high density ($10x10^6$ cells/ml) in complete medium and treated with PBS, 200ng/ml HMGB1, 500ng/ml HMGB1 or 10μg/ml neutralising anti-RAGE antibody. Increasing doses of HMGB1 were used to recapitulate the CLL plasma concentrations previously determined by our ELISA results (Figure 4-4A). Cells were cultured for 48 hours or 120 hours prior to staining with Annexin V-FITC and PI. CLL cells rapidly die in culture upon removal from niche sites rich in supporting microenvironment signals; therefore, a 48-hour time point was used to assess cells before committing to spontaneous cell death, and a longer time point of 120 hours to capture spontaneous cell death. Using the Annexin V assay, alive (PI-/Annexin V-), apoptotic (PI-/Annexin V+) and dead cells (PI+/Annexin V+) were distinguished (Figure 4-12A). There was no difference in cell survival *in vitro* at the 48 or 120-hour time points in response to HMGB1 stimulation or RAGE blockade for CLL patient PBMCs (Figure 4-12B and C).

CLL patients exhibit varying CLL-cell purity in PB, with infiltrating cell subsets supporting and maintaining CLL cell survival, particularly M2- polarised macrophage cell subsets. Next, we assessed the effect of HMGB1 and RAGE blockade directly on isolated pure CLL B-cell populations by using CD19+ positive selection and negative selection kits. CD19 positive selection isolates CD19+ B-cells by using CD19-conjugated magnetic beads. B-CLL negative selection works in reverse, and depletes the PBMC of other cell populations by using conjugated magnetic microbeads to a panel of cell surface markers. Both isolation methods were used to account for possible CD19-mediated cell stimulation via microbead conjugation. Our data shows CD19-positive and CLL-negative isolated cells are more susceptible to spontaneous cell death *in vitro* (Figure 4-13). This result was expected, as CLL cells heavily rely on the surrounding microenvironment for survival signals and anti-apoptotic signals that are not intrinsic to CLL cells.[337] Exogenous HMGB1 and RAGE blockade had no significant effect on cell survival *in vitro* on our isolated CLL-cell population (Figure 4-13).

An *in vitro* experimental setting is not an ideal model system to perform a CLL cell survival assay.[338] CLL dependence on growth signals and microenvironment support, as established in CLL LNs, outweighs experimental modifications as performed here, and rapidly leads to *in vitro* spontaneous cell death. Therefore, we could not successfully model the effect of HMGB1 on CLL cell proliferation or survival in this study.

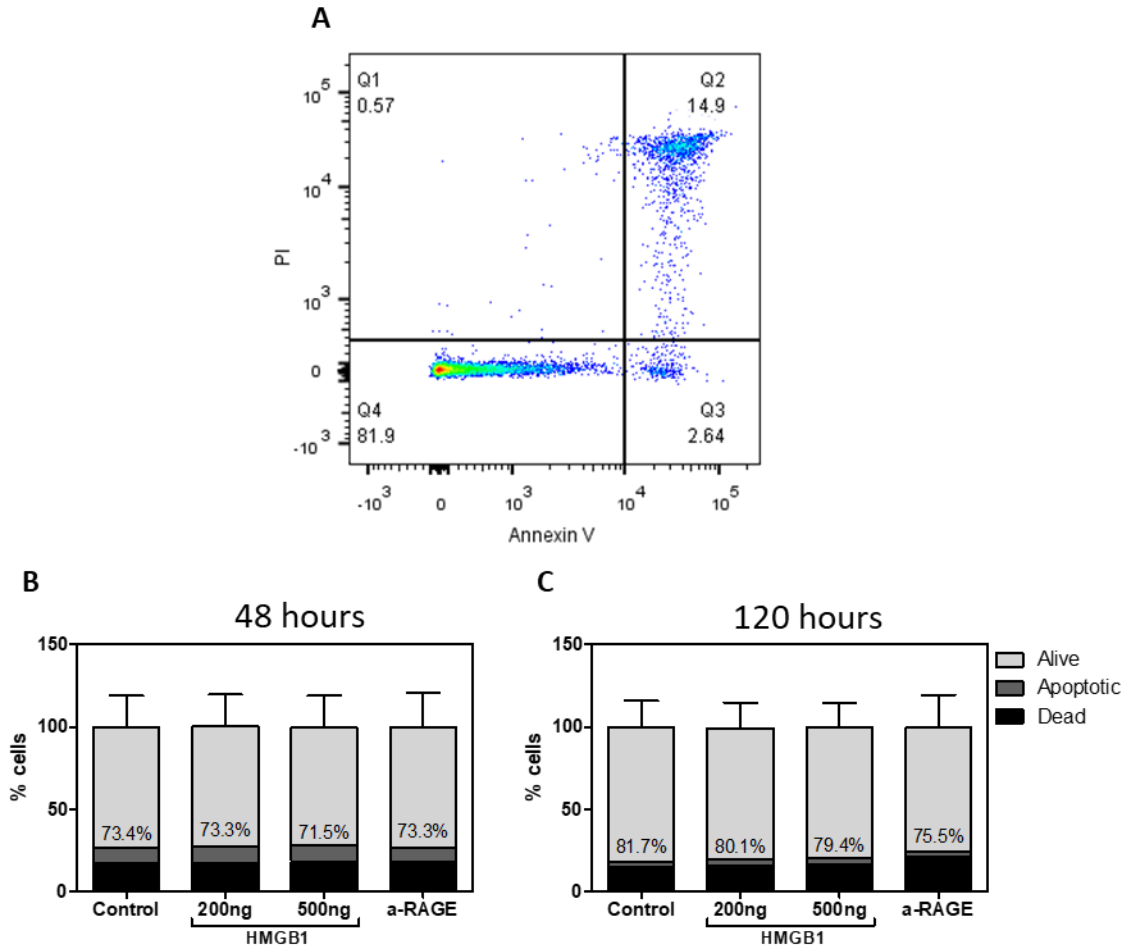

Figure 4-12 Evaluation of cell survival in fresh primary CLL PBMCs in response to exogenous HMGB1 stimulation and RAGE blockade *in vitro*

Fresh CLL patients PBMCs were stimulated with 200ng/ml and 500ng/ml HMGB1 or blocked with 10µg/ml neutralising anti-RAGE antibody before measuring cell death using the Annexin V assay. Dead cells (PI+/Annexin V+), apoptotic cells (PI-/Annexin V+) and live cells (PI-/Annexin V-) were measured by flow cytometry; representative flow plot (A). PBMCs were cultured for 48 (B) or 120 hours (C) before cell survival was assessed. Data are presented as mean ± SD and statistical differences between samples was analysed by Two-way ANOVA; n= 11 patients. The percentages on graph bars are the % of live cells measured as PI-/Annexin V-.

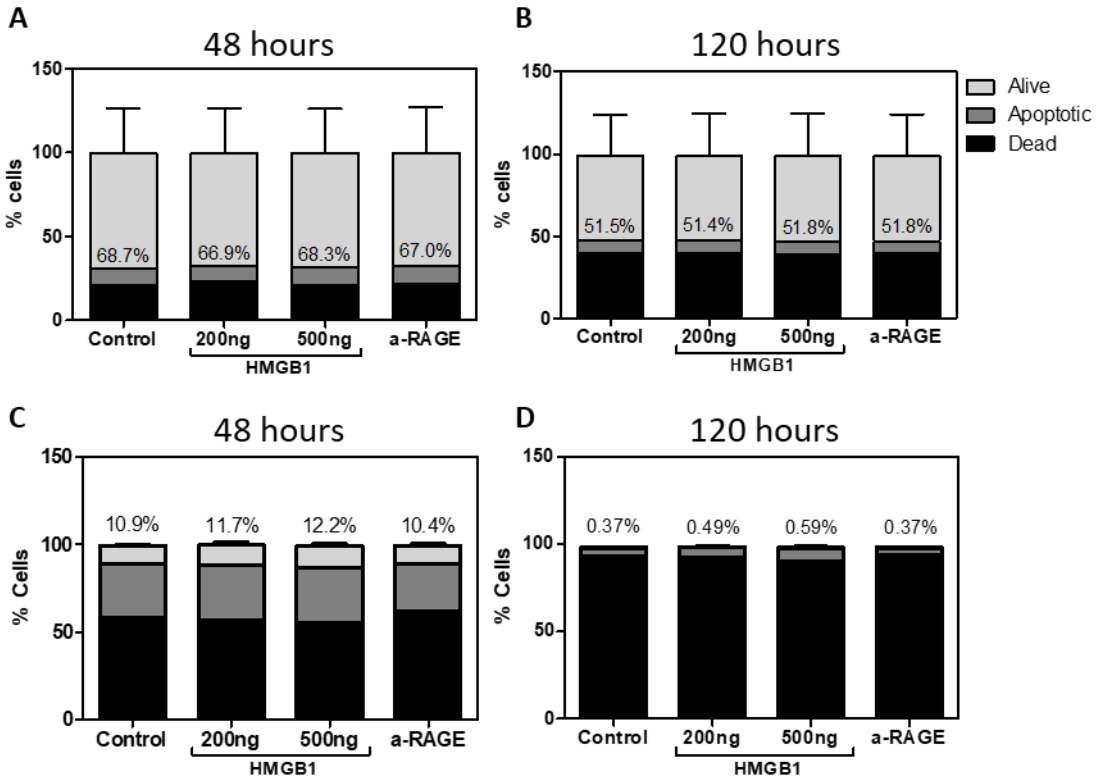

Figure 4-13 Evaluation of cell survival in fresh CD19-positive selection or CLL-negative isolated CLL cells in response to exogeneous HMGB1 stimulation and RAGE blockade *in vitro*

CD19+ B-cells were isolated from fresh CLL PBMCs by CD19+ MACS selection (A-B) and CLL cells were isolated from fresh PBMCs by B-CLL negative selection kit (C-D). Freshly separated cells were treated with 200ng/ml and 500ng/ml HMGB1 and RAGE blocked with 10µg/ml neutralising anti-RAGE antibody and cultured for 48 (A and C) and 120 (B and D) hours. Cells death was assessed by Annexin V assay and data for dead cells (PI-/Annexin V-), apoptotic cells (PI-/Annexin V+) and live cells (PI+/Annexin V+) was recorded. Data are presented as the mean ± SD and statistical difference between samples was analysed by Two-way ANOVA; n=4 for CD19+ selection and n=2 for B-CLL negative selection. The percentages on graph bars = % of live cells measured as PI-/Annexin V-.

4.3 Discussion

In this chapter, we have confirmed plasma HMGB1 levels are significantly increased in untreated and relapsed patients, compared to S100B and antagonistic sRAGE. Extracellular HMGB1 and sRAGE levels are CLL subset independent, and HMGB1 receptor expression is more prevalent in CD19+ B-cells in CLL PB. Although we could not model the outcome of HMGB1 stimulation in CLL B-cells *in vitro*, the work in this study strengthens the clinical relevance of HMGB1 and RAGE in CLL disease pathogenesis.

RAGE and TLR9 mRNA expression is increased in CLL B-cells compared to healthy controls, but other leukocyte subsets also express these receptors.[316] Surface RAGE MFI was higher in circulating CD14+ monocytes in PB, but intracellular RAGE was significantly higher in circulating CD19+ B-cells. When we consider CD19+ B-cells make up >90% of the PBMC population, HMGB1 ligand will clearly be sequestered by receptors on CD19+ B-cells and activate signalling pathways predominately in this cell subset. Higher intracellular levels of RAGE in B-cells hint at receptor internalisation – a key mechanism involved in mediating RAGE signalling.[194] These results, combined with RAGE and TLR9 LN expression, provide rationale to further investigate HMGB1 signalling directly in CLL B-cells.

RAGE is a key mediator between acute and chronic inflammation implicated in several pathological diseases.[176] To perform this function, RAGE binds various DAMPs via 3 extracellular Ig-domains. The main ligands include HMGB1, S100 proteins (family of 21 members) and AGEs. Although extracellular ligand-RAGE signalling contributes to tumour progression, as occurs continuously within the tumour microenvironment,[339] S100B is the only other RAGE ligand (aside from HMGB1) with a defined prognostic association with patient outcome in cancer – specifically, melanoma.[333] Our results show HMGB1 levels are significantly higher than S100B in CLL, and compared to healthy controls, demonstrating HMGB1-RAGE is more prevalent in CLL. However, the extracellular role of HMGB1 is dependent on its redox state.[346] Fully oxidised HMGB1 at Cys23, Cys45 and Cys106 is inactive but promotes immune tolerance [347]. Disulphide HMGB1 between Cys23-Cys45 has cytokine activity and drives leukocyte activation, and all-thiol HMGB1 with fully reduced Cys23, Cys45 and Cys106 displays chemokine activity.[348] Oxidative stress was detected in CLL patients and associated with poor prognosis [349]. It is likely all 3 states occur in the tumour microenvironment as the extracellular redox status within the tumour vicinity is continually changing. Few studies have successfully reported HMGB1 post-translational modifications, due to the unavailability of antibodies specific to the different functional isoforms of HMGB1.[346] In CLL, increased levels of HMGB1 may not possess biological functional activity if fully oxidised which we have not measured here, but we propose a cycle of

reduction upon entering and leaving CLL LNs and BM, key sites of disease pathogenesis, and re-oxidation when released into PB.

Soluble RAGE circulating in human plasma, is modulated in chronic diseases impacted by RAGE and its ligands. The extracellular pool of sRAGE derives from 2 origins – membrane shedding catalysed by ADAM10 as an anti-inflammatory mechanism, or alternative splicing to produce an endogenous-secreted RAGE isoform.[192,215] Membrane shedding is a tightly controlled process under normal physiological conditions, but is deregulated in pathological conditions that display altered metalloproteinase activity, as observed in this study.[219] Tracking levels of sRAGE is increasingly gaining recognition as a biomarker for inflammatory chronic disease.[350-352] Surprisingly we observed higher levels of sRAGE in CLL compared to healthy controls, the opposite result to down-modulated sRAGE levels frequently reported in solid cancer.[353] Extracellular HMGB1 levels are significantly higher than sRAGE in CLL so will fail to fully inhibit HMGB1, but this highlights that increased sRAGE may be due to ligand-induced membrane receptor shedding catalysed by ADAM10 activity. Moreover, the involvement ADAM10 may be a side-product of NOTCH1 signalling in CLL.[218] We identified higher extracellular sRAGE levels confer a protective effect in CLL so further investigation of sRAGE origin and involvement of ADAM10, as described in Chapter VI, will pinpoint the precise role of sRAGE in CLL.

U-CLL status and PB ZAP70 expression are powerful, associated prognosticators for CLL disease. The association with either U-CLL or ZAP70+ expression helps to determine the severity of other molecular markers, i.e. RAGE and HMGB1. Although the standard prevalence of ZAP70-/M-CLL to ZAP70+/U-CLL disease is usually 60%:40%;[50] ZAP70+ expression to ZAP70- was 29:16 for our cohort of CLL patients by in-house flow cytometry. The ZAP70 MFI T-cell/CLL-cell ratio method is the most robust method to date, following extensive testing across diagnostic laboratories with different commercial antibodies. The skewing of our cohort of CLL patients towards ZAP70+ may be due to our patient inclusion criteria rather than experimental false positives. Recent improvements in the ZAP70 MFI flow cytometry method to increase robustness, include correcting T-cell and CLL-cell ZAP70 MFI by removing background fluorescence with an isotype-matched control.[299] However, this method currently has no validated data range or cut off-value, so the traditional ZAP70 MFI ratio was used in this study instead. These results demonstrate that RAGE expression in CLL LN may be linked to disease severity, but HMGB1 release is independent of CLL subtype.

To functionally investigate the biological effect of high HMGB1 plasma levels we assessed the longer-term outcome of HMGB1 signalling *in vitro*. CLL-cells circulating in PB undergo cell cycle arrest and are resistant to programmed cell death, contributing to chemotherapy resistance in

CLL.[354] However, as soon as cells are removed *ex vivo*, CLL-cells rapidly lose their anti-apoptotic mechanisms and undergo spontaneous cell death *in vitro*.[338] To dissect a direct role for HMGB1 in CLL B-cell proliferation, we tried to model and investigate if HMGB1 contributes to the acquired anti-apoptotic mechanisms for CLL-cell survival *in vitro*. HMGB1 is a known inducer of NLC differentiation, and this cell population is observed *in vitro* following 1 week of culture, after an initial drop in CLL-cell viability.[76,337] However, without the support of other key growth factors and co-culture with stromal cells, particularly using time-points prior to NLC differentiation, we did not measure a direct difference in HMGB1-induced cell survival with this *in vitro* model.

In summary, these results demonstrate that the HMGB1-RAGE signalling axis is more prevalent in CLL than other RAGE ligands, or in other cell populations. HMGB1 release is CLL-subset independent, but the signalling capacity of HMGB1 will likely coincide with BCR-signalling responsiveness. sRAGE levels are deregulated in CLL, compared to the classical inverse trend between HMGB1 and sRAGE observed in the healthy controls, but confers a protective effect. These results demonstrate extracellular HMGB1 and cellular RAGE are clinically relevant, and deciphering the signalling pathways activated by these proteins will reveal key targets for therapeutic intervention.

Chapter V

Determine HMGB1-mediated cell signalling activation

5.1 Introduction

We have identified an association between extracellular HMGB1 levels and receptor expression, RAGE, with poor CLL disease outcome but the functional significance of these results in CLL is currently not known. Although we could not model the direct impact of HMGB1 on CLL cell survival *in vitro*, these results give us rationale to further investigate the HMGB1-RAGE signalling axis and demonstrates a pro-tumour role for the DAMP. Insight into the HMGB1 phosphoproteome will reveal receptor usage, co-activation of other unidentified HMGB1 signalling pathways, and potential therapeutic targets for the treatment of CLL.

Identified receptors for inflammatory DAMP, HMGB1, include RAGE and TLRs 2, 4 and 9.[146] Receptor selection heavily relies on the cell-type specific expression profile; i.e. activation of TLRs are responsible for myeloid cells and RAGE in endothelial cells.[146] The full HMGB1 signalling pathway is not fully elucidated, but has been demonstrated to activate NF-κB and stimulate IFN-α, TNF, IL-6 and IL-12 production and can contribute to both pro- and anti-tumour responses.[145,149] To fulfil its role as a DAMP, HMGB1 can function as a free molecule or complex with other ligands/signalling mediators to increase their immunogenicity.[131] This renders HMGB1 particularly difficult to target, as the preference in signalling pathway activation is dependent on the presence of other ligands and cell type;[144] moreover, HMGB1 blockade could result in a bias towards pro- or anti-tumour activity.

A B-cell specific synergism has been observed between RAGE and TLR9 following HMGB1 stimulation. HMGB1 can bind to DNA in a sequence independent manner, and has demonstrated ability to bind to both A and B classes of CpG-ODNs.[145,149] For SLE B-cells, DNA-containing autoimmune complexes are internalised by BCR endocytosis,[260] but an autoantibody-independent mechanism exists. Double stranded extracellular DNA bound to HMGB1 is internalised via RAGE, and stimulates TLR9 activity.[145] Our group previously demonstrated that extracellular HMGB1 levels positively correlate with extracellular DNA levels in CLL, indicative of passive HMGB1 release.[76] Therefore, it is plausible that HMGB1 exists in DNA-bound complexes circulating in CLL disease. Following TLR9 engagement, CpG-ODN drives dichotic responses in CLL dependent on ZAP70 expression.[96] Our group have already shown RAGE/TLR9 dependent differentiation of NLCs in response to HMGB1,[76] but whether RAGE and TLR9 function in a co-linked manner directly in CLL cells, as is observed in CLL NLCs, and lead to the activation of NF-κB is unknown. Using 2 imaging approaches and an unbiased phosphoproteomic approach, we will be able to assess whole cell signalling network activation following treatment with RAGE agonist, HMGB1, a TLR9 agonist, CpG-ODN (B-class).

The work in this chapter will determine i) the main HMGB1 receptor in CLL; ii) HMGB1-mediated colocalization of RAGE and TLR9; iii) HMGB1-mediated activation of cell signalling pathways.

5.2 Results

5.2.1 RAGE and TLR9 are the most likely binding partners of HMGB1 in CLL B-cells

We have demonstrated increased gene expression of HMGB1 receptors, RAGE and TLR9, in CLL patients compared to age-matched healthy controls using available gene expression datasets,[316] and overexpression of RAGE in CLL LNs confers a worse overall survival for CLL patients. However, the signalling capacity of these receptors in response to HMGB1 stimulation in CLL cells is unknown. HMGB1 can potentially interact with multiple cellular receptors leading to the activation of several signalling pathways that are cell-type specific.[76,149,281] In combination with the gene expression data from Chapter III, we first assessed the binding affinities of multiple receptors for HMGB1 using available online database, STRING (https://string-db.org/), to determine the main functional HMGB1 receptors in CLL.[355]

The main receptors for HMGB1 include TLR1, 2, 4, 9 and RAGE (Figure 5-1). STRING computes a protein-protein association functional score from 0-1 based on high-throughput experimental data, online database mining, literature searches and predictions from genomic context analysis.[356] TLR1, TLR2, TLR4 and RAGE displayed the highest scores for HMGB1 functional associations of >0.9 (0.900, 0.997, 0.998 and 0.972, respectively; Table 9). TLR9 displayed a functional score of 0.8 and all other TLRs displayed little or no functional association with HMGB1, displaying scores <0.1 (Table 9). We demonstrated decreased gene expression of TLR1, TLR2 and TLR4 in CLL compared to age-matched healthy controls (Figure 3-1), but this does not give an indication of receptor protein levels. Performing a literature search, TLR4 lacks expression at the protein level in CLL B-cells, so will not mediate HMGB1 cell activation directly in CLL cells (Table 9). The other 4 HMGB1 receptors with high functional association scores, TLR1, TLR2, TLR9 and RAGE, are expressed to protein level in CLL. The TLR expression profile in CLL cells is similar to a mature B-cell phenotype, and we previously demonstrated RAGE and TLR9 mRNA expression was significantly increased in CLL PB cells compared to healthy controls, and (Figure 3-1).[317] Taking this data together, we hypothesise that extracellular HMGB1 in the CLL microenvironment interacts with high affinity to RAGE and could lead to the co-activation of intracellular receptor TLR9 as previously reported in B-cells.

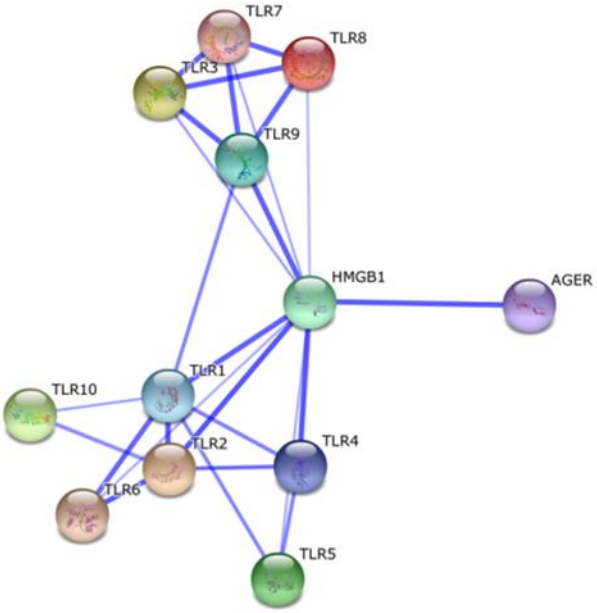

Figure 5-1 Interaction network map of HMGB1 and its receptors predicted by STRING database
The functional association scores and interaction map were calculated and produced by STRING database.[355] Each node represents a different protein and the thickness of each connecting line represents the degree of functional association between two proteins; the thicker the line, the higher the association score. AGER = RAGE.

Table 9. STRING HMGB1 receptor functional association scores, mRNA expression and evidence of protein expression in CLL

Receptor	Functional association score	Gene expression transformed count	Protein expression in CLL (Refs)
RAGE	0.972	2.98	+ [76]
TLR1	0.900	3.92	+ [317,357]
TLR2	0.997	2.55	+ [317,357]
TLR3	0.073	2.93	-
TLR4	0.998	3.74	- [76,317]
TLR5	0.073	2.52	-
TLR6	0.073	3.43	+ [317,357]
TLR7	0.073	4.86	+ [317,318]
TLR8	0.073	2.82	-
TLR9	0.800	6.09	+ [76,96,317]
TLR10	0	5.99	+ [357]

Note: Functional association score extracted from STRING database;[356] gene expression transformed count represents log2 transformed and RMA normalised mRNA expression data from online GEO dataset (GSE22529).[316]

5.2.2 Treatment with recombinant HMGB1 mediates RAGE/TLR9 colocalization

HMGB1 links RAGE and TLR9 in an inflammatory triad, as an established DNA and CpG-ODN binding partner.[145,149] This signalling triad is responsible for the activation of NF-κB in malignant and non-malignant inflammatory conditions.[76,145,281] Our group previously reported HMGB1-mediated activation of RAGE and TLR9, driving CLL NLC differentiation.[76] Moreover, the HMGB1-RAGE signalling axis poses as a BCR-independent route for nuclear complex internalisation, and activation of TLR9 by presentation of CpG-ODN ligand in autoreactive B-cells.[145] It is currently unknown whether HMGB1 induces RAGE and TLR9 colocalization and signalling activation in CLL B-cells.

We used 2 imaging systems to qualitatively and quantitatively measure protein colocalization and nuclear translocation. Immunofluorescent microscopy was used as a qualitative technique to investigate protein expression with additional spatial localisation information, and can reveal protein-protein interactions.[303] Imagestream X Mark II flow cytometry was employed as a quantitative comparison – the combination of flow cytometry with fluorescence microscopy allows for acquisition of statistically powerful data and detailed morphological fluorescence information of every cell.[304]

Using fluorescent microscopy, we determined the activation of RAGE and TLR9 in response to exogenous HMGB1 treatment in primary CLL cells. Protein colocalization was measured with ImageJ analysis software using dual colour images to perform the pixel intensity spatial correlation analysis. The Pearson's correlation coefficient measures the degree of colocalization of fluorescent pixels in two colour channels, i.e. RAGE in the red channel and TLR9 in the green channel; a coefficient of +1 indicates perfect correlation, 0 for no correlation and -1 for perfect anti-correlation. We observed strong colocalization of RAGE and TLR9 in primary CLL cells following exogenous treatment with 200ng/ml HMGB1 for 2 and 4 hours (yellow aggregates indicate pixel overlap and colocalization; Figure 5-2A), and following *in vitro* culture for 1 week, conditions which induce HMGB1 release into cell culture medium to levels of 150ng/ml (Figure 5-2A).[76] RAGE and TLR9 protein colocalization was significantly higher than untreated 0 hour control sample after 2 hours HMGB1 stimulation (0hr control mean Rr= 0.36, 2hr HMGB1 mean Rr= 0.59; $P<0.01$; Figure 5-2B) and 4 hours HMGB1 stimulation (0hr control mean Rr= 0.36, 4hr HMGB1 mean Rr= 0.57; $P<0.05$; Figure 5-2B). Treatment with 10μg/ml neutralising anti-RAGE antibody, followed by addition of 200ng/ml HMGB1 for 2 and 4 hours prevented (not significant) HMGB1-mediated RAGE and TLR9 colocalization (Figure 5-2B).

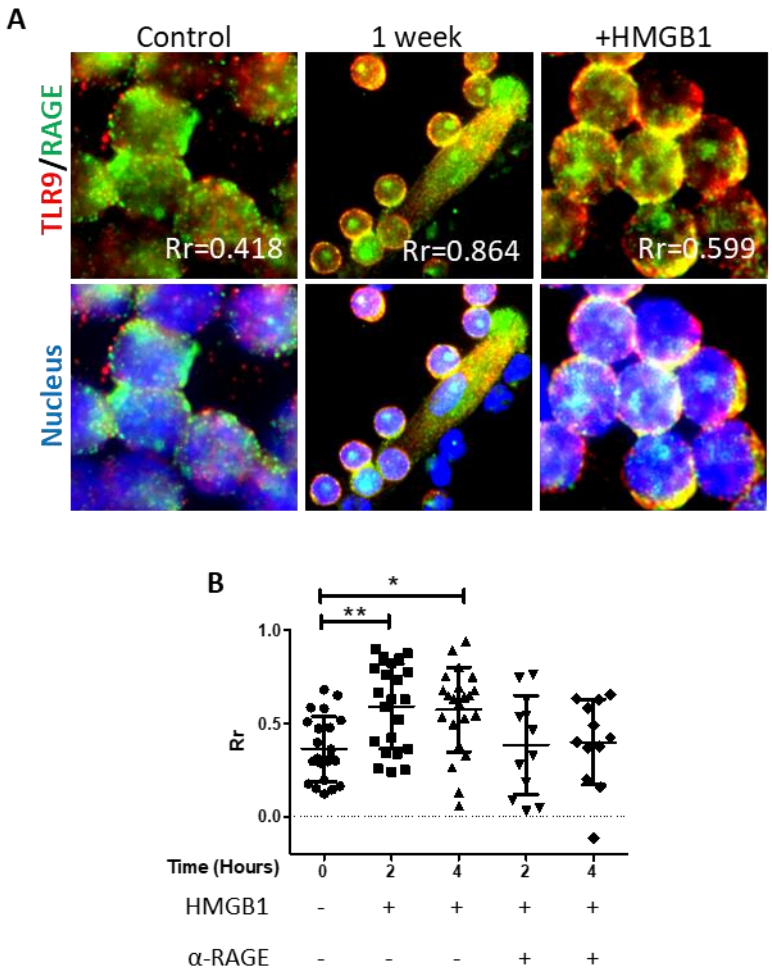

Figure 5-2 Fluorescent microscopy analysis of HMGB1-mediated RAGE and TLR9 colocalisation in primary CLL cells

(A) Representative images of RAGE and TLR9 colocalization. Fresh CLL cells (control), cells cultured for 1 week (1 week), or cells treated with 200ng/ml HMGB1 for 2 hours (+ HMGB1) were fixed and permeabilized on slides. Cells were then co-stained with anti-RAGE/AF-488 and anti-TLR9/AF-546 antibodies. Areas where green pixels (RAGE) and red pixels (TLR9) overlap give yellow aggregates, representing protein colocalization. Magnification x60 and x100. (B) Pixel intensity spatial correlation analysis of HMGB1-mediated colocalization of RAGE and TLR9. Fresh CLL cells were left untreated for 0-hours or incubated with 200ng/ml HMGB1 for 2 and 4 hours with or without 10µg/ml neutralising anti-RAGE antibody (α-RAGE). RAGE and TLR9 protein colocalization was analysed using ImageJ software and 'Rr' indicates Pearson's correlation coefficient. Data are mean ± SD from 5 individual CLL patients and differences compared with unpaired t test; $P<0.05$*, $P<0.01$**. 5 images were analysed per patient sample. Immunofluorescence was observed at 100x magnification using the Nikon eclipse Ci-E fluorescence microscope using the green, blue and red channels.

To confirm this quantitatively, on a larger population of cells, we performed ImageStream X Mark II flow cytometry. Using this method, we can collect fluorescence intensity and microscopy images of 5000 cells simultaneously. Protein colocalization was measured in the same manner as the pixel intensity spatial correlation analysis with ImageJ. The ImageStream IDEAS software removes background fluorescence to concentrate bright spots, and calculates the Pearson's correlation coefficient for each pixel in the dual-colour image. The Pearson's correlation coefficient is then log transformed to give the similarity bright detail score (SBDS) – the higher the SBDS, the higher the level of pixel overlap and protein colocalization. The colocalization of RAGE and TLR9 was significantly higher following treatment with 200ng/ml HMGB1 for 2 and 4 hours compared to the untreated control cells (2 hours untreated mean SBDS=1.263, HMGB1=1.282, $P<0.01$; 4 hours untreated mean SBDS=1.250, HMGB1 1.278; $P<0.001$, respectively; Figure 5-3). Treatment with 10µg/ml neutralising anti-RAGE antibody and 200ng/ml HMGB1 addition abrogated HMGB1-mediated RAGE and TLR9 colocalization at 4 hours (4 hours HMGB1 mean SBDS=1.278, anti-RAGE=1.250, $P<0.001$; Figure 5-3), but not at 2 hours (2 hours HMGB1 SBDS=1.282, anti-RAGE=1.274; Figure 5-3). In both fluorescence microscopy and ImageStream images, internalization of RAGE is visible following addition of HMGB1, compared to the localization of RAGE at the cell membrane in non-stimulated or RAGE-neutralised cells.

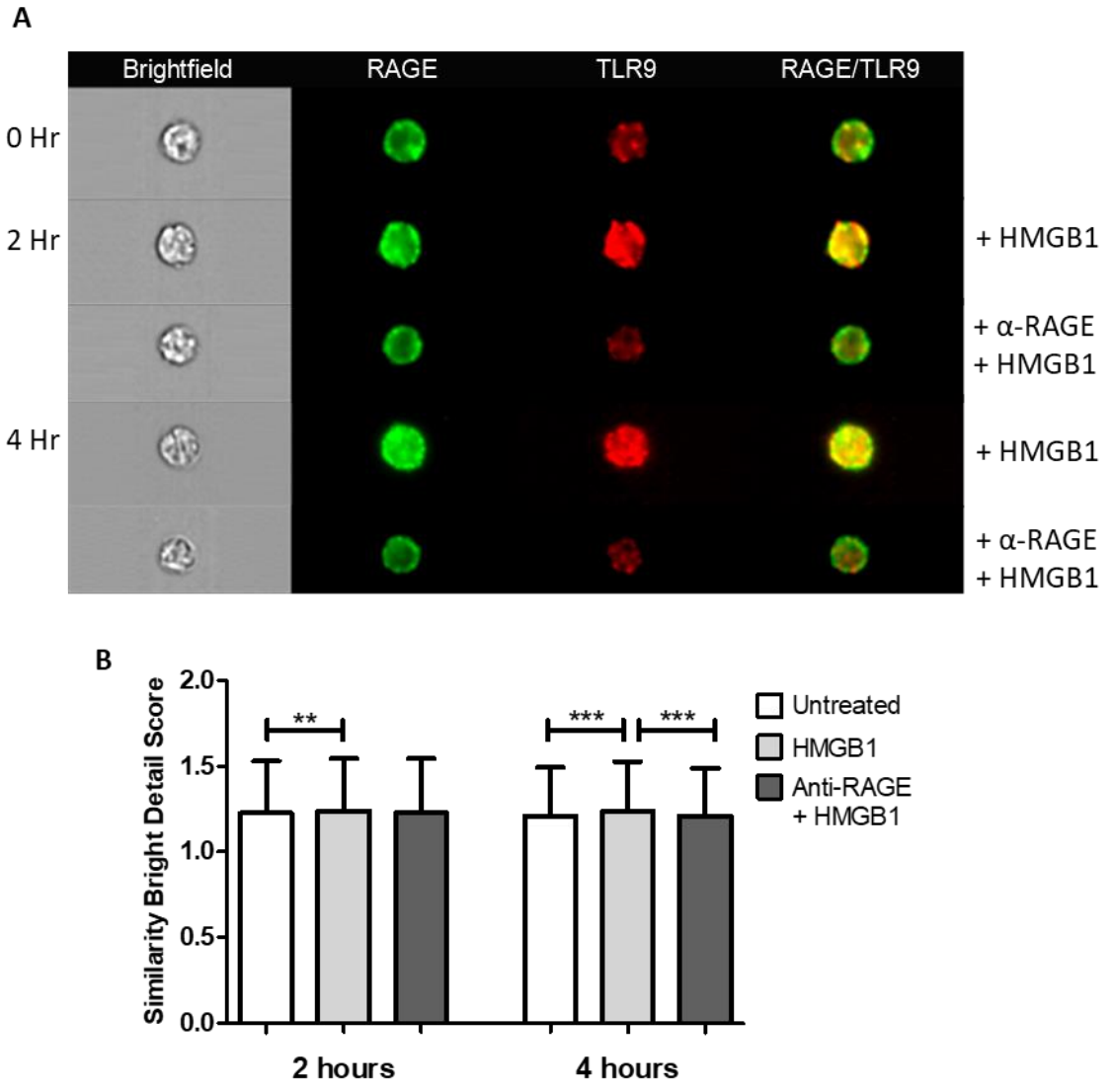

Figure 5-3 ImageStream analysis of HMGB1-mediated RAGE and TLR9 colocalisation in primary CLL cells

(A) Representative images of RAGE and TLR9 colocalization captured by the ImageStream X Mark II flow cytometer; magnification x40. Fresh CLL cells were treated with 200ng/ml HMGB1 (+ HMGB1) with or without 10µg/ml goat anti-RAGE neutralising antibody (α-RAGE) for 2 and 4 hours. Cells were fixed/permeabilised, co-stained with anti-RAGE/AF-488 and anti-TLR9/AF-647 antibodies and data/images assessed by ImageStream flow cytometry and colocalizaiotn analysed by IDEAS software. (B) Statistical analysis of RAGE and TLR9 protein colocalization using the IDEAS software. Protein colocalization was measured as the log transformed Pearson's correlation coefficient termed the Similarity Bright Detail Score, and was measured for every cell recorded in 5 patients. Data are presented as median with interquartile range. 2 hours untreated n= 17428, HMGB1 n=16604, anti-RAGE n=10007; 4 hours untreated n=13348, HMGB1 n=13752, anti-RAGE n=7192. Differences were compared with an unpaired Mann Whitney U test; *P*<0.01**, *P*<0.001***.

Next, we assessed the colocalization of TLR9 and MyD88 in the same cohort of patients, as an indicator of TLR9 signalling pathway activation. Using fluorescent microscopy, TLR9 and MyD88 colocalization was not increased following 2 and 4 hours stimulation with 200ng/ml HMGB1 compared to fresh untreated CLL cells (0-hour control Rr=0.38, 2 hours HMGB1 Rr=0.44, 4 hours HMGB1 Rr=0.37; Figure 5-4). However, surface RAGE neutralisation with 10µg/ml goat anti-RAGE antibody significantly decreased HMGB1-mediated TLR9 and MyD88 colocalization after 2 hours, but not at 4 hours compared to stimulation alone with HMGB (2 hours HMGB1 Rr=0.44, anti-RAGE Rr=0.23, $P<0.05$; 4 hours HMGB1 Rr=0.37, anti-RAGE Rr=0.23; Figure 5-4). Using quantitative ImageStream flow cytometry for the same patient samples, 200ng/ml HMGB1 stimulation induced significantly higher TLR9 and MyD88 protein colocalization following 4 hours stimulation compared to untreated controls (4 hours untreated mean SBDS=1.117, HMGB1=1.135, $P<0.05$; Figure 5-5), but not at 2 hours (2 hours untreated mean SBDS=1.059, HMGB1=1.086; Figure 5-5). Blockade of RAGE with 10µg/ml neutralising anti-RAGE antibody significantly abrogated HMGB1-mediated TLR9 and MyD88 colocalization at both 2 and 4 hours (2 hours HMGB1 mean SBDS=1.086, anti-RAGE=1.067, $P<0.001$; 4 hours HMGB1 mean SBDS=1.135, anti-RAGE=1.061, $P<0.001$; Figure 5-5).

Taken together, these results demonstrate that HMGB1 does mediate RAGE and TLR9 colocalization, which is blocked when surface RAGE is neutralised. We did observe TLR9 and MyD88 colocalization at longer time points, but the nature of RAGE and TLR9, and TLR9 and MyD88 interactions need further investigation.

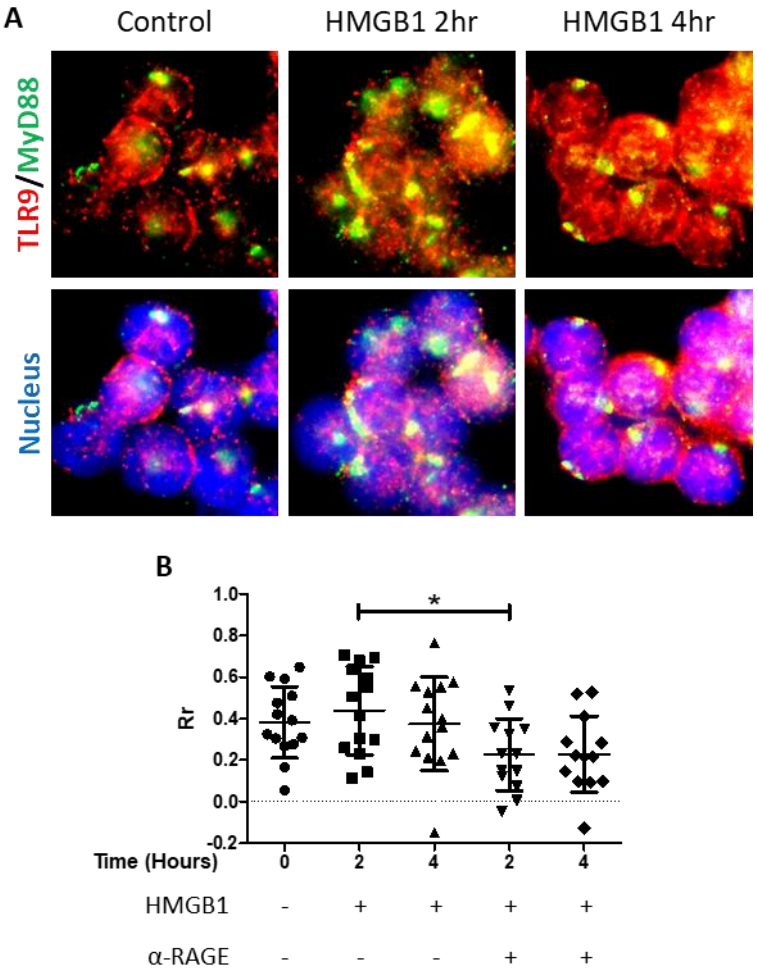

Figure 5-4 Fluorescent microscopy analysis of HMGB1-mediated TLR9 and MyD88 colocalisation in primary CLL cells

(A) Representative images of TLR9 and MyD88 colocalization. Fresh CLL cells were left untreated for 0 hour (control), or cells were treated with 200ng/ml HMGB1 for 2 hours (HMGB1 2hr) and 4 hours (HMGB1 4hr) and then fixed and permeabilized on slides. Cells were co-stained with anti-MyD88/AF-488 and anti-TLR9/AF-546 antibodies. Areas where green pixels (MyD88) and red pixels (TLR9) overlap give yellow aggregates, representing protein colocalization. Magnification x100. (B) Pixel intensity spatial correlation analysis of HMGB1-mediated colocalization of TLR9 and MyD88. Fresh CLL cells were left untreated for 0-hours or incubated with 200ng/ml HMGB1 for 2 and 4 hours with or without 10µg/ml neutralising anti-RAGE antibody (α-RAGE). TLR9 and MyD88 protein colocalization was analysed using ImageJ software and 'Rr' indicates Pearson's correlation coefficient. Data are mean ± SD from 4 individual CLL patients and differences compared with an unpaired student t test; $P<0.05$*. 5 images were analysed per patient sample.

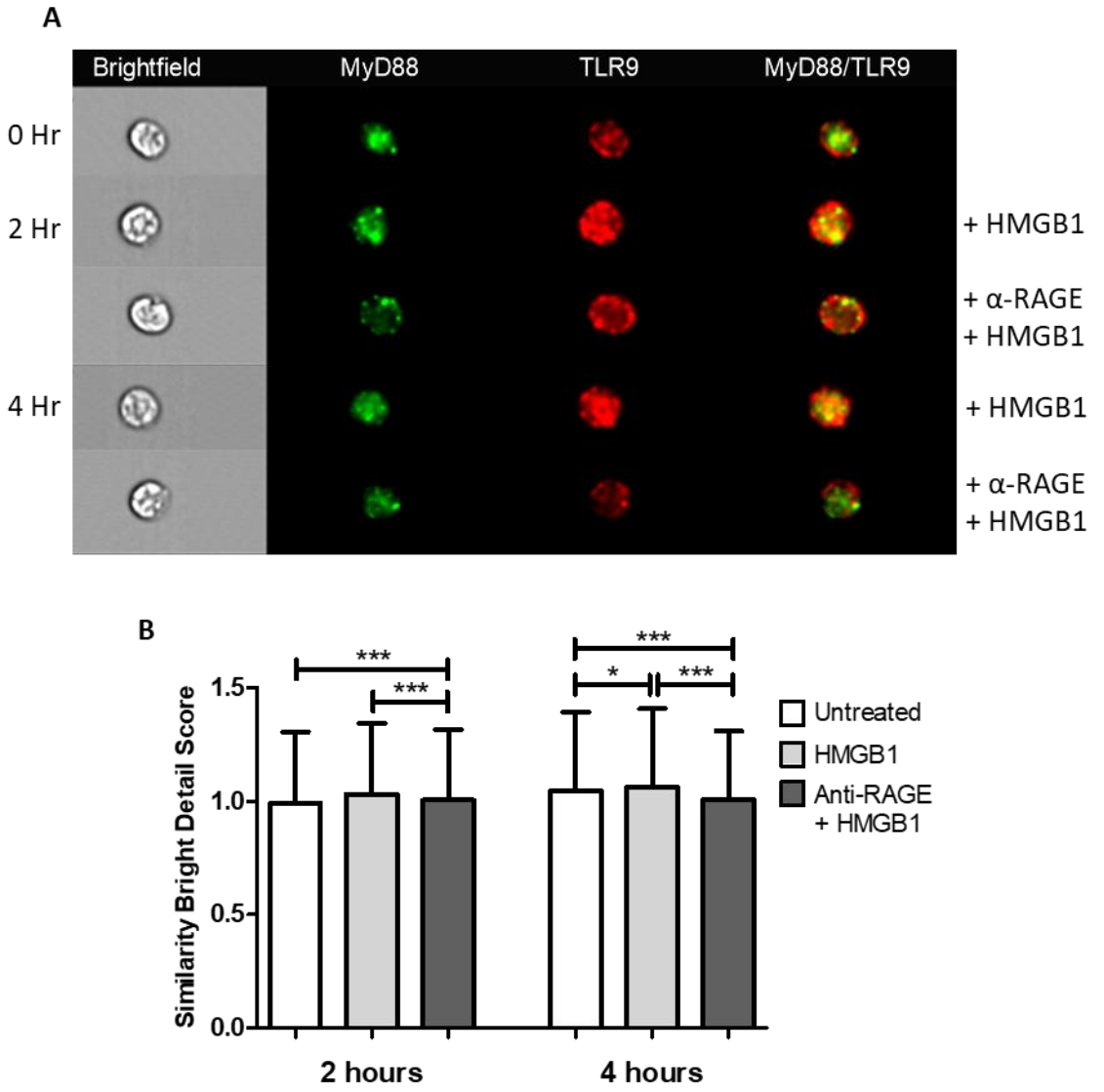

Figure 5-5 ImageStream analysis of HMGB1-mediated TLR9 and MyD88 colocalisation in primary CLL cells

(A) Representative images of TLR9 and MyD88 colocalization captured by the ImageStream X Mark II flow cytometer; magnification x40. Fresh CLL cells were treated with 200ng/ml HMGB1 (+ HMGB1) with or without 10µg/ml goat anti-RAGE neutralising antibody (α-RAGE) for 2 and 4 hours. Cells were fixed/permeabilised, co-stained with anti-MyD88/AF-488 and anti-TLR9/AF-647 antibodies and data/images assessed by ImageStream flow cytometry and colocalization analysed by IDEAS software. (B) Statistical analysis of TLR9 and MyD88 protein colocalization using the IDEAS software. The Similarity Bright Detail Score was measured for every cell recorded in 5 patients. Data are presented as median with interquartile range. 2 hours untreated n= 10489, HMGB1 n=10610, anti-RAGE n=10536; 4 hours untreated n=13185, HMGB1 n=14778, anti-RAGE n=10668. Differences were compared with an unpaired Mann Whitney U test; $P<0.05$*, $P<0.01$**, $P<0.001$***.

5.2.3 Treatment with recombinant HMGB1 results in the nuclear translocation of transcription factor NF-κB

TLR9 signalling results in the activation of transcription factor, NF-κB, resulting in inflammatory cytokine induction. We further investigated whether activation of RAGE and TLR9 receptors with HMGB1 stimulates signal transduction pathways by assessing the activation of transcription factor NF-κB. Nuclear translocation of the p65 NF-κB subunit elicits activation of this transcription factor, therefore, fluorescence microscopy and ImageStream flow cytometry were used to assess p65 nuclear translocation by measuring pixel colocalization with nuclear fluorescent dye, DAPI.

Stimulation of fresh primary CLL cells with recombinant HMGB1 for 2 and 4 hours significantly induced p65 NF-κB nuclear translocation compared to the untreated 0-hour control (0-hour control Rr=0.11; 2 hours HMGB1 Rr=0.33, $P<0.05$; 4 hours HMGB1 Rr=0.35, $P<0.01$; Figure 5-6). Consistent with RAGE and TLR9 colocalization, RAGE blockade with 10μg/ml neutralising anti-RAGE antibody significantly decreased HMGB1-mediated p65 NF-κB nuclear translocation at 4 hours (4 hours HMGB1 Rr=0.35, anti-RAGE=0.07; $P<0.01$; Figure 5-6). Overall, the fluorescence microscopy images reveal p65 localised to the cytoplasm of unstimulated cells, and bright expression of NF-κB in the nuclei of cells following HMGB1 stimulation (Figure 5-6A). We further investigated HMGB1-mediated activation of NF-κB using the nuclear translocation ImageStream flow cytometry technique. The similarity eroded score (SEC) is the background-eroded, log transformed Pearson's correlation coefficient that measured the degree of colocalization between nuclear stain, DAPI, and NF-κB fluorescence. Using this method, no difference was measured in NF-κB nuclear translocation between untreated, 200ng/ml HMGB1 treated and anti-RAGE neutralised cells at 2 hours (2 hours untreated mean SEC=1.506, HMGB1 mean SEC=1.510, anti-RAGE mean SEC=1.489; Figure 5-7). After 4 hours treatment, cells treated with 200ng/ml HMGB1 displayed significantly higher NF-κB nuclear translocation compared to untreated cells, and neutralising anti-RAGE antibody blocked HMGB1-mediated NF-κB activation (4 hours untreated mean SEC=1.435, HMGB1 mean SEC=1.520, anti-RAGE mean SEC=1.496; Figure 5-7). These results demonstrate that HMGB1-mediated activation of RAGE/TLR9 pathways in CLL cells leads to the activation of NF-κB.

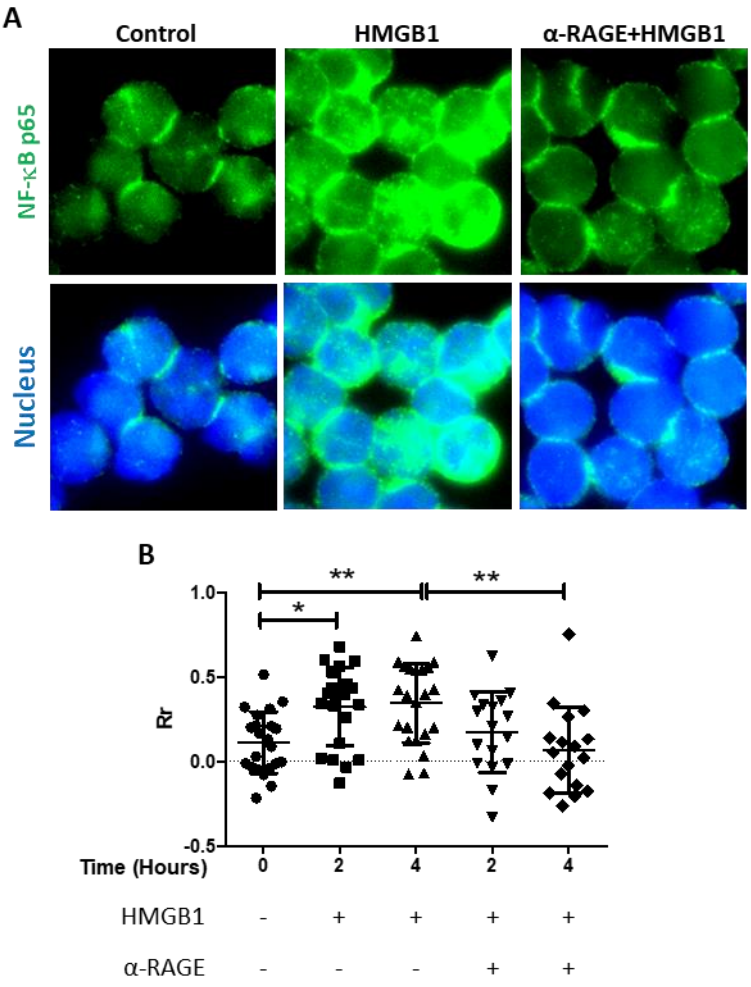

Figure 5-6 Fluorescent microscopy analysis of HMGB1-mediated NF-κB activation
(A) Representative images of p65 NF-κB nuclear translocation. Fresh CLL cells were left untreated for 0 hour (control), or cells were treated with 200ng/ml HMGB1 for 2 hours (HMGB1) or with 10μg/ml neutralising anti-RAGE antibody (α-RAGE) and then fixed and permeabilized on slides. Cells were co-stained with anti—p65 NF-κB/AF-488 antibodies and nuclear stain DAPI. Areas where green pixels (NF-κB) and blue nuclei (DAPI) overlap give light blue aggregates, representing nuclear translocation. Magnification x100. (B) Pixel intensity spatial correlation analysis of HMGB1-mediated nuclear translocation of p65 NF-κB. Fresh CLL cells were left untreated for 0-hours or incubated with 200ng/ml HMGB1 for 2 and 4 hours with or without 10μg/ml neutralising anti-RAGE antibody (α-RAGE). P65 NF-κB nuclear translocation was analysed using ImageJ software and 'Rr' indicates Pearson's correlation coefficient. Data are mean ± SD from 4 individual CLL patients and differences compared with an unpaired student t test; $P<0.05$*, $P<0.01$**. 5 images were analysed per patient sample.

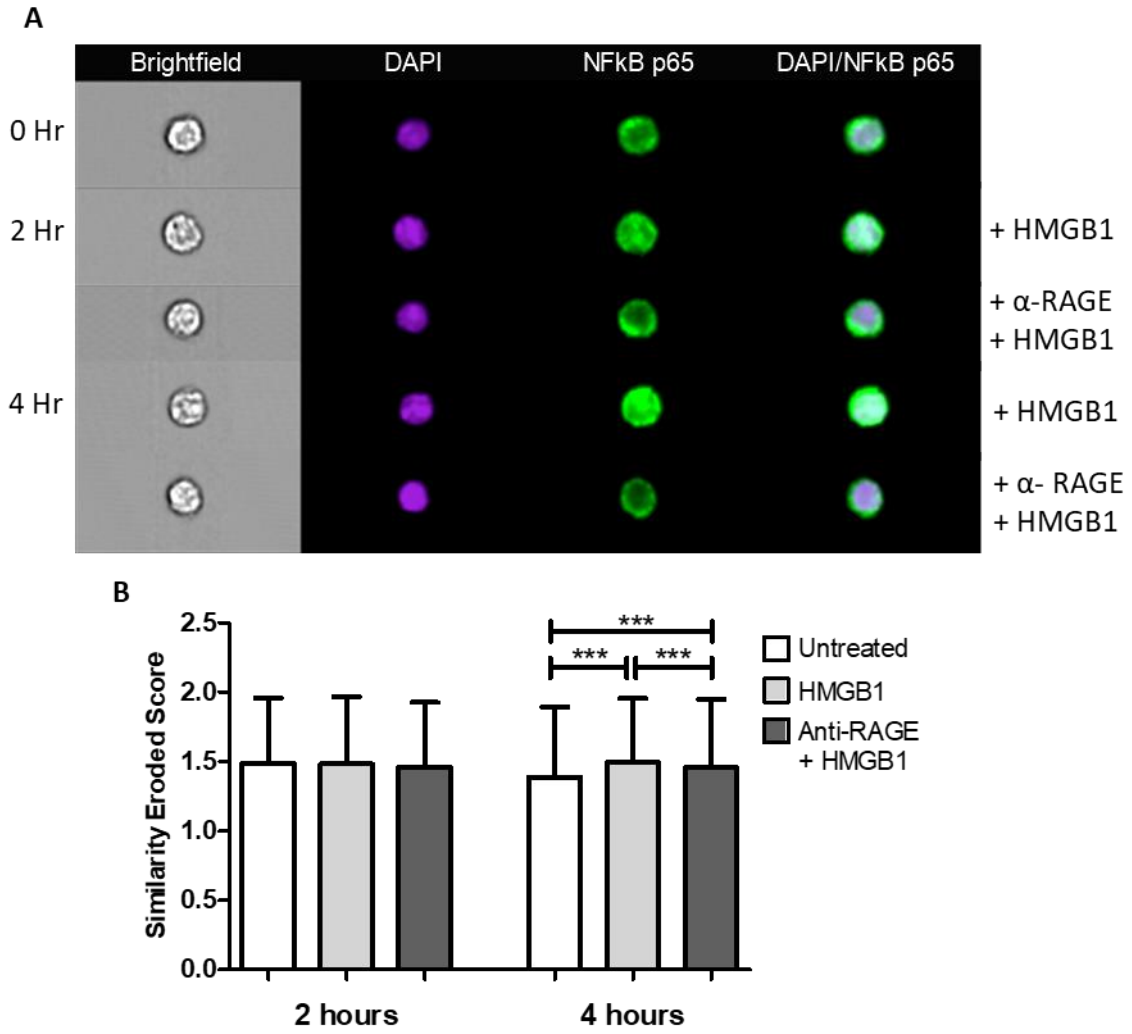

Figure 5-7 ImageStream analysis of HMGB1-mediated p65 NF-κB nuclear translocation in primary CLL cells

(A) Representative images of p65 NF-κB nuclear translocation captured by the ImageStream X Mark II flow cytometer; magnification x40. Fresh CLL cells were treated with 200ng/ml HMGB1 (+ HMGB1) with or without 10μg/ml goat anti-RAGE neutralising antibody (α-RAGE) for 2 and 4 hours. Cells were fixed/permeabilised, co-stained with anti-p65 NF-κB/AF-488 647 antibodies and nuclei stained with DAPI. Data and images were assessed by ImageStream flow cytometry and nuclear translocation analysed by IDEAS software. (B) Statistical analysis of p65 NF-κB nuclear translocation using the IDEAS software. The Similarity Eorded Score was measured for every cell recorded in 4 patients. Data are presented as median with interquartile range. 2 hours untreated n= 14468, HMGB1 n=13980, anti-RAGE n=14341; 4 hours untreated n=13432, HMGB1 n=13537, anti-RAGE n=13300. Differences were compared by an unpaired Mann Whitney U test; P<0.001***.

5.2.4 HMGB1 does not mediate a stable interaction between RAGE and TLR9 in CLL cells

Colocalization of RAGE and TLR9 assessed by immunofluorescence does not indicate a direct protein-protein interaction. RAGE and TLR9 play pivotal roles in mediating HMGB1 inflammatory signalling activation, with evidence of direct binding and recruitment/activation of MyD88 in CLL NLCs, transfected HEK293 cells and lung epithelial cells.[76,145,358] Therefore, we evaluated whether HMGB1 induces an interaction between TLR9 with RAGE, and TLR9 with MyD88 using co-IP.

Fresh CLL cells were cultured for 2 hours with PBS control, 200ng/ml HMGB1, 10µg/ml anti-RAGE with addition of HMGB1 or 1µM CpG-ODN positive control. After 2 hours, cells were lysed and 300µg of cell lysate incubated with 5µg of mouse anti-TLR9 antibody conjugated to Dynabead™ Protein A. TLR9-containing protein complexes were removed from the cell lysate by magnetic precipitation and denatured protein complexes were separated by gel electrophoresis. Blots were probed for RAGE, MyD88 and TLR9; co-IP with mouse anti-IgG antibody was used as a negative control. Using this method, no binding was observed between endogenous RAGE and TLR9, or TLR9 and MyD88 following treatment with HMGB1 for 2 hours (Figure 5-8) in 3 independent co-IPs performed with 3 fresh primary CLL samples. Moreover, CpG-ODN failed to induce an interaction between TLR9 and MyD88, an established agonist of TLR9 signalling and MyD88 receptor recruitment.[253] We failed to observe a band for TLR9 post-co-IP for all 3 patient samples, demonstrating unsuccessful attempts at precipitating TLR9 (Figure 5-8). Input cell lysates, pre-co-IP, express MyD88, RAGE and TLR9 (Figure 5-8). Therefore, co-IP was repeated for 1 patient sample using rabbit anti-RAGE antibody for precipitation. However, we failed to observe RAGE IP or TLR9 and MyD88 co-IP (data not shown). These results demonstrate we could not detect a stable interaction between RAGE and TLR9 or TLR9 and MyD88 in CLL cells, but these proteins do colocalise following stimulation with HMGB1. This suggests that the interaction between these proteins may be indirect via other protein(s) in CLL cells.

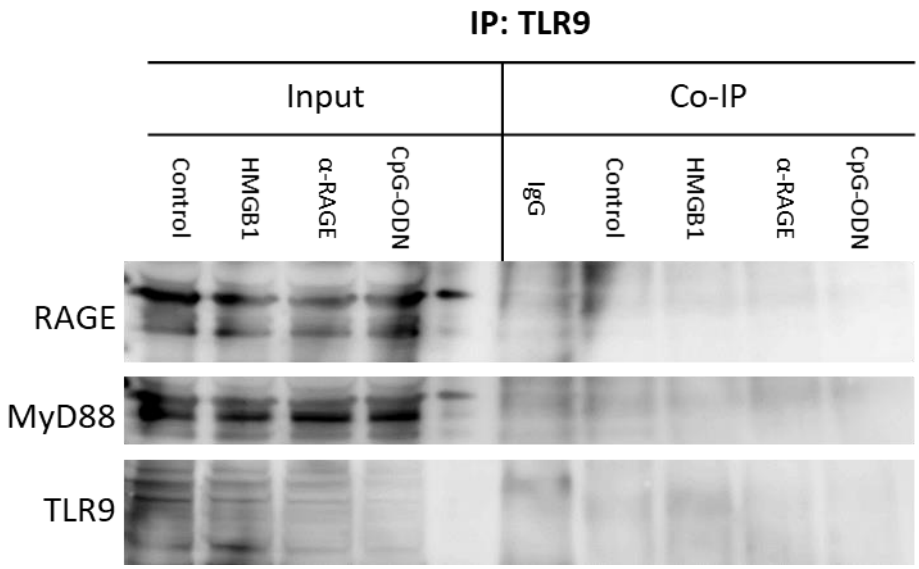

Figure 5-8 Co-IP of TLR9 and RAGE and MyD88 in CLL cells.
Fresh CLL cells were treated with 200ng/ml HMGB1 with or without 10μg/ml goat anti-RAGE blocking antibody for 2 hours. TLR9 agonist 1μM CpG-ODN was included as a positive control for TLR9 and MyD88 interaction. 5μg mouse anti-TLR9 antibody was incubated with Dynabeads protein A and then incubated with 300μg protein lysate. IP with 5μg mouse anti-IgG was used as a negative control. Pre-co-IP cell lysates and co-IP proteins were separated by gel electrophoresis and proteins probed with rabbit anti-RAGE and rabbit anti-MyD88. Immunoprecipitation of TLR9 was checked by probing with mouse anti-TLR9 antibody. Data are representative of 3 patients (10904).

5.2.5 Deciphering HMGB1-mediated intracellular signalling networks using comparative phosphoproteomics

To fully investigate the signalling capacity of HMGB1 and synergism with TLR9 signalling pathway, we assessed intracellular signalling network activation using a phosphoproteomic approach. TLR and TLR9 signalling pathways are fully deciphered,[246] while the precise signalling capacity of RAGE is unclear and highly cell-type specific. Although the 40-amino acid cytoplasmic tail of RAGE does not contain any known signalling motifs, it is vital for RAGE-mediated signalling,[359] while other reports demonstrate the importance of receptor internalisation for HMGB1-mediated responses.[194] On the other hand, HMGB1 has been identified as a component of autoantigens in SLE disease pathogenesis, and may play a role in CLL BCR activation.[260] The full signaling pathways of HMGB1 and RAGE, or synergy with TLR9 signalling are currently not known.

Using an unbiased phosphoproteomic approach with the help of Dr David Britton and Dr Pedro Cutillas's mass spectrometry laboratory, we will be able to identify the signalling pathways activated following HMGB1 stimulation and synergy with CpG-ODN TLR9 agonist. We chose 2 patient samples with high CLL purity (patient ID 8231: 97.2%; patient ID 6799: 94.3%; Figure 5-9) and from our earlier ZAP70 expression analysis, patient 8231 was ZAP70+ and patient 6799 was ZAP70- (Section 4.2.4; Appendix II, Table P). Both patients had not required therapy at the time of phosphoproteomic analysis (Appendix II, Table P). High CLL purity is important to ensure phosphorylated peptide signals originate from CLL cells, not contaminated by other cell types, particularly macrophages and dendritic cells for HMGB1 biology. Samples were stimulated for 15 minutes, to capture rapid short-term signalling pathways, and 2 hours to assess downstream kinase cascade signalling. 200ng/ml HMGB1 alone, 1µM CpG-ODN alone, and 200ng/ml HMGB1 + 1µM CpG-ODN combined stimulation was assessed at 15 minutes and 2 hour time-points, and 10µg/ml anti-RAGE antibody blockade and 200ng/ml HMGB1 stimulation combined was assessed at 2 hours. PBS stimulation was performed as baseline comparison controls at both 15 minutes and 2 hours.

5.2.5.1 Comparing the abundance of phosphorylated and de-phosphorylated peptides between patients

We analysed 2 independent patient samples and each experiment was performed for three times. Following phosphopeptide enrichment, a total of 4185 unique phosphorylated peptide ions across 7 different experimental conditions and the 2 patient samples were detected. The abundance of phosphorylated peptide ions in each experimental condition was compared to the PBS baseline control. The significance of the difference in the means of log2-transformed data

across samples was assessed by Student's t test, and an increased abundance phosphopeptide threshold was set log2 fold change ≥1 and $P<0.05$ compared to PBS treated sample; a decreased abundance threshold was set at log2 fold change ≤-1 and $P<0.05$ compared to PBS treated sample (Table 10).

For both patient 8231 and 6799, 15 minutes stimulation with HMGB1 alone did not induce the phosphorylation of many peptides compared to PBS alone (32 and 20, respectively; Table 10). 15 minutes CpG-ODN stimulation alone induced the significant phosphorylation of 119 phosphopeptides in patient 8231 (ZAP70+ patient) compared to the PBS control, whereas this remained low in patient 6799 (36 phosphopeptides; ZAP70- patient). The combination of HMGB1 and CpG-ODN at 15 minutes induced the phosphorylation of a similar number of phosphopeptides compared to CpG-ODN alone in patient 8231 (125 phosphopeptides), and a similar number of phosphopeptides that were significantly de-phosphorylated compared to the PBS control (11 for CpG-ODN 15 minutes alone; 18 for HMGB1 and CpG-ODN 15 minutes; Table 10). Although patient 6799 demonstrated a much higher abundance of phosphopeptides following HMGB1 and CpG-ODN stimulation at 15 minutes, when comparing to the abundance of phosphopeptides following to CpG-ODN alone (189 and 36, respectively), the abundance of dephosphorylated peptides for HMGB1 and CpG-ODN combined, was more than phosphorylated peptides (219; Table 10).

The 2-hour time-point for all experimental conditions demonstrated an increase in cell signalling activity, based on the abundance of phosphorylated and dephosphorylated peptides, compared to PBS baseline. For patient 8231, HMGB1 alone at 2 hours resulted in 125 significantly abundant phosphopeptides compared to baseline, and 12 phosphopeptides down-regulated. Again, patient 6799 had a low amount of abundant phosphopeptides at 2 hours following stimulation with HMGB1 alone (55; Table 10), but a high level of down-regulated phosphopeptides compared to baseline (232; Table 10). CpG-ODN alone had an impact on the phosphoproteome for both patients. Patient 8231 demonstrated the abundance of 401 significantly phosphorylated peptides, and the down-regulation of 212 phosphopeptides compared to PBS baseline. Patient 6799 had a similar level of phosphorylated peptides, but a high number of de-phosphorylated peptides compared to baseline (477 and 407, respectively). The combination of HMGB1 and CpG-ODN together induced the phosphorylation of 655 peptides for patient 8231 at 2 hours, and the down-regulation of 212 phosphopeptides compared to baseline control. A similar number of peptides were phosphorylated following HMGB1 and CpG-ODN stimulation combined compared to CpG-ODN alone for patient 6799 (493 and 477, respectively). Again, the combination of HMGB1 and CpG-ODN resulted in the abundance of more phosphopeptides that were significantly dephosphorylated compared to PBS control at 15 minutes and 2 hours for

patient 6799 (530 down-regulated at 2 hours; Table 10). Pre-blockade of RAGE for 30 minutes before addition of HMGB1 for 2 hours, resulted in the up-regulation of 107 phosphopeptides and the down-regulation of 15 phosphopeptides compared to PBS baseline for patient 8231, and the up-regulation 152 phosphopeptides and down-regulation of 445 for patient 6799. These results give an indication of cell activity but investigating the specific peptides and kinases with increased or decreased activity under each experimental condition, and their respective signalling pathways, will give further insight into the mechanism of HMGB1 biology.

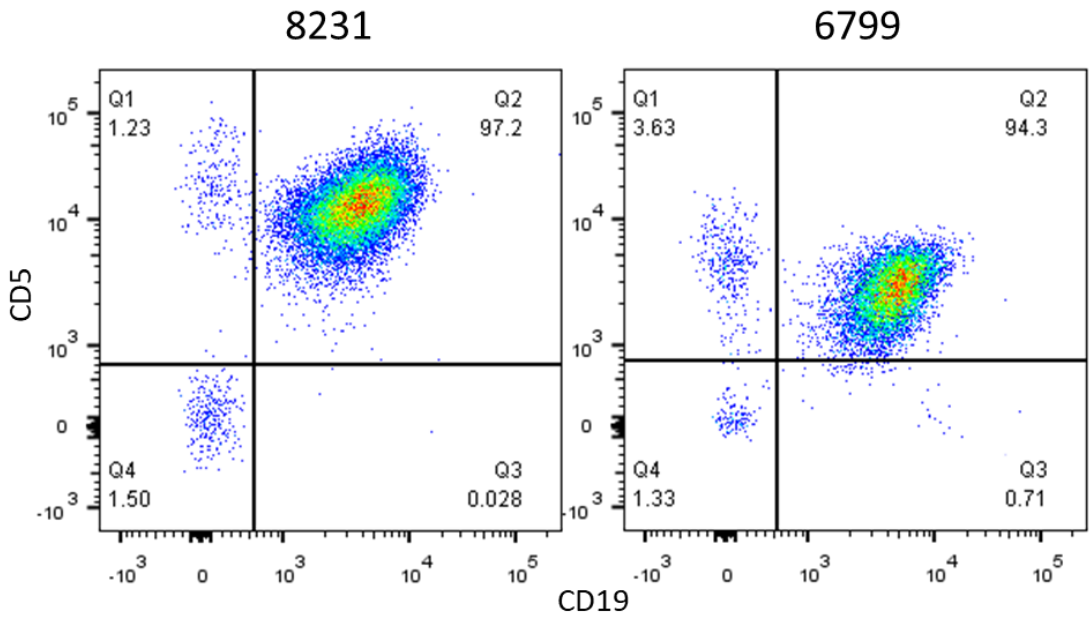

Figure 5-9. Representative flow plots for CD19+/CD5+ CLL purity
The CLL-cell purity of freshly isolated CLL PBMCs from patient 8231 and 6799 was assessed by flow cytometry. Non-permeabilised fresh PBMCs were stained for surface markers CD5 and CD19, using anti-CD5-PE/Cy7 and anti-CD19-APC, respectively. Positive fluorescence was gated by comparing to isotype-matched controls, and the purity of CLL cells was the % of cells that were CD5+/CD19+ (gate Q2).

Table 10. Abundance of significantly phosphorylated and dephosphorylated peptides across each experimental condition compared to PBS baseline control

	8231		6799	
	Up	Down	Up	Down
HMGB1 15 mins	32	12	20	11
CpG 15 mins	124	11	36	47
HMGB1 + CpG 15 mins	119	18	189	219
HMGB1 2 hours	125	12	55	232
CpG 2 hours	401	212	477	407
HMGB1 + CpG 2 hours	655	212	493	530
Anti-RAGE and HMGB1 2 hours	107	15	152	445

Note: Up-regulated threshold set at log2 fold change ≥1 and $P<0.05$ compared to PBS treated sample; down-regulated threshold set at log2 fold change ≤-1 and $P<0.05$ compared to PBS treated sample.

5.2.5.2 HMGB1 treatment alone modulates the activity of the MAPK pathway following 15 minutes stimulation for the ZAP70 positive patient

First, we aimed to assess the impact of HMGB1 treatment at 15 minutes and 2 hours on whole-cell signalling pathways compared to PBS baseline control. To decipher the signalling pathways that correspond to the significantly abundant phosphopeptides in Table 10 (log2 fold change ≥1 and P<0.05), the Database for Annotation, Visualization and Integrated Discovery (DAVID) online bioinformatics resource (https://david.ncifcrf.gov/home.jsp) was used. The uniprot IDs (i.e. gene list) for the list of phosphopeptides significantly abundant following 15 minutes HMGB1 treatment (patient 8231, 32 phosphopeptides; patient 6799, 20 phosphopeptides; Table 10) and 2 hours HMGB1 treatment (patient 8231, 125 phosphopeptides; patient 6799, 55 phosphopeptides; Table 10) were submitted to DAVID bioinformatics (Appendix II; Table N) and pathway functional annotation was assessed using KEGG pathway mapping. Using this available online database, the list of uniprot IDs/gene list can be mapped to known signalling pathways based on experimental knowledge. The KEGG pathway output gives:

i) a list of signalling pathways associated with the gene list input

ii) the number of genes involved in the signalling pathway from the input list

iii) the percentage of involved genes compared to total genes from the input list

iv) the modified fisher exact P-value, i.e. the smaller the P-value the more enriched the pathway is with genes from the input list

Following 15 minutes HMGB1 stimulation, 3/32 input genes from patient 8231 are associated with herpes simplex infection, only. For patient 6799, 2/20 input genes following 15 minutes HMGB1 stimulation are associated with spliceosome signalling, only. No other signalling pathways were identified from each gene list at this time-point.

At 2 hours HMGB1 treatment for patient 8231, 14 signalling pathway groups were identified (Table 11) that are associated with the 125 uniprot IDs for the up-regulated phosphopeptides in Table 10; 10/125 are associated with spliceosome signalling, 6/125 are associated with oxidative phosphorylation and the others are linked to inflammatory conditions. The gene list for the 55 abundant phosphopeptides following 2 hours HMGB1 treatment for patient 6799 yielded no results. When we input the list of 232 down-regulated phosphopeptides from patient 6799 following 2 hours HMGB1 stimulation, 17 signalling pathway groups were identified. Of interest, 3/6 of the top associated pathways from the KEGG pathway results were associated with metabolism (glycolysis/gluconeogenesis, carbon metabolism, pyruvate metabolism) indicating a down-regulation of anaerobic metabolism, and a switch to oxidative phosphorylation following HMGB1 treatment for 2 hours for patient 6799.

Table 11. Patient 8231 2 hours HMGB1 treatment KEGG pathway results for upregulated phoshopeptides

Signalling pathways	Gene count	%	P-Value
Spliceosome	10	8.9	9.70E-07
Parkinson's disease	8	7.1	1.30E-04
Alzheimer's disease	7	6.2	2.20E-03
Alcoholism	7	6.2	2.90E-03
Oxidative phosphorylation	6	5.4	4.30E-03
Huntington's disease	7	6.2	4.40E-03
Systemic lupus erythematosus	6	5.4	4.40E-03
Cardiac muscle contraction	4	3.6	2.30E-02
Gap junction	4	3.6	3.40E-02
Serotonergic synapse	4	3.6	6.10E-02
Carbon metabolism	4	3.6	6.30E-02
Pathogenic Escherichia coli infection	3	2.7	6.40E-02
Long-term depression	3	2.7	8.50E-02
Pathways in cancer	7	6.2	9.70E-02

Table 12. Patient 6799 2 hours HMGB1 treatment KEGG pathways results for downregulated phosphopeptides

Signalling pathways	Gene count	%	P-Value
Spliceosome	15	7.4	1.30E-08
Glycolysis / Gluconeogenesis	9	4.5	7.80E-06
Carbon metabolism	10	5	5.70E-05
Pathogenic Escherichia coli infection	7	3.5	1.20E-04
Biosynthesis of antibiotics	12	5.9	4.10E-04
Pyruvate metabolism	5	2.5	3.20E-03
Shigellosis	5	2.5	1.70E-02
Herpes simplex infection	8	4	2.30E-02
Biosynthesis of amino acids	5	2.5	2.70E-02
Phagosome	7	3.5	3.10E-02
Viral carcinogenesis	8	4	3.90E-02
Salmonella infection	5	2.5	3.90E-02
Fc gamma R-mediated phagocytosis	5	2.5	4.10E-02
Alzheimer's disease	7	3.5	4.60E-02
Ribosome	6	3	5.90E-02
Parkinson's disease	6	3	6.90E-02
SNARE interactions in vesicular transport	3	1.5	9.70E-02

Next, to infer pathway activity, we used a computational approach developed by Dr Pedro Cutillas, termed kinase-substrate enrichment analysis (KSEA), to determine the activation of given kinase pathways from mass spectrometry–based phosphoproteomic analysis.[310] As phosphorylation sites are the result of kinase activity (i.e. kinase substrates), using several known phosphorylation sites downstream of each kinase, it is possible to use this data as a way to quantify kinase activity - the master regulators of signalling pathways. This is a better measure of overall global signalling activity, as an individual phosphorylation site may be targeted by multiple kinases, the nature of this post-translational modification is dynamic and can quickly change, along with experimental stress that all impact protein kinase activity, and impact signal-to-noise ratio. Therefore, using this approach, we can gain deeper and more reliable biological insight on the activity of kinase pathways from MS-based phosphoproteomics.

Substrate groups enriched for different kinases was calculated using the KSEA algorithm (with the PhosphoSite database: https://www.phosphosite.org), and fold-enrichment was based on the abundance of phosphopeptides under each experimental condition, divided by the abundance in the PBS treated cells. The unique 4185 phosphopeptide ions detected in this dataset correspond to 330 kinase substrate groups in total.

Focusing on substrate groups with significant activity compared to PBS baseline control following 15 minutes HMGB1 stimulation, 18 substrate groups were identified with significant activity in patient 8231 with ZAP70+ expression status (column of interest indicated by arrow; (Figure 5-10) and 0 substrate groups with significant activity in patient 6799 with ZAP70- expression status. 12/18 substrate groups for patient 8231 demonstrated an increase in abundancy, shown in red in the heat map for Figure 5-10 (corresponding to kinases MEK2, AurA, Ret, JAK2, PLK3, JNK2, ERK7, MEK1, VRK1, PKR, CDK19 and HcK) and 6/18 substrate groups demonstrated a decrease in abundancy in blue shades in the heat map (corresponding to kinases MEKK3, LRRK2, LOK, GRK2, Cot, PKCT; Figure 5-10). Of interest, MEK2, Ret, JAK2, MEK1 significantly contribute to the activation of the MAPK pathway, via the phosphorylation of MAPK1 (at tyrosine 187 and threonine 185) and MAPK1 (tyrosine 204 and threonine 202) substrates. PLK3, JNK2, ERK7 and VRK1 contribute to the activation of transcription factor AP-1, by the phosphorylation of Jun (at serine 73).

Interestingly, the substrate groups leading to MAPK pathway activation (corresponding to kinases MEK2, Ret, JAK2, MEK1) at 15 minutes, are not significantly enriched at 2 hours, whereas the substrate groups for AP-1 activation (due to kinases PLK3, JNK2, ERK7 and VRK1) are enriched (patient 8231 comparing 15 minutes HMGB1 column and 2 hours HMGB1 column; Figure 5-10). The substrate groups with significant abundancy (increased or decreased) in

patient 8231 following 15 minutes HMGB1 treatment, do not overlap with patient 6799, as the 15 minutes HMGB1 column for patient 6799 in Figure 5-10 does not contain notable enrichment or any significant results.

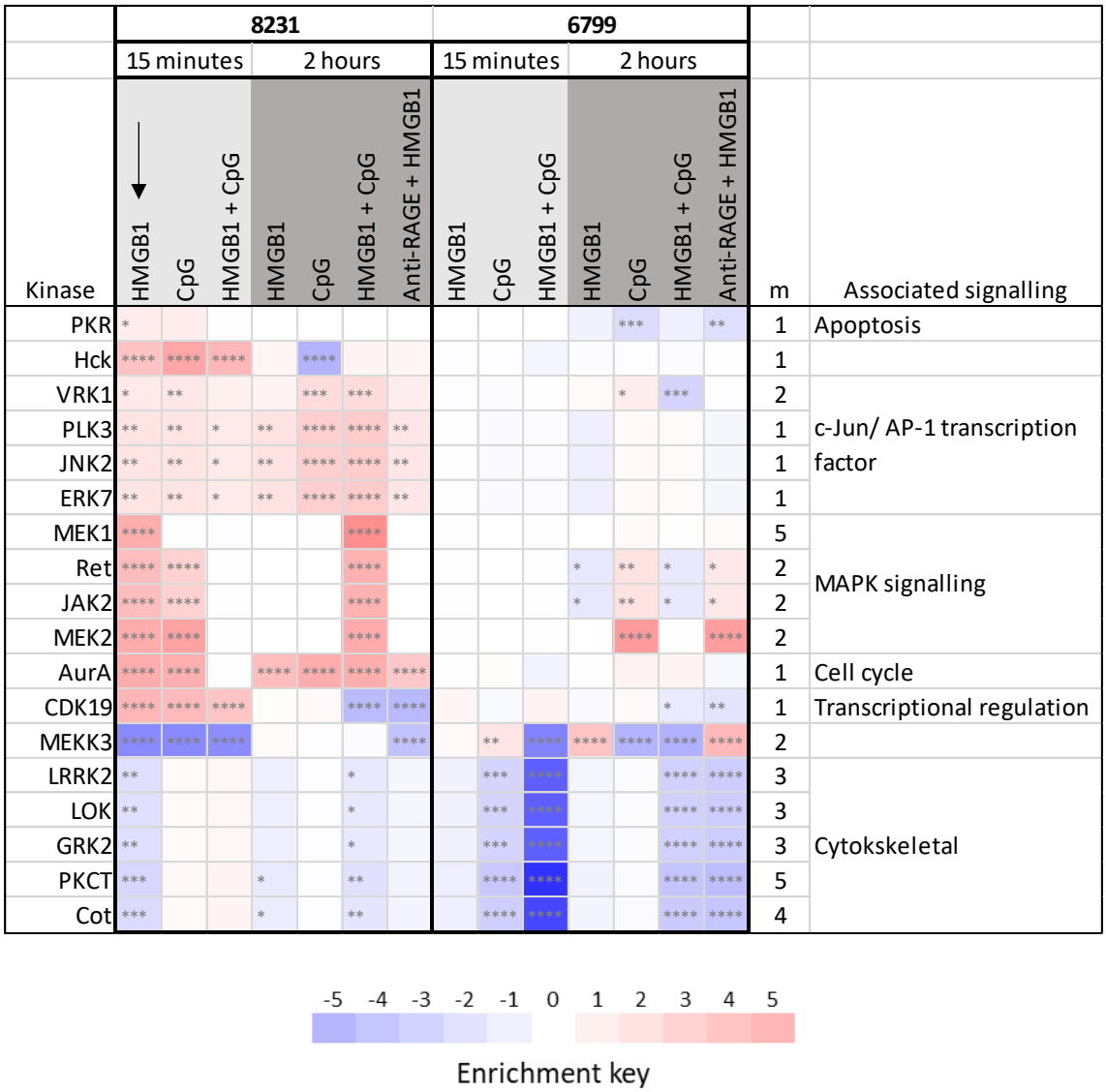

Figure 5-10. Heat map showing the enrichment of substrate groups for the different kinases calculated by KSEA algorithm with significant abundance following 15 minutes HMGB1 treatment for patient 8231

Fresh CLL cells were treated with 200ng/ml HMGB1 alone, 1µM CpG-ODN alone, 200ng/ml HMGB1 and 1µM CpG-ODN combined for 15 minutes and 2 hours. Blockade of surface RAGE was performed with 10µg/ml goat anti-RAGE neutralising antibody for 30 minutes before addition of 200ng/ml HMGB1 for 2 hours. Cell lysates were processed for mass spectrometry and phosphorylated peptides were enriched with TiO_2 and identified and quantified by LC-MS/MS. Enrichment of substrate groups was calculated by the KSEA algorithm and divided by the abundance of phosphopeptides in the PBS treated sample. The coloured enrichment key indicates -5 to +5-fold enrichment compared to PBS treated sample. Statistical significance of these changes was calculated by Student's t test compared to PBS treated samples; *P*<0.05*, *P*<0.01**, *P*<0.001***, *P*<0.0001****. 'm', number of substrates in the indicated kinase substrate group. KSEA results were filtered based on significantly abundant substrate groups for patient 8231 following 15 minutes HMGB1 treated (column indicated by arrow).

After 2 hours HMGB1 treatment, patient 8231 demonstrated the significant abundancy of 8 substrate groups (column of interest indicated by arrow; Figure 5-11) and patient 6799 demonstrated the abundancy of 9 substrate groups (column of interest indicated by arrow; Figure 5-12). For patient 8231, substrate groups for AurA, PLK3, JNK2, ERK7, Cot and PKCT overlap with 15 minutes HMGB1 treatment. Of these, substrates for PLK3, JNK2 and ERK7 with significant increased abundancy contribute to the activation of transcription factor AP-1 via Jun phosphorylation at serine 73. Cot and PKCT substrate groups with significant decreased phosphorylated abundancy, act as cross-linkers between plasma membranes and actin-based cytoskeletons. Again, these significantly abundant substrate groups for patient 8231 following 2 hours' HMGB1 treatment, do not overlap with significant results for patient 6799 under the same experimental condition (Figure 5-11).

For patient 6799 with ZAP70- expression status, substrate groups for kinases Wee1, Myt1, HER2 and MEKK3 showed increased significant enrichment following 2 hours HMGB1 treatment (column of interest indicated by arrow; Figure 5-12). Of these, Wee1, Myt1 and Her2 substrate groups are associated with the phosphorylation of CDK1 and CDK2, vital components of cell cycle transitions. Whereas substrate groups Ret, JAK2, GSK3A, JNK3 and Syk demonstrated decreased significant abundancy in patient 6799 following 2 hours HMGB1 treatment, components of MAPK and MYC signalling. This result demonstrates a decrease in activity of MAPK and MYC signalling for patient 6799 following longer-term HMGB1 signalling compared to the PBS baseline control.

Taken together, this data demonstrates 2 hours HMGB1 stimulation results in opposing MAPK signalling pathway activity in 2 patients with different clinical background and ZAP70 expression status.

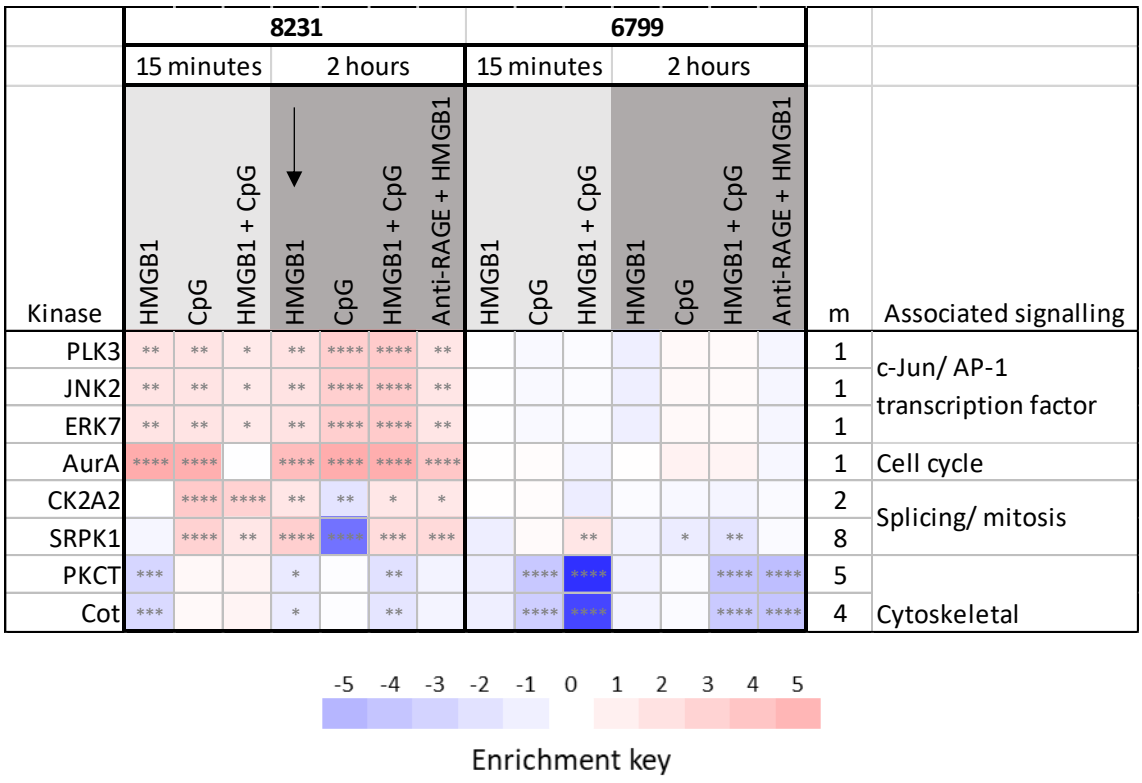

Figure 5-11. Heat map showing the enrichment of substrate groups for the different kinases calculated by KSEA algorithm, with significant abundance following 2 hours HMGB1 treatment for patient 8231
Cell samples were treated, processed and phosphopeptides quantified by LC/MS-MS as previously described in Figure 5-10. Enrichment of substrate groups was calculated by the KSEA algorithm and divided by the abundance of phosphopeptides in the PBS treated sample. The coloured enrichment key indicates -5 to +5-fold enrichment compared to PBS treated sample. Statistical significance of these changes was calculated by Student's t test compared to PBS treated samples; P<0.05*, P<0.01**, P<0.001***, P<0.0001****. 'm', number of substrates in the indicated kinase substrate group. KSEA results were filtered based on significantly abundant substrate groups for patient 8231 following 2 hours HMGB1 treated (column indicated by arrow).

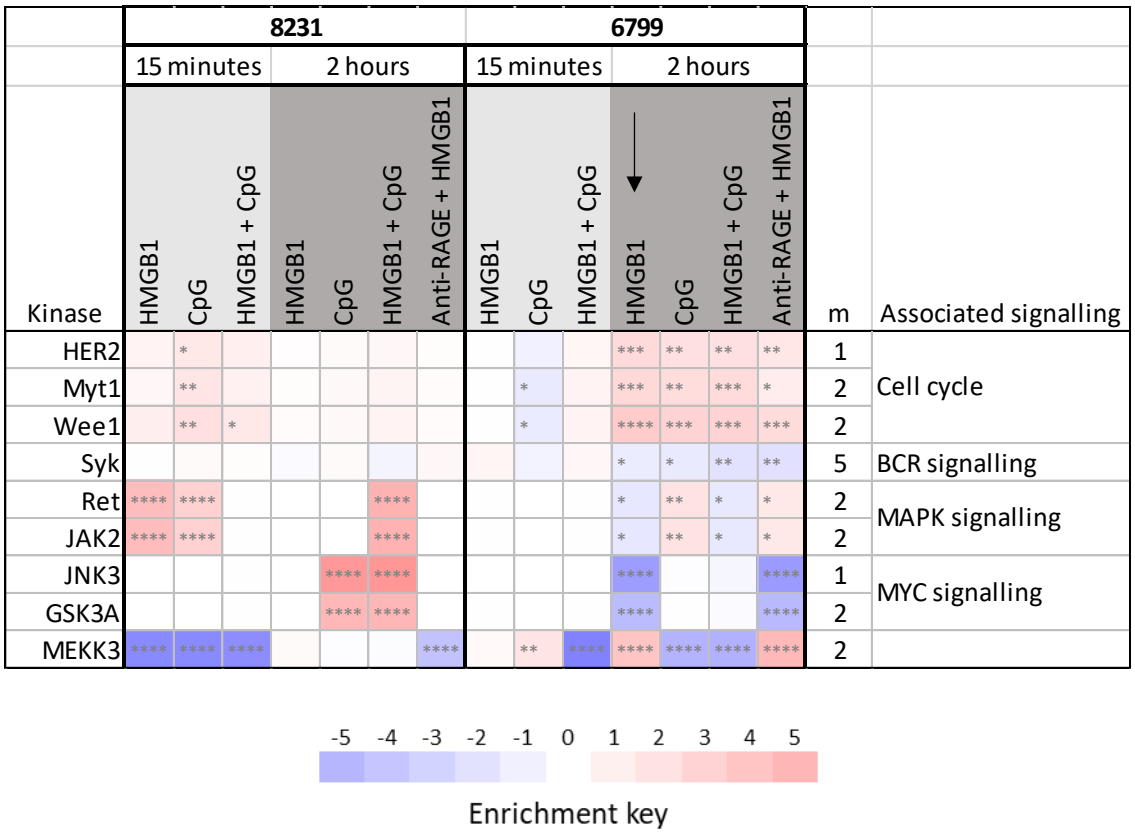

Figure 5-12. Heat map showing the enrichment of substrate groups for the different kinases calculated by KSEA algorithm, with significant abundance following 2 hours HMGB1 treatment for patient 6799
Cell samples were treated, processed and phosphopeptides quantified by LC/MS-MS as previously described in Figure 5-10. Enrichment of substrate groups was calculated by the KSEA algorithm and divided by the abundance of phosphopeptides in the PBS treated sample. The coloured enrichment key indicates -5 to +5-fold enrichment compared to PBS treated sample. Statistical significance of these changes was calculated by Student's t test compared to PBS treated samples; P<0.05*, P<0.01**, P<0.001***, P<0.0001****. 'm', number of substrates in the indicated kinase substrate group. KSEA results were filtered based on significantly abundant substrate groups for patient 6799 following 2 hours HMGB1 treated (column indicated by arrow).

5.2.5.3 HMGB1 combined with CpG-ODN results in the phosphorylation of more peptides in ZAP70 positive cells compared to CpG-ODN alone

A synergistic mode of action has been demonstrated for CpG-ODN and HMGB1 in autoimmune disease and lung cancer.[145,148,149] Next, we aimed to investigate any synergistic signalling between HMGB1 and CpG-ODN (class B) in a CLL setting, by phosphoproteomic analysis of primary CLL cells following individual and combined HMGB1 and CpG-ODN treatment for 15 minutes and 2 hours. Referring to the relevant data from Table 10, Table 13 outlines the number of significantly increased and decreased abundant phosphopeptides in HMGB1 alone, CpG-ODN alone and combined HMGB1 and CpG-ODN treated samples. For patient 8231, the combination of HMGB1 and CpG-ODN at 15 minutes resulted in a similar number of increased and decreased phosphopeptides as CpG-ODN alone when compared to PBS baseline; at 2 hours, the combination of HMGB1 and CpG-ODN induces the phosphorylation of 154 more peptides than CpG-ODN alone. For patient 6799, both 15 minutes and 2 hours combined HMGB1 and CpG-ODN treatment results in more abundant phosphopeptides (either increased or decreased), compared to CpG-ODN alone. However, whether the same phosphopeptide ions and signalling pathways are modulated in response to combined stimulation, requires further investigation of specific kinase cascades.

Table 13. Comparing the abundance of significantly increased and decreased phosphopeptides in HMGB1 alone, CpG-ODN alone and HMGB1 + CpG-ODN treated samples

	8231		6799	
	Up-regulated	Down-regulated	Up-regulated	Down-regulated
HMGB1 15 mins	32	12	20	11
CpG 15 mins	124	11	36	47
HMGB1 + CpG 15 mins	119	18	189	219
HMGB1 2 hours	125	12	55	232
CpG 2 hours	401	212	477	407
HMGB1 + CpG 2 hours	655	212	493	530

Note: Data from Table 10. Up-regulated threshold set at log2 fold change ≥1 and $P<0.05$ compared to PBS treated sample; down-regulated threshold set at log2 fold change ≤-1 and $P<0.05$ compared to PBS treated sample.

DAVID bioinformatics and KEGG pathway functional annotation resource was used to initially assess overlap of signalling pathways, across experimental conditions, for the phosphopeptides with increased significant abundancy. For patient 8231, the list of uniprot IDs for abundant phosphopeptides at 15 minutes HMGB1 alone, CpG-ODN alone, or combined HMGB1 and CpG-ODN, did not yield many pathway results (Table 14). Following 2 hours treatment, combined HMGB1 and CpG-ODN resulted in more than double the signalling pathway hits than HMGB1 or CpG-ODN alone (30 for combined HMGB1 and CpG-ODN, 12 for CpG-ODN alone, 14 for HMGB1

alone; Table 14). Main signalling pathways such as MAPK, BCR and mTOR overlapped in both CpG-ODN alone and combined HMGB1 and CpG-ODN; whereas other signaling pathway hits in both experimental conditions were linked to clinical conditions and had a low gene count (≤2 genes) out of all input gene from the uniprot ID list. For patient 6799 the input gene list corresponding to HMGB1 alone and CpG-ODN alone at both 15 minutes and 2 hours, resulted in less than 4 results (Table 14). Upon combining HMGB1 and CpG-ODN, the number of KEGG pathway outputs containing genes from the input list is notably increased (41 pathways for 15 minutes, 34 pathways for 2 hours; Table 14). Again, the core pathways of this list include BCR, MAPK, mTOR and ErbB signalling.

Table 14. KEGG pathway results for upregulated phoshopeptides in patient 8231 and 6799 following HMGB1 alone, CpG alone and HMGB1 and CpG combined treated samples

	8231		6799	
	15 mins	2 hours	15 mins	2 hours
HMGB1 alone	1	14	1	0
CpG alone	5	12	1	4
HMGB1 + CpG	2	30	41	34

Although KEGG pathway functional annotation can offer insight into the main signalling pathway(s) utilised based on gene name for significantly up-regulated phosphopeptides, this method loses detailed information that is gained from phosphoproteomic analysis. This includes information regarding the specific phosphorylation site(s) per protein, the magnitude of up-regulation/down-regulation of these phosphorylation sites, upstream information regarding the kinase responsible, and corresponding increased or decreased kinase activity across different experimental conditions. Therefore, to fully investigate and compare signalling pathway activation across HMGB1 and CpG-ODN experimental conditions, KSEA was performed to gain a better insight into kinase activity.

KSEA of the phosphoproteome was performed for each patient following 15 minutes and 2 hours CpG-ODN and HMGB1 combined treatment, to identify substrate groups of kinases with significant activity compared to PBS baseline controls. For patient 8231, 15 minutes HMGB1 and CpG-ODN combined treatment demonstrated the significant abundancy (increased or decreased) of 9 substrate groups (column of interest indicated by arrow; Figure 5-13). Of these, 8/9 kinases had increased activity compared to PBS baseline and 1 had decreased activity. All 9 of these kinases overlap with kinases with significant activity following 15 minutes CpG-ODN treatment alone (Figure 5-13; Appendix II Figure 11). The signalling pathways and cellular activity associated with these kinases and substrate groups include cell cycle signalling, c-Jun oncogene activation, transcriptional regulation and RNA splicing. MAPK signalling was the only signalling

pathway demonstrating activation following 15 minutes CpG-ODN treatment, but not when HMGB1 and CpG were combined at this time points (Figure 5-13; Appendix II Figure 11).

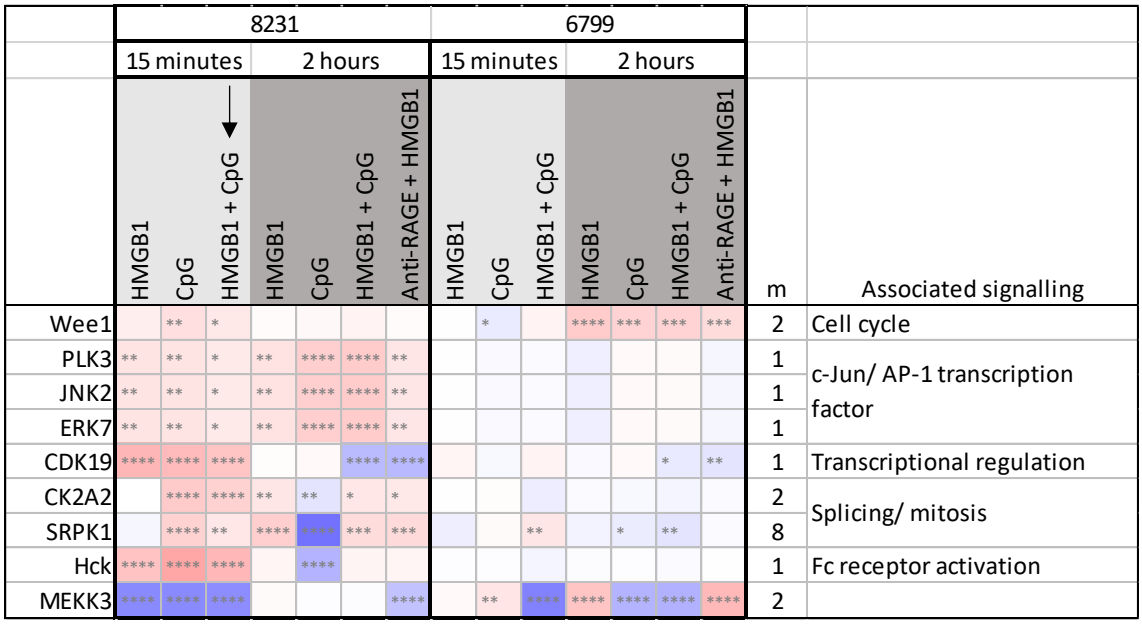

Figure 5-13. Heat map showing the enrichment of substrate groups for the different kinases calculated by KSEA algorithm, with significant abundance following HMGB1 and CpG treatment for 15 minutes for patient 8231

Cell samples were treated, processed and phosphopeptides quantified by LC/MS-MS as previously described in Figure 5-10. Enrichment of substrate groups was calculated by the KSEA algorithm and divided by the abundance of phosphopeptides in the PBS treated sample. Heat map colours correspond to the coloured enrichment key in Figure 5-10 and indicates -5 to +5-fold enrichment compared to PBS treated sample. Statistical significance of these changes was calculated by Student's t test compared to PBS treated samples; P<0.05*, P<0.01**, P<0.001***, P<0.0001****. 'm', number of substrates in the indicated kinase substrate group. KSEA results were filtered based on significantly abundant substrate groups for patient 8231 following HMGB1 and CpG-B class for 15 minutes (column indicated by arrow).

For patient 6799, 15 minutes HMGB1 and CpG-ODN combined treatment demonstrated the significant abundancy (increased or decreased) of 14 substrate groups (column of interest indicated by arrow; Figure 5-14). For this patient (ZAP70-), most substrate groups were negatively enriched following combined treatment, with 11/14 kinases demonstrating decreased activity compared to PBS baseline. This translates into a decrease in clathrin-mediated endocytosis, cytoskeletal rearrangement and chemotaxis (CXCR4 mediated) activity. These substrate groups overlap with significant kinase activity following CpG-ODN alone stimulation, except for GRK6 involved in CXCR4 chemotaxis, and PIKCI and ROCK1 involved in cytoskeletal reorganisation (Figure 5-14; Appendix II Figure 12). P38B, CK2A1 and SRPK1 demonstrate increased kinase activity following combined HMGB1 and CpG-ODN treatment, but not after CpG-ODN treatment alone (Figure 5-14). These kinases and substrate groups correspond to MAPK signalling, a central kinase for multiple cellular processes, and RNA splicing, respectively. For this patient, 15 minutes CpG-ODN stimulation alone resulted in 12 kinases with significant activity; 11 with decreased activity compared to baseline and 1 with increased activity (Appendix II Figure 12). The down-regulated substrate groups correspond to clathrin-mediated endocytosis, cytoskeletal regulation (consistent with combined HMGB1 and CpG-ODN treatment), cell cycle signalling and the unfolded protein response.

Interestingly, MAPK signalling was uniquely induced in the ZAP70- patient (6799) following HMGB1 and CpG-ODN combined, but not by CpG-ODN alone, whereas the opposite was observed in the ZAP70+ patient (8231); CpG-ODN alone induced MAPK signalling in patient 8231, which showed little activity following HMGB1 and CpG-ODN combined.

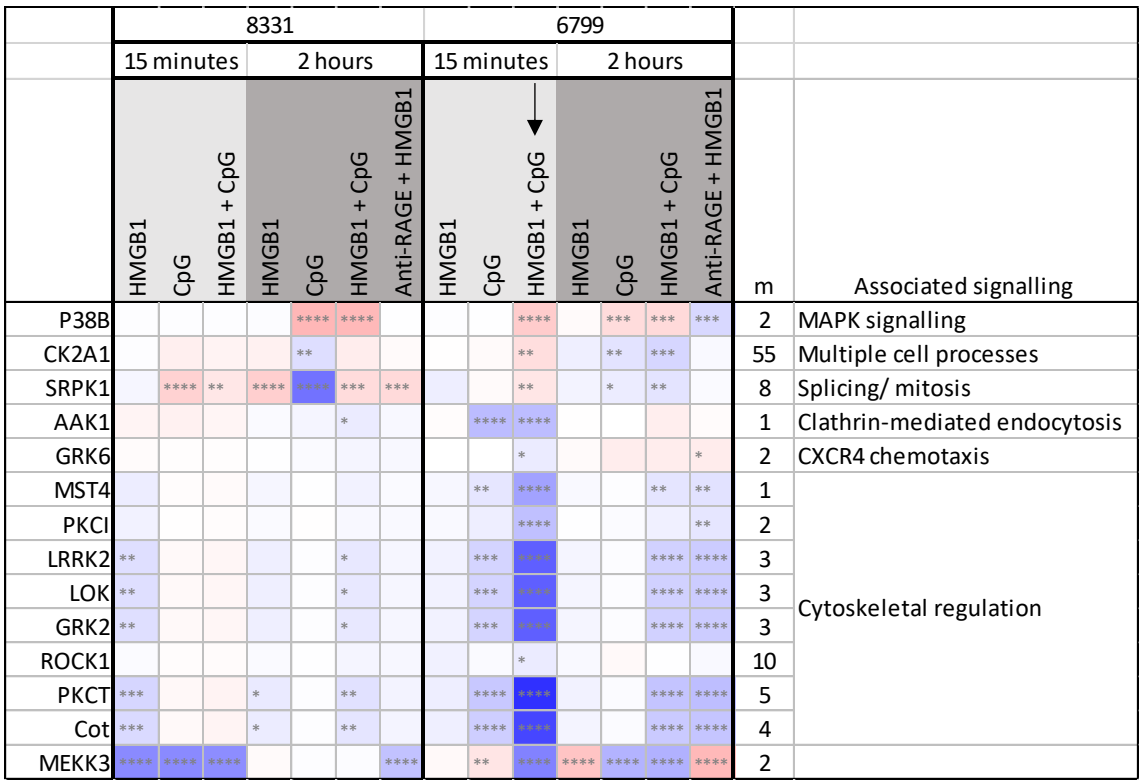

Figure 5-14. Heat map showing the enrichment of substrate groups for the different kinases calculated by KSEA algorithm, with significant abundance following HMGB1 and CpG-ODN treatment for 15 minutes for patient 6799

Cell samples were treated, processed and phosphopeptides quantified by LC/MS-MS as previously described in Figure 5-10. Enrichment of substrate groups was calculated by the KSEA algorithm and divided by the abundance of phosphopeptides in the PBS treated sample. Heat map colours correspond to the coloured enrichment key in Figure 5-10 and indicates -5 to +5-fold enrichment compared to PBS treated sample. Statistical significance of these changes was calculated by Student's t test compared to PBS treated samples; P<0.05*, P<0.01**, P<0.001***, P<0.0001****. 'm', number of substrates in the indicated kinase substrate group. KSEA results were filtered based on significantly abundant substrate groups for patient 6799 following HMGB1 and CpG-B class for 15 minutes (column indicated by arrow).

At the longer 2-hour time-point, KSEA of the phosphoproteome for patient 8231 revealed the significant activity of 28 substrate groups and respective kinases (Figure 5-15); 21 with increased activity compared to PBS baseline and 7 kinases with decreased activity. The up-regulated substrate groups correspond to mTORC1 regulation, MAPK signalling, c-Jun oncogene activation, MYC signalling, RNA splicing activity and microtubule regulation. Of these abundant substrate groups and respective associated signalling pathways, only kinases corresponding to mTORC1 regulation (mTOR) and MAPK signalling (ERK1, MEK2, Ret, JAK2, MEK1) have unique increased activity following 2 hours combined HMGB1 and CpG-ODN, when comparing to the KSEA results following 2 hours CpG-ODN alone for patient 8231 (Figure 5-15; Appendix II Figure 13). Therefore, at 15 minutes for this ZAP70+ patient, CpG-ODN alone stimulates MAPK activity, whereas by 2 hours treatment, MAPK signalling has ceased following CpG-ODN alone but is induced following HMGB1 and CpG-ODN combined. The increased mTOR activity following HMGB1 and CpG-ODN combined treatment suggests the involvement of the PI3K/Akt pathway

at this longer time-point. Interestingly, the response to RNA processing and splicing is reversed when HMGB1 and CpG-ODN is combined (Figure 5-15); CpG-ODN alone for 2 hours results in decreased CK2A2 and SRPK1, whereas combined HMGB1 and CpG-ODN results in increased kinase activity.

The 7 down-regulated substrate groups following 2 hours combined treatment, are unique to HMGB1 and CpG-ODN combined, and not significant following CpG-ODN alone (Figure 5-15; Appendix II Figure 13). These substrate groups are associated with clathrin-mediated endocytosis, transcriptional regulation and cytoskeletal regulation/reorganisation. Following 2 hours CpG-ODN stimulation alone (Appendix II Figure 13), all significant enriched substrate groups overlap with significant results for 2 hours HMGB1 and CpG-ODN combined.

Therefore, these results demonstrate that for this ZAP70+ patient, HMGB1 and CpG do act synergistically by inducing long-term MAPK activation, which is observed at 15 minutes HMGB1 alone (Figure 5-12) or CpG-ODN alone (Appendix II Figure 13), but ceased by 2 hours.

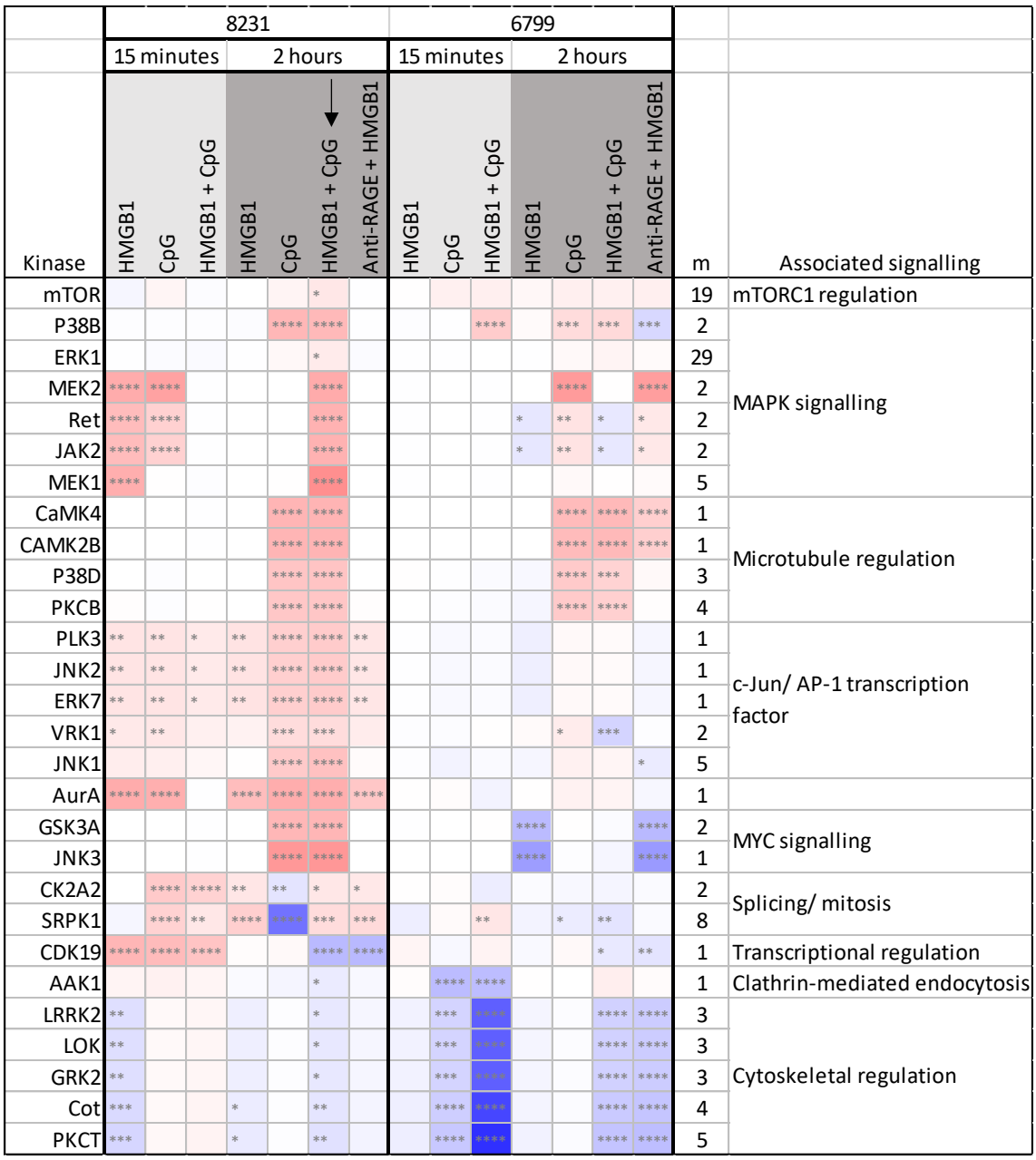

Figure 5-15. Heat map showing the enrichment of substrate groups for the different kinases calculated by KSEA algorithm, with significant abundance following HMGB1 and CpG treatment for 2 hours for patient 8231

Cell samples were treated, processed and phosphopeptides quantified by LC/MS-MS as previously described in Figure 5-10. Enrichment of substrate groups was calculated by the KSEA algorithm and divided by the abundance of phosphopeptides in the PBS treated sample. Heat map colours correspond to the coloured enrichment key in Figure 5-10 and indicates -5 to +5-fold enrichment compared to PBS treated sample. Statistical significance of these changes was calculated by Student's t test compared to PBS treated samples; P<0.05*, P<0.01**, P<0.001***, P<0.0001****. 'm', number of substrates in the indicated kinase substrate group. KSEA results were filtered based on significantly abundant substrate groups for patient 8231 following HMGB1 and CpG-B class for 2 hours (column indicated by arrow).

For patient 6799, KSEA of the phosphoproteome following 2 hours combined HMGB1 and CpG-ODN treatment revealed the significant enrichment of 29 substrate groups and respective kinases (Figure 5-16); 15/29 of these demonstrated increased activity compared to PBS baseline and 14/29 kinases with decreased activity. Comparing to the KSEA results following CpG-ODN alone 2 hours treatment for this patient (Appendix II Figure 14), nearly all 23 significant kinases under this experimental condition overlap with combined HMGB1 and CpG-ODN 2 hours, except for PKR and MEK2 in the CpG-ODN alone cohort (Appendix II Figure 14).

The substrate groups with significant enrichment following combined 2 hours HMGB1 and CpG-ODN treatment, correspond to PKC signalling, TLR9 signalling, PI3K/mTOR signalling, cell cycle and microtubule regulation (Figure 5-16). For this patient, kinases involved in MAPK signalling have demonstrated differing activity; HMGB1 and CpG-ODN combined 15 minutes treatment and 2 hours CpG-ODN alone treatment resulted in increased MAPK kinase activity, whereas 2 hours HMGB1 treatment alone resulted in decreased MAPK activity. For the 4 substrate groups under MAPK signalling with significant enrichment following HMGB1 and CpG-ODN combined treatment in patient 6799, 2 respective kinases had increased activity, and 2 with decreased activity (Figure 5-16).

For the 14/29 substrate groups with decreased enrichment compared to PBS baseline following combined HMGB1 and CpG-ODN treatment, some overlap with the direction of kinase activity following 2 hours CpG-ODN alone. These include kinases associated with BCR signalling, CK2 family of kinases and splicing/mitosis (Figure 5-16). The decreased activity of kinases associated with c-Jun activation, transcriptional regulation and cytoskeletal regulation, are unique to combined HMGB1 and CpG-ODN 2 hours alone.

These results do not reveal the increased activity of any alternative signalling pathways on the combination of HMGB1 and CpG-ODN compared to either alone. However, we have identified differing MAPK pathway activity, dependent on the length of time of stimulation and whether CpG-ODN was combined with HMGB1.

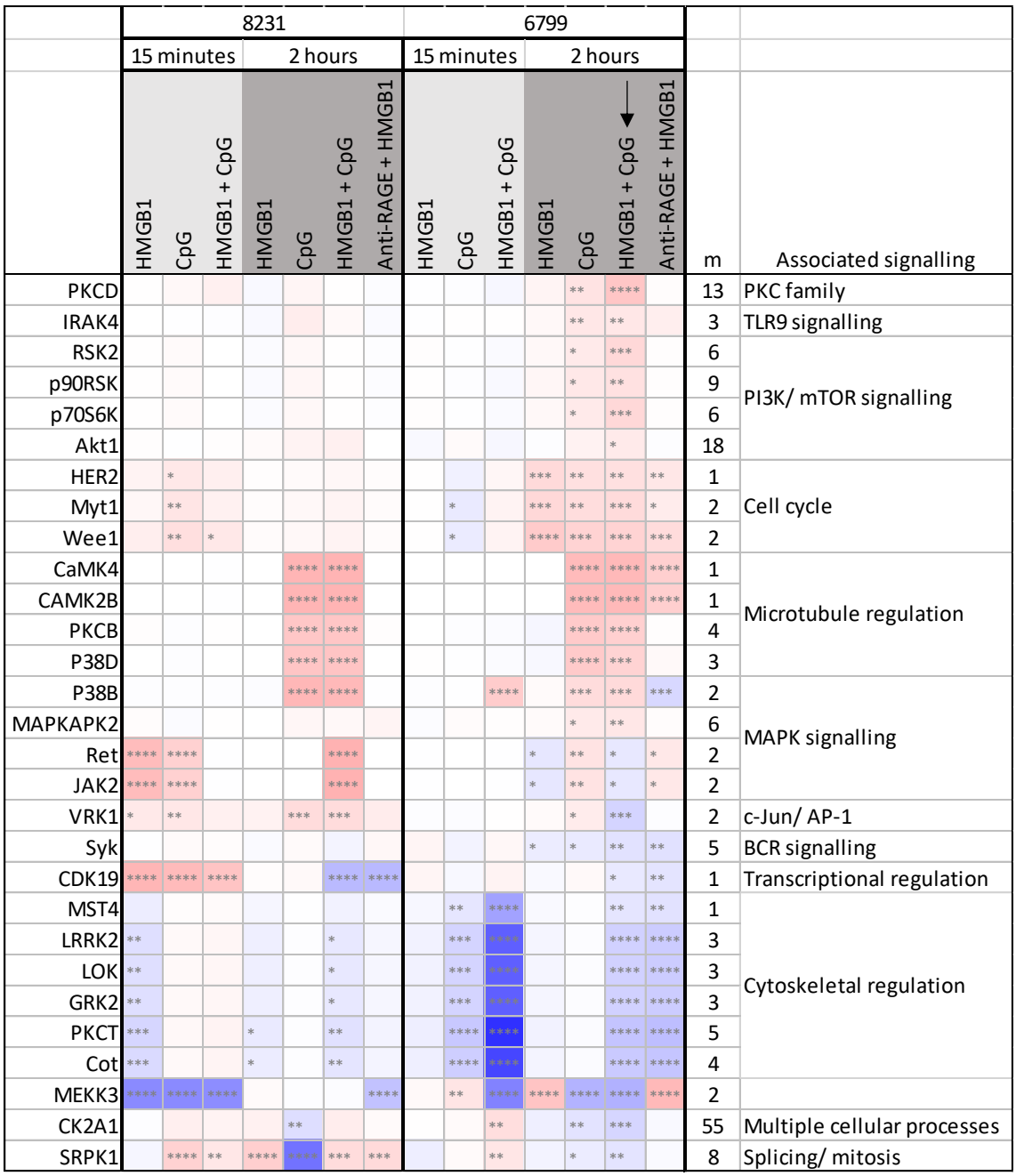

Figure 5-16. Heat map showing the enrichment of substrate groups for the different kinases calculated by KSEA algorithm, with significant abundance following HMGB1 and CpG treatment for 2 hours for patient 6799

Cell samples were treated, processed and phosphopeptides quantified by LC/MS-MS as previously described in Figure 5-10. Enrichment of substrate groups was calculated by the KSEA algorithm and divided by the abundance of phosphopeptides in the PBS treated sample. Heat map colours correspond to the coloured enrichment key in Figure 5-10 and indicates -5 to +5-fold enrichment compared to PBS treated sample. Statistical significance of these changes was calculated by Student's t test compared to PBS treated samples; P<0.05*, P<0.01**, P<0.001***, P<0.0001****. 'm', number of substrates in the indicated kinase substrate group. KSEA results were filtered based on significantly abundant substrate groups for patient 6799 following HMGB1 and CpG-B class for 2 hours (column indicated by arrow).

5.2.5.4 Anti-RAGE blockade does not neutralise HMGB1 activity

Finally, using phosphoproteomics we aimed to determine the impact of surface-RAGE blockade on 2 hours HMGB1 signalling, by assessing whole-cell signalling pathways. Referring to the relevant data from Table 10, Table 15 outlines the number of significantly increased and decreased abundant phosphopeptides in HMGB1-treated and anti-RAGE pre-blockade treated samples.

Table 15. Comparing the abundance of significantly increased and decreased phosphopeptides in HMGB1-stimulated samples with or without RAGE blockade

	8231		6799	
2 hours:	Up	Down	Up	Down
HMGB1	125	12	55	232
Anti-RAGE and HMGB1	107	15	152	445

Note: Data from Table 10. Up-regulated threshold set at log2 fold change ≥1 and $P<0.05$ compared to PBS treated sample; down-regulated threshold set at log2 fold change ≤-1 and $P<0.05$ compared to PBS treated sample.

HMGB1 treatment for 2 hours resulted in the up-regulation of 125 phosphopeptides and downregulation of 12 phosphopeptides for patient 8231, while pre-blockade of RAGE for 30 minutes before addition of HMGB1 for 2 hours, resulted in the up-regulation of 107 phosphopeptides and the down-regulation of 15 phosphopeptides compared to PBS baseline.

HMGB1 treatment for 2 hours resulted in the up-regulation of 55 phosphopeptides and down-regulation of 232 phosphopeptides for patient 6799; while pre-blockade of RAGE for 30 minutes before addition of HMGB1 for 2 hours, resulted in the up-regulation of 152 phosphopeptides and the down-regulation of 445 phosphopeptides compared to PBS baseline.

Anti-RAGE blockade does not have much impact on the abundance of increased or decreased phosphopeptides for patient 8231, but these may be of different phosphorylation sites; whereas there is a big increase in the abundance of both increased and decreased phosphopeptides for patient 6799. Assessing the signalling pathways affected using DAVID bioinformatics resource and KSEA of the phosphoproteomes will reveal the true impact of RAGE blockade on kinase activity.

The list of uniprot IDs for the significantly increased abundant phosphopeptides following 2 hours anti-RAGE blockade with HMGB1 were submitted to DAVID bioinformatics (Appendix II; Table O) and pathway functional annotation was assessed using KEGG pathway mapping. 14 signalling pathways were identified with genes associated with the input uniprot ID list following 2 hours HMGB1 stimulation alone for patient 8231 (5.2.5.2; Table 11). Addition of pre-RAGE blockade for 30 minutes, followed by 2 hours HMGB1 stimulation gave 10 KEGG pathway results

(Table 16). 9/10 of these pathways overlap with results from 2 hours HMGB1 stimulation alone for patient 8231, except for glycolysis/gluconeogenesis. For patient 6799, the list of uniprot IDs for the significantly increased abundant phosphopeptides following 2 hours treatment with HMGB1 yielded 0 results for association with signalling pathways - this result was maintained upon addition of pre-RAGE blockade for 30 minutes.

The KEGG pathway results for patient 8231 imply similar pathways are activated by HMGB1, regardless of RAGE-blockade. However, prior *in vivo* cell activation may contribute to the activation of some observed pathways through KEGG analysis (i.e. the pathways associated with pathological conditions), and the gene count for the observed pathways is not consistent between HMGB1 alone stimulation, and RAGE blockade with HMGB1. Further investigation of kinase activity may reveal inhibition of certain pathways and switching to others due to RAGE blockade.

Table 16. Patient 8231 2 hours anti-RAGE and HMGB1 treatment KEGG pathway results for upregulated phoshopeptides

Signalling pathways	Gene count	%	P-Value
Spliceosome	7	7	2.30E-04
Alcoholism	7	7	1.00E-03
Parkinson's disease	6	6	2.40E-03
Pathogenic Escherichia coli infection	4	4	4.60E-03
Huntington's disease	6	6	8.60E-03
Systemic lupus erythematosus	5	5	1.20E-02
Alzheimer's disease	5	5	2.50E-02
Carbon metabolism	4	4	3.90E-02
Oxidative phosphorylation	4	4	5.80E-02
Glycolysis / Gluconeogenesis	3	3	7.30E-02

KSEA of the phosphoproteome was performed for each patient following 2 hours anti-RAGE and HMGB1 combined treatment, to identify substrate groups of kinases with significant activity compared to PBS baseline controls. For patient 8231, 2 hours HMGB1 treatment alone, demonstrated the significant abundancy (increased or decreased) of 8 substrate groups (column of interest indicated by arrow; Figure 5-11). When RAGE was neutralised for 30 minutes prior to addition of HMGB1, 9 substrate groups were identified with significant abundancy (increased or decreased; column of interest indicated by arrow; Figure 5-17). Comparing these results to KSEA for patient 8231 following 2 hours HMGB1 treatment alone (Figure 5-11), substrates of AurA, PLK3, JNK2 and ERK7 are still significantly enriched despite RAGE blockade, contributing to the activation of transcription factor AP-1, via Jun phosphorylation at serine 73. Other substrate

groups that remained significantly enriched include those of CK2A2 and SRPK1 - both with roles in the regulation of alternative splicing. DYRK1A, CDK19 and MEKK3 are the only substrate groups with significant negative enrichment compared to the PBS baseline, and the only results that were not significant for 2 hours HMGB1 treatment alone. RCAN1 regulates transcriptional responses and is a mutual substrate for both DYRK1A and MEKK3. Decreased phosphorylation of RCAN1, as observed following anti-RAGE blockade, relieves the inhibitor function of RCAN1, allowing transcriptional activity to occur. An interesting result was a decrease in the enrichment of substrates for CDK19, which showed significantly increased enrichment following 15 minutes HMGB1 treatment alone for patient 8231. CDK19 is a component of the Mediator coactivator complex, responsible for the regulation of several transcription factors. In this setting, decreased CDK19 activity was due to a decrease in PAK1 phosphorylation. The significant KSEA results for RAGE blockade for patient 8231 do not overlap with patient 6799.

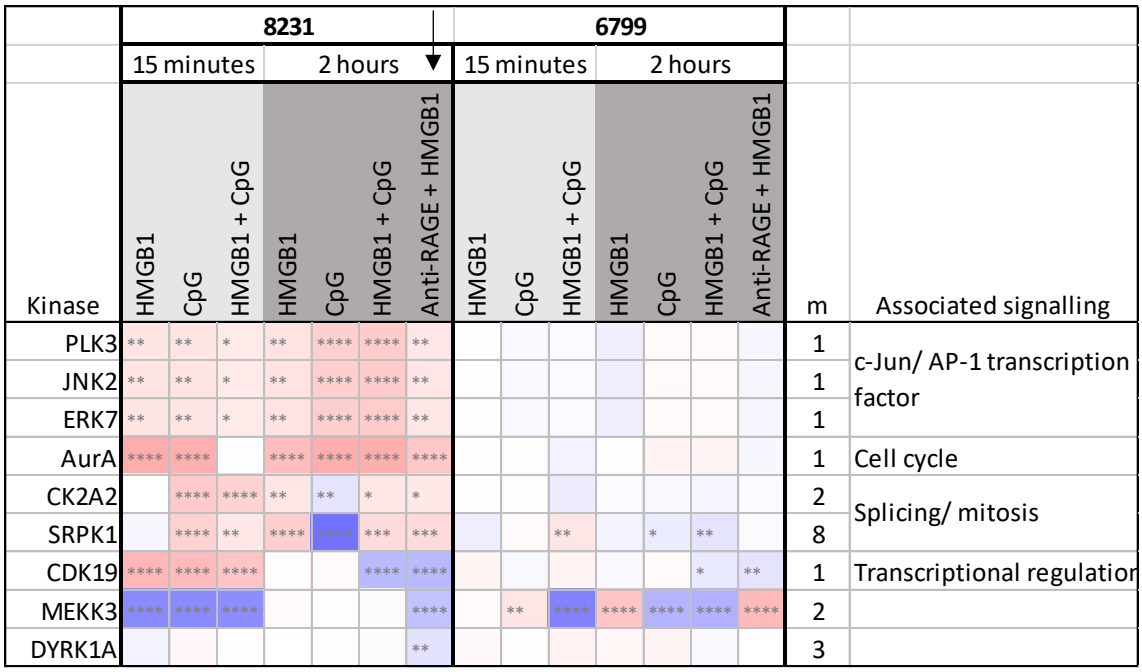

Figure 5-17 Heat map showing the enrichment of substrate groups for the different kinases calculated by KSEA algorithm, with significant abundance following pre-RAGE blockade for 30 minutes and addition of HMGB1 for 2 hours for patient 8231

Cell samples were treated, processed and phosphopeptides quantified by LC/MS-MS as previously described in Figure 5-10. Enrichment of substrate groups was calculated by the KSEA algorithm and divided by the abundance of phosphopeptides in the PBS treated sample. Heat map colours correspond to the coloured enrichment key in Figure 5-10 and indicates -5 to +5-fold enrichment compared to PBS treated sample. Statistical significance of these changes was calculated by Student's t test compared to PBS treated samples; P<0.05*, P<0.01**, P<0.001***, P<0.0001****. 'm', number of substrates in the indicated kinase substrate group. KSEA results were filtered based on significantly abundant substrate groups for patient 8231 following RAGE blockade for 30 minutes and addition of HMGB1 for 2 hours (column indicated by arrow).

For patient 6799, KSEA of the phosphoproteome following 2 hours HMGB1 treatment alone, resulted in 9 enriched substrate groups (column of interest indicated by arrow; Figure 5-12). Pre-blockade of RAGE followed by 2 hours HMGB1 treatment, resulted in the enrichment of 25 substrate groups (column of interest indicated by arrow; Figure 5-18). Comparing the KSEA results, all 9 enriched substrate groups following 2 hours HMGB1 treatment (HER2, Myt1, Wee1, Syk, Ret, JAK2, JNK3, GSK2A, MEKK3) were also significantly enriched in the same direction (increased or decreased) despite RAGE blockade (Figure 5-18). BCR and MYC signalling activity (via Syk, and JNK3 and GSK3A, respectively) was still decreased compared to the PBS baseline. Moreover, RAGE blockade failed to supress cell cycle signalling (via HER2, Myt1, Wee1) and MAPK signalling (via Ret, JAK2). RAGE blockade further induced the activity of MEK2, contributing to MAPK signalling, and the activity of GRK6 enhancing CXCR4 chemotactic activity.

The enrichment of substrate groups for CDK19, P38B, PKR, MST4, PKCI, Akt2, LRRK2, LOK, GRK2, PKCT and Cot, were significantly decreased compared to PBS baseline, and enrichment levels were different when comparing to 2 hours' HMGB1 alone (Figure 5-18). Decreased CDK19 activity was due to decreased PAK1 phosphorylation at serine 174; PAK1 regulates cytoskeleton reorganisation. The decrease in P38B activity is indicative of decreased RPTOR phosphorylation at serine 863 – a key activating phosphorylation site important for the positive regulation of mTORC1 activity, cell growth and cell survival. The decrease in activity of MST4 through to Cot is due to the decreased phosphorylation of EZR (threonine 567), RDX (threonine 564) and MSN (threonine 558). These 3 substrates function as cross-linkers between the plasma membrane and actin-based cytoskeleton.

Therefore, anti-RAGE blockade and HMGB1 treatment combined, does not impact HMGB-mediated outcome on increased MAPK and cell cycle signalling, or decreased BCR and MYC signalling. However, RAGE blockade does appear to have an inhibitory action on cytoskeletal reorganisation and cell motility signalling pathways for patient 6799 (ZAP70- patient).

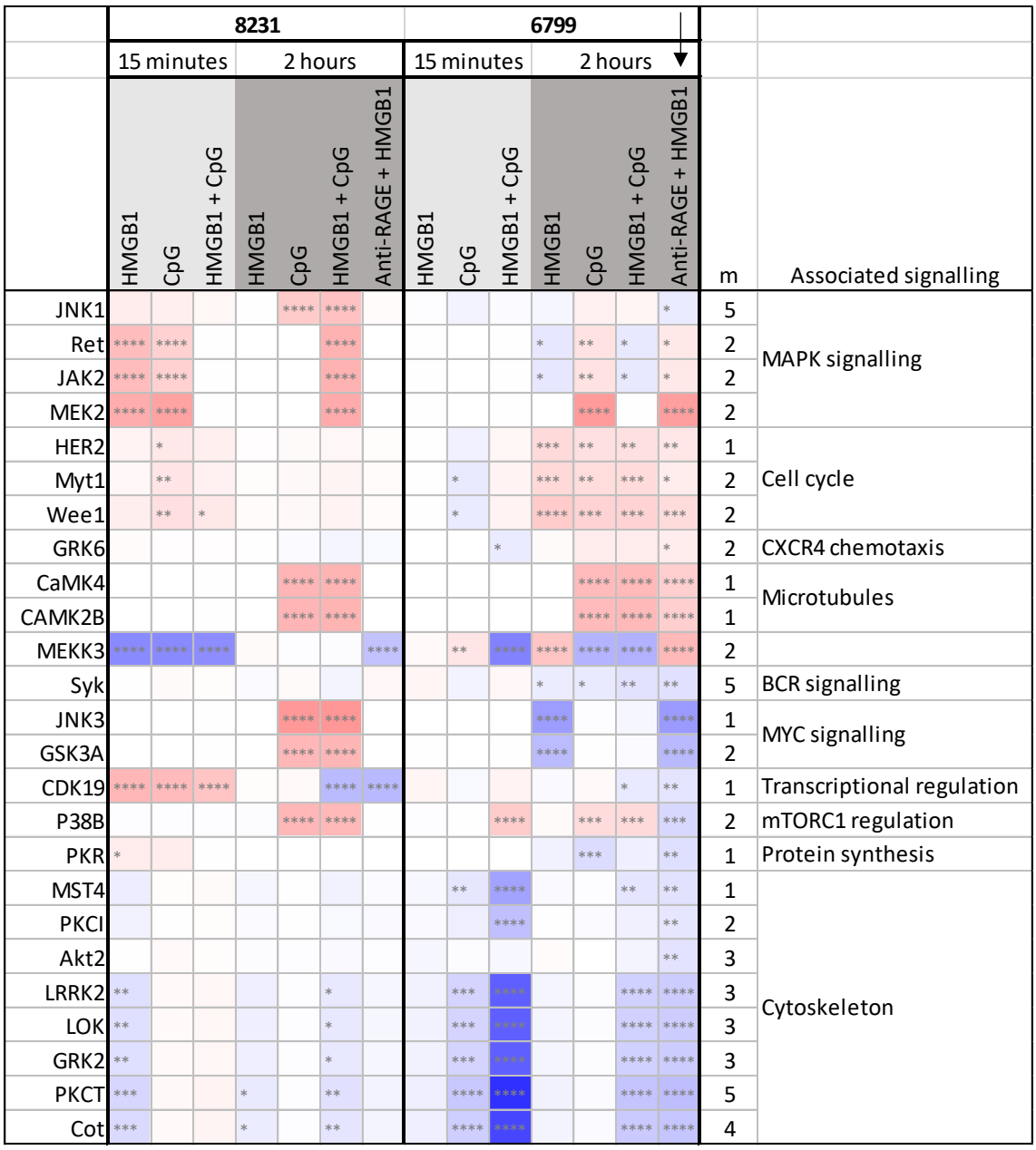

Figure 5-18. Heat map showing the enrichment of substrate groups for the different kinases calculated by KSEA algorithm, with significant abundance following pre-RAGE blockade for 30 minutes and addition of HMGB1 for 2 hours for patient 6799

Cell samples were treated, processed and phosphopeptides quantified by LC/MS-MS as previously described in Figure 5-10. Enrichment of substrate groups was calculated by the KSEA algorithm and divided by the abundance of phosphopeptides in the PBS treated sample. Heat map colours correspond to the coloured enrichment key in Figure 5-10 and indicates -5 to +5-fold enrichment compared to PBS treated sample. Statistical significance of these changes was calculated by Student's t test compared to PBS treated samples; P<0.05*, P<0.01**, P<0.001***, P<0.0001****. 'm', number of substrates in the indicated kinase substrate group. KSEA results were filtered based on significantly abundant substrate groups for patient 6799 following RAGE blockade for 30 minutes and addition of HMGB1 for 2 hours (column indicated by arrow).

5.3 Discussion

In this chapter, we have demonstrated RAGE and TLR9 as the most likely binding partners of HMGB1 using available bioinformatic databases. RAGE and TLR9 colocalise in CLL cells following HMGB1 stimulation, although this interaction is not stable by co-IP. Using an unbiased phosphoproteomic approach to assess cellular signalling networks, we identified MAPK signalling as a key pathway mediator of HMGB1 signalling. Blockade of RAGE did not inhibit MAPK signalling induced by HMGB1.

HMGB1 receptor selection and signalling pathway activation has not been fully elucidated in CLL B-cells. To successfully act as a DAMP, HMGB1 needs the ability to activate a variety of cell types, under stressed conditions.[131] To fulfil this role, HMGB1 targets several receptors (TLR1, 2, 4, 9 and RAGE), with the ability to bind other ligands and gain wider access to further receptors.[123,148] Using a combination of available online sources and literature search for receptor protein expression in CLL B-cells, we hypothesised RAGE and TLR9 as the most likely binding partners for HMGB1 in CLL B-cells. RAGE is highly expressed in epithelium of the lung and gastrointestinal tract and up-regulated in activated endothelium and immune cells following receptor engagement.[146] TLR9 is highly expressed in antigen presenting cells of the immune system, localised intracellularly in endosomes.[360] These expression patterns ensure rapid activation and removal of any exogenous or endogenous pathogenic threats. In the CLL B-cell setting, TLR9 activation results on dichotic cell responses, reliant on the expression of ZAP70 to engage BCR signalling pathway;[96] RAGE does not have a clear defined function in CLL B-cells so far. Further, previous studies in CLL NLCs and autoreactive B-cells, demonstrate cross-linked activity of RAGE and TLR9, and support a co-linked function of these receptors in HMGB1 biology.[76,145,260]

To infer linked activity of these receptors, we used two different imaging techniques to assess RAGE and TLR9 colocalisation following HMGB1 stimulation or blockade. Using fluorescent microscopy and ImageStream flow cytometry, we demonstrated the colocalisation of RAGE and TLR9 following 2 and 4 hours' exogenous HMGB1 treatment, consistent with the findings in CLL NLCs.[76] Both techniques were employed to gain quantitative and qualitative assessment of RAGE and TLR9 localisation.[304] While fluorescent microscopy at a magnification of 100x provides detailed morphological information, the number of cells imaged and analysed by ImageJ pixel intensity spatial correlation analysis makes this technique quantitatively unpowerful and could result in false conclusions. ImageStream flow cytometry overcomes this, by imaging 5000 cells at a magnification at 60x.[304] However, a stable interaction was not identified between RAGE and TLR9, or MyD88 and TLR9, following HMGB1 stimulation by co-IP.[76] Downstream from RAGE and TLR9 colocalisation, HMGB1, RAGE and TLR9 form an inflammatory triad contributing to the

activation of NF-κB in NLCs and autoreactive B-cells;[76,260,281] we demonstrated the nuclear translocation of NF-κB p65 subunit to the nuclei of CLL B-cells.

The entire HMGB1 signalling pathway has not been fully elucidated,[195] so assessment of cell signalling by biased approaches, such as Western blotting may miss important signalling events. We utilised an unbiased phosphoproteomic approach to assess HMGB1 signalling, synergy with CpG-ODN, and RAGE blockade in primary CLL B-cell samples.[311] Further, we analysed our phosphoproteomic dataset using KSEA, to measure the change of abundance of phosphosites between initial and treated samples, and therefore, infer differences in kinase activity.[310] We selected 2 fresh CLL patient samples with CD5+/CD19+ cell purity >90% to ensure phosphoproteomic signals were sourced from CLL B-cells, and with opposing ZAP70 expression status (assessed in-house using our method optimised in Chapter 4). ZAP70+ status correlates with IGHV mutational status, which was not performed at clinical diagnosis for our patient cohort.[91,92] The subsets differ by their signalling responsiveness to IgM antigen and CpG-ODN ligand.[95,96] Our phosphoproteomic data demonstrate ZAP70+ patient (Pat ID: 8231) with a higher number of significantly up-regulated phosphopeptides than down-regulated phosphopeptides, following HMGB1, CpG-ODN and HMGB1 and CpG-ODN combined; while patient 6799 had more down-regulated phosphopeptides than up-regulated under the same treatment conditions. These results reflect different signalling responsiveness of ZAP70+ and ZAP70- patient samples *in vitro*.[95,96]

HMGB1 has extensive roles in leukocyte biology, including apoptosis, chemotaxis and immune activation.[116,122,123] HMGB1 signalling pathways remain elusive, due to the complexity in receptor usage, ligand-synergy with IL-1, CXCL12, DNA, RNA, histones, CpG-ODN or LPS,[346] and cell-type selection and dependence on HMGB1 redox status.[139] In myeloid cells, HMGB1-TLR activation is one route leading to the activation and maturation of dendritic cells, monocytes and macrophages in innate immunity, and characterised by the up-regulation of the IFN response and pro-inflammatory cytokines.[146] Phosphorylation and activation of IRAK1,2,4, TRAF6, IKKα or IKKβ leads to NF-κB, IRF3 and IRF7 transcription factor activation is involved in the TLR signalling cascade.[253] The full RAGE signalling pathways is not well defined, but RAGE engagement in cells of myeloid and lymphoid lineage, endothelial cells and lung epithelial cells,[146] frequently results in the activation of MAPK, RAS pathways and NF-κB.[147] Our phosphoprotemic results for patient 8231 demonstrates the activation of MAPK signalling, AP-1 transcription factor activation, cell cycle regulation following 15 minutes HMGB1 stimulation, indicative of RAGE signalling. At 2 hours HMGB1 stimulation, AP-1 transcription factor activation is sustained. However, HMGB1 had no significant positive impact on the ZAP70- patient 6799, with no significant results following 15 minutes stimulation but induced the down-regulation of MAPK, BCR and Myc

signalling following 2 hours HMGB1 compared to the PBS baseline. These results reflect different signalling responsiveness profile of ZAP70+ and ZAP70- patients in the 2 patients included in this study, and demonstrate that HMGB1 has an anti-tumour effect in ZAP70- cells.[93,95,96]

HMGB1 can function synergistically with other cytokines, enhancing the immunogenicity of many ligands and giving HMGB1 the ability to target the various arms of immunological responses.[148] CXCL12 and CpG-ODN are widely known co-ligands of HMGB1. Moreover, CpG-ODN alone, and HMGB1 and CpG-ODN combined have demonstrated roles in CLL.[76,96] For patient 8231 (ZAP70+), our phosphoproteomic dataset demonstrates 15 minutes CpG-ODN alone induces up-regulation of cell cycle signalling, Fc receptor activation, AP-1 transcription factor activation and MAPK signalling; at 2 hours, AP-1 transcription factor activation and MAPK signalling are sustained along with activation of MYC signalling, while Fc receptor activation is down-regulated. Addition of HMGB1 with CpG-ODN for this patient for 15 minutes' stimulation, reduced MAPK signalling. This may be the result of different receptor usage, compared to CpG alone. At 2 hours' combined HMGB1 and CpG-ODN treatment, a higher number of phosphopeptides involved in MAPK signalling are up-regulated compared to 2 hours CpG-ODN alone; activation of mTOR signalling was identified following 2 hours' combined HMGB1 and CpG-ODN stimulation, while Myc signalling, microtubule regulation and AP-1 transcription factor activation are sustained upon addition of HMGB1 with CpG-ODN. HMGB1 bound to extracellular CpG-ODN and circulating immune complexes is responsible for the activation of TLR9 and BCR in B-cells, respectively.[149] Although our data reflects the up-regulation of more phosphopeptides following 2 hours' combined HMGB1 and CpG treatment for patient 8231, it is not distinctly clear whether this is due to dual use of TLR9 and HMGB1 pathways, or due to effective delivery of more CpG-OND ligand by HMGB1-RAGE.

For patient 6799 (ZAP70-), 15 minutes HMGB1 and CpG-ODN combined treatment results in the activation of MAPK compared to CpG-ODN alone. The down-regulation of phosphopeptides involved in cytoskeletal rearrangement and clathrin-mediated endocytosis are common to both CpG-ODN alone and CpG-ODN with HMGB1. At 2 hours, combination of HMGB1 with CpG-ODN did not result in the up-regulation and activation of any unique signalling pathways compared to CpG-ODN alone. However, while all MAPK phosphopeptides were upregulated after 2 hours CpG-ODN alone, some phosphopeptides had opposing down-regulated status following the combination of HMGB1 and CpG-ODN. In CLL cells, CpG-ODN signalling results in dichotic responses, dependent on the expression of ZAP70. In ZAP70+ cells, TLR9 signalling can fully engage the BCR pathway via ZAP70 and Syk crosslinking leading to proliferation; in ZAP70- cells, this crosslink does not occur and TLR9 signalling leads to apoptosis.[96] In our dataset, MYC signalling is up-regulated following 2 hours CpG-ODN in the ZAP70+ patient, and BCR signalling

is down-regulated under the same conditions for the ZAP70- patient; these results reflect previously published work on CpG-ODN stimulation in CLL cells.[96] Whereas HMGB1 and CpG-ODN enhances the activity of proliferative signalling kinases in the ZAP70+ patient, there is little impact of the addition of HMGB1 with CpG-ODN in the ZAP70- patients, and actually induced the opposing kinase activity score of some kinases involved in MAPK signalling. These results demonstrate HMGB1 induces dichotic responses dependent on the ZAP70 status, in line with the signalling responsiveness to CpG-ODN.

Elevated expression and perpetuation of RAGE signalling and associated inflammatory loops, has been demonstrated in a variety of cancers and chronic inflammatory disorders.[123,182-185,224] Intracellular RAGE signalling is not well defined, but evidence for the activation of MAPK pathway (via ERK1/2, p38 activation), PI3K and AKT, and JAK-STAT pathway has been established in a variety of cell types.[145,196,197] Our phosphoprotemic dataset demonstrates the activation of MAPK following HMGB1 treatment, suggesting the use of RAGE signalling cascade. Due to the uncertainty of intracellular RAGE mediators across multiple cell types, current RAGE antagonists target the membrane-bound receptor.[235-237] In this study, we used a monoclonal RAGE antibody to block HMGB1 from binding to the ligand-binding site of membrane-RAGE, which was previously used to ameliorate sepsis and tumour progression in animal models.[168,238] Anti-RAGE antibody successfully blocked HMGB1-mediated NLC differentiation in CLL,[76] and blocked RAGE and TLR9 colocalization in our study. However, assessing kinase activity scores, 2 hours anti-RAGE antibody and HMGB1 combined treatment did not block signalling pathways activated following 2 hours HMGB1 alone in our phosphoproteomic dataset for both patients. Interestingly, blockade of RAGE in the ZAP70- patient 6799 induced the activation of Ret, JAK2 and MEK2, reversing the status of MAPK signalling. These results demonstrate membrane RAGE blockade does not affect HMGB1 signalling in CLL cells, suggesting other receptor usage, or that anti-RAGE blockade did not fully block membrane RAGE. Further studies are required with MAPK signalling inhibitors to fully investigate the association between HMGB1, RAGE and MAPK signalling in ZAP70+ patients. Moreover, RAGE blockade has a pro-tumour effect in ZAP70- CLL cells; this result combined with the down-regulation of MAPK signalling following HMGB1 alone in the ZAP70- patient suggests HMGB1 contributes to anti-tumour signalling. Further studies with a larger cohort of ZAP70+ and ZAP70- are required to confirm this observation.

In summary, our results demonstrate that MAPK is a central pathway involved in HMGB1 signalling. With the limited sample size we have assessed in our study, our preliminary results suggest a dichotic response to HMGB1 in CLL patients, dependent on ZAP70 expression status. Further experiments with MAPK and TLR inhibitors in a larger cohort of patients will help decipher key mediators in HMGB1 signalling and signalling outcomes.

Chapter VI

Determine the origin of soluble RAGE in CLL

6.1 Introduction

Extracellular sRAGE sequesters extracellular RAGE ligands and displays 'decoy' receptor ability. We determined significantly increased levels of extracellular sRAGE in CLL patients compared to healthy controls, the reverse of down-modulated levels measured in the plasma of patients with cancer or autoimmune disease.[128] Extracellular sRAGE displays a protective effect in CLL and correlates with time to first treatment, but the origin of extracellular sRAGE and functional impact in CLL has not been studied. Further insight into the functional significance of sRAGE as an antagonist of HMGB1, could provide an intrinsic mechanism to regulate HMGB1-mediated CLL disease pathogenesis.

The pool of sRAGE derives from 2 main sources – alternative splicing to produce endogenous secreted RAGE (esRAGE), or from surface RAGE ectodomain shedding. The es-RAGE isoform lacks the transmembrane region found in FL-RAGE but contains a C-terminal amino acid sequence that differentiates this isoform from the FL-RAGE sequence. Membrane RAGE shedding is catalysed by ADAM10 (a disintegrin and metalloproteinases), member of a zinc-dependent family of metalloproteases. In a healthy setting, HMGB1 and sRAGE plasma levels are inversely correlated.[209] Although extracellular HMGB1 concentration always exceeds sRAGE in healthy subjects, elevated levels of sRAGE regulates inflammatory responses by neutralising circulating ligands. In chronic disease, the HMGB1-sRAGE inverse relationship breaks down.[361] Lower levels of sRAGE are associated with a higher risk of disease or poor disease outcome for patients with type 2 diabetes, rheumatoid arthritis, SLE, malignant melanoma, advanced pancreatic cancer and breast cancer.[158,228,350,352,353,362] For these reasons, easily attainable extracellular sRAGE levels pose as a suitable plasma marker for chronic inflammation monitoring in pathological conditions.

Artificially inducing intrinsic receptor ectodomain shedding could provide beneficial RAGE ligand neutralisation - an area of current active research. Surface RAGE undergoes proteolysis dependent on ADAM10 γ-secretase activity.[215] Deregulation of extracellular sRAGE in CLL may be due to altered levels of ADAM10 expression, commonly observed in various pathological diseases.[363] Moreover, production of sRAGE may be a by-product of Notch cleavage/signalling catalysed by ADAM10 in CLL, and levels of sRAGE could be associated with NOTCH1 mutations (~10% prevalence in CLL).[364] Ligand-RAGE binding affects the accessibility of ADAM10 to the RAGE cleavage site, 12 amino acids upstream of the transmembrane region, rather than altering the cleavage site motif.[219] Therefore, saturating levels of RAGE ligand such as HMGB1, combined with increased expression of ADAM10 could be the driving factor behind sRAGE production in CLL; It is currently unknown whether saturating levels of HMGB1 observed in CLL could

functionally induce RAGE shedding. Es-RAGE and sRAGE produced by cleavage are functionally similar, as they both share identical ligand-binding sites, but the full extracellular roles of sRAGE in disease pathogenesis are still unclear.

The work in this chapter will determine if i) the origin of sRAGE in CLL; ii) if RAGE shedding is ADAM10-dependent and HMGB1 can induce RAGE cleavage in CLL; iii) if sRAGE antagonises HMGB1-mediated differentiation of NLCs.

6.2 Results

6.2.1 Extracellular sRAGE levels are stable for untreated CLL patients

We observed significantly higher extracellular sRAGE levels in the plasma of CLL patients compared to healthy controls assessed by ELISA, contrary to the frequent downregulation reported in inflammatory disease settings.[128,353] A lack of correlation between HMGB1 and sRAGE plasma levels in CLL suggest deregulated control of sRAGE isoform expression or RAGE membrane shedding. Although extracellular sRAGE levels confer a protective effect for CLL patients, whether extracellular sRAGE levels remain stable over the course of the disease is not known.

In our study, extracellular sRAGE levels were significantly higher in CLL patients compared to healthy controls (median 60.0pg/ml and 31.0pg/ml, respectively; Figure 4-6). High extracellular sRAGE levels were associated with a longer time to first treatment, but plasma sRAGE levels may not be stable over time. We assessed temporal sRAGE levels by using consecutive CLL patient plasma samples from 10 CLL patients. Plasma sRAGE levels were relatively stable (Figure 6-1), 9/10 patients had a coefficient of variation (CV) below 30% when comparing sRAGE levels across different time points (Table 17). For the 7 patients who did not undergo therapy at the time of plasma isolation, 5 patient plasma samples displayed a negative Pearson's correlation coefficient, highlighting a gradual decline in extracellular sRAGE levels over the course of the disease (Table 17; Figure 6-1). 3 CLL patients who progressed to front-line therapy (patient ID 8550, 7888, 8553), displayed higher sRAGE levels following therapy (of differing treatment regimens) and positive Pearson's correlation coefficients (coloured arrows indicate time of treatment; Figure 6-1; Table 17). These 3 patients reached partial remission. In our cohort of 54 patients, patients with samples assayed while in remission did not have significantly higher levels of sRAGE compared to plasma samples assayed from untreated or relapsed patients (Figure 4-8C); these temporal plasma results do indicate there is an initial increase in extracellular sRAGE following treatment. This could be due to treatment-related release of DAMPs and cell debris, that stimulate RAGE membrane shedding and metalloproteinase activity.

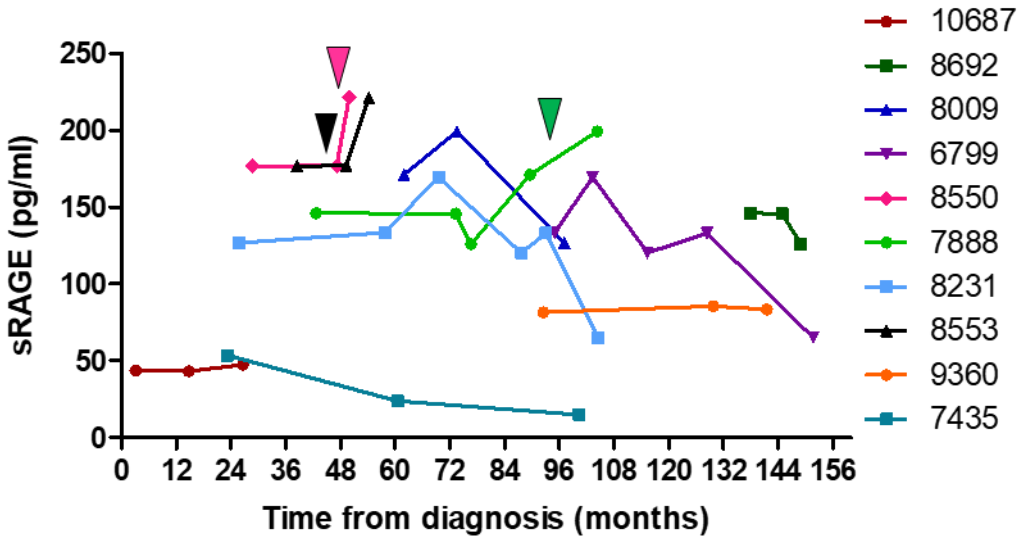

Figure 6-1 Evaluation of plasma sRAGE levels over time
Consecutive plasma samples from 10 CLL patients were assayed by ELISA to determine extracellular sRAGE concentration. Date of diagnosis and date and type of treatment was extracted from our tissue bank clinical database. 9 CLL patients remained untreated for the duration of these sample collection timepoints, and 3 CLL patients received treatment during these timepoints. Coloured lines represent different patients, linked to patient ID. For the 3 patients which received treatment, the same coloured arrows indicate time of treatment with details of their treatment in Table 17 below.

Table 17 Coefficient of variation and Pearson's correlation coefficient for consecutive extracellular sRAGE levels for 10 CLL patients

Pat ID	CV (%)	Pearson's correlation coefficient	Treatment
10687	5.09	0.82	
8692	8.24	-0.79	
8009	22.02	-0.75	
6799	30.45	-0.82	
8550	13.41	0.60	FCR
7888	17.90	0.68	FC
8231	27.15	-0.45	
8553	13.41	0.56	Lenalidomide
9360	2.36	0.69	
7435	65.71	-0.95	

Note: CV= coefficient of variation; FC= fludarabine, cyclophosphamide; R=Rituximab.

6.2.2 sRAGE originates from ectodomain shedding in CLL patient plasma

Understanding the origin of deregulated sRAGE levels will aid in understanding the driving mechanism behind sRAGE release in CLL. Moreover, this molecular understanding could reveal intrinsic antagonistic methods to dampen HMGB1-mediated inflammatory signalling and/or provide an easily attainable patient plasma marker that is coupled to chronic inflammatory dysregulation.

First, we assessed patient plasma sRAGE molecular weight to determine the main origin of extracellular RAGE. Cleaved RAGE produced by membrane RAGE shedding is of shorter length than endogenous secreted RAGE (alternatively spliced RAGE; 37kDa), and both are smaller than the main isoform full-length RAGE (42kDa). Using SDS-PAGE to denature and linearise RAGE isoforms, we can assess RAGE size based on protein mass alone, rather than shape. Human plasma is densely concentrated with extracellular proteins, particularly serum albumin and IgG, forming protein aggregates during protein denaturation steps for Western blotting. For these reasons, ELISA is the easiest and most quantitative method of choice when assessing plasma proteins but does not give an indication of protein size. Plasma protein concentration was measured by Bradford assay to ensure 40µg of protein was loaded per patient, and to limit albumin and IgG protein aggregation. We compared sRAGE from 6 CLL patient plasma samples with high levels of extracellular sRAGE, to a healthy control plasma sample (C90) and 1 matched patient CLL B-cell lysate (Figure 6-2). By Western blotting, the molecular weight of sRAGE in CLL patient plasma is of shorter length than FL-RAGE and es-RAGE in the patient whole cell lysate, indicating plasma RAGE originates from membrane receptor shedding. Transferrin expression (80kDa) was used as a loading control. However, Western blot protein smears caused by IgG heavy chain (50kDa) and albumin (66.5kDa) protein aggregates made it difficult to clearly evaluate transferrin expression (Appendix Figure 9). The same smearing was observed with Ponceau Red staining. Overall, as Western blotting was used here to assess protein size rather than for quantitative purposes, these results demonstrate membrane RAGE ectodomain shedding contributes to the pool of extracellular sRAGE.

ADAM10 is the main reported metalloproteinase that catalyses RAGE ectodomain shedding.[215] We compared patient extracellular HMGB1 and sRAGE concentrations to ADAM10 whole cell expression by using matched plasma samples and cryopreserved PBMCs. ADAM10 precursor (90kDa) is processed in the endoplasmic reticulum to give the cleaved active form (68kDa) expressed on the cell surface. Assessing ADAM10 whole cell expression in patients with high or low HMGB1 and sRAGE plasma levels revealed expression of ADAM10, and processing to produce the active form, is independent of extracellular HMGB1 and sRAGE (Figure 6-3). These

results demonstrate that CLL cells do express ADAM10 and extracellular sRAGE in CLL disease pathogenesis is primarily from RAGE ectodomain shedding.

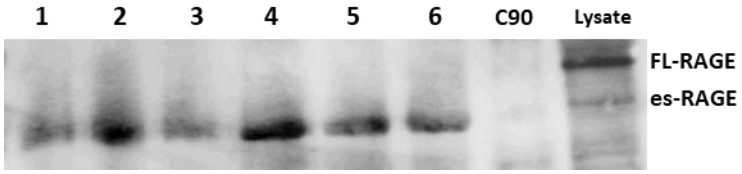

Figure 6-2 Western Blotting analysis of sRAGE isoforms in CLL patient plasma.
Extracellular RAGE protein mass was assessed in 40µg of plasma protein from 6 CLL patients with high sRAGE (lanes 1-6) and compared with healthy control patient plasma (C90) and CLL patient (5959) whole cell lysate. CLL patient and healthy control extracellular sRAGE concentration outlined in Table 18. FL-RAGE = Full-length RAGE, and es-RAGE = alternatively spliced endogenous secreted RAGE isoform whole cell lysate expression labelled in figure.

Table 18 sRAGE plasma concentration in CLL patients and healthy control (C90) from Figure 6-2

Lane	1	2	3	4	5	6	7
Pat ID	5959	9746	9853	5313	T-2472	8692	C90
sRAGE (pg/ml)	156.7	103.1	108.7	133.4	114.5	144.2	9.6

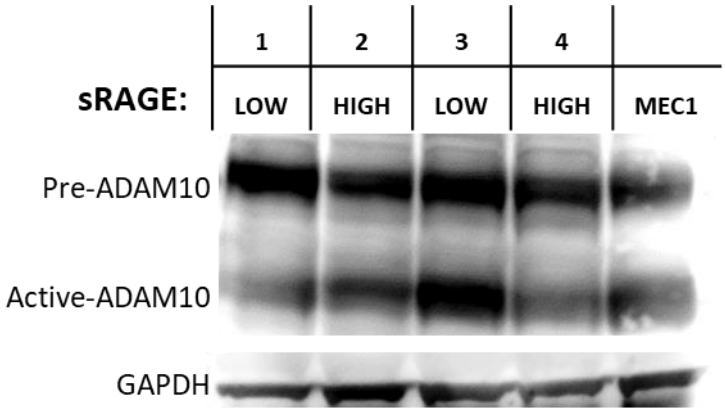

Figure 6-3 Western Blotting analysis of ADAM10 in CLL whole cell lysates.
ADAM10 whole cell expression was assessed in 50µg of whole cell lysate protein from 4 CLL patients that demonstrated high or low sRAGE plasma levels measured previously by ELISA, outlined in Table 19. Mec1 whole cell lysate was used as an ADAM10 expression control and GAPDH was probed as a loading control. Precursor ADAM10 (Pre-ADAM10, 90kDa) is cleaved to give active ADAM10 (68kDa).

Table 19 sRAGE and HMGB1 plasma concentrations in CLL patients from Figure 6-3

Lane	1	2	3	4
Pat ID	8921	T-1789	10450	8009
sRAGE (pg/ml)	1.47	136.4	0	101.89
HMGB1 (ng/ml)	78.9	205.9	72.7	394.1

6.2.3 Producing RAGE-transfected HEK293 cell line

We have demonstrated a protective effect for soluble RAGE in CLL, which is predominately produced by RAGE ectodomain shedding. To investigate the functional significance of RAGE shedding and sRAGE, we produced FL-RAGE transfected HEK293 cells, and es-RAGE-containing conditioned media from es-RAGE transfected HEK293 cells.

sRAGE cannot be purchased commercially so FL-RAGE and es-RAGE pcDNA3 plasmids were purchased from HMGBiotech (Appendix I; Figure 1). Plasmid numbers were expanded by transforming DH5α™ competent cells with FL-RAGE pcDNA3, es-RAGE pcDNA3 and pCU19 empty vector control plasmids. Plasmid DNA was purified from bacterial inoculation by plasmid midiprep and DNA concentration measured using Nanodrop spectrometer. To confirm we expanded and isolated the correct plasmid products, we quantified purified plasmid DNA by restriction digest and agarose gel electrophoresis (Figure 6-4A). We used SmaI and BamHI restriction enzymes, as both enzymes have cut sites in the pcDNA3 backbone and RAGE gene sequence. To differentiate between FL-RAGE and es-RAGE plasmids, FL-RAGE gene sequence has 2x BamHI and 1x SmaI cut sites in the gene sequence, compared to 1x BamHI and 1x SmaI cut site in es-RAGE gene sequence (Appendix I; Figure 2). The restriction digest products confirmed we isolated the correct plasmids; SmaI produced 2 bands from 2x cut sites in the es-RAGE-pcDNA3 and FL-RAGE-pcDNA3 plasmids, and BamHI produced 2 bands from 2x cut sites in es-RAGE-pcDNA3 plasmid and 3 bands from 3x cut sites in FL-RAGE-pcDNA3 plasmid (Figure 6-4A).

HEK293 cell line was transfected with 5µg purified plasmid DNA using JetPRIME transfection reagent. Lipid-based transfection reagent interacts with negatively charged plasmid DNA to produce transfection complexes. The positive charge from the transfection reagent allows the complex to interact with heparan sulphate proteoglycans on the cell surface and promote endocytosis. Plasmid DNA enters the nucleus and is transiently expressed following genome integration. We used a GFP expressing plasmid under the same conditions as FL-RAGE, es-RAGE and pCU19 plasmid transfections to assess transfection efficiency. 24 hours post transfection, nearly all HEK293 cells express GFP, indicating very high transfection efficiency (Figure 6-4B). Western blot analysis using cell lysates from FL-RAGE and es-RAGE transfected HEK293 cells confirmed cellular expression of the correct RAGE isoforms, and little RAGE was detected in the pCU19 control HEK293 cells (Figure 6-4C). Cell culture supernatant was collected from all transfected cells 24 hours-post transfection (transfection reagent removed before 24-hour culture; Figure 6-4C). Western blotting analysis and measurement of sRAGE concentration by ELISA confirmed es-RAGE was released into cell culture medium (2.4ng/ml), FL-RAGE resulted in

some RAGE release (1.1ng/ml) and pCU19 empty control vector displayed little RAGE shedding after 24 hours (23pg/ml). Using this method, FL-RAGE HEK293 cells can be used for downstream experiments, but not enough sRAGE was collected from es-RAGE cell culture medium (2.4ng/ml) to use for HMGB1 inhibitor functional studies.

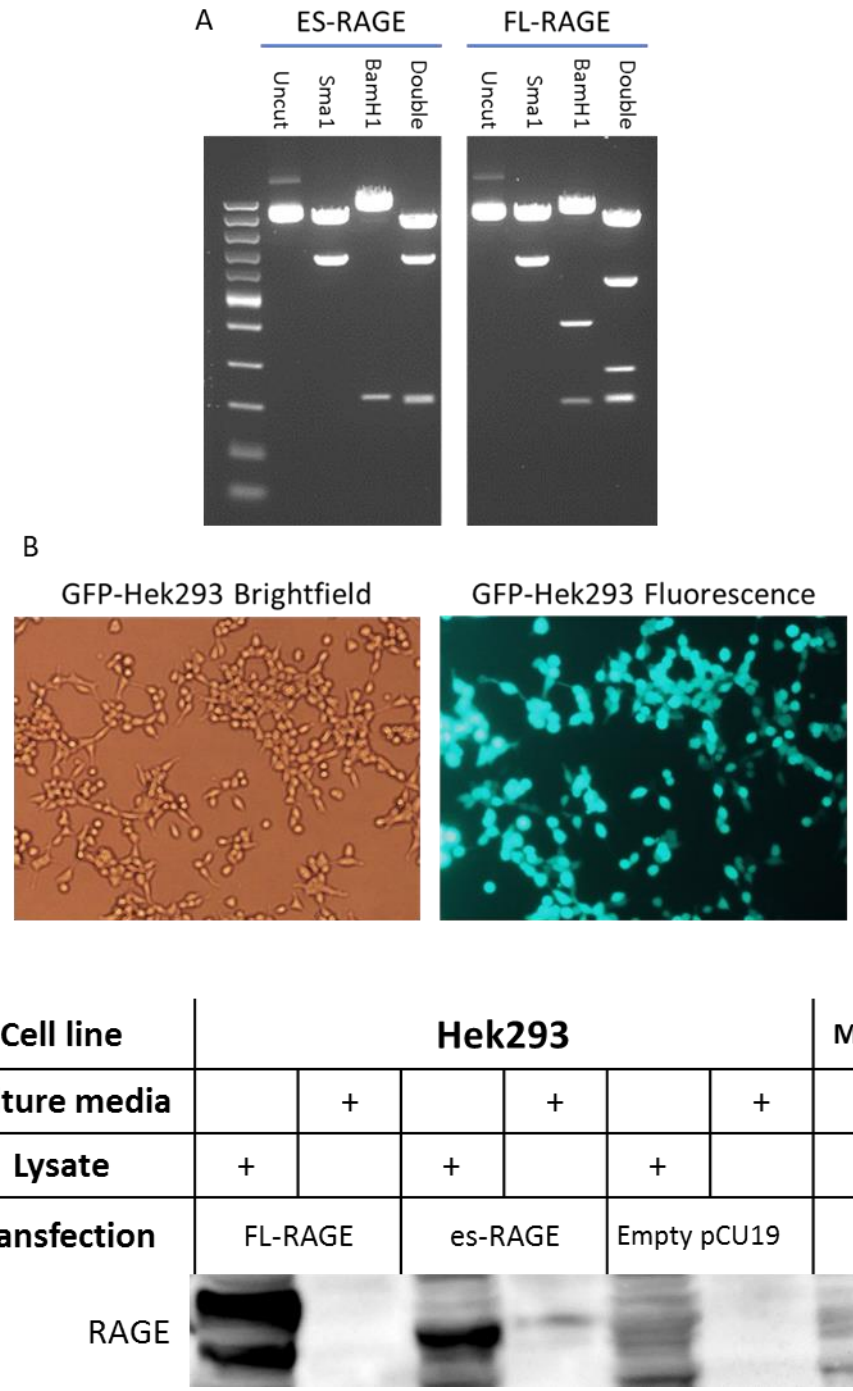

Figure 6-4 Producing FL-RAGE and es-RAGE transfected HEK293 cell line for sRAGE production.
FL-RAGE and es-RAGE expressing pcDNA3 plasmids were purified from transformed DH5α competent bacteria and quantified by restriction enzyme digest. (A) FL-RAGE and es-RAGE plasmids were digested with SmaI and BamHI restriction enzymes individually and subject to double digest. Digest products were separated by agarose gel electrophoresis and resulting bands were imaged. (B) HEK293 cells were transfected with 5µg of purified plasmid DNA and transfection efficiency was assessed with a GFP expressing plasmid control using brightfield and fluorescent microscopy; magnification x40. (C) FL-RAGE, es-RAGE and empty pCU19 vector expression was assessed by western blot analysis of conditioned media and cell lysates collected 24-hours post-transfection from HEK293 cells. A Mec1 cell lysate was included as a positive control.

6.2.4 RAGE shedding could be induced with ionomycin and HMGB1, and blocked with specific ADAM10 inhibitor

Our results show sRAGE originates from ectodomain shedding and CLL cells express ADAM10, but whether saturating levels of HMGB1 can stimulate RAGE shedding, or if ADAM10 is the specific RAGE sheddase in CLL, is currently unknown. We investigated RAGE shedding into cell culture medium following ADAM10 stimulation and ADAM10 inhibition in FL-RAGE transfected HEK293 cell line, Mec1 cell line and primary CLL cells.

We have demonstrated PB CLL B-cells express lower levels of surface RAGE compared to CD14+ monocytes, but higher levels of intracellular RAGE. To reliably assess the specific role of ADAM10 in surface RAGE shedding we established a transiently transfected HEK293 cell line with the FL-RAGE gene sequence. HEK293 cells normally express low levels of RAGE (Figure 6-4C), so any RAGE shedding measured in cell culture medium by ELISA is produced directly by RAGE shedding from FL-RAGE transfection. ADAM10 activity can be experimentally induced using calcium ionophore, ionomycin, in a PKCα/β1-dependent manner and by phorbol-12-myristate 13-acetate (PMA).[214,215] In this study, ADAM10 activity was induced by stimulating cells for 1 hour with ionomycin,[215] and ADAM10 activity blocked with specific inhibitor, GI254023X, for 1 hour prior to another hour of ionomycin stimulation in combination with the inhibitor. We assessed if saturating levels of RAGE ligand, HMGB1, also induced RAGE shedding; sRAGE released into cell culture supernatant was measured by ELISA, and cell surface expression of RAGE and ADAM10 by flow cytometry.

FL-RAGE transfected HEK293 cells expressed high levels of surface RAGE (MFI of 2426), and stimulation with 500nM ionomycin for 1 hour induced significant release of RAGE into cell culture medium compared to PBS and DMSO controls (PBS 1095pg/ml and ionomycin 2270pg/ml; $P<0.01$; Figure 6-5C). Moreover, when HEK293 cells were pre-treated for 1 hour with increasing doses of ADAM10 inhibitor, GI254023X, followed by stimulation with ionomycin, RAGE shedding was completely abrogated (GI254023X 5μM 45.6pg/ml, 10μM 30.1pg/ml, 20μM 49.4pg/ml; $P<0.0001$; Figure 6-5C). This observed shedding induced by ionomycin was not due to cell death (Appendix Figure 10). Levels of surface RAGE and ADAM10 were not altered when cells were treated with PBS and DMSO controls, or with ionomycin and ADAM10 inhibition (Figure 6-5A-B). We next investigated if increasing HMGB1 concentrations induces RAGE shedding using our FL-RAGE transfected HEK293 cell line model. HEK293 cell stimulation with 50ng, 200ng and 500ng HMGB1 did not result in ligand-induced RAGE shedding (PBS 1095pg/ml, HMGB1 50ng 1088pg/ml, 200ng 1316pg/ml, 500ng 1135pg/ml; Figure 6-5F). These results demonstrate ADAM10 is responsible for RAGE shedding.

We performed the same treatments and measurements in a CLL-specific cell line, Mec1. Surface RAGE expression was much lower compared to FL-RAGE transfected HEK293 cells, and stimulation with ionomycin did not induce measurable RAGE shedding into cell culture medium (PBS 7.9pg/ml, ionomycin 0.0pg/ml; Figure 6-6C). ADAM10 inhibition also failed to block RAGE shedding and we did not observe any changes in surface RAGE or ADAM10 expression (Figure 6-6A-C). Moreover, when we stimulate RAGE with increasing doses of HMGB1, in a B-cell line model, there were no measurable changes in RAGE shedding into cell culture medium (PBS 7.6pg/ml, HMGB1 50ng 16.4pg/ml, 200ng 0.0pg/ml, 500ng 6.8pg/ml; Figure 6-6F).

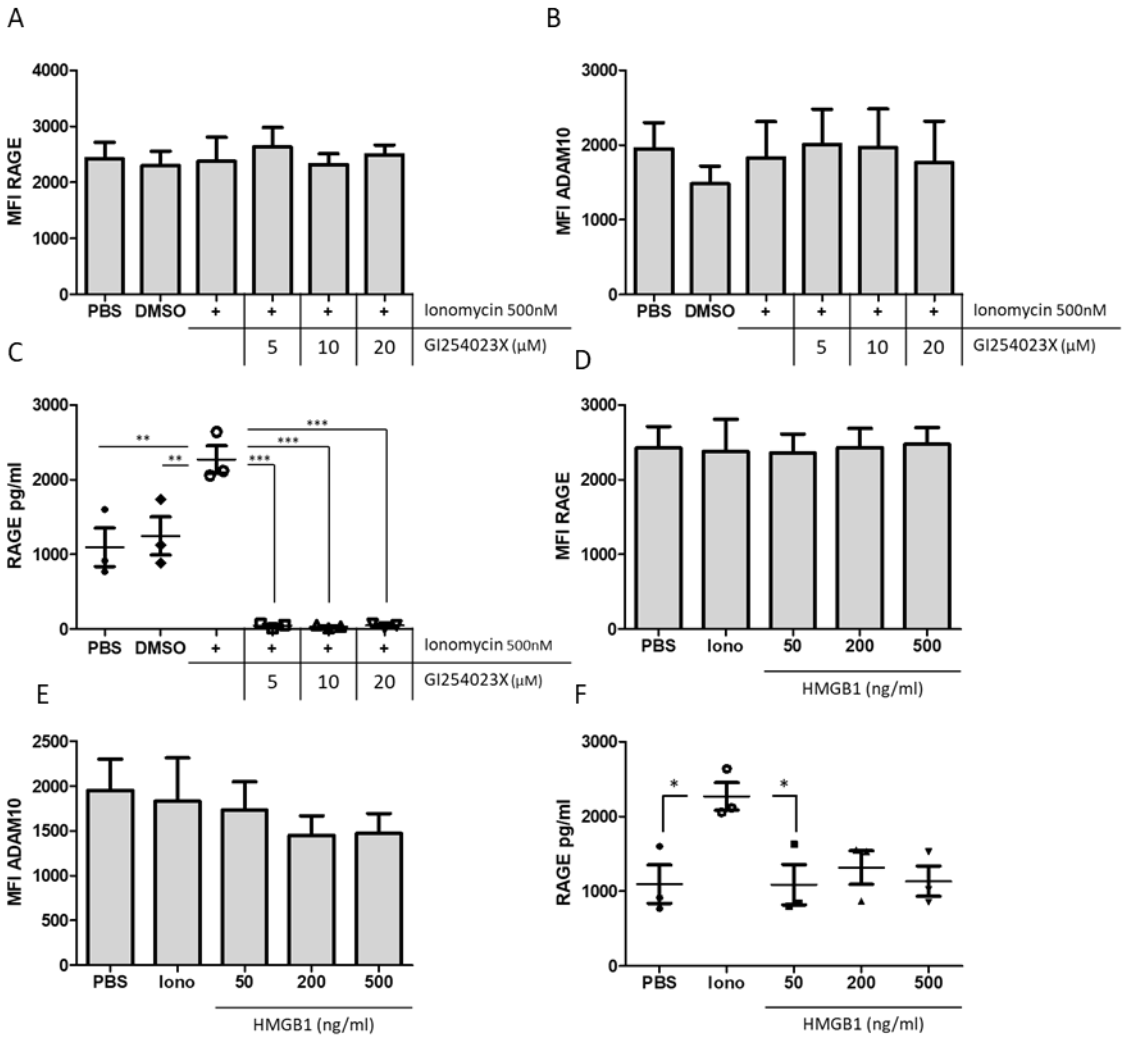

Figure 6-5 Evaluation of RAGE shedding in FL-RAGE transfected HEK293 cell line.
RAGE shedding in FL-RAGE transfected HEK293 cells was measured following ADAM10 stimulation with 500nM ionomycin for 1-hour or ADAM10 inhibition with GI254023X 5μM, 10μM and 20μM for 1-hour prior to addition of 500nM ionomycin. Cell surface RAGE (A) and ADAM10 (B) expression were assessed by flow cytometry with primary antibodies to rabbit anti-RAGE and rabbit anti-ADAM10 before labelling with AF-647 conjugated secondary antibodies. RAGE shedding into cell culture medium was measured by ELISA (C) following the same treatments. Ligand-induced RAGE shedding was measured in FL-RAGE transfected HEK293 cells by 1-hour stimulation with 50ng, 200ng and 500ng exogenous HMGB1. Cell surface RAGE (D) and ADAM10 (E) levels were assessed by flow cytometry and RAGE shedding measured in cell culture medium by ELISA (F). PBS and DMSO were used as vehicle controls and data are presented as the mean ±SD; n=3. *P*<0.05*, *P*<0.01**, *P*<0.0001***. + indicates addition of 500nM ionomycin; iono = ionomycin.

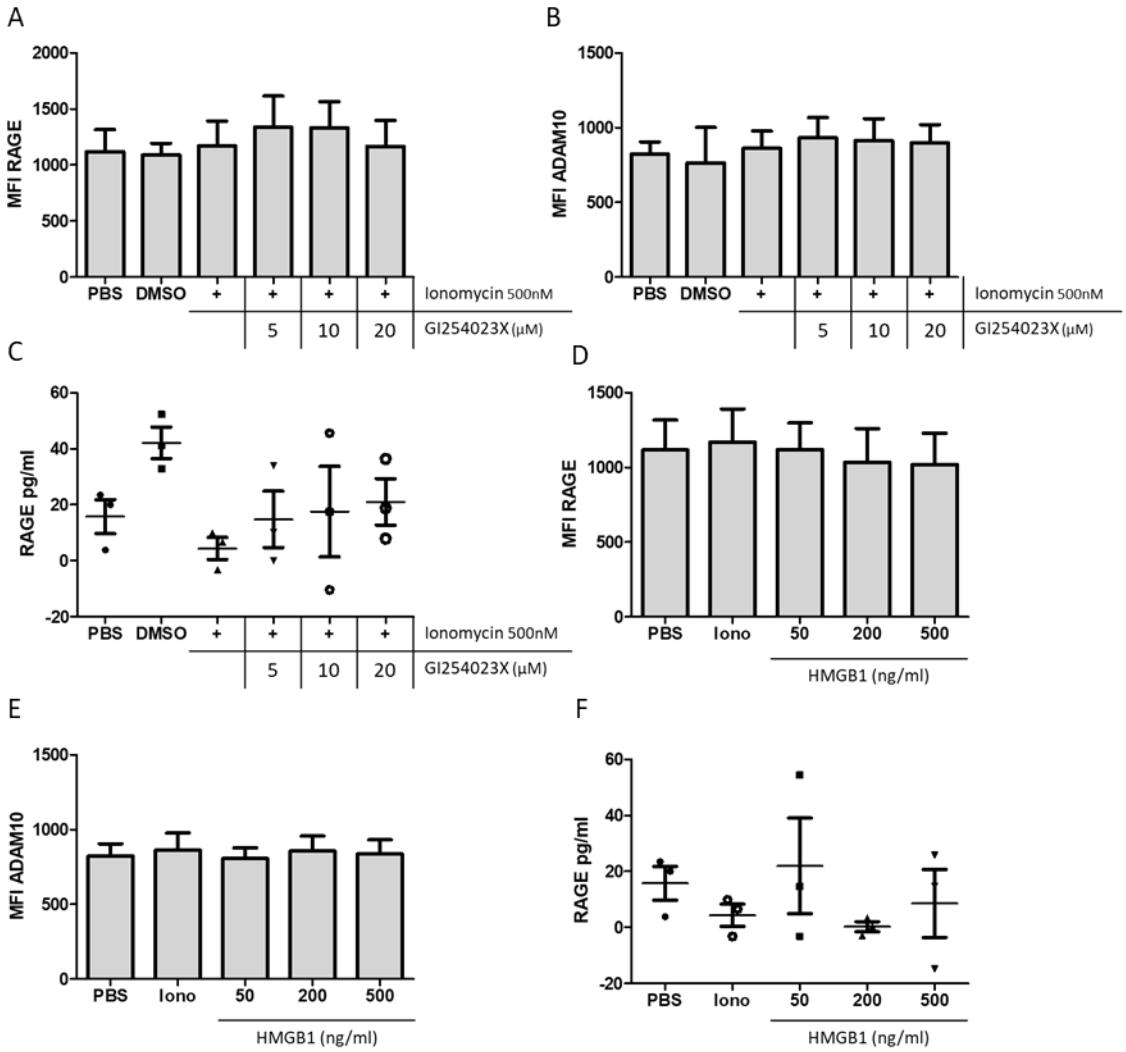

Figure 6-6 Evaluation of RAGE shedding Mec1 cell line.
RAGE shedding in CLL cell line, Mec1, was measured following ADAM10 stimulation with 500nM ionomycin for 1-hour or ADAM10 inhibition with GI254023X 5μM, 10μM and 20μM for 1-hour prior to addition of 500nM ionomycin. Cell surface RAGE (A) and ADAM10 (B) MFI levels were assessed by flow cytometry with primary antibodies to rabbit anti-RAGE and rabbit anti-ADAM10 before labelling with AF-647 conjugated secondary antibodies. RAGE shedding into cell culture medium was measured by ELISA (C) following the same treatments. Ligand-induced RAGE shedding was measured in Mec1 cells by 1-hour stimulation with 50ng, 200ng and 500ng exogenous HMGB1. Cell surface RAGE (D) and ADAM10 (E) MFI were assessed by flow cytometry and RAGE shedding measured in cell culture medium by ELISA (F). PBS and DMSO were used as vehicle controls and data are presented as the mean ±SD; n=3. + indicates addition of 500nM ionomycin; iono= ionomycin.

As we induced artificially high levels of FL-RAGE expression in HEK293 cells, and Mec1 cell line express low levels of surface RAGE, we next investigated RAGE shedding in 6 primary CLL patient samples. We previously demonstrated CLL cells express variable levels of RAGE on the cell surface, and high intracellular expression which is likely due to ligand-induced receptor internalisation and signalling. Whether saturating levels of HMGB1 induce RAGE shedding in CLL cells is unknown. Pre-treatment with ADAM10 inhibitor, GI254023X induced apoptosis in primary CLL cells so only ligand-induced receptor shedding was compared to ADAM10 positive stimulation with ionomycin. After 1-hour treatment, 500nM ionomycin and 500ng HMGB1 induced RAGE shedding into cell culture medium compared to PBS control (PBS 23.2pg/ml, ionomycin 41.3pg/ml, 500ng HMGB1 33.9pg/ml; $P<0.05$; Figure 6-7C). Surface levels of RAGE and ADAM10 remain unaltered (Figure 6-7A-B). Taking these data together, ionomycin stimulated ADAM10 activity in transfected HEK293 cells and primary CLL cells resulting in RAGE shedding into cell culture medium, dependent on ADAM10, which was also inducible by high levels of HMGB1 in primary CLL cells.

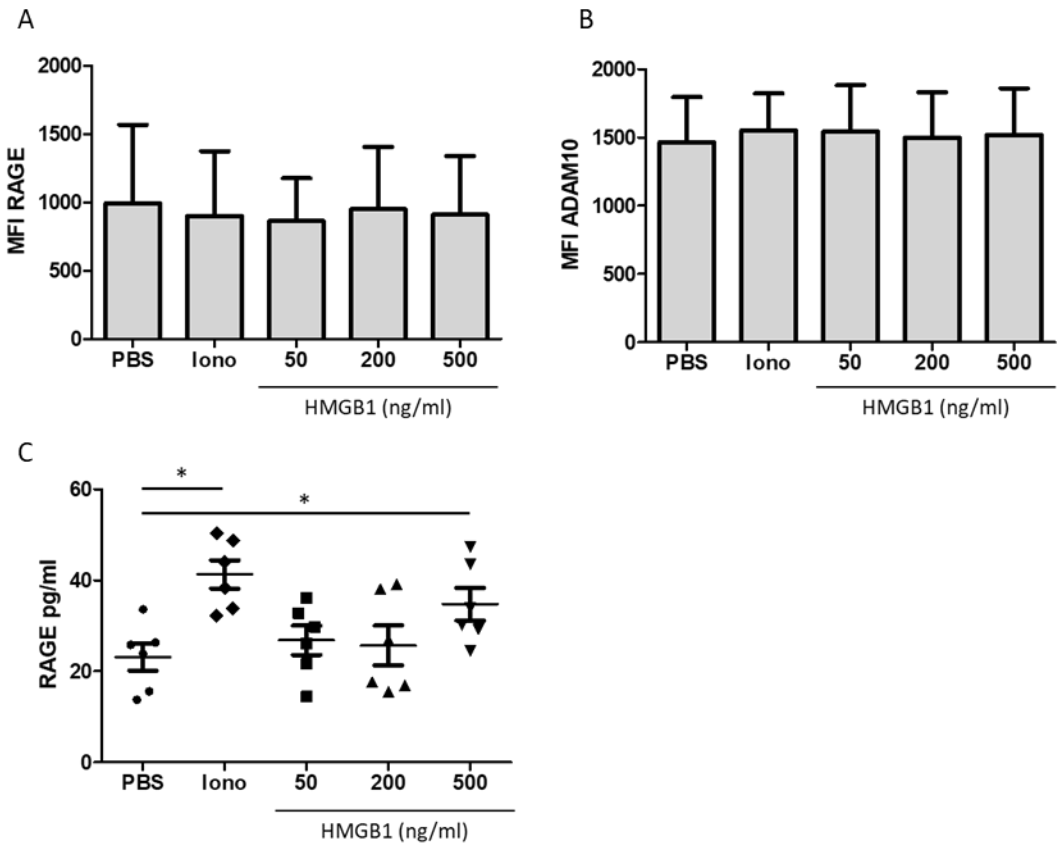

Figure 6-7 Evaluation of RAGE shedding in primary CLL cells.
Ligand-induced RAGE shedding was measured in 6 primary CLL patient samples following 1-hour stimulation with 50ng, 200ng and 500ng exogenous HMGB1. Cell surface RAGE (A) and ADAM10 (B) MFI levels were assessed by flow cytometry and RAGE shedding measured into cell culture medium by ELISA (C). PBS was used as a vehicle control and data are presented as the mean ±SD; n=6. $P<0.05$*; iono = ionomycin. ADAM10 inhibitor treatment, GI254023X, followed by ionomycin treatment induced apoptosis in primary CLL cells.

6.3 Discussion

In this chapter, we have demonstrated sRAGE levels are variable over time between patients, and display treatment-induced release. Extracellular sRAGE protein mass is shorter than FL-RAGE and es-RAGE indicating sRAGE derives predominantly from ectodomain shedding. ADAM10 is responsible for RAGE shedding in our transfected HEK293 cell line model, and HMGB1 could induce RAGE release in primary CLL samples.

Attention on the clinical applicability of measuring extracellular sRAGE levels in chronic pathological conditions is increasing. There is a clear association between low plasma sRAGE levels and poor outcome in cancer.[228,353,362] Moreover, we have identified a protective effect of extracellular sRAGE in CLL, but plasma levels were not altered between patients who were either untreated, reached remission or who had relapsed diseased. However, the patient-specific variability in extracellular sRAGE levels are unknown. Patient sRAGE extracellular levels were constant and stable in diabetic patients with vascular risk across a 3-year period, highlighting plasma sRAGE concentration could be measured at any time point to evaluate disease risk.[365] In our study, extracellular sRAGE levels slightly dropped for CLL patients who did not require treatment, but increased in patient plasma samples post-treatment, regardless of the treatment regime. We previously demonstrated a lack of inverse correlation between extracellular HMGB1 and sRAGE in CLL, highlighting DAMP-mediated deregulation of HMGB1 and sRAGE plasma levels in CLL. The increase in sRAGE levels following treatment is most likely due to treatment-related release of DAMPs during apoptosis and necrosis, driving RAGE ectodomain shedding.[121,366] Repeating the measurement of sRAGE plasma samples in conjunction with extracellular HMGB1 and S100B would confirm this. Regardless, patients who received treatment and displayed increased extracellular sRAGE levels reached partial remission.

The pool of extracellular sRAGE originates from alternative splicing or membrane RAGE shedding. The FL-RAGE and esRAGE spliced isoforms are the only isoforms of RAGE to reach protein expression.[210] It is not clear if RAGE alternative splicing is regulated upon different conditions; the ratio between FL-RAGE and es-RAGE expression is highly cell-type specific.[212] ADAM10 metalloproteinase is responsible for cleaving membrane FL-RAGE approximately 12 amino acids upstream of the transmembrane region.[219] Ligand-RAGE binding facilitates increased RAGE shedding, thereby dampening inflammatory responses, by increasing the accessibility of ADAM10 to the RAGE cleavage site, rather than revealing a cleavage motif.[219] In most chronic disease states, either cleaved RAGE or esRAGE contributes to the pool of sRAGE, compared to an equal combination of both, but the origin in CLL has not been investigated before.[215] By Western blotting, extracellular sRAGE in CLL is of shorter length than FL-RAGE and es-RAGE indicating sRAGE production is from membrane RAGE ectodomain shedding. Using an

antibody raised against the sequence-specific es-RAGE C-terminal end for Western blotting will confirm the origin of sRAGE in CLL patient plasma, but this antibody is not currently commercially available. Our results suggest sRAGE derives from ectodomain shedding, utilising this intrinsic mechanism to drive further RAGE release could dampen HMGB1 responses.

Surface RAGE ectodomain shedding is solely dependent on ADAM10 activity, and not reliant on shared-substrate metalloprotease ADAM17.[215] CLL cells express ADAM10, but protein levels and activation status are not associated with extracellular sRAGE levels. RAGE ectodomain shedding can be induced *in vitro* using PMA or calcium ionophore, ionomycin, using FL-RAGE transfected HEK293 cell line, which was recapitulated in this study.[214,215] We confirmed ADAM10 is the main RAGE sheddase using ADAM10 inhibitor GI254023X, and could induce RAGE shedding into culture medium following ionomycin stimulation in our HEK293 model. HMGB1 induces a conformational change in the membrane receptor, facilitating ADAM10 access to the cleavage site, but we did not observe RAGE shedding following HMGB1 stimulation in our HEK293 model.[219] FL-RAGE transfected HEK293 cells lack the intracellular signalling pathways downstream of RAGE expressed in B-cells; similar to ionomycin PKC-mediated ADAM10 activation, ligand-induced RAGE shedding may require activation of intracellular signalling, in combination with ligand-mediated conformational changes in the RAGE ectodomain structure to activate membrane RAGE shedding. Saturating levels of HMGB1 induced RAGE shedding into cell culture medium in primary CLL patient samples *in vitro,* but not in CLL cell line, Mec1. ADAM10 is responsible for the cleavage of several inflammatory and chemokine receptors, particularly the Notch receptor in CLL.[367] Using fresh CLL samples, ADAM10 may be in a higher primed state of activation reflecting prior *in vivo* activation when compared to ADAM10 expressed in the Mec1 cell line. Taken together, our results demonstrate ADAM10 activity and RAGE shedding can be induced in CLL *in vitro*. However, ionomycin and HMGB1 are not suitable stimulatory candidates to drive sRAGE production. A physiological approach could be the use of Lovastatin, a cholesterol-lowering agent that induces RAGE shedding *in vitro* in a ADAM10-dependent manner.[241] Although statins reportedly interfere with Rituximab efficacy, by inducing conformational changes in CD20,[242] patients with relapsed/refractory CLL displayed improved outcome when treated with FCR therapy while using statins and aspirin.[368] Moreover, inducing ADAM10 activity in CLL *in vivo* may stimulate Notch signalling that would drive CLL-cell survival.[369]

Although the regulation of RAGE ectodomain shedding is well documented, the biological function of sRAGE as an antagonist of RAGE ligands has only recently undergone functional investigation.[219] RAGE ectodomain shedding limited the migration of RAGE transfected C6 glioma cells. Although sRAGE decreased cell migration by sequestering RAGE ligands,

downstream signalling of the cleaved RAGE intracellular domain (ICD) revealed a more complex signalling network that contributed to a decrease in cell migration. We have shown sRAGE confers a protective effect in CLL and originates from ectodomain shedding; RAGE cleavage may produce a signalling-competent ICD that contributes to a favourable outcome compared to extracellular decoy receptor ability alone. In this study, we did not investigate the decoy receptor ability of esRAGE or the functional implication of endogenous RAGE ectodomain shedding. Modelling the biological effect of RAGE shedding in primary CLL cells or a B-cell line would be difficult. Comparison of FL-RAGE and cleavage-resistant FL-RAGE isoforms would help identify the role of RAGE ICD, but B-cells are notoriously difficult to successfully transfect. Secondly, inducing RAGE shedding with calcium ionophore, ionomycin, would lead to the activation of various off-target signalling pathways following calcium influx. Further functional studies into the intrinsic RAGE shedding mechanism in CLL are required for sRAGE or RAGE cleavage to fully define its role in CLL disease pathogenesis, and as a HMGB1 antagonist.

In summary, these results demonstrate that surface RAGE ectodomain shedding contributes to the pool of sRAGE in CLL. High levels of HMGB1 activate ADAM10-mediated RAGE shedding, contributing to sRAGE deregulation in CLL. This work demonstrates extracellular levels of HMGB1 and sRAGE as suitable, easily-attainable, circulating markers of chronic inflammation.

Chapter VII

Discussion

This thesis has investigated the roles of HMGB1 and RAGE in CLL disease progression. The involvement of HMGB1 in CLL disease pathogenesis is not well known, and the implications of the HMGB1-RAGE signalling axis in inflammatory disorders is only just starting to undergo investigation in clinical intervention studies.[128] To elucidate the roles of HMGB1 and RAGE in CLL, four main aims were set out for this study:

1. Assess the prognostic impact of RAGE and TLR9 receptors and effect on CLL overall survival
2. Determine the clinical relevance of the HMGB1-RAGE signalling axis
3. Determine HMGB1-mediated cellular signalling pathway
4. Determine the origin of soluble RAGE in CLL

7.1 Summarised findings addressing aims of PhD

7.1.1 Assess the prognostic impact of RAGE and TLR9 receptors and effect on CLL overall survival

Finding: RAGE and TLR9 are heterogeneously expressed in CLL patients LNs

Prior to assessing the prognostic impact of RAGE and TLR9 expression in Chapter 3, we first determined expression levels of HMGB1 receptors, RAGE and TLR9 in CLL. The results demonstrate RAGE and TLR9 gene expression is significantly higher in CLL cells compared to healthy controls using GEO datasets, while other HMGB1 receptors, TLR2 and TLR4 were significantly lower in CLL cells. When we assessed receptor expression in CD5+ CLL LN using TMAs comprised of 80 patient samples, an important site of CLL disease pathogenesis and microenvironment interactions, we found RAGE and TLR9 expression was significantly lower compared to reactive LN, and CLL LN expression of both receptors was highly heterogeneous in CLL patients, reflecting the clinical heterogeneity and variability in microenvironment dependence among CLL patients.

Finding: Higher RAGE expression in CLL LNs positively correlated with established proliferation marker, Ki67, and aggressive disease marker, ZAP70

ZAP70 is an established poor prognostic marker for CLL disease.[93] TLR9 and RAGE LN staining was compared to Ki67 and ZAP70 LN staining performed on the same CLL TMAs used in this study to gain insight into the association with poor prognosis. RAGE LN expression levels

positively and significantly correlated with both Ki67 and ZAP70 LN markers, indicating an association with aggressive disease for this cohort of patients. TLR9 expression had no association with ZAP70 expression, but TLR9 has established opposing roles in both ZAP70+ and ZAP70- CLL subsets, so this result was expected.[96,271,273]

Finding: CLL patients with high RAGE expression have a shorter overall survival

RAGE has not been studied in CLL before, so there is no indication of whether the HMGB1 receptor has a pro-tumour or anti-tumour function in CLL. We assessed the prognostic impact of RAGE expression, in CLL LNs, to assess whether expression is associated with CLL disease outcome, and further provide us with rationale to move forward with functional studies.

The results in Chapter 3 demonstrate for the first time that CLL patients with higher RAGE expression have a shorter OS when assessed by Kaplan Meier analysis, with data cut points determined by X-tile software. Moreover, using the same data cut points, high RAGE expression demonstrates prognostic significance using categorical univariate cox regression analysis. Interestingly, the prognostic significance of high RAGE expression increased when stratified with ZAP70 and Ki67 categorical variables for patients with CLL, meaning patients with high RAGE expression, Ki67 and ZAP70 LN staining had the poorest disease clinical outcome. However, we also demonstrated that RAGE expression in CLL-LN is lower than reactive-LN; these results highlight the routine role of RAGE in a healthy setting as an endogenous stress-response receptor and the involvement in inflammatory LN biology. The results from Chapter 3 demonstrate RAGE plays an important microenvironmental role in CLL LNs for further investigation, but the clinical applicability of RAGE as a prognostic marker requires further validation in independent data cohorts using the data cut points generated by X-tile.

7.1.2 Determine the clinical relevance of the HMGB1-RAGE signalling axis

Finding: Plasma HMGB1 levels are higher than other RAGE ligand, S100B, in CLL patients

In chapter 3 we established RAGE LN expression was associated with shorter CLL patient overall survival, and previous work in our group demonstrated increased levels of plasma HMGB1 in CLL patients compared to healthy controls. Prior to performing functional studies on HMGB1 and RAGE, it was important to assess the plasma levels of another main RAGE ligand, S100B, to ensure S100B-RAGE signalling does not dominate HMGB1-RAGE signalling in CLL. The results from chapter 4 demonstrate HMGB1 plasma levels are significantly higher than S100B in CLL patients.

Finding: Plasma HMGB1 levels are higher than plasma decoy receptor, soluble RAGE, and both plasma isoforms are independent of patient ZAP70 expression status

High plasma levels of HMGB1 in CLL may be signalling-incompetent if the RAGE ligand is sequestered by similar levels of 'decoy receptor' sRAGE. Further to the previous finding regarding S100B plasma levels, it was important to establish plasma levels of sRAGE in CLL. The results from chapter 4 demonstrate plasma levels of HMGB1 were significantly higher than sRAGE (ng levels vs pg levels, respectively) in our cohort of CLL patients. To assess if plasma protein levels were CLL subset specific, we compared the plasma concentrations of these proteins in ZAP70+ and ZAP70- cohorts; both plasma isoforms were independent of ZAP70 expression status.

Finding: Higher levels of soluble RAGE correlate with a longer time to first treatment

Lower plasma sRAGE levels compared to healthy controls is frequently reported in cancer, and is associated with progression of different types of solid cancer.[128] Surprisingly, our results demonstrate significantly higher levels of plasma sRAGE in CLL patients compared to healthy controls. An explanation for increased levels of sRAGE in CLL patients may be due to increased ligand-induced membrane receptor shedding catalysed by ADAM10 protease, indicative of ongoing chronic inflammation.[215,219] This is supported by a lack of inverse correlation observed for plasma sRAGE and HMGB1 levels in our cohort of CLL patients, that is classically observed in a healthy setting;[128,209] ie in a healthy setting, increasing levels of HMGB1 drives RAGE shedding, and plasma sRAGE consequently sequesters free plasma HMGB1. Although increased sRAGE levels in CLL was a surprising result compared to healthy controls in our study, we observed that CLL patients with high sRAGE levels had a longer time to first treatment, conferring a protective effect in CLL.

7.1.3 Determine HMGB1-mediated cellular signalling pathway

Finding: Recombinant HMGB1 induces the colocalization of RAGE and TLR9 assessed by imaging methods

Consistent with previous fluorescent microscopy results in CLL NLCs,[76] the results from chapter 5 demonstrate RAGE and TLR9 colocalization assessed by 2 imaging methods, following longer-term HMGB1 stimulation for 2 and 4 hours in primary CLL cell samples. Our fluorescent microscopy / ImageStream results indicate HMGB1 induces RAGE and TLR9 colocalization, suggesting the possibility of co-linked cell signalling; however, a stable interaction was not

detected between RAGE and TLR9 by co-IP. We identified downstream translocation of NF-κB p65 subunit to the nuclei following HMGB1 treatment, which was blocked following RAGE neutralisation with anti-RAGE antibody, but as HMGB1 signalling is unknown, we may be missing key signalling events. To support these initial results, and fully decipher HMGB1 signalling and synergism with TLR9 signalling, phosphoproteomics was performed to measure kinase activity under different experimental conditions.

Finding: Phosphoproteomic analysis of HMGB1-stimulated CLL samples identified the activation of MAPK substrate groups in the ZAP70+ patient, but RAGE blockade did not neutralise HMGB1 activity

The full HMGB1 and RAGE signalling pathways have not been fully elucidated,[195] so assessment of cell signalling by biased approaches, such as Western blotting may miss important signalling events. We analysed our phosphoproteomic dataset using KSEA, to measure the change of abundance of phosphosites between initial and treated samples, and therefore, infer differences in kinase activity.[310] The results from chapter 5 demonstrate the ZAP70+ patient as more signalling responsive to HMGB1 than the ZAP70- patient. MAPK pathway activity was significantly and rapidly increased following short-term HMGB1 treatment for the ZAP70+ patient. This had ceased by 2 hours, but the increased activity of kinases involved in c-Jun transcription factor activation was sustained. For this patient, blocking membrane bound RAGE with neutralising anti-RAGE antibody had little impact on HMGB1 signalling kinase activity. The signalling activity of the ZAP70- patient reflected the signalling profile responsiveness already established for ZAP70- CLL patients; short-term HMGB1 stimulation yielded no significant results compared to PBS baseline, and 2 hours HMGB1 treatment led to decreased activity of kinases involved in BCR, MAPK and MYC signalling pathways. Surprisingly, when RAGE blockade was performed for this patient, BCR, mTOR, and MYC signalling remained downregulated while the status of MAPK signalling switched to increased kinase activity. These results suggest HMGB1 elicits pro- and anti-tumour effects dependent on the CLL subset.

Finding: HMGB1 and CpG-ODN combined treatment activates and sustains MAPK signalling

TLR9 agonist, CpG-ODN, results in opposing responses in U-CLL and M-CLL subsets, dependent on the expression of ZAP70.[96,273] In autoreactive SLE B-cells, HMGB1 is an essential component of DNA-containing immune complexes that stimulate RAGE internalisation and TLR9 activation.[145,260] After recapitulating RAGE and TLR9 colocalization in response to HMGB1 stimulation alone in CLL cells, as is observed in NLCs,[76] the next step was to investigate a synergistic relationship between HMGB1 and CpG-ODN using an unbiased whole cell signalling phosphoproteomic approach. The results did not reveal activation of signalling pathways unique

to either CpG-ODN, or CpG-ODN combined with HMGB1 in either patient, but we did identify sustained MAPK signalling at the longer timepoint in the ZAP70+ patient when HMGB1 and CpG-ODN was combined, highlighting a pro-tumour role. In the ZAP70- patient, the status of MAPK signalling was variable depending on whether CpG-ODN was combined with HMGB1 and if assessing the short- or long-term timepoint. Taken together, these results confirm previously published data on the outcome of CpG-ODN stimulation in CLL sample with opposing ZAP70 expression status, and suggests the responsiveness of the MAPK signalling pathway to HMGB1 stimulation, appears to depend on the CLL subset. MAPK signalling should be assessed in a larger cohort of patients to confirm these initial findings.

7.1.4 Determine the origin of soluble RAGE in CLL

Finding: Extracellular sRAGE protein mass is shorter than FL-RAGE and es-RAGE, indicating sRAGE derives predominantly from ectodomain shedding

To ascertain why patient plasma sRAGE levels were higher in CLL patients compared to healthy controls, we first assessed which RAGE isoform constitutes the majority of sRAGE. Our data demonstrates that sRAGE is shorter than FL-RAGE and es-RAGE, therefore originating from ectodomain shedding, in line with previous studies.[215,219] This result indicates that smouldering ongoing chronic inflammation driving CLL disease pathogenesis, including high levels of HMGB1, activates RAGE shedding and contributes to sRAGE deregulation in CLL.

Finding: ADAM10 is the protease responsible for RAGE shedding in a transfected HEK293 cell line model

Previous studies have identified ADAM10 as the sole RAGE metalloprotease.[215] Using a transfected HEK293 cell line model, ADAM10 inhibitor and RAGE ectodomain shedding stimulator (ionomycin), the results from chapter 6 confirm ADAM10 as the main RAGE sheddase in a HEK293 cell line model. Once these conditions were established in a RAGE-expressing cell line model, we could further investigate this in primary CLL cells.

Finding: RAGE shedding could be induced with ionomycin and HMGB1 in fresh primary CLL samples

In chapter 4 we observed that patients with higher levels of sRAGE had a longer time to first treatment, and that extracellular sRAGE in CLL originates from ectodomain shedding in chapter 6. Investigating methods to induce RAGE shedding could help us understand why sRAGE levels are higher in CLL compared to healthy controls, and possibly utilise intrinsic mechanisms to

increase levels of sRAGE to confer a protective effect. Although we could not experimentally measure ADAM10 inhibition in CLL samples, our results demonstrate calcium ionophore, ionomycin, and HMGB1 as stimulators of RAGE ectodomain shedding in primary CLL samples *in vitro*. Although this data *in vitro* suggests HMGB1 directly drives RAGE ectodomain shedding, we did not observe a significant correlation (either positive or negative) for these 2 proteins in CLL plasma samples (results from chapter 4). Taken together, while ongoing chronic inflammation in CLL (including increased levels of HMGB1) could drive increased RAGE ectodomain shedding, there is a breakdown in the negative inflammatory feedback loop; plasma sRAGE levels are not fully controlling HMGB1 inflammatory dysregulation established in CLL but does elicit a protective effect. Further investigational work is required to decipher the function and antagonistic potential of sRAGE.

7.2 Limitations of thesis

7.2.1 Clinical constraints

Limited independent TMA patient cohorts: An independent patient TMA cohort to confirm our findings from chapter 3 using our in-house TMAs would have been useful. This would allow us to validate and strengthen our conclusion that high RAGE LN expression has prognostic significance in CLL and support further studies to translate this finding to an easily attainable clinical marker, as IHC is not routinely performed in clinic for CLL diagnosis.

Limited patient clinical data: Detailed patient clinical information, including lymphocyte counts, cytogenetics, CLL-cell immunophenotype, IGHV mutational status, disease progression, treatment regimen and patient outcome would have strengthened our results that show an association with risk factors / disease outcome. Further, this information would have facilitated investigation of our functional results with different subsets and risk factors established in CLL. For example, although plasma HMGB1 and sRAGE levels are independent of ZAP70 expression, our results indicate RAGE LN expression is associated with poor-risk patients and signalling responsiveness to HMGB1 appear to be CLL-subset specific. Expanding our cohort of patients, with pre-selected cytogenetic / IGHV mutational status / prognostic clinical background will enrich this study.

7.2.2 Biological constraints

Selection and preparation of LNs for TMAs and IHC staining: When preparing TMAs, LN tissue is assessed for representative malignant areas following haematoxylin and eosin staining of a

3µm LN cross section. Malignant-rich areas are excised and 1mm^2 cores arrayed in triplicate per patient into a recipient paraffin block to ensure enough of the malignant area is represented. 3µm thick sections are cut and transferred onto glass slides to make a TMA. This does introduce a degree of selection bias; although LN cores are arrayed in triplicate, and are representative of malignant areas, this is performed in a 2D fashion using a LN cross section. Staining of TMAs is performed using consecutive 3µm cuts; this means the LN composition slightly changes with each TMA slide. Consecutive staining is a method to overcome this - slides are stained as per the protocol in chapter 2 with a purple chromogen (Vips) instead of DAB. Once image analysis is performed for the first batch of staining, antibody binding is stripped by performing heat induced antigen retrieval outlined in section 2.3.2. However, when this method was tested in our study, residual antibody remained from the previous batch of staining. Therefore, to reduce large changes in LN composition, consecutive TMA cuts were used and stained for our proteins of interest in this study.

Age of healthy control plasma samples: Unfortunately, we were unable to obtain age-matched controls for our healthy control plasma cohort. Previous work in CLL assessed HMGB1 CLL plasma compared to healthy age matched controls, identifying increased levels in CLL.[76] Therefore expanding our cohort of patients, with age-matched healthy controls for sRAGE plasma levels will strengthen our findings.

Measuring anti-RAGE antibody blockade: To confirm use of neutralising anti-RAGE antibody successfully blocked membrane RAGE activity, it would have been useful to have a RAGE signalling endpoint to measure; but RAGE signalling is not fully deciphered and is cell-type specific. Our phosphoproteomic dataset demonstrates RAGE blockade had little effect on MAPK signalling in the ZAP70+ patient, but we need to confirm if RAGE activity was inhibited, or HMGB1 was utilising another receptor. In our imaging studies, RAGE blockade prevented the colocalization of RAGE and TLR9 assessed by ImageStream but not by fluorescent microscopy. The effect of RAGE blockade on TLR9/MyD88 colocalization and NF-κB nuclear translocation was more prominent at the longer 4 hours timepoint. In combination with out phosphoproteomic data, it appears RAGE and TLR9 colocalization is not a signalling-inducing event, and / or MAPK signalling is activated by a different receptor following HMGB1 stimulation. Therefore, the studies using anti-RAGE blocking antibody were exploratory, and further confirmation with other RAGE and MAPK inhibitors are required to confirm the outcome of RAGE blockade and HMGB1 signalling.

Healthy B-cells as a comparison for signalling studies: CLL B-cell BCR signalling kinetics is subset dependent, leading to proliferation or anergy.[53,70] In our study, we did not assess HMGB1

signalling in B-cells from healthy donors. Anergic responses are observed in a subset of mature B-cells from healthy individuals.[370] Results from our phosphoproteomic dataset suggest opposing signalling responsiveness to HMGB1 for the 2 patients assessed that were ZAP70+ or ZAP70-. Expanding these findings with data from healthy B-cells would be helpful to examine the impact of HMGB1 under homeostatic conditions, and support further studies assessing the impact of HMGB1 blockade/inhibition on healthy B-cells and CLL B-cells.

7.2.3 Statistical constraints

Testing X-tile data cut points: Categorical separation of biomarker expression is a clinically relevant method to define the threshold of a given prognostic marker for disease severity grading. For example, estrogen receptor, progesterone receptor and HER2 expression is scored using IHC in clinical breast cancer grading.[371] There is currently no standardised statistical method to determine optimal data cut points for expression variables that don't have prior defined subsets, but using X-tile helps to identify sub-populations of expression biomarkers rooted with unknown biology which would otherwise be left unnoticed. In this study, we used X-tile as an unbiased approach to determine the optimal data cut points for RAGE and TLR9 LN expression. Although this method splits the data cohort into test and validation sets we did not have an independent TMA patient cohort to test these data cut points and strengthen our finding that high RAGE LN expression had prognostic significance.

Limited power: A larger cohort of patients would greatly improve the statistical power and accuracy of our results, as with many scientific studies. Confirming the IHC and plasma HMGB1 and sRAGE findings in a larger cohort of CLL patients would ensure our results are indicative of the wider CLL population. For functional RAGE shedding and phosphoproteomic studies, where we have used fresh CLL samples, expanding this work with a larger cohort of patients and appropriate healthy controls will build on these initial results and allow solid conclusions to be made. A larger cohort for my studies would also allow investigation of different CLL risk groups.

Selection bias: For the fresh CLL patient sample studies, we were limited to patients who were willing to donate material for research purposes, were treatment and steroid free for 6 months, with a lymphocyte count of greater than 20×10^9/L, and PBMC samples with high CLL B-cell % to perform functional studies with. This does mean we were likely selecting for patients with high CLL-cell numbers in PB, and missing patients with aggressive disease requiring therapy, or patients with indolent disease (as they were below the lymphocyte count set to obtain enough patient material).

7.3 Future work

7.3.1 Clinical / therapeutic future directions

- Confirmation of our CLL LN TMA results with an independent patient cohort:
  Our finding that high RAGE LN expression is associated with shorter overall survival for patients with CLL warrants further investigation in a larger cohort of patients, and in independent data sets, to ensure our results are indicative of the CLL population. Such data would enhance our knowledge of CLL LN biology and aid in design of further inhibitor functional studies for RAGE.

- Investigation to translate our CLL LN TMA results into PB clinical marker:
  Although investigating CLL LN biology is of mechanistic interest to further understand the drivers of CLL-cell survival in proliferation centres, any LN marker that is an indication of disease outcome would not routinely be assessed for every patient at diagnosis. It would be extremely useful if we could translate our findings to an easily attainable PB marker. In this study, we assessed RAGE expression in different cell types by flow cytometry with fresh CLL PBMCs, but this will be difficult to perform with fresh LN samples to compare. Once full TMA analysis has been performed with independent datasets, further investigation of RAGE gene expression will be assessed in matched LN and PB samples. PBMCs and LNs can be lysed and cryostored upon arrival, and gene expression analysis performed with the whole cohort of patients, instead of flow cytometry with fresh samples Moreover, gene expression analysis will allow us to assess the expression of different RAGE isoforms.

- Long-term tracking of HMGB1 and sRAGE plasma levels with patient outcome:
  Our initial results indicate that HMGB1 and sRAGE plasma levels are increased in patients with CLL compared to healthy controls. We assessed sRAGE levels in consecutive CLL patient plasma samples, which demonstrate sRAGE levels to be relatively stable over the course of disease and increased following treatment for the 3 patients that progressed to therapy. Further investigation of HMGB1 and sRAGE samples over the course of disease will allow deeper understanding of the relationship between these 2 markers, and if they are reliable and stable plasma markers that reflect disease progression.

7.3.2 Biological future directions

- Expand our signalling studies with a larger cohort of patients from U-CLL and M-CLL subsets:

We have assessed RAGE and TLR9 colocalization, and HMGB1 signalling in this study. Although we do not know the CLL subsets of the patients assessed in our imaging studies, our phosphoproteomic results in this thesis indicate that HMGB1 signalling may be CLL-subset specific. We cannot make conclusive outcomes from a cohort of 2 patients, so further signalling studies in a larger cohort of patients, and confirmation by western blotting for key signalling mediators, are vital to assess HMGB1 signalling outcomes in CLL B-cells.

- Assess the effect of MAPK and TLR signalling inhibitors on HMGB1 signalling:
  To further tease apart the main signalling mediators in HMGB1 signalling, the next step would be to use specific inhibitors for the pathways of interest. Firstly, we would use TLR9 and TLR inhibitors for HMGB1 alone, CpG-ODN alone, and HMGB1 and CpG-ODN combined treatment conditions to investigate the impact of TLR inhibition on HMGB1-mediated cell signalling and pathway selection. Secondly, our initial results indicate MAPK pathway of importance in HMGB1 signalling. Further investigation of HMGB1 signalling in combination with MAPK inhibitors will highlight if this is a central pathway in HMGB1 signalling in CLL B-cells, and indicate other signalling pathways with increased activity when MAPK is blocked.

- Investigate the effect of different HMGB1 redox states on HMGB1 CLL-cell signalling:
  Complex post-translational modifications regulate the extracellular function of HMGB1, dependent on the mode of cell death, metabolism and HMGB1 biology. The redox status of the 3 cysteine residues is specifically linked to HMGB1 cytokine or chemokine activity.[139] Fully reduced HMGB1 displays chemotactic activity, disulphide HMGB1 has cytokine activity, and fully oxidised HMGB1 has no immunostimulatory activity. We did not assess the difference in redox status on HMGB1 signalling in this study. To directly measure the impact of fully reduced (chemotactic) and disulphide HMGB1 (cytokine) on HMGB1 signalling, these 2 forms are commercially available to investigate *in vitro*. Stimulation and signalling studies using these 2 HMGB1 forms will help define any differences in HMGB1 signalling based on redox status in CLL samples.

- Investigate the antagonistic effect of sRAGE:
  Once full signalling studies have identified the key mediators of HMGB1 signalling, the next step would be to assess the antagonistic effect of sRAGE on CLL-cells. It would be interesting to assess if sRAGE could be a direct competitor for HMGB1 *in vitro* by measuring the activation of key signalling mediators identified in our study; our es-RAGE HEK293 transfection cell line model did not produce a high enough concentration of

sRAGE in conditioned media to inhibit HMGB1, so further work is needed to investigate commercially available sRAGE. On a larger scale, *in vivo* work would be useful in assessing if higher levels of sRAGE contribute to the microenvironmental milieu towards immunogenic cell death, conferring a protective effect.

7.4 Concluding remarks

While the results in this thesis provide strong evidence for the importance of HMGB1 and RAGE expression in CLL microenvironmental disease pathogenesis, further complexity that remains to be addressed is the precise CLL subset-specific roles of HMGB1 and RAGE, and the antagonistic effect of sRAGE in CLL. In a larger context, established prognostic indicators are of great use in clinically defining CLL risk, but for a disease that is a model system for inflammatory-driven cancer progression, there are no established markers to track chronic inflammation or give insight into the proliferative communication occurring in CLL LNs.[82] Within an established prognostic CLL subset, it's not clear how powerful chronic inflammatory dysregulation is in shaping the outcome of CLL disease. As we move forward with targeted treatment options that modulate proliferative signalling pathways, acquired immune deficiency and immune checkpoints,[102] tracking early responses to these therapies with a combination of markers covering many aspects of CLL biology would be helpful, in combination with clinical features and lymphocyte counts.

CLL is a highly diverse and heterogeneous disease, reflected in variations in clinical manifestations, prognostic biomarkers and need and type of therapeutic management. This was observed in our study with highly variable CLL LN TLR9 and RAGE expression, and variable plasma HMGB1 and sRAGE levels among CLL patients. Although CLL cells circulate in peripheral blood, the LN harbours the proliferative CLL fraction in specialised structures called proliferation centres.[46] This niche site is enriched with tumour-associated non-neoplastic cells and encompasses key microenvironment-CLL interactions;[72] i.e. HMGB1-induced differentiation of NLCs and in turn, prolonged CLL survival.[76] CLL LN biology offers great insight into the proliferative fraction of CLL and disease pathogenesis,[47] but owing to the invasiveness of the procedure and LN-tissue handling, CLL LN biopsies are not routinely removed and examined to aid in CLL diagnosis or disease staging. Risk stratification is performed based on clinical features and PB samples, comprised of quiescent CLL cells. The results from this thesis indicate for the first time that RAGE LN expression has prognostic significance in CLL. Although we need to further confirm our results with independent data cohorts, it would be highly useful to translate these findings to a marker that was clinically applicable.

The clinical course of CLL disease is highly variable - some patients do not require treatment for years, if at all, whereas other patients rapidly develop high-risk disease and require treatment immediately.[58] Following diagnosis and collection of extensive clinical information (cytogenetics, prognostic markers, IGHV somatic mutation status), frequent observation / monitoring and disease management algorithms are followed to assess for indicators for therapy.[58] Assessment includes tracking lymphocyte doubling time, disease-related symptoms, or advanced stage Rai / Binet disease.[58] These are effective measures to manage disease, but as treatment options become more targeted, better insight into treatment effectiveness is needed at an earlier stage, along with inflammatory and proliferative markers. Inflammatory PB markers could be useful to track inflammatory dysregulation over the course of CLL disease. In this study, we have assessed HMGB1 and sRAGE plasma levels, which are promising clinical markers for disease progression in autoimmune disease and cancer.[361] Serum levels of sRAGE are easily attainable and powerful circulating disease biomarkers in patients undergoing chemotherapy in advanced pancreatic cancer.[228,229] Although HMGB1 and sRAGE plasma markers measured here are not linked to the effectiveness of a specific treatment, our initial results comparing plasma levels to available clinical information, combined with studies in other disease settings,[361] indicate these plasma markers as promising circulating inflammatory biomarkers. Further investigation is required in CLL with detailed clinical data and downstream functional studies.

A powerful gene expression analysis of matched CLL cells from peripheral blood, bone marrow and lymph nodes identified enhanced activation of BCR-associated signalling pathways and NF-κB activation in CLL lymph nodes; this was significantly higher in U-CLL.[47] BCR signalling is a central pathway in CLL B-cell proliferation, knowledge of which has translated into therapy options for the treatment of CLL.[88,115] The outcome of BCR signalling is heterogeneous in CLL; antigen engagement results in B-cell activation/proliferation, or anergy.[70] Moreover, the response to TLR9 agonists in CLL is dependent on the expression of ZAP70.[96,273] Although HMGB1 plasma levels are ZAP70 expression independent, our initial phosphoproteomic results indicate the signalling response to HMGB1 could be CLL subset-specific in the 2 patients we investigated. This requires further investigation with a larger cohort of ZAP70+ / ZAP70- patients. HMGB1 has a demonstrated role in smouldering chronic tumour-associated inflammation, and immunogenic malignant-cell death in cancer pathogenesis.[151] The overall molecular and cellular components of the tumour microenvironment will largely decide the polarisation of the HMGB1 response in tumour-associated inflammation; but on a molecular lever, further investigation is required to assess if HMGB1 signalling is truly dichotic in ZAP70+ and ZAP70- CLL-cell samples.

In summary, CLL is still an incurable disease and relapse is common for high-risk patients. Current targeted therapies lead to high overall response rates but complete responses are not

common.[115] A deeper understanding of molecular mechanisms contributing to disease pathogenesis, particularly microenvironmental interactions occurring in the LN, will aid in the development of new therapeutic agents and better risk stratification for patients with CLL. In combination with HMGB1-driven differentiation of NLCs, the results in this thesis support a direct role for HMGB1 in CLL B-cells. Further insight into this signalling pathway in different CLL risk groups, and overall microenvironment interactions, will support further HMGB1 / RAGE functional and intervention studies.

References

1 Medzhitov, R. Origin and physiological roles of inflammation. *Nature* **454**, 428-435, doi:10.1038/nature07201 (2008).

2 Majno, G. The Healing Hand - Man and wound in the ancient world. *Cambridge, MA: Harvard University Press* (1975).

3 Medzhitov, R. Inflammation 2010: new adventures of an old flame. *Cell* **140**, 771-776, doi:10.1016/j.cell.2010.03.006 (2010).

4 Nathan, C. Points of control in inflammation. *Nature* **420**, 846-852, doi:10.1038/nature01320 (2002).

5 Takeda, K. & Akira, S. Toll-like receptors in innate immunity. *International immunology* **17**, 1-14, doi:10.1093/intimm/dxh186 (2005).

6 Tauber, A. I. Metchnikoff and the phagocytosis theory. *Nature reviews. Molecular cell biology* **4**, 897-901, doi:10.1038/nrm1244 (2003).

7 Nathan, C. Neutrophils and immunity: challenges and opportunities. *Nat Rev Immunol* **6**, 173-182, doi:10.1038/nri1785 (2006).

8 Murray, P. J. & Wynn, T. A. Protective and pathogenic functions of macrophage subsets. *Nat Rev Immunol* **11**, 723-737 (2011).

9 Bianchi, M. E. DAMPs, PAMPs and alarmins: all we need to know about danger. *J Leukoc Biol* **81**, 1-5, doi:10.1189/jlb.0306164 (2007).

10 Hanahan, D. & Weinberg, R. A. Hallmarks of cancer: the next generation. *Cell* **144**, 646-674, doi:10.1016/j.cell.2011.02.013 (2011).

11 Balkwill, F. R. & Mantovani, A. Cancer-related inflammation: common themes and therapeutic opportunities. *Seminars in cancer biology* **22**, 33-40, doi:10.1016/j.semcancer.2011.12.005 (2012).

12 Mantovani, A., Allavena, P., Sica, A. & Balkwill, F. Cancer-related inflammation. *Nature* **454**, 436-444, doi:10.1038/nature07205 (2008).

13 Burger, J. A. & Gribben, J. G. The microenvironment in chronic lymphocytic leukemia (CLL) and other B cell malignancies: Insight into disease biology and new targeted therapies. *Semin Cancer Biol*, doi:S1044-579X(13)00087-4 [pii]

10.1016/j.semcancer.2013.08.011 (2013).

14 Bachireddy, P., Burkhardt, U. E., Rajasagi, M. & Wu, C. J. Haematological malignancies: at the forefront of immunotherapeutic innovation. *Nat Rev Cancer*, doi:10.1038/nrc3907 (2015).

15 Chen, W. *et al.* Conversion of peripheral CD4+CD25- naive T cells to CD4+CD25+ regulatory T cells by TGF-beta induction of transcription factor Foxp3. *J Exp Med* **198**, 1875-1886, doi:10.1084/jem.20030152 (2003).

16 Balkwill, F. & Mantovani, A. Inflammation and cancer: back to Virchow? *Lancet* **357**, 539-545, doi:10.1016/S0140-6736(00)04046-0 (2001).

17 Balkwill, F., Charles, K. A. & Mantovani, A. Smoldering and polarized inflammation in the initiation and promotion of malignant disease. *Cancer Cell* **7**, 211-217, doi:10.1016/j.ccr.2005.02.013 (2005).

18 Rous, P. & Kidd, J. G. CONDITIONAL NEOPLASMS AND SUBTHRESHOLD NEOPLASTIC STATES : A STUDY OF THE TAR TUMORS OF RABBITS. *J Exp Med* **73**, 365-390 (1941).

19 Borrello, M. G. *et al.* Induction of a proinflammatory program in normal human thyrocytes by the RET/PTC1 oncogene. *Proc Natl Acad Sci U S A* **102**, 14825-14830, doi:10.1073/pnas.0503039102 (2005).

20 Fan, Y., Mao, R. & Yang, J. NF-kappaB and STAT3 signaling pathways collaboratively link inflammation to cancer. *Protein & cell* **4**, 176-185, doi:10.1007/s13238-013-2084-3 (2013).

21 Aggarwal, B. B., Vijayalekshmi, R. V. & Sung, B. Targeting inflammatory pathways for prevention and therapy of cancer: short-term friend, long-term foe. *Clinical cancer*

research : an official journal of the American Association for Cancer Research **15**, 425-430, doi:10.1158/1078-0432.ccr-08-0149 (2009).

22 Coussens, L. M. & Werb, Z. Inflammation and cancer. *Nature* **420**, 860-867, doi:10.1038/nature01322 (2002).

23 Yoshida, T. *et al.* Activation of STAT3 by the Hepatitis C Virus Core Protein Leads to Cellular Transformation. *J Exp Med* **196**, 641-653, doi:10.1084/jem.20012127 (2002).

24 Takahashi, H., Ogata, H., Nishigaki, R., Broide, D. H. & Karin, M. Tobacco smoke promotes lung tumorigenesis by triggering IKKbeta- and JNK1-dependent inflammation. *Cancer Cell* **17**, 89-97, doi:10.1016/j.ccr.2009.12.008 (2010).

25 Dvorak, H. F. Tumors: wounds that do not heal. Similarities between tumor stroma generation and wound healing. *N Engl J Med* **315**, 1650-1659, doi:10.1056/NEJM198612253152606 (1986).

26 Mantovani, A., Sozzani, S., Locati, M., Allavena, P. & Sica, A. Macrophage polarization: tumor-associated macrophages as a paradigm for polarized M2 mononuclear phagocytes. *Trends Immunol* **23**, 549-555 (2002).

27 Schafer, M. & Werner, S. Cancer as an overhealing wound: an old hypothesis revisited. *Nature reviews. Molecular cell biology* **9**, 628-638, doi:10.1038/nrm2455 (2008).

28 Vakkila, J. & Lotze, M. T. Inflammation and necrosis promote tumour growth. *Nat Rev Immunol* **4**, 641-648, doi:10.1038/nri1415 (2004).

29 Grivennikov, S. I., Greten, F. R. & Karin, M. Immunity, inflammation, and cancer. *Cell* **140**, 883-899, doi:10.1016/j.cell.2010.01.025 (2010).

30 Diakos, C. I., Charles, K. A., McMillan, D. C. & Clarke, S. J. Cancer-related inflammation and treatment effectiveness. *The Lancet. Oncology* **15**, e493-503, doi:10.1016/s1470-2045(14)70263-3 (2014).

31 DuPage, M., Mazumdar, C., Schmidt, L. M., Cheung, A. F. & Jacks, T. Expression of tumour-specific antigens underlies cancer immunoediting. *Nature* **482**, 405-409, doi:10.1038/nature10803 (2012).

32 Matsushita, H. *et al.* Cancer exome analysis reveals a T-cell-dependent mechanism of cancer immunoediting. *Nature* **482**, 400-404, doi:10.1038/nature10755 (2012).

33 Laurence, A., Belkaid, Y. & O'Shea, J. J. A degrading view of regulatory T cells. *Immunity* **39**, 201-203, doi:10.1016/j.immuni.2013.08.017 (2013).

34 Coussens, L. M., Zitvogel, L. & Palucka, A. K. Neutralizing tumor-promoting chronic inflammation: a magic bullet? *Science* **339**, 286-291, doi:10.1126/science.1232227 (2013).

35 Hallek, M. *et al.* Guidelines for the diagnosis and treatment of chronic lymphocytic leukemia: a report from the International Workshop on Chronic Lymphocytic Leukemia updating the National Cancer Institute-Working Group 1996 guidelines. *Blood* **111**, 5446-5456, doi:10.1182/blood-2007-06-093906 (2008).

36 Williams, C. S., Mann, M. & DuBois, R. N. The role of cyclooxygenases in inflammation, cancer, and development. *Oncogene* **18**, 7908-7916, doi:10.1038/sj.onc.1203286 (1999).

37 Reddy, B. S. *et al.* Chemoprevention of colon cancer by specific cyclooxygenase-2 inhibitor, celecoxib, administered during different stages of carcinogenesis. *Cancer research* **60**, 293-297 (2000).

38 Thun, M. J., Namboodiri, M. M., Calle, E. E., Flanders, W. D. & Heath, C. W., Jr. Aspirin use and risk of fatal cancer. *Cancer research* **53**, 1322-1327 (1993).

39 Anglesio, M. S. *et al.* IL6-STAT3-HIF Signaling and Therapeutic Response to the Angiogenesis Inhibitor Sunitinib in Ovarian Clear Cell Cancer. *Clinical Cancer Research* **17**, 2538-2548, doi:10.1158/1078-0432.ccr-10-3314 (2011).

40 Qian, B. Z. *et al.* CCL2 recruits inflammatory monocytes to facilitate breast-tumour metastasis. *Nature* **475**, 222-225, doi:10.1038/nature10138 (2011).

41 Konstantinopoulos, P. A. & Papavassiliou, A. G. Seeing the future of cancer-associated transcription factor drug targets. *Jama* **305**, 2349-2350, doi:10.1001/jama.2011.727 (2011).

42 Buchert, M., Burns, C. J. & Ernst, M. Targeting JAK kinase in solid tumors: emerging opportunities and challenges. *Oncogene* **35**, 939-951, doi:10.1038/onc.2015.150 (2016).

43 Hallek, M. *et al.* Addition of rituximab to fludarabine and cyclophosphamide in patients with chronic lymphocytic leukaemia: a randomised, open-label, phase 3 trial. *Lancet* **376**, 1164-1174, doi:10.1016/s0140-6736(10)61381-5 (2010).

44 Poole, R. M. Pembrolizumab: first global approval. *Drugs* **74**, 1973-1981, doi:10.1007/s40265-014-0314-5 (2014).

45 Ding, W. *et al.* Pembrolizumab in patients with chronic lymphocytic leukemia with Richter's transformation and relapsed CLL. *Blood*, doi:10.1182/blood-2017-02-765685 (2017).

46 Burger, J. A. Targeting the microenvironment in chronic lymphocytic leukemia is changing the therapeutic landscape. *Curr Opin Oncol* **24**, 643-649, doi:10.1097/CCO.0b013e3283589950 (2012).

47 Herishanu, Y. *et al.* The lymph node microenvironment promotes B-cell receptor signaling, NF-kappaB activation, and tumor proliferation in chronic lymphocytic leukemia. *Blood* **117**, 563-574, doi:10.1182/blood-2010-05-284984 (2011).

48 Chen, L. S., Balakrishnan, K. & Gandhi, V. Inflammation and survival pathways: chronic lymphocytic leukemia as a model system. *Biochemical pharmacology* **80**, 1936-1945, doi:10.1016/j.bcp.2010.07.039 (2010).

49 Fabbri, G. & Dalla-Favera, R. The molecular pathogenesis of chronic lymphocytic leukaemia. *Nature reviews. Cancer* **16**, 145-162, doi:10.1038/nrc.2016.8 (2016).

50 Hamblin, T. J., Davis, Z., Gardiner, A., Oscier, D. G. & Stevenson, F. K. Unmutated Ig V(H) genes are associated with a more aggressive form of chronic lymphocytic leukemia. *Blood* **94**, 1848-1854 (1999).

51 Damle, R. N. *et al.* Ig V gene mutation status and CD38 expression as novel prognostic indicators in chronic lymphocytic leukemia. *Blood* **94**, 1840-1847 (1999).

52 Chiorazzi, N. & Ferrarini, M. Cellular origin(s) of chronic lymphocytic leukemia: cautionary notes and additional considerations and possibilities. *Blood* **117**, 1781-1791, doi:10.1182/blood-2010-07-155663 (2011).

53 Packham, G. *et al.* The outcome of B-cell receptor signaling in chronic lymphocytic leukemia: proliferation or anergy. *Haematologica* **99**, 1138-1148, doi:10.3324/haematol.2013.098384 (2014).

54 Kipps, T. J. *et al.* Developmentally restricted immunoglobulin heavy chain variable region gene expressed at high frequency in chronic lymphocytic leukemia. *Proc Natl Acad Sci U S A* **86**, 5913-5917 (1989).

55 Fais, F. *et al.* Chronic lymphocytic leukemia B cells express restricted sets of mutated and unmutated antigen receptors. *Journal of Clinical Investigation* **102**, 1515-1525 (1998).

56 Agathangelidis, A. *et al.* Stereotyped B-cell receptors in one-third of chronic lymphocytic leukemia: a molecular classification with implications for targeted therapies. *Blood* **119**, 4467-4475, doi:10.1182/blood-2011-11-393694 (2012).

57 Widhopf, G. F., 2nd *et al.* Chronic lymphocytic leukemia B cells of more than 1% of patients express virtually identical immunoglobulins. *Blood* **104**, 2499-2504, doi:10.1182/blood-2004-03-0818 (2004).

58 Kipps, T. J. *et al.* Chronic lymphocytic leukaemia. *Nature reviews. Disease primers* **3**, 16096, doi:10.1038/nrdp.2016.96 (2017).

59 Dohner, H. *et al.* Genomic aberrations and survival in chronic lymphocytic leukemia. *N Engl J Med* **343**, 1910-1916, doi:10.1056/nejm200012283432602 (2000).

60 Klein, U. *et al.* The DLEU2/miR-15a/16-1 cluster controls B cell proliferation and its deletion leads to chronic lymphocytic leukemia. *Cancer Cell* **17**, 28-40, doi:10.1016/j.ccr.2009.11.019 (2010).
61 Pleasance, E. D. *et al.* A comprehensive catalogue of somatic mutations from a human cancer genome. *Nature* **463**, 191-196, doi:10.1038/nature08658 (2010).
62 Fabbri, G. *et al.* Analysis of the chronic lymphocytic leukemia coding genome: role of NOTCH1 mutational activation. *J Exp Med* **208**, 1389-1401, doi:10.1084/jem.20110921 (2011).
63 Puente, X. S. *et al.* Whole-genome sequencing identifies recurrent mutations in chronic lymphocytic leukaemia. *Nature* **475**, 101-105, doi:10.1038/nature10113 (2011).
64 Landau, D. A. *et al.* Mutations driving CLL and their evolution in progression and relapse. *Nature* **526**, 525-530, doi:10.1038/nature15395

http://www.nature.com/nature/journal/v526/n7574/abs/nature15395.html#supplementary-information (2015).
65 Damm, F. *et al.* Acquired initiating mutations in early hematopoietic cells of CLL patients. *Cancer discovery* **4**, 1088-1101, doi:10.1158/2159-8290.cd-14-0104 (2014).
66 Puente, X. S. *et al.* Non-coding recurrent mutations in chronic lymphocytic leukaemia. *Nature* **526**, 519-524, doi:10.1038/nature14666

http://www.nature.com/nature/journal/v526/n7574/abs/nature14666.html#supplementary-information (2015).
67 Calin, G. A. *et al.* Frequent deletions and down-regulation of micro- RNA genes miR15 and miR16 at 13q14 in chronic lymphocytic leukemia. *Proc Natl Acad Sci U S A* **99**, 15524-15529, doi:10.1073/pnas.242606799 (2002).
68 Kulis, M. *et al.* Epigenomic analysis detects widespread gene-body DNA hypomethylation in chronic lymphocytic leukemia. *Nat Genet* **44**, 1236-1242, doi:10.1038/ng.2443 (2012).
69 Stevenson, F. K., Krysov, S., Davies, A. J., Steele, A. J. & Packham, G. B-cell receptor signaling in chronic lymphocytic leukemia. *Blood* **118**, 4313-4320, doi:10.1182/blood-2011-06-338855 (2011).
70 Mockridge, C. I. *et al.* Reversible anergy of sIgM-mediated signaling in the two subsets of CLL defined by VH-gene mutational status. *Blood* **109**, 4424-4431, doi:10.1182/blood-2006-11-056648 (2007).
71 Duhren-von Minden, M. *et al.* Chronic lymphocytic leukaemia is driven by antigen-independent cell-autonomous signalling. *Nature* **489**, 309-312, doi:10.1038/nature11309 (2012).
72 Ten Hacken, E. & Burger, J. A. Microenvironment interactions and B-cell receptor signaling in Chronic Lymphocytic Leukemia: Implications for disease pathogenesis and treatment. *Biochim Biophys Acta* **1863**, 401-413, doi:10.1016/j.bbamcr.2015.07.009 (2016).
73 Shain, K. H. & Tao, J. The B-cell receptor orchestrates environment-mediated lymphoma survival and drug resistance in B-cell malignancies. *Oncogene* **33**, 4107-4113, doi:10.1038/onc.2013.379 (2014).
74 Endo, T. *et al.* BAFF and APRIL support chronic lymphocytic leukemia B-cell survival through activation of the canonical NF-kappaB pathway. *Blood* **109**, 703-710, doi:10.1182/blood-2006-06-027755 (2007).
75 O'Hayre, M. *et al.* Elucidating the CXCL12/CXCR4 signaling network in chronic lymphocytic leukemia through phosphoproteomics analysis. *PLoS One* **5**, e11716, doi:10.1371/journal.pone.0011716 (2010).
76 Jia, L. *et al.* Extracellular HMGB1 promotes differentiation of nurse-like cells in chronic lymphocytic leukemia. *Blood* **123**, 1709-1719, doi:10.1182/blood-2013-10-529610 (2014).

77 Aguilar-Hernandez, M. M. *et al.* IL-4 enhances expression and function of surface IgM in CLL cells. *Blood*, doi:10.1182/blood-2015-11-682906 (2016).

78 McClanahan, F. *et al.* PD-L1 checkpoint blockade prevents immune dysfunction and leukemia development in a mouse model of chronic lymphocytic leukemia. *Blood* **126**, 203-211, doi:10.1182/blood-2015-01-622936 (2015).

79 Yu, J. *et al.* Wnt5a induces ROR1/ROR2 heterooligomerization to enhance leukemia chemotaxis and proliferation. *The Journal of clinical investigation* **126**, 585-598, doi:10.1172/jci83535 (2016).

80 Seke Etet, P. F., Vecchio, L. & Nwabo Kamdje, A. H. Interactions between bone marrow stromal microenvironment and B-chronic lymphocytic leukemia cells: any role for Notch, Wnt and Hh signaling pathways? *Cellular signalling* **24**, 1433-1443, doi:10.1016/j.cellsig.2012.03.008 (2012).

81 Burger, J. A., Burger, M. & Kipps, T. J. Chronic lymphocytic leukemia B cells express functional CXCR4 chemokine receptors that mediate spontaneous migration beneath bone marrow stromal cells. *Blood* **94**, 3658-3667 (1999).

82 Rozovski, U., Keating, M. J. & Estrov, Z. Targeting inflammatory pathways in chronic lymphocytic leukemia. *Critical reviews in oncology/hematology* **88**, 655-666, doi:10.1016/j.critrevonc.2013.07.011 (2013).

83 Delgado, J. & Villamor, N. Chronic lymphocytic leukemia in young individuals revisited. *Haematologica* **99**, 4-5, doi:10.3324/haematol.2013.096297 (2014).

84 Rai, K. R. *et al.* Clinical staging of chronic lymphocytic leukemia. *Blood* **46**, 219-234 (1975).

85 Binet, J. L. *et al.* A clinical staging system for chronic lymphocytic leukemia: prognostic significance. *Cancer* **40**, 855-864 (1977).

86 Pflug, N. *et al.* Development of a comprehensive prognostic index for patients with chronic lymphocytic leukemia. *Blood* **124**, 49-62, doi:10.1182/blood-2014-02-556399 (2014).

87 Rossi, D. *et al.* Integrated mutational and cytogenetic analysis identifies new prognostic subgroups in chronic lymphocytic leukemia. *Blood* **121**, 1403-1412, doi:10.1182/blood-2012-09-458265 (2013).

88 Nabhan, C. & Rosen, S. T. Chronic lymphocytic leukemia: a clinical review. *Jama* **312**, 2265-2276, doi:10.1001/jama.2014.14553 (2014).

89 Hallek, M. *et al.* Serum beta(2)-microglobulin and serum thymidine kinase are independent predictors of progression-free survival in chronic lymphocytic leukemia and immunocytoma. *Leukemia & lymphoma* **22**, 439-447, doi:10.3109/10428199609054782 (1996).

90 Thompson, P. A. *et al.* Complex karyotype is a stronger predictor than del(17p) for an inferior outcome in relapsed or refractory chronic lymphocytic leukemia patients treated with ibrutinib-based regimens. *Cancer* **121**, 3612-3621, doi:10.1002/cncr.29566 (2015).

91 Gaidano, G., Foa, R. & Dalla-Favera, R. Molecular pathogenesis of chronic lymphocytic leukemia. *The Journal of clinical investigation* **122**, 3432-3438, doi:10.1172/jci64101 (2012).

92 Wiestner, A. *et al.* ZAP-70 expression identifies a chronic lymphocytic leukemia subtype with unmutated immunoglobulin genes, inferior clinical outcome, and distinct gene expression profile. *Blood* **101**, 4944-4951, doi:10.1182/blood-2002-10-3306 (2003).

93 Pede, V. R., A; Verhasselt, B; Philippe J. The Biological Relevance of ZAP-70 in CLL. *www.intechopen.com* (2012).

94 Penna, D. *et al.* Degradation of ZAP-70 Following Antigenic Stimulation in Human T Lymphocytes: Role of Calpain Proteolytic Pathway. *The Journal of Immunology* **163**, 50-56 (1999).

95 Gobessi, S. *et al.* ZAP-70 enhances B-cell-receptor signaling despite absent or inefficient tyrosine kinase activation in chronic lymphocytic leukemia and lymphoma B cells. *Blood* **109**, 2032-2039, doi:10.1182/blood-2006-03-011759 (2007).

96 Wagner, M. *et al.* Integration of innate- into adaptive- immune responses in ZAP-70 positive chronic lymphocytic leukaemia. *Blood*, doi:10.1182/blood-2015-05-646935 (2015).

97 Goede, V. *et al.* Obinutuzumab plus chlorambucil in patients with CLL and coexisting conditions. *N Engl J Med* **370**, 1101-1110, doi:10.1056/NEJMoa1313984 (2014).

98 Hillmen, P. *et al.* Chlorambucil plus ofatumumab versus chlorambucil alone in previously untreated patients with chronic lymphocytic leukaemia (COMPLEMENT 1): a randomised, multicentre, open-label phase 3 trial. *Lancet* **385**, 1873-1883, doi:10.1016/s0140-6736(15)60027-7 (2015).

99 Gentile, M. *et al.* Combination of bendamustine and rituximab as front-line therapy for patients with chronic lymphocytic leukaemia: multicenter, retrospective clinical practice experience with 279 cases outside of controlled clinical trials. *European journal of cancer (Oxford, England : 1990)* **60**, 154-165, doi:10.1016/j.ejca.2016.03.069 (2016).

100 Thompson, P. A. *et al.* Fludarabine, cyclophosphamide, and rituximab treatment achieves long-term disease-free survival in IGHV-mutated chronic lymphocytic leukemia. *Blood* **127**, 303-309, doi:10.1182/blood-2015-09-667675 (2016).

101 Rossi, D. *et al.* Molecular prediction of durable remission after first-line fludarabine-cyclophosphamide-rituximab in chronic lymphocytic leukemia. *Blood* **126**, 1921-1924, doi:10.1182/blood-2015-05-647925 (2015).

102 Cuneo, A. *et al.* Modern treatment in chronic lymphocytic leukemia: impact on survival and efficacy in high-risk subgroups. *Cancer Med* **3**, 555-564, doi:10.1002/cam4.226 (2014).

103 Jain, N. & O'Brien, S. Targeted therapies for CLL: Practical issues with the changing treatment paradigm. *Blood reviews*, doi:10.1016/j.blre.2015.12.002 (2015).

104 Byrd, J. C. *et al.* Ibrutinib versus ofatumumab in previously treated chronic lymphoid leukemia. *N Engl J Med* **371**, 213-223, doi:10.1056/NEJMoa1400376 (2014).

105 Burger, J. A. *et al.* Ibrutinib as Initial Therapy for Patients with Chronic Lymphocytic Leukemia. *N Engl J Med* **373**, 2425-2437, doi:10.1056/NEJMoa1509388 (2015).

106 Furman, R. R. *et al.* Idelalisib and rituximab in relapsed chronic lymphocytic leukemia. *N Engl J Med* **370**, 997-1007, doi:10.1056/NEJMoa1315226 (2014).

107 Roberts, A. W. *et al.* Targeting BCL2 with Venetoclax in Relapsed Chronic Lymphocytic Leukemia. *N Engl J Med* **374**, 311-322, doi:10.1056/NEJMoa1513257 (2016).

108 Cervantes-Gomez, F. *et al.* Pharmacological and Protein Profiling Suggests Venetoclax (ABT-199) as Optimal Partner with Ibrutinib in Chronic Lymphocytic Leukemia. *Clinical cancer research : an official journal of the American Association for Cancer Research* **21**, 3705-3715, doi:10.1158/1078-0432.ccr-14-2809 (2015).

109 Thijssen, R. *et al.* Resistance to ABT-199 induced by microenvironmental signals in chronic lymphocytic leukemia can be counteracted by CD20 antibodies or kinase inhibitors. *Haematologica* **100**, e302-306, doi:10.3324/haematol.2015.124560 (2015).

110 Sharma, P. & Allison, J. P. The future of immune checkpoint therapy. *Science* **348**, 56-61, doi:10.1126/science.aaa8172 (2015).

111 Khouri, I. F. *et al.* Nonmyeloablative allogeneic stem cell transplantation in relapsed/refractory chronic lymphocytic leukemia: long-term follow-up, prognostic factors, and effect of human leukocyte histocompatibility antigen subtype on outcome. *Cancer* **117**, 4679-4688, doi:10.1002/cncr.26091 (2011).

112 Porter, D. L. *et al.* Chimeric antigen receptor T cells persist and induce sustained remissions in relapsed refractory chronic lymphocytic leukemia. *Science translational medicine* **7**, 303ra139, doi:10.1126/scitranslmed.aac5415 (2015).

113 Fraietta, J. A. *et al.* Ibrutinib enhances chimeric antigen receptor T-cell engraftment and efficacy in leukemia. *Blood* **127**, 1117-1127, doi:10.1182/blood-2015-11-679134 (2016).

114 Tsiodras, S., Samonis, G., Keating, M. J. & Kontoyiannis, D. P. Infection and Immunity in Chronic Lymphocytic Leukemia. *Mayo Clinic Proceedings* **75**, 1039-1054, doi:http://dx.doi.org/10.4065/75.10.1039 (2000).

115 Jain, N. & O'Brien, S. *Initial treatment of CLL: integrating biology and functional status*. Vol. 126 (2015).

116 Tang, D., Kang, R., Zeh, H. J. & Lotze, M. T. High-mobility group box 1 and cancer. *Biochim Biophys Acta* **1799**, 131-140, doi:10.1016/j.bbagrm.2009.11.014 (2010).

117 Laudet, V., Stehelin, D. & Clevers, H. Ancestry and diversity of the HMG box superfamily. *Nucleic Acids Res* **21**, 2493-2501 (1993).

118 Bustin, M., Hopkins, R. B. & Isenberg, I. Immunological relatedness of high mobility group chromosomal proteins from calf thymus. *The Journal of biological chemistry* **253**, 1694-1699 (1978).

119 Calogero, S. *et al.* The lack of chromosomal protein Hmg1 does not disrupt cell growth but causes lethal hypoglycaemia in newborn mice. *Nat Genet* **22**, 276-280, doi:10.1038/10338 (1999).

120 Wang, H. *et al.* HMG-1 as a late mediator of endotoxin lethality in mice. *Science* **285**, 248-251 (1999).

121 Tang, D. *et al.* HMGB1 release and redox regulates autophagy and apoptosis in cancer cells. *Oncogene* **29**, 5299-5310, doi:10.1038/onc.2010.261 (2010).

122 Schiraldi, M. *et al.* HMGB1 promotes recruitment of inflammatory cells to damaged tissues by forming a complex with CXCL12 and signaling via CXCR4. *J Exp Med* **209**, 551-563, doi:10.1084/jem.20111739 (2012).

123 Sims, G., Rowe, D., Rietdijk, S., Herbst, R. & Coyle, A. HMGB1 and RAGE in inflammation and cancer. *Annu Rev Immunol* **28**, 367-388, doi:10.1146/annurev.immunol.021908.132603 (2010).

124 Pil, P. M., Chow, C. S. & Lippard, S. J. High-mobility-group 1 protein mediates DNA bending as determined by ring closures. *Proceedings of the National Academy of Sciences of the United States of America* **90**, 9465-9469 (1993).

125 Ura, K., Nightingale, K. & Wolffe, A. P. Differential association of HMG1 and linker histones B4 and H1 with dinucleosomal DNA: structural transitions and transcriptional repression. *The EMBO Journal* **15**, 4959-4969 (1996).

126 Dumitriu, I. E., Baruah, P., Manfredi, A. A., Bianchi, M. E. & Rovere-Querini, P. HMGB1: guiding immunity from within. *Trends in Immunology* **26**, 381-387, doi:http://dx.doi.org/10.1016/j.it.2005.04.009 (2005).

127 Bonaldi, T. *et al.* Monocytic cells hyperacetylate chromatin protein HMGB1 to redirect it towards secretion. *The EMBO Journal* **22**, 5551-5560, doi:10.1093/emboj/cdg516 (2003).

128 Pilzweger, C. & Holdenrieder, S. Circulating HMGB1 and RAGE as Clinical Biomarkers in Malignant and Autoimmune Diseases. *Diagnostics* **5**, 219 (2015).

129 Krysko, D. V. *et al.* Immunogenic cell death and DAMPs in cancer therapy. *Nat Rev Cancer* **12**, 860-875, doi:10.1038/nrc3380

nrc3380 [pii] (2012).

130 Yang, H. *et al.* Reversing established sepsis with antagonists of endogenous high-mobility group box 1. *Proc Natl Acad Sci U S A* **101**, 296-301, doi:10.1073/pnas.2434651100 (2004).

131 Li, G., Liang, X. & Lotze, M. T. HMGB1: The Central Cytokine for All Lymphoid Cells. *Frontiers in immunology* **4**, 68, doi:10.3389/fimmu.2013.00068 (2013).

132 Rovere-Querini, P. *et al.* HMGB1 is an endogenous immune adjuvant released by necrotic cells. *EMBO Rep* **5**, 825-830, doi:10.1038/sj.embor.7400205 (2004).

133 Zhao, T. *et al.* Rituximab-induced HMGB1 release is associated with inhibition of STAT3 activity in human diffuse large B-cell lymphoma. *Oncotarget* **6**, 27816-27831, doi:10.18632/oncotarget.4816 (2015).

134 Scaffidi, P., Misteli, T. & Bianchi, M. E. Release of chromatin protein HMGB1 by necrotic cells triggers inflammation. *Nature* **418**, 191-195, doi:10.1038/nature00858 (2002).

135 Yamada, Y. *et al.* The release of high mobility group box 1 in apoptosis is triggered by nucleosomal DNA fragmentation. *Archives of biochemistry and biophysics* **506**, 188-193, doi:10.1016/j.abb.2010.11.011 (2011).

136 Gauley, J. & Pisetsky, D. S. The translocation of HMGB1 during cell activation and cell death. *Autoimmunity* **42**, 299-301 (2009).

137 Stros, M. HMGB proteins: interactions with DNA and chromatin. *Biochim Biophys Acta* **1799**, 101-113, doi:10.1016/j.bbagrm.2009.09.008 (2010).

138 Gardella, S. *et al.* The nuclear protein HMGB1 is secreted by monocytes via a non-classical, vesicle-mediated secretory pathway. *EMBO Rep* **3**, 995-1001, doi:10.1093/embo-reports/kvf198 (2002).

139 Venereau, E. *et al.* Mutually exclusive redox forms of HMGB1 promote cell recruitment or proinflammatory cytokine release. *J Exp Med* **209**, 1519-1528, doi:10.1084/jem.20120189 (2012).

140 Yang, H. *et al.* A critical cysteine is required for HMGB1 binding to Toll-like receptor 4 and activation of macrophage cytokine release. *Proc Natl Acad Sci U S A* **107**, 11942-11947, doi:10.1073/pnas.1003893107 (2010).

141 Yang, H. *et al.* Redox modification of cysteine residues regulates the cytokine activity of high mobility group box-1 (HMGB1). *Molecular medicine (Cambridge, Mass.)* **18**, 250-259, doi:10.2119/molmed.2011.00389 (2012).

142 Antoine, D. J., Williams, D. P., Kipar, A., Laverty, H. & Park, B. K. Diet restriction inhibits apoptosis and HMGB1 oxidation and promotes inflammatory cell recruitment during acetaminophen hepatotoxicity. *Molecular medicine (Cambridge, Mass.)* **16**, 479-490, doi:10.2119/molmed.2010.00126 (2010).

143 Musumeci, D., Roviello, G. N. & Montesarchio, D. An overview on HMGB1 inhibitors as potential therapeutic agents in HMGB1-related pathologies. *Pharmacology & therapeutics* **141**, 347-357, doi:10.1016/j.pharmthera.2013.11.001 (2014).

144 Avalos, A. M. *et al.* RAGE-independent autoreactive B cell activation in response to chromatin and HMGB1/DNA immune complexes. *Autoimmunity* **43**, 103-110, doi:10.3109/08916930903384591 (2010).

145 Tian, J. *et al.* Toll-like receptor 9-dependent activation by DNA-containing immune complexes is mediated by HMGB1 and RAGE. *Nat Immunol* **8**, 487-496, doi:10.1038/ni1457 (2007).

146 Yanai, H., Ban, T. & Taniguchi, T. High-mobility group box family of proteins: ligand and sensor for innate immunity. *Trends in Immunology* **33**, 633-640, doi:10.1016/j.it.2012.10.005.

147 Lotze, M. T. & Tracey, K. J. High-mobility group box 1 protein (HMGB1): nuclear weapon in the immune arsenal. *Nat Rev Immunol* **5**, 331-342, doi:10.1038/nri1594 (2005).

148 Wang, C. *et al.* HMGB1 was a pivotal synergistic effecor for CpG oligonucleotide to enhance the progression of human lung cancer cells. *Cancer biology & therapy* **13**, 727-736, doi:10.4161/cbt.20555 (2012).

149 Ivanov, S. *et al.* A novel role for HMGB1 in TLR9-mediated inflammatory responses to CpG-DNA. *Blood* **110**, 1970-1981, doi:10.1182/blood-2006-09-044776 (2007).

150 Jiao, Y., Wang, H. C. & Fan, S. J. Growth suppression and radiosensitivity increase by HMGB1 in breast cancer. *Acta pharmacologica Sinica* **28**, 1957-1967, doi:10.1111/j.1745-7254.2007.00669.x (2007).

151 Kang, R., Zhang, Q., Zeh, H. J., Lotze, M. T. & Tang, D. HMGB1 in cancer: good, bad, or both? *Clinical cancer research : an official journal of the American Association for Cancer Research* **19**, 4046-4057, doi:10.1158/1078-0432.CCR-13-0495 (2013).

152 Fucikova, J. *et al.* Human tumor cells killed by anthracyclines induce a tumor-specific immune response. *Cancer research* **71**, 4821-4833, doi:10.1158/0008-5472.can-11-0950 (2011).

153 Ito, N. *et al.* Cytolytic cells induce HMGB1 release from melanoma cell lines. *J Leukoc Biol* **81**, 75-83, doi:10.1189/jlb.0306169 (2007).

154 Dong Xda, E. *et al.* High mobility group box I (HMGB1) release from tumor cells after treatment: implications for development of targeted chemoimmunotherapy. *Journal of immunotherapy (Hagerstown, Md. : 1997)* **30**, 596-606, doi:10.1097/CJI.0b013e31804efc76 (2007).

155 Krysko, D. V. *et al.* Immunogenic cell death and DAMPs in cancer therapy. *Nature Reviews Cancer* **12**, 860-875, doi:10.1038/nrc3380 (2012).

156 Liu, Z., Falo, L. D., Jr. & You, Z. Knockdown of HMGB1 in tumor cells attenuates their ability to induce regulatory T cells and uncovers naturally acquired CD8 T cell-dependent antitumor immunity. *Journal of immunology (Baltimore, Md. : 1950)* **187**, 118-125, doi:10.4049/jimmunol.1003378 (2011).

157 Peltz, E. D. *et al.* HMGB1 IS MARKEDLY ELEVATED WITHIN 6 HOURS OF MECHANICAL TRAUMA IN HUMANS. *Shock (Augusta, Ga.)* **32**, 17-22 (2009).

158 Ma, C. Y. *et al.* Elevated plasma level of HMGB1 is associated with disease activity and combined alterations with IFN-alpha and TNF-alpha in systemic lupus erythematosus. *Rheumatology international* **32**, 395-402, doi:10.1007/s00296-010-1636-6 (2012).

159 Li, J. *et al.* Expression of high mobility group box chromosomal protein 1 and its modulating effects on downstream cytokines in systemic lupus erythematosus. *The Journal of rheumatology* **37**, 766-775, doi:10.3899/jrheum.090663 (2010).

160 Li, Y. *et al.* Serum high mobility group box protein 1 as aclinical marker for ovarian cancer. *Neoplasma* **61**, 579-584, doi:10.4149/neo_2014_070 (2014).

161 Shang, G. H. *et al.* Serum high mobility group box protein 1 as a clinical marker for non-small cell lung cancer. *Respiratory medicine* **103**, 1949-1953, doi:10.1016/j.rmed.2009.05.019 (2009).

162 Cheng, B. Q. *et al.* Serum high mobility group box chromosomal protein 1 is associated with clinicopathologic features in patients with hepatocellular carcinoma. *Digestive and liver disease : official journal of the Italian Society of Gastroenterology and the Italian Association for the Study of the Liver* **40**, 446-452, doi:10.1016/j.dld.2007.11.024 (2008).

163 Taniguchi, N. *et al.* High mobility group box chromosomal protein 1 plays a role in the pathogenesis of rheumatoid arthritis as a novel cytokine. *Arthritis and rheumatism* **48**, 971-981, doi:10.1002/art.10859 (2003).

164 Fang, W.-H. *et al.* The Significance of Changes in High Mobility Group-1 Protein mRNA Expression in Rats After Thermal Injury. *Shock* **17**, 329-333 (2002).

165 Pallier, C. *et al.* Association of chromatin proteins high mobility group box (HMGB) 1 and HMGB2 with mitotic chromosomes. *Molecular biology of the cell* **14**, 3414-3426, doi:10.1091/mbc.E02-09-0581 (2003).

166 Schlueter, C. *et al.* Angiogenetic signaling through hypoxia: HMGB1: an angiogenetic switch molecule. *The American journal of pathology* **166**, 1259-1263, doi:10.1016/s0002-9440(10)62344-9 (2005).

167 van Beijnum, J. R., Buurman, W. A. & Griffioen, A. W. Convergence and amplification of toll-like receptor (TLR) and receptor for advanced glycation end products (RAGE) signaling pathways via high mobility group B1 (HMGB1). *Angiogenesis* **11**, 91-99, doi:10.1007/s10456-008-9093-5 (2008).

168 Taguchi, A. *et al.* Blockade of RAGE-amphoterin signalling suppresses tumour growth and metastases. *Nature* **405**, 354-360, doi:10.1038/35012626 (2000).

169 Yang, R. *et al.* Anti-HMGB1 neutralizing antibody ameliorates gut barrier dysfunction and improves survival after hemorrhagic shock. *Molecular medicine (Cambridge, Mass.)* **12**, 105-114, doi:10.2119/2006-00010.Yang (2006).

170 Kokkola, R. *et al.* Successful treatment of collagen-induced arthritis in mice and rats by targeting extracellular high mobility group box chromosomal protein 1 activity. *Arthritis and rheumatism* **48**, 2052-2058, doi:10.1002/art.11161 (2003).

171 Shin, J. H. *et al.* Ethyl pyruvate inhibits HMGB1 phosphorylation and release by chelating calcium. *Molecular medicine (Cambridge, Mass.)* **20**, 649-657, doi:10.2119/molmed.2014.00039 (2014).

172 Kim, Y. M. *et al.* Ethyl pyruvate inhibits the acetylation and release of HMGB1 via effects on SIRT1/STAT signaling in LPS-activated RAW264.7 cells and peritoneal macrophages. *International immunopharmacology* **41**, 98-105, doi:10.1016/j.intimp.2016.11.002 (2016).

173 Park, S. Y., Yi, E. Y., Jung, M., Lee, Y. M. & Kim, Y. J. Ethyl pyruvate, an anti-inflammatory agent, inhibits tumor angiogenesis through inhibition of the NF-kappaB signaling pathway. *Cancer letters* **303**, 150-154, doi:10.1016/j.canlet.2010.12.024 (2011).

174 Kao, K. K. & Fink, M. P. The biochemical basis for the anti-inflammatory and cytoprotective actions of ethyl pyruvate and related compounds. *Biochemical pharmacology* **80**, 151-159, doi:10.1016/j.bcp.2010.03.007 (2010).

175 Bennett-Guerrero, E. *et al.* A phase II multicenter double-blind placebo-controlled study of ethyl pyruvate in high-risk patients undergoing cardiac surgery with cardiopulmonary bypass. *Journal of cardiothoracic and vascular anesthesia* **23**, 324-329, doi:10.1053/j.jvca.2008.08.005 (2009).

176 Riehl, A., Nemeth, J., Angel, P. & Hess, J. The receptor RAGE: Bridging inflammation and cancer. *Cell communication and signaling : CCS* **7**, 12, doi:10.1186/1478-811x-7-12 (2009).

177 Kierdorf, K. & Fritz, G. RAGE regulation and signaling in inflammation and beyond. *Journal of Leukocyte Biology* **94**, 55-68, doi:10.1189/jlb.1012519 (2013).

178 Chavakis, T., Bierhaus, A. & Nawroth, P. P. RAGE (receptor for advanced glycation end products): a central player in the inflammatory response. *Microbes and infection / Institut Pasteur* **6**, 1219-1225, doi:10.1016/j.micinf.2004.08.004 (2004).

179 Kokkola, R. *et al.* RAGE is the major receptor for the proinflammatory activity of HMGB1 in rodent macrophages. *Scandinavian journal of immunology* **61**, 1-9, doi:10.1111/j.0300-9475.2005.01534.x (2005).

180 Hori, O. *et al.* The receptor for advanced glycation end products (RAGE) is a cellular binding site for amphoterin. Mediation of neurite outgrowth and co-expression of rage and amphoterin in the developing nervous system. *The Journal of biological chemistry* **270**, 25752-25761 (1995).

181 Chavakis, T. *et al.* The pattern recognition receptor (RAGE) is a counterreceptor for leukocyte integrins: a novel pathway for inflammatory cell recruitment. *J Exp Med* **198**, 1507-1515, doi:10.1084/jem.20030800 (2003).

182 Cai, Z. *et al.* Role of RAGE in Alzheimer's Disease. *Cellular and molecular neurobiology*, doi:10.1007/s10571-015-0233-3 (2015).

183 Buraczynska, M., Zaluska, W., Buraczynska, K., Markowska-Gosik, D. & Ksiazek, A. Receptor for advanced glycation end products (RAGE) gene polymorphism and cardiovascular disease in end-stage renal disease patients. *Human immunology*, doi:10.1016/j.humimm.2015.09.046 (2015).

184 Cohen, M. M., Jr. Perspectives on RAGE signaling and its role in cardiovascular disease. *Am J Med Genet A* **161a**, 2750-2755, doi:10.1002/ajmg.a.36181 (2013).

185 Yamagishi, S. & Matsui, T. Role of receptor for advanced glycation end products (RAGE) in liver disease. *European journal of medical research* **20**, 15, doi:10.1186/s40001-015-0090-z (2015).

186 Kierdorf, K. & Fritz, G. RAGE regulation and signaling in inflammation and beyond. *J Leukoc Biol* **94**, 55-68, doi:10.1189/jlb.1012519 (2013).

187 Fritz, G. RAGE: a single receptor fits multiple ligands. *Trends Biochem Sci* **36**, 625-632, doi:10.1016/j.tibs.2011.08.008 (2011).

188 Huttunen, H. J., Fages, C. & Rauvala, H. Receptor for advanced glycation end products (RAGE)-mediated neurite outgrowth and activation of NF-kappaB require the

cytoplasmic domain of the receptor but different downstream signaling pathways. *The Journal of biological chemistry* **274**, 19919-19924 (1999).

189 Srikrishna, G. *et al.* Carboxylated N-glycans on RAGE promote S100A12 binding and signaling. *Journal of cellular biochemistry* **110**, 645-659, doi:10.1002/jcb.22575 (2010).

190 Xie, J. *et al.* Structural basis for pattern recognition by the receptor for advanced glycation end products (RAGE). *The Journal of biological chemistry* **283**, 27255-27269, doi:10.1074/jbc.M801622200 (2008).

191 Hudson, B. I. *et al.* Identification, classification, and expression of RAGE gene splice variants. *FASEB journal : official publication of the Federation of American Societies for Experimental Biology* **22**, 1572-1580, doi:10.1096/fj.07-9909com (2008).

192 Sterenczak, K. A., Nolte, I. & Murua Escobar, H. RAGE splicing variants in mammals. *Methods in molecular biology (Clifton, N.J.)* **963**, 265-276, doi:10.1007/978-1-62703-230-8_16 (2013).

193 Sterenczak, K. A. *et al.* Cloning, characterisation, and comparative quantitative expression analyses of receptor for advanced glycation end products (RAGE) transcript forms. *Gene* **434**, 35-42, doi:10.1016/j.gene.2008.10.027 (2009).

194 Sevillano, N. *et al.* Internalization of the receptor for advanced glycation end products (RAGE) is required to mediate intracellular responses. *Journal of biochemistry* **145**, 21-30, doi:10.1093/jb/mvn137 (2009).

195 Rai, V. *et al.* Signal transduction in receptor for advanced glycation end products (RAGE): solution structure of C-terminal rage (ctRAGE) and its binding to mDia1. *The Journal of biological chemistry* **287**, 5133-5144, doi:10.1074/jbc.M111.277731 (2012).

196 Batkulwar, K. B. *et al.* Investigation of Phosphoproteome in RAGE signaling. *Proteomics*, doi:10.1002/pmic.201400169 (2014).

197 Ibrahim, Z. A., Armour, C. L., Phipps, S. & Sukkar, M. B. RAGE and TLRs: relatives, friends or neighbours? *Mol Immunol* **56**, 739-744, doi:10.1016/j.molimm.2013.07.008 (2013).

198 Fiuza, C. *et al.* Inflammation-promoting activity of HMGB1 on human microvascular endothelial cells. *Blood* **101**, 2652-2660, doi:10.1182/blood-2002-05-1300 (2003).

199 Yeh, C. H. *et al.* Requirement for p38 and p44/p42 mitogen-activated protein kinases in RAGE-mediated nuclear factor-kappaB transcriptional activation and cytokine secretion. *Diabetes* **50**, 1495-1504 (2001).

200 Yang, D. *et al.* High mobility group box-1 protein induces the migration and activation of human dendritic cells and acts as an alarmin. *J Leukoc Biol* **81**, 59-66, doi:10.1189/jlb.0306180 (2007).

201 Li, J. & Schmidt, A. M. Characterization and functional analysis of the promoter of RAGE, the receptor for advanced glycation end products. *The Journal of biological chemistry* **272**, 16498-16506 (1997).

202 Gebhardt, C. *et al.* RAGE signaling sustains inflammation and promotes tumor development. *J Exp Med* **205**, 275-285, doi:10.1084/jem.20070679 (2008).

203 Perrone, L., Peluso, G. & Melone, M. A. RAGE recycles at the plasma membrane in S100B secretory vesicles and promotes Schwann cells morphological changes. *Journal of cellular physiology* **217**, 60-71, doi:10.1002/jcp.21474 (2008).

204 Hsieh, H. L., Schafer, B. W., Weigle, B. & Heizmann, C. W. S100 protein translocation in response to extracellular S100 is mediated by receptor for advanced glycation endproducts in human endothelial cells. *Biochem Biophys Res Commun* **316**, 949-959, doi:10.1016/j.bbrc.2004.02.135 (2004).

205 Frommhold, D. *et al.* RAGE and ICAM-1 cooperate in mediating leukocyte recruitment during acute inflammation in vivo. *Blood* **116**, 841-849, doi:10.1182/blood-2009-09-244293 (2010).

206 Metz, V. V., Kojro, E., Rat, D. & Postina, R. Induction of RAGE shedding by activation of G protein-coupled receptors. *PLoS One* **7**, e41823, doi:10.1371/journal.pone.0041823 (2012).

207 Galichet, A., Weibel, M. & Heizmann, C. W. Calcium-regulated intramembrane proteolysis of the RAGE receptor. *Biochem Biophys Res Commun* **370**, 1-5, doi:10.1016/j.bbrc.2008.02.163 (2008).

208 Kalea, Anastasia Z., Schmidt, Ann M. & Hudson, Barry I. RAGE: a novel biological and genetic marker for vascular disease. *Clinical Science* **116**, 621-637, doi:10.1042/cs20080494 (2009).

209 Fukami, A. *et al.* Factors associated with serum high mobility group box 1 (HMGB1) levels in a general population. *Metabolism: clinical and experimental* **58**, 1688-1693, doi:10.1016/j.metabol.2009.05.024 (2009).

210 Kalea, A. Z., Schmidt, A. M. & Hudson, B. I. Alternative splicing of RAGE: roles in biology and disease. *Frontiers in bioscience (Landmark edition)* **16**, 2756-2770 (2011).

211 Yonekura, H. *et al.* Novel splice variants of the receptor for advanced glycation end-products expressed in human vascular endothelial cells and pericytes, and their putative roles in diabetes-induced vascular injury. *The Biochemical journal* **370**, 1097-1109, doi:10.1042/bj20021371 (2003).

212 Schlueter, C., Hauke, S., Flohr, A. M., Rogalla, P. & Bullerdiek, J. Tissue-specific expression patterns of the RAGE receptor and its soluble forms--a result of regulated alternative splicing? *Biochim Biophys Acta* **1630**, 1-6 (2003).

213 Nakamura, K. *et al.* Serum levels of soluble form of receptor for advanced glycation end products (sRAGE) are positively associated with circulating AGEs and soluble form of VCAM-1 in patients with type 2 diabetes. *Microvasc Res* **76**, 52-56, doi:10.1016/j.mvr.2007.09.004 (2008).

214 Zhang, L. *et al.* Receptor for advanced glycation end products is subjected to protein ectodomain shedding by metalloproteinases. *The Journal of biological chemistry* **283**, 35507-35516, doi:10.1074/jbc.M806948200 (2008).

215 Raucci, A. *et al.* A soluble form of the receptor for advanced glycation endproducts (RAGE) is produced by proteolytic cleavage of the membrane-bound form by the sheddase a disintegrin and metalloprotease 10 (ADAM10). *FASEB journal : official publication of the Federation of American Societies for Experimental Biology* **22**, 3716-3727, doi:10.1096/fj.08-109033 (2008).

216 Chantry, A., Gregson, N. & Glynn, P. Degradation of myelin basic protein by a membrane-associated metalloprotease: Neural distribution of the enzyme. *Neurochemical Research* **17**, 861-867, doi:10.1007/bf00993261 (1992).

217 Carey, R. M., Blusztajn, J. K. & Slack, B. E. Surface expression and limited proteolysis of ADAM10 are increased by a dominant negative inhibitor of dynamin. *BMC cell biology* **12**, 20, doi:10.1186/1471-2121-12-20 (2011).

218 Gibb, D. R., Saleem, S. J., Chaimowitz, N. S., Mathews, J. & Conrad, D. H. The emergence of ADAM10 as a regulator of lymphocyte development and autoimmunity. *Mol Immunol* **48**, 1319-1327, doi:10.1016/j.molimm.2010.12.005 (2011).

219 Braley, A. *et al.* Regulation of Receptor for Advanced Glycation End Products (RAGE) Ectodomain Shedding and Its Role in Cell Function. *The Journal of biological chemistry* **291**, 12057-12073, doi:10.1074/jbc.M115.702399 (2016).

220 Endres, K. & Fahrenholz, F. Upregulation of the alpha-secretase ADAM10--risk or reason for hope? *The FEBS journal* **277**, 1585-1596, doi:10.1111/j.1742-4658.2010.07566.x (2010).

221 Tousseyn, T. *et al.* ADAM10, the Rate-limiting Protease of Regulated Intramembrane Proteolysis of Notch and Other Proteins, Is Processed by ADAMS-9, ADAMS-15, and the γ-Secretase. *The Journal of biological chemistry* **284**, 11738-11747, doi:10.1074/jbc.M805894200 (2009).

222 Sternberg, Z. *et al.* Reduced expression of membrane-bound (m)RAGE is a biomarker of multiple sclerosis disease progression. *Immunobiology*, doi:10.1016/j.imbio.2015.09.007 (2015).

223 Litwinoff, E., Hurtado Del Pozo, C., Ramasamy, R. & Schmidt, A. M. Emerging Targets for Therapeutic Development in Diabetes and Its Complications: The RAGE Signaling Pathway. *Clinical pharmacology and therapeutics* **98**, 135-144, doi:10.1002/cpt.148 (2015).

224 Tesarova, P., Cabinakova, M., Mikulova, V., Zima, T. & Kalousova, M. RAGE and its ligands in cancer - culprits, biomarkers, or therapeutic targets? *Neoplasma* **62**, 353-364 (2015).

225 Abe, R. & Yamagishi, S. AGE-RAGE system and carcinogenesis. *Current pharmaceutical design* **14**, 940-945 (2008).

226 Chen, X. *et al.* RAGE Expression in Tumor-associated Macrophages Promotes Angiogenesis in Glioma. *Cancer research*, doi:10.1158/0008-5472.can-14-1240 (2014).

227 Kang, R. *et al.* The HMGB1/RAGE inflammatory pathway promotes pancreatic tumor growth by regulating mitochondrial bioenergetics. *Oncogene* **33**, 567-577, doi:10.1038/onc.2012.631 (2014).

228 Wittwer, C. *et al.* Circulating nucleosomes and immunogenic cell death markers HMGB1, sRAGE and DNAse in patients with advanced pancreatic cancer undergoing chemotherapy. *International journal of cancer. Journal international du cancer* **133**, 2619-2630, doi:10.1002/ijc.28294 (2013).

229 Wittwer, C. & Holdenrieder, S. in *Laboratoriumsmedizin* Vol. 37 29 (2013).

230 Tesarova, P. *et al.* Receptor for advanced glycation end products (RAGE)--soluble form (sRAGE) and gene polymorphisms in patients with breast cancer. *Cancer investigation* **25**, 720-725, doi:10.1080/07357900701560521 (2007).

231 Jing, R., Cui, M., Wang, J. & Wang, H. Receptor for advanced glycation end products (RAGE) soluble form (sRAGE): a new biomarker for lung cancer. *Neoplasma* **57**, 55-61 (2010).

232 Grote, V. A. *et al.* The associations of advanced glycation end products and its soluble receptor with pancreatic cancer risk: a case-control study within the prospective EPIC Cohort. *Cancer epidemiology, biomarkers & prevention : a publication of the American Association for Cancer Research, cosponsored by the American Society of Preventive Oncology* **21**, 619-628, doi:10.1158/1055-9965.epi-11-1139 (2012).

233 He, L. *et al.* Circulating soluble advanced glycation end product is inversely associated with the significant risk of developing cancer: evidence from a meta-analysis. *Tumour biology : the journal of the International Society for Oncodevelopmental Biology and Medicine* **35**, 8749-8755, doi:10.1007/s13277-014-2122-7 (2014).

234 Kalea, A. Z. *et al.* Alternatively spliced RAGEv1 inhibits tumorigenesis through suppression of JNK signaling. *Cancer research* **70**, 5628-5638, doi:10.1158/0008-5472.can-10-0595 (2010).

235 Han, Y. T. *et al.* Ligand-based design, synthesis, and biological evaluation of 2-aminopyrimidines, a novel series of receptor for advanced glycation end products (RAGE) inhibitors. *Journal of medicinal chemistry* **55**, 9120-9135, doi:10.1021/jm300172z (2012).

236 Walker, D., Lue, L. F., Paul, G., Patel, A. & Sabbagh, M. N. Receptor for advanced glycation endproduct modulators: a new therapeutic target in Alzheimer's disease. *Expert opinion on investigational drugs* **24**, 393-399, doi:10.1517/13543784.2015.1001490 (2015).

237 Galasko, D. *et al.* Clinical trial of an inhibitor of RAGE-Abeta interactions in Alzheimer disease. *Neurology* **82**, 1536-1542, doi:10.1212/wnl.0000000000000364 (2014).

238 Christaki, E. *et al.* A monoclonal antibody against RAGE alters gene expression and is protective in experimental models of sepsis and pneumococcal pneumonia. *Shock* **35**, 492-498, doi:10.1097/SHK.0b013e31820b2e1c (2011).

239 Park, L. *et al.* Suppression of accelerated diabetic atherosclerosis by the soluble receptor for advanced glycation endproducts. *Nat Med* **4**, 1025-1031, doi:10.1038/2012 (1998).

240 Goova, M. T. *et al.* Blockade of receptor for advanced glycation end-products restores effective wound healing in diabetic mice. *The American journal of pathology* **159**, 513-525, doi:10.1016/s0002-9440(10)61723-3 (2001).

241 Quade-Lyssy, P., Kanarek, A. M., Baiersdorfer, M., Postina, R. & Kojro, E. Statins stimulate the production of a soluble form of the receptor for advanced glycation end products. *Journal of lipid research* **54**, 3052-3061, doi:10.1194/jlr.M038968 (2013).

242 Winiarska, M. *et al.* Statins impair antitumor effects of rituximab by inducing conformational changes of CD20. *PLoS medicine* **5**, e64, doi:10.1371/journal.pmed.0050064 (2008).

243 Krieg, A. M. TLR9 and DNA 'feel' RAGE. *Nat Immunol* **8**, 475-477, doi:ni0507-475 [pii]

10.1038/ni0507-475 (2007).

244 Chen, K. *et al.* Toll-like receptors in inflammation, infection and cancer. *International immunopharmacology* **7**, 1271-1285, doi:10.1016/j.intimp.2007.05.016 (2007).

245 Hemmi, H. *et al.* A Toll-like receptor recognizes bacterial DNA. *Nature* **408**, 740-745, doi:10.1038/35047123 (2000).

246 Akira, S. & Takeda, K. Toll-like receptor signalling. *Nat Rev Immunol* **4**, 499-511, doi:10.1038/nri1391 (2004).

247 Ahmad-Nejad, P. *et al.* Bacterial CpG-DNA and lipopolysaccharides activate Toll-like receptors at distinct cellular compartments. *European Journal of Immunology* **32**, 1958-1968 (2002).

248 Rutz, M. *et al.* Toll-like receptor 9 binds single-stranded CpG-DNA in a sequence- and pH-dependent manner. *Eur J Immunol* **34**, 2541-2550, doi:10.1002/eji.200425218 (2004).

249 Ohto, U. *et al.* Structural basis of CpG and inhibitory DNA recognition by Toll-like receptor 9. *Nature* **520**, 702-705, doi:10.1038/nature14138 (2015).

250 Verthelyi, D. & Zeuner, R. A. Differential signaling by CpG DNA in DCs and B cells: not just TLR9. *Trends Immunol* **24**, 519-522 (2003).

251 Slack, J. L. *et al.* Identification of two major sites in the type I interleukin-1 receptor cytoplasmic region responsible for coupling to pro-inflammatory signaling pathways. *The Journal of biological chemistry* **275**, 4670-4678 (2000).

252 Dunne, A. & O'Neill, L. A. The interleukin-1 receptor/Toll-like receptor superfamily: signal transduction during inflammation and host defense. *Science's STKE : signal transduction knowledge environment* **2003**, re3, doi:10.1126/stke.2003.171.re3 (2003).

253 Dunne, A., Ejdeback, M., Ludidi, P. L., O'Neill, L. A. & Gay, N. J. Structural complementarity of Toll/interleukin-1 receptor domains in Toll-like receptors and the adaptors Mal and MyD88. *The Journal of biological chemistry* **278**, 41443-41451, doi:10.1074/jbc.M301742200 (2003).

254 Karin, M. & Ben-Neriah, Y. Phosphorylation meets ubiquitination: the control of NF-[kappa]B activity. *Annu Rev Immunol* **18**, 621-663, doi:10.1146/annurev.immunol.18.1.621 (2000).

255 Wesche, H. *et al.* IRAK-M is a novel member of the Pelle/interleukin-1 receptor-associated kinase (IRAK) family. *The Journal of biological chemistry* **274**, 19403-19410 (1999).

256 Dalpke, A. H., Opper, S., Zimmermann, S. & Heeg, K. Suppressors of cytokine signaling (SOCS)-1 and SOCS-3 are induced by CpG-DNA and modulate cytokine responses in APCs. *Journal of immunology (Baltimore, Md. : 1950)* **166**, 7082-7089 (2001).

257 Chuang, T. H. & Ulevitch, R. J. Triad3A, an E3 ubiquitin-protein ligase regulating Toll-like receptors. *Nat Immunol* **5**, 495-502, doi:10.1038/ni1066 (2004).

258 Leadbetter, E. A. *et al.* Chromatin-IgG complexes activate B cells by dual engagement of IgM and Toll-like receptors. *Nature* **416**, 603-607, doi:10.1038/416603a (2002).

259 Boule, M. W. *et al.* Toll-like receptor 9-dependent and -independent dendritic cell activation by chromatin-immunoglobulin G complexes. *J Exp Med* **199**, 1631-1640, doi:10.1084/jem.20031942 (2004).

260 Frese, S. & Diamond, B. Structural modification of DNA[mdash]a therapeutic option in SLE? *Nat Rev Rheumatol* **7**, 733-738 (2011).

261 Viglianti, G. A. *et al.* Activation of autoreactive B cells by CpG dsDNA. *Immunity* **19**, 837-847 (2003).

262 Eckl-Dorna, J. & Batista, F. D. BCR-mediated uptake of antigen linked to TLR9 ligand stimulates B-cell proliferation and antigen-specific plasma cell formation. *Blood* **113**, 3969-3977, doi:10.1182/blood-2008-10-185421 (2009).

263 Krieg, A. M. Toll-like receptor 9 (TLR9) agonists in the treatment of cancer. *Oncogene* **27**, 161-167 (0000).

264 Adams, S. Toll-like receptor agonists in cancer therapy. *Immunotherapy* **1**, 949-964, doi:10.2217/imt.09.70 (2009).

265 Belmont, L. *et al.* Expression of TLR9 in tumor-infiltrating mononuclear cells enhances angiogenesis and is associated with a worse survival in lung cancer. *International journal of cancer. Journal international du cancer* **134**, 765-777, doi:10.1002/ijc.28413 (2014).

266 Kauppila, J. H. *et al.* Toll-like receptor 9 mediates invasion and predicts prognosis in squamous cell carcinoma of the mobile tongue. *Journal of oral pathology & medicine : official publication of the International Association of Oral Pathologists and the American Academy of Oral Pathology* **44**, 571-577, doi:10.1111/jop.12272 (2015).

267 Olbert, P. J. *et al.* TLR4- and TLR9-dependent effects on cytokines, cell viability, and invasion in human bladder cancer cells. *Urologic oncology* **33**, 110.e119-127, doi:10.1016/j.urolonc.2014.09.016 (2015).

268 Decker, T. *et al.* Immunostimulatory CpG-oligonucleotides cause proliferation, cytokine production, and an immunogenic phenotype in chronic lymphocytic leukemia B cells. *Blood* **95**, 999-1006 (2000).

269 Jahrsdorfer, B. *et al.* Immunostimulatory oligodeoxynucleotides induce apoptosis of B cell chronic lymphocytic leukemia cells. *J Leukoc Biol* **77**, 378-387, doi:10.1189/jlb.0604373 (2005).

270 Tarnani, M. *et al.* The proliferative response to CpG-ODN stimulation predicts PFS, TTT and OS in patients with chronic lymphocytic leukemia. *Leukemia research* **34**, 1189-1194, doi:10.1016/j.leukres.2009.12.020 (2010).

271 Tromp, J. M. *et al.* Dichotomy in NF-kappaB signaling and chemoresistance in immunoglobulin variable heavy-chain-mutated versus unmutated CLL cells upon CD40/TLR9 triggering. *Oncogene* **29**, 5071-5082, doi:10.1038/onc.2010.248 (2010).

272 Busconi, L. *et al.* Functional outcome of B cell activation by chromatin immune complex engagement of the B cell receptor and TLR9. *Journal of immunology (Baltimore, Md. : 1950)* **179**, 7397-7405 (2007).

273 Bekeredjian-Ding, I. *et al.* TLR9-activating DNA up-regulates ZAP70 via sustained PKB induction in IgM+ B cells. *J Immunol* **181**, 8267-8277 (2008).

274 Jahrsdorfer, B. *et al.* B-cell lymphomas differ in their responsiveness to CpG oligodeoxynucleotides. *Clinical cancer research : an official journal of the American Association for Cancer Research* **11**, 1490-1499, doi:10.1158/1078-0432.ccr-04-1890 (2005).

275 Weihrauch, M. R. *et al.* Phase I clinical study of the toll-like receptor 9 agonist MGN1703 in patients with metastatic solid tumours. *European Journal of Cancer* **51**, 146-156, doi:https://doi.org/10.1016/j.ejca.2014.11.002 (2015).

276 Balak, D. M. *et al.* IMO-8400, a toll-like receptor 7, 8, and 9 antagonist, demonstrates clinical activity in a phase 2a, randomized, placebo-controlled trial in patients with moderate-to-severe plaque psoriasis. *Clinical immunology (Orlando, Fla.)* **174**, 63-72, doi:10.1016/j.clim.2016.09.015 (2017).

277 Wang, D. *et al.* Overexpression of the Receptor for Advanced Glycation Endproducts (RAGE) is associated with poor prognosis in gastric cancer. *PLoS One* **10**, e0122697, doi:10.1371/journal.pone.0122697 (2015).

278 Xu, X. C., Gao, H., Zhang, W. B., Abuduhadeer, X. & Wang, Y. H. Clinical significance of immunogenic cell death biomarker rage and early growth response 1 in human primary gastric adenocarcinoma. *International journal of immunopathology and pharmacology* **26**, 485-493 (2013).

279 Kotrashetti, V. S., Nayak, R., Bhat, K., Hosmani, J. & Somannavar, P. Immunohistochemical expression of TLR4 and TLR9 in various grades of oral epithelial dysplasia and squamous cell carcinoma, and their roles in tumor progression: a pilot study. *Biotechnic & histochemistry : official publication of the Biological Stain Commission* **88**, 311-322, doi:10.3109/10520295.2013.785592 (2013).

280 Paz, S. *et al.* The Distinct and Cooperative Roles of Toll-Like Receptor 9 and Receptor for Advanced Glycation End Products in Modulating In Vivo Inflammatory Responses to Select CpG and Non-CpG Oligonucleotides. *Nucleic acid therapeutics*, doi:10.1089/nat.2017.0668 (2017).

281 Nogueira-Machado, J. A., Volpe, C. M., Veloso, C. A. & Chaves, M. M. HMGB1, TLR and RAGE: a functional tripod that leads to diabetic inflammation. *Expert opinion on therapeutic targets* **15**, 1023-1035, doi:10.1517/14728222.2011.575360 (2011).

282 Masters, J. R. W. Human cancer cell lines: fact and fantasy. *Nature reviews. Molecular cell biology* **1**, 233-236, doi:http://www.nature.com/nrm/journal/v1/n3/suppinfo/nrm1200_233a_S1.html (2000).

283 Stacchini, A. *et al.* MEC1 and MEC2: two new cell lines derived from B-chronic lymphocytic leukaemia in prolymphocytoid transformation. *Leukemia research* **23**, 127-136 (1999).

284 Thomas, P. & Smart, T. G. HEK293 cell line: a vehicle for the expression of recombinant proteins. *Journal of pharmacological and toxicological methods* **51**, 187-200, doi:10.1016/j.vascn.2004.08.014 (2005).

285 Barnes, D. & Sato, G. Serum-free cell culture: a unifying approach. *Cell* **22**, 649-655 (1980).

286 Walker, R. A. Quantification of immunohistochemistry--issues concerning methods, utility and semiquantitative assessment I. *Histopathology* **49**, 406-410, doi:10.1111/j.1365-2559.2006.02514.x (2006).

287 Taylor, C. R. & Levenson, R. M. Quantification of immunohistochemistry--issues concerning methods, utility and semiquantitative assessment II. *Histopathology* **49**, 411-424, doi:10.1111/j.1365-2559.2006.02513.x (2006).

288 Rait, V. K., Xu, L., O'Leary, T. J. & Mason, J. T. Modeling formalin fixation and antigen retrieval with bovine pancreatic RNase A II. Interrelationship of cross-linking, immunoreactivity, and heat treatment. *Laboratory investigation; a journal of technical methods and pathology* **84**, 300-306, doi:10.1038/labinvest.3700041 (2004).

289 Fowler, C. B. *et al.* Tissue microarrays: construction and uses. *Methods in molecular biology (Clifton, N.J.)* **724**, 23-35, doi:10.1007/978-1-61779-055-3_2 (2011).

290 Greaves, P. *et al.* Expression of FOXP3, CD68, and CD20 at diagnosis in the microenvironment of classical Hodgkin lymphoma is predictive of outcome. *Journal of clinical oncology : official journal of the American Society of Clinical Oncology* **31**, 256-262, doi:10.1200/jco.2011.39.9881 (2013).

291 Liapis, K. *et al.* The microenvironment of AIDS-related diffuse large B-cell lymphoma provides insight into the pathophysiology and indicates possible therapeutic strategies. *Blood* **122**, 424-433, doi:10.1182/blood-2013-03-488171 (2013).

292 Norton, A. J., Jordan, S. & Yeomans, P. Brief, high-temperature heat denaturation (pressure cooking): a simple and effective method of antigen retrieval for routinely processed tissues. *The Journal of pathology* **173**, 371-379, doi:10.1002/path.1711730413 (1994).

293 Ramos-Vara, J. A. Principles and methods of immunohistochemistry. *Methods Mol Biol* **691**, 83-96, doi:10.1007/978-1-60761-849-2_5 (2011).

294 Radcliff, G. & Jaroszeski, M. J. Basics of flow cytometry. *Methods in molecular biology (Clifton, N.J.)* **91**, 1-24 (1998).

295 Kamentsky, L. A., Melamed, M. R. & Derman, H. Spectrophotometer: new instrument for ultrarapid cell analysis. *Science* **150**, 630-631 (1965).

296 Jaroszeski, M. J. & Radcliff, G. Fundamentals of flow cytometry. *Mol Biotechnol* **11**, 37-53, doi:10.1007/bf02789175 (1999).

297 Tung, J. W., Parks, D. R., Moore, W. A., Herzenberg, L. A. & Herzenberg, L. A. New approaches to fluorescence compensation and visualization of FACS data. *Clinical immunology (Orlando, Fla.)* **110**, 277-283, doi:10.1016/j.clim.2003.11.016 (2004).

298 Letestu, R. *et al.* Evaluation of ZAP-70 expression by flow cytometry in chronic lymphocytic leukemia: A multicentric international harmonization process. *Cytometry. Part B, Clinical cytometry* **70**, 309-314, doi:10.1002/cyto.b.20132 (2006).

299 Marquez, M. E., Deglesne, P. A., Suarez, G. & Romano, E. MFI ratio estimation of ZAP-70 in B-CLL by flow cytometry can be improved by considering the isotype-matched antibody signal. *International journal of laboratory hematology* **33**, 194-200, doi:10.1111/j.1751-553X.2010.01263.x (2011).

300 Koopman, G. *et al.* Annexin V for flow cytometric detection of phosphatidylserine expression on B cells undergoing apoptosis. *Blood* **84**, 1415-1420 (1994).

301 Martin, S. J. *et al.* Early redistribution of plasma membrane phosphatidylserine is a general feature of apoptosis regardless of the initiating stimulus: inhibition by overexpression of Bcl-2 and Abl. *J Exp Med* **182**, 1545-1556 (1995).

302 Chiorazzi, N., Rai, K. R. & Ferrarini, M. Chronic lymphocytic leukemia. *N Engl J Med* **352**, 804-815, doi:10.1056/NEJMra041720 (2005).

303 Wu, Y., Zinchuk, V., Grossenbacher-Zinchuk, O. & Stefani, E. Critical evaluation of quantitative colocalization analysis in confocal fluorescence microscopy. *Interdisciplinary sciences, computational life sciences* **4**, 27-37, doi:10.1007/s12539-012-0117-x (2012).

304 Zuba-Surma, E. K. & Ratajczak, M. Z. Analytical capabilities of the ImageStream cytometer. *Methods in cell biology* **102**, 207-230, doi:10.1016/b978-0-12-374912-3.00008-0 (2011).

305 Ortyn, W. E. *et al.* Sensitivity measurement and compensation in spectral imaging. *Cytometry. Part A : the journal of the International Society for Analytical Cytology* **69**, 852-862, doi:10.1002/cyto.a.20306 (2006).

306 Zuba-Surma, E. K., Kucia, M., Abdel-Latif, A., Lillard, J. W., Jr. & Ratajczak, M. Z. The ImageStream System: a key step to a new era in imaging. *Folia histochemica et cytobiologica / Polish Academy of Sciences, Polish Histochemical and Cytochemical Society* **45**, 279-290 (2007).

307 Towbin, H., Staehelin, T. & Gordon, J. Electrophoretic transfer of proteins from polyacrylamide gels to nitrocellulose sheets: procedure and some applications. *Proc Natl Acad Sci U S A* **76**, 4350-4354 (1979).

308 Bradford, M. M. A rapid and sensitive method for the quantitation of microgram quantities of protein utilizing the principle of protein-dye binding. *Anal Biochem* **72**, 248-254 (1976).

309 Rajeeve, V., Vendrell, I., Wilkes, E., Torbett, N. & Cutillas, P. R. Cross-species proteomics reveals specific modulation of signaling in cancer and stromal cells by phosphoinositide 3-kinase (PI3K) inhibitors. *Mol Cell Proteomics* **13**, 1457-1470, doi:10.1074/mcp.M113.035204 (2014).

310 Casado, P. *et al.* Kinase-substrate enrichment analysis provides insights into the heterogeneity of signaling pathway activation in leukemia cells. *Sci Signal* **6**, rs6, doi:10.1126/scisignal.2003573 (2013).

311 Wirbel, J., Cutillas, P. & Saez-Rodriguez, J. in *Cancer Systems Biology: Methods and Protocols* (ed Louise von Stechow) 103-132 (Springer New York, 2018).

312 Budczies, J. *et al.* Cutoff Finder: A Comprehensive and Straightforward Web Application Enabling Rapid Biomarker Cutoff Optimization. *PLOS ONE* **7**, e51862, doi:10.1371/journal.pone.0051862 (2012).

313 Camp, R. L., Dolled-Filhart, M. & Rimm, D. L. X-tile: a new bio-informatics tool for biomarker assessment and outcome-based cut-point optimization. *Clin Cancer Res* **10**, 7252-7259, doi:10.1158/1078-0432.ccr-04-0713 (2004).

314 Rosenquist, R., Cortese, D., Bhoi, S., Mansouri, L. & Gunnarsson, R. Prognostic markers and their clinical applicability in chronic lymphocytic leukemia: where do we stand? *Leukemia & lymphoma* **54**, 2351-2364, doi:10.3109/10428194.2013.783913 (2013).

315 Stilgenbauer, S. & Hallek, M. [Chronic lymphocytic leukemia. Treatment and genetic risk profile]. *Der Internist* **54**, 164, 166-170, doi:10.1007/s00108-012-3153-z (2013).

316 Gutierrez, A., Jr. *et al.* LEF-1 is a prosurvival factor in chronic lymphocytic leukemia and is expressed in the preleukemic state of monoclonal B-cell lymphocytosis. *Blood* **116**, 2975-2983, doi:10.1182/blood-2010-02-269878 (2010).

317 Rozkova, D. *et al.* Toll-like receptors on B-CLL cells: expression and functional consequences of their stimulation. *International journal of cancer. Journal international du cancer* **126**, 1132-1143, doi:10.1002/ijc.24832 (2010).

318 Chatzouli, M. *et al.* Heterogeneous functional effects of concomitant B cell receptor and TLR stimulation in chronic lymphocytic leukemia with mutated versus unmutated Ig genes. *Journal of immunology (Baltimore, Md. : 1950)* **192**, 4518-4524, doi:10.4049/jimmunol.1302102 (2014).

319 Spaner, D. E. *et al.* Immunomodulatory effects of Toll-like receptor-7 activation on chronic lymphocytic leukemia cells. *Leukemia* **20**, 286-295, doi:10.1038/sj.leu.2404061 (2006).

320 Scholzen, T. & Gerdes, J. The Ki-67 protein: from the known and the unknown. *Journal of cellular physiology* **182**, 311-322, doi:10.1002/(sici)1097-4652(200003)182:3<311::aid-jcp1>3.0.co;2-9 (2000).

321 Rassenti, L. Z. *et al.* ZAP-70 compared with immunoglobulin heavy-chain gene mutation status as a predictor of disease progression in chronic lymphocytic leukemia. *N Engl J Med* **351**, 893-901, doi:10.1056/NEJMoa040857 (2004).

322 Arvaniti, E. *et al.* Toll-like receptor signaling pathway in chronic lymphocytic leukemia: distinct gene expression profiles of potential pathogenic significance in specific subsets of patients. *Haematologica* **96**, 1644-1652, doi:10.3324/haematol.2011.044792 (2011).

323 Ciccone, M. *et al.* Proliferation centers in chronic lymphocytic leukemia: correlation with cytogenetic and clinicobiological features in consecutive patients analyzed on tissue microarrays. *Leukemia* **26**, 499-508, doi:10.1038/leu.2011.247 (2012).

324 Gine, E. *et al.* Expanded and highly active proliferation centers identify a histological subtype of chronic lymphocytic leukemia ("accelerated" chronic lymphocytic leukemia) with aggressive clinical behavior. *Haematologica* **95**, 1526-1533, doi:10.3324/haematol.2010.022277 (2010).

325 Herreros, B. *et al.* Proliferation centers in chronic lymphocytic leukemia: the niche where NF-[kappa]B activation takes place. *Leukemia* **24**, 872-876, doi:http://www.nature.com/leu/journal/v24/n4/suppinfo/leu2009285s1.html (2010).

326 De Silva, N. S. & Klein, U. Dynamics of B cells in germinal centres. *Nat Rev Immunol* **15**, 137-148, doi:10.1038/nri3804 (2015).

327 Basso, K. & Dalla-Favera, R. Germinal centres and B cell lymphomagenesis. *Nat Rev Immunol* **15**, 172-184, doi:10.1038/nri3814 (2015).

328 Burger, J. A. The times they are a-changin': prognostic markers in the new era of BCR-targeting therapies for CLL. *Expert opinion on medical diagnostics* **6**, 49-57, doi:10.1517/17530059.2012.637108 (2012).

329 Stilgenbauer, S. Prognostic markers and standard management of chronic lymphocytic leukemia. *Hematology / the Education Program of the American Society of Hematology.*

American Society of Hematology. Education Program **2015**, 368-377, doi:10.1182/asheducation-2015.1.368 (2015).

330 Oscier, D. G. *et al.* Multivariate analysis of prognostic factors in CLL: clinical stage, IGVH gene mutational status, and loss or mutation of the p53 gene are independent prognostic factors. *Blood* **100**, 1177-1184 (2002).

331 Rosenwald, A. *et al.* Relation of gene expression phenotype to immunoglobulin mutation genotype in B cell chronic lymphocytic leukemia. *J Exp Med* **194**, 1639-1647 (2001).

332 Krober, A. *et al.* V(H) mutation status, CD38 expression level, genomic aberrations, and survival in chronic lymphocytic leukemia. *Blood* **100**, 1410-1416 (2002).

333 Hauschild, A. *et al.* S100B protein detection in serum is a significant prognostic factor in metastatic melanoma. *Oncology* **56**, 338-344, doi:11989 (1999).

334 Ramasamy, R., Yan, S. F. & Schmidt, A. M. RAGE: therapeutic target and biomarker of the inflammatory response--the evidence mounts. *J Leukoc Biol* **86**, 505-512, doi:10.1189/jlb.0409230 (2009).

335 Munoz, L. *et al.* Comparative analysis of ZAP-70 expression and Ig VH mutational status in B-cell chronic lymphocytic leukemia. *Cytometry. Part B, Clinical cytometry* **72**, 96-102, doi:10.1002/cyto.b.20149 (2007).

336 Wang, Y.-H., Fan, L., Xu, W. & Li, J.-Y. Detection methods of ZAP-70 in chronic lymphocytic leukemia. *Clinical and Experimental Medicine* **12**, 69-77, doi:10.1007/s10238-011-0148-3 (2012).

337 Burger, J. A. *et al.* Blood-derived nurse-like cells protect chronic lymphocytic leukemia B cells from spontaneous apoptosis through stromal cell-derived factor-1. *Blood* **96**, 2655-2663 (2000).

338 Collins, R. J. *et al.* Spontaneous programmed death (apoptosis) of B-chronic lymphocytic leukaemia cells following their culture in vitro. *British journal of haematology* **71**, 343-350 (1989).

339 Bresnick, A. R., Weber, D. J. & Zimmer, D. B. S100 proteins in cancer. *Nat Rev Cancer* **15**, 96-109, doi:10.1038/nrc3893 (2015).

340 Orchard, J. A. *et al.* ZAP-70 expression and prognosis in chronic lymphocytic leukaemia. *Lancet* **363**, 105-111, doi:10.1016/s0140-6736(03)15260-9 (2004).

341 Zucchetto, A. *et al.* ZAP-70 expression in B-cell chronic lymphocytic leukemia: evaluation by external (isotypic) or internal (T/NK cells) controls and correlation with IgV(H) mutations. *Cytometry. Part B, Clinical cytometry* **70**, 284-292, doi:10.1002/cyto.b.20127 (2006).

342 Shenkin, M. & Maiese, R. Use of a blocking antibody method for the flow cytometric measurement of ZAP-70 in B-CLL. *Cytometry. Part B, Clinical cytometry* **70**, 251-258, doi:10.1002/cyto.b.20125 (2006).

343 Bakke, A. C., Purtzer, Z., Leis, J. & Huang, J. A robust ratio metric method for analysis of Zap-70 expression in chronic lymphocytic leukemia (CLL). *Cytometry Part B: Clinical Cytometry* **70B**, 227-234, doi:10.1002/cyto.b.20079 (2006).

344 Rossi, F. M. *et al.* Prognostic impact of ZAP-70 expression in chronic lymphocytic leukemia: mean fluorescence intensity T/B ratio versus percentage of positive cells. *Journal of translational medicine* **8**, 23, doi:10.1186/1479-5876-8-23 (2010).

345 Shankey, T. V. *et al.* An optimized whole blood method for flow cytometric measurement of ZAP-70 protein expression in chronic lymphocytic leukemia. *Cytometry. Part B, Clinical cytometry* **70**, 259-269, doi:10.1002/cyto.b.20135 (2006).

346 Yang, H., Antoine, D. J., Andersson, U. & Tracey, K. J. The many faces of HMGB1: molecular structure-functional activity in inflammation, apoptosis, and chemotaxis. *J Leukoc Biol* **93**, 865-873, doi:10.1189/jlb.1212662 (2013).

347 Janko, C. *et al.* Redox modulation of HMGB1-related signaling. *Antioxid Redox Signal* **20**, 1075-1085, doi:10.1089/ars.2013.5179 (2014).

348 Janko, C. *et al.* Redox Modulation of HMGB1-Related Signaling. *Antioxidants & Redox Signaling* **20**, 1075-1085, doi:10.1089/ars.2013.5179 (2014).

349 D'Arena, G. *et al.* Prognostic relevance of oxidative stress measurement in chronic lymphocytic leukaemia. *European journal of haematology* **99**, 306-314, doi:10.1111/ejh.12918 (2017).

350 Nakamura, K. *et al.* Circulating advanced glycation end products (AGEs) and soluble form of receptor for AGEs (sRAGE) are independent determinants of serum monocyte chemoattractant protein-1 (MCP-1) levels in patients with type 2 diabetes. *Diabetes/metabolism research and reviews* **24**, 109-114, doi:10.1002/dmrr.766 (2008).

351 Kalousová, M. *et al.* Soluble Receptor for Advanced Glycation End Products in Patients With Decreased Renal Function. *American Journal of Kidney Diseases* **47**, 406-411, doi:http://dx.doi.org/10.1053/j.ajkd.2005.12.028 (2006).

352 Chen, Y.-S., Yan, W., Geczy, C. L., Brown, M. A. & Thomas, R. Serum levels of soluble receptor for advanced glycation end products and of S100 proteins are associated with inflammatory, autoantibody, and classical risk markers of joint and vascular damage in rheumatoid arthritis. *Arthritis Research & Therapy* **11**, R39, doi:10.1186/ar2645 (2009).

353 Wagner, N. B. *et al.* Diminished levels of the soluble form of RAGE are related to poor survival in malignant melanoma. *International journal of cancer. Journal international du cancer* **137**, 2607-2617, doi:10.1002/ijc.29619 (2015).

354 McConkey, D. J. *et al.* Apoptosis sensitivity in chronic lymphocytic leukemia is determined by endogenous endonuclease content and relative expression of BCL-2 and BAX. *Journal of immunology (Baltimore, Md. : 1950)* **156**, 2624-2630 (1996).

355 Szklarczyk, D. *et al.* STRING v10: protein-protein interaction networks, integrated over the tree of life. *Nucleic Acids Res* **43**, D447-452, doi:10.1093/nar/gku1003 (2015).

356 von Mering, C. *et al.* STRING: known and predicted protein-protein associations, integrated and transferred across organisms. *Nucleic Acids Res* **33**, D433-437, doi:10.1093/nar/gki005 (2005).

357 Muzio, M. *et al.* Expression and function of toll like receptors in chronic lymphocytic leukaemia cells. *Br J Haematol* **144**, 507-516, doi:10.1111/j.1365-2141.2008.07475.x

BJH7475 [pii] (2009).

358 Hiraku, Y. *et al.* Multi-walled carbon nanotube induces nitrative DNA damage in human lung epithelial cells via HMGB1-RAGE interaction and Toll-like receptor 9 activation. *Particle and fibre toxicology* **13**, 16, doi:10.1186/s12989-016-0127-7 (2016).

359 Rai, V. *et al.* Signal Transduction in Receptor for Advanced Glycation End Products (RAGE): SOLUTION STRUCTURE OF C-TERMINAL RAGE (ctRAGE) AND ITS BINDING TO mDia1. *The Journal of biological chemistry* **287**, 5133-5144, doi:10.1074/jbc.M111.277731 (2012).

360 Krieg, A. M. Toll-like receptor 9 (TLR9) agonists in the treatment of cancer. *Oncogene* **27**, 161, doi:10.1038/sj.onc.1210911 (2008).

361 Pilzweger C, H. S. Circulating HMGB1 and RAGE as clinical biomarkers in malignant and autoimmune diseases. *Diagnostics* **4** (2014).

362 Stoetzer, O. J. *et al.* Circulating immunogenic cell death biomarkers HMGB1 and RAGE in breast cancer patients during neoadjuvant chemotherapy. *Tumour biology : the journal of the International Society for Oncodevelopmental Biology and Medicine* **34**, 81-90, doi:10.1007/s13277-012-0513-1 (2013).

363 Lee, S. B. *et al.* ADAM10 is upregulated in melanoma metastasis compared with primary melanoma. *J Invest Dermatol* **130**, 763-773, doi:10.1038/jid.2009.335 (2010).

364 Foa, R., Del Giudice, I., Guarini, A., Rossi, D. & Gaidano, G. Clinical implications of the molecular genetics of chronic lymphocytic leukemia. *Haematologica* **98**, 675-685, doi:10.3324/haematol.2012.069369 (2013).

365 Bower, J. K. *et al.* Three-year variability in plasma concentrations of the soluble receptor for advanced glycation end products (sRAGE). *Clinical biochemistry* **47**, 132-134, doi:10.1016/j.clinbiochem.2013.11.005 (2014).

366 Liu, L. *et al.* HMGB1-induced autophagy promotes chemotherapy resistance in leukemia cells. *Leukemia* **25**, 23-31 (2011).

367 Pruessmeyer, J. & Ludwig, A. The good, the bad and the ugly substrates for ADAM10 and ADAM17 in brain pathology, inflammation and cancer. *Seminars in cell & developmental biology* **20**, 164-174, doi:10.1016/j.semcdb.2008.09.005 (2009).

368 Chae, Y. K. *et al.* Statin and aspirin use is associated with improved outcome of FCR therapy in relapsed/refractory chronic lymphocytic leukemia. *Blood* **123**, 1424-1426, doi:10.1182/blood-2013-07-517102 (2014).

369 Rossi, D., Ciardullo, C., Spina, V. & Gaidano, G. Molecular bases of chronic lymphocytic leukemia in light of new treatments. *Immunol Lett* **155**, 51-55, doi:10.1016/j.imlet.2013.09.010 (2013).

370 Duty, J. A. *et al.* Functional anergy in a subpopulation of naive B cells from healthy humans that express autoreactive immunoglobulin receptors. *J Exp Med* **206**, 139-151, doi:10.1084/jem.20080611 (2009).

371 Onitilo, A. A., Engel, J. M., Greenlee, R. T. & Mukesh, B. N. Breast cancer subtypes based on ER/PR and Her2 expression: comparison of clinicopathologic features and survival. *Clin Med Res* **7**, 4-13, doi:10.3121/cmr.2009.825 (2009).

Appendices

Appendix I

1. Cell lines and cell culture

Materials:

- Heat Inactivated Fetal Bovine Serum (FBS) – Gibco Life Technologies 10500
- Penicillin and Streptomycin (P/S) – Sigma Aldrich P4333
- RPMI 1640 – Sigma Aldrich R8758

1.1 Cell culture medium preparation

Heat inactivated FBS (56°C for 30 minutes with mixing) was used to ensure complement proteins were inactivated. P/S was supplemented into cell culture medium to control bacterial contamination. RPMI 1640 medium contains sodium bicarbonate as a buffering system, L-gluatmine as an amino acid supplement and phenol red to detect changes in medium pH. 55ml FBS and 5ml P/S (100x) was added to RPMI 1640 medium to give a final concentration of 10% heat inactivated FBS, 2.0mM L-glutamine, 100U/ml Penicillin and 100µg/ml Streptomycin. Cell culture medium was stored at 4°C and pre-warmed to 37°C in a water bath before addition to cells.

1.2 Measurement of cell viability

Cell viability and cell count was measured using the Luna-II™ Automated Cell Counter (Logos Biosystems L10001). 10µl of cell culture suspension was mixed with Trypan Blue in a 1:1 ratio (Cell Viability PN 2100102) before loading 10µl onto disposable Luna™ Cell Counting Slides (Logos Biosystems L12001). Trypan Blue is not absorbed by viable cells but traverses the damaged plasma membrane in dead cells staining cells blue, while live cells remain unstained. The Luna-II automated cell counter distinguishes dead cells from live cells and gives a measure of cell viability and total cell count.

2. Patient Samples

Materials:

- Lymphoprep – Axis-Shield 1114547
- CD19 MicroBeads human – MACS Miltenyi Biotech 130-050-301
- B-CLL Cell Isolation Kit human – MACS Miltenyi Biotech 130-103-466
- LS Columns - MACS Miltenyi Biotech 130-042-401
- MACS Multistands - MACS Miltenyi Biotech 130-090-976
- QuadroMACS separator - MACS Miltenyi Biotech – 130-042-303

- Bovine serum albumin (BSA) – Sigma Aldrich A7906
- Phosphate Buffered Saline (PBS) – Sigma Aldrich D8537

2.1 0.5% bovine serum albumin-phosphate buffered saline MACS LS column wash buffer

250mg of BSA was diluted in 50ml sterile PBS to give 0.5% BSA in PBS.

3. Immunohistochemistry

Materials:

- Superfrost Plus slides – VWR 631-0108
- Xylene – VWR Chemicals 28975.325
- Industrial Methylated Spirit (IMS) – Fisher Scientific 11482874
- Peroxidase – VWR Chemicals 23619.264
- Unmasking Solution – Vector Laboratories H3300
- 10x Dako wash buffer – Dako S3006
- ImmEdge Hydrophobic Barrier PAP Pen – Vector Laboratories H-4000
- Antibody Diluent – Zytomed ZUC025-500
- Super Sensitive Polymer-Horseradish Peroxidase IHC Detection System – BioGenex QD430-XAKE. Kit includes:
    - SS label
    - Super Enhancer
    - Stable DAB buffer
    - Liquid DAB
- Mayer Haematoxylin – Gill's II
- DPX mountant (Distrene 80, Dibutyl phthalate and Xylene) – VWR 360294H

3.1 Peroxidase blocking buffer

2% hydrogen peroxide in 100% IMS

3.2 Unmasking solution

30ml of citrate-based pH 6 unmasking solution was diluted 1:100 into 3L of distilled water. 1x unmasking solution was pre-heated to 400°C in a pressure cooker before slides were added.

3.3 Wash buffer

100ml of 10x Dako wash buffer was diluted in 900ml of distilled water to give 0.05 M Tris /HCl, 0.15 M NaCl, 0.05% Tween-20, pH 7.6 (±1) working solution.

3.4 Antibody dilutions

Table A. Primary antibodies used in this study

Antibody	Clone	Species	Company (Cat. No)	Antigen Retrieval	Dilution
RAGE	Monoclonal	Mouse	Abcam - ab54741	Heat induced	1:100
TLR9	26C593	Mouse	Abcam - ab12121	Heat induced	1:1000
Ki67	MIB-1	Mouse	Dako – M7240	Heat induced	1:1250
ZAP70	YE291	Rabbit	Abcam – ab32429	Heat induced	1:100
CD5	4C7	Mouse	Leica Biosystems - CD5-4C7-L-CE	Heat induced	1:500

3.5 Dako autostainer programme

Table B. The Dako autostainer was set up for immunostaining using the following programme.

Reagent	Incubation time
Primary antibody	40 minutes
Dako wash buffer	Rinse
Super-enhancer	20 minutes
Dako wash buffer	Rinse
SS-label	30 minutes
Dako wash buffer	Rinse
DAB	10 minutes
dH_2O	Rinse

3.6 3,3'-diaminobenzidine (DAB)

DAB was prepared immediately before use. 1 drop (38µl) was added to 1ml stable DAB buffer included in the detection kit.

3.7 Acid Alcohol

1% HCl acid in 70% IMS

3.8 DPX

A commercially purchased ready to use, xylene-based permanent mountant used to coverslip TMA slides.

4. Flow Cytometry

Materials:

- Human γ-Globulin (HAG) – Sigma 4386
- BD Cytofix/Cytoperm Solution – BD Biosciences 554722
- PBS – Sigma Aldrich D8537
- FBS - Gibco Life Technologies 10500
- 4', 6'-Diamidino-2-Phenylindole, Dihydrochloride (DAPI) – Sigma D9564
- Deoxyribonuclease I from bovine pancreas (DNase) – Sigma D4513
- Recombinant Human HMGB1 – R&D Systems 1690-HMB-050
- Polyclonal neutralising goat anti-RAGE IgG antibody – R&D Systems AF1145
- FITC Annexin V Apoptosis Detection Kit I – BD Biosciences 556547. Kit includes:
    - 10X Annexin V Binding Buffer
    - FITC Annexin V
    - Propidium Iodide Staining Solution
- Ionomycin – Sigma I0634
- GI254023X – Sigma SML0789

4.1 2% Human γ-Globulin (HAG)

1g HAG was dissolved in 50ml sterile PBS for 30 minutes at room temperature and store in 0.5ml aliquots at -20°C. 50µl per $1x10^6$ cells was used as blocking buffer and antibody diluent.

4.2 2% FBS flow cytometry wash buffer

Flow cytometry wash buffer was prepared by diluting 1ml FBS in 50ml PBS (2%).

4.3 Antibodies and dilutions used for flow cytometry

Table C. Conjugated, primary and secondary antibodies used in this study

Antibody	Clone	Isotype	Fluorochrome	Company (cat. No)	Dilution for 10^6 cells
RAGE	Polyclonal	Rabbit, IgG	-	Abcam ab37647	1:100
TLR9	26C593.2	Mouse, IgG	-	Abcam ab12121	1:100
TLR9	5G5	Mouse, IgG2a κ	FITC	Abcam ab58864	1:50
CD14	61D3	Mouse, IgG1 κ	PE-Cy5	Abcam ab25395	1:20

CD19	SJ25-C1	Mouse, IgG1 κ	PE-Cy7	Abcam ab81997	1:20
CD19	HIB19	Mouse, IgG1 κ	APC	BD Biosciences 555415	1:5
CD3	UCHT1	Mouse, IgG1 κ	FITC	DAKO F0818	1:20
CD3	UCHT1	Mouse, IgG1 κ	APC	BD Biosciences 555335	1:20
CD5	UCHT2	Mouse, IgG1 κ	APC-Cy7	BD Biosciences 563516	1:20
CD5	UCHT2	Mouse, IgG 1κ	PE/Cy7	eBioscience 25-0059-42	1:20
CD163	GH1/61	Mouse, IgG1 κ	APC	Biolegend 333609	1:20
CD68	Y1/82A	Mouse, IgG1 κ	PE	Biolegend 333808	1:20
ZAP70	IE7.2	Mouse, IgG1 κ	AF-488	ThermoFisher MHZAP7020	1:20
ADAM10 N-terminal	Polyclonal	Rabbit, IgG	-	Abcam ab39153	1:100
Rabbit IgG	Polyclonal	Goat, whole IgG	AF-488	Invitrogen A11034	1:200
Rabbit IgG	Polyclonal	Goat, whole IgG	AF-647	Invitrogen A21244	1:200
Mouse IgG	Polyclonal	Donkey, whole IgG	AF-647	Invitrogen A31571	1:200
Mouse IgG1 κ	-	-	FITC	BD Biosciences 556028	1:20
Mouse IgG1 κ	-	-	APC	BD Biosciences 555751	1:20
Mouse IgG1 κ	-	-	APC/Cy7	BD Biosciences 557873	1:20
Mouse IgG1 κ	-	-	PE/Cy7	BD Biosciences 557872	1:20

4.4 DAPI working solution (Sigma D9564)

10mg DAPI was dissolved in 2ml DMSO to give 50mg/ml the first stock solution which was 1:10 diluted with DMSO to make the second stock solution (50µg/ml). Aliquots were stored at -20°C in the dark. For flow cytometry, DAPI was diluted 1:1000 in 2% FBS wash buffer to give a working solution of 50ng/ml.

4.5 2% FBS flow cytometry wash buffer with DAPI

Cells were collected in 300µl 2% flow wash buffer with 50ng/ml DAPI for flow cytometry.

4.6 Deoxyribonuclease I from bovine pancreas (Sigma D4513)

10µg Deoxyribonuclease I (DNase) was diluted in 10ml sterile PBS to give 1µg/ml and stored at -20°C in 1ml aliquots.

4.7 Preparation of FITC Annexin V Apoptosis Detection Kit I (BD Biosciences 556547)

1X Annexin V Binding buffer (0.1M Hepes/NaOH (pH 7.4), 1.4M NaCl, 25mM $CaCl_2$) was prepared by diluting 1ml 10X Annexin V Binding Buffer in 9ml sterile distilled water; 100µl was used per $1x10^6$ cells. Annexin V-FITC and PI was ready-to-use on arrival; 5µl of each stain was used per $1x10^6$ cells.

5. Enzyme-Linked Immunosorbant Assay (ELISA)

Materials:

- Human HMGB1 ELISA Kit – IBL International ST51011. Kit includes:
    - Microtiter Plate (96 wells coated with polyclonal anti-HMGB1)
    - Peroxidase Enzyme Conjugate
    - HMGB1 Standard (from pig)
    - HMGB1 Positive Control (from pig)
    - Diluent Buffer
    - Enzyme Conjugate Diluent
    - 5X Wash Buffer (phosphate buffer, <0.5% Tween 20)
    - Colour Reagent A (TMB)
    - Colour Reagent B (0.005M hydrogen peroxide)
    - Colour Stop Solution (0.35M H_2SO_4)
    - Adhesive Foil
- Human S100B ELISA Kit – EMD Millipore EZHS100B-33K. Kit includes:
    - S100B ELISA Plate (96 wells pre-titered with human S100B antibodies)
    - 10X HRP Wash Buffer Concentrate (Tris-Buffered Saline with Tween-20)
    - S100B Standard
    - S100B Quality Control 1 and 2
    - Matrix Solution
    - 1X Assay Buffer
    - S100B Detection Antibody
    - Enzyme Solution (pre-titres streptavidin-horseradish peroxidase conjugate)
    - Substrate (3,3',5,5'-tetramethylbenzidine)
    - Stop Solution (0.3M HCl)
- Human RAGE ELISA Kit – Abcam ab100632. Kit includes:
    - RAGE ELISA Plate (96 wells pre-titre with anti-RAGE antibody)

- 20X Wash Buffer Concentrate
- Assay Diluent A
- 5X Assay Diluent B
- Biotinylated Anti-human RAGE
- Recombinant Human RAGE Standard
- 200X HRP-Streptavidin Concentrate
- TMB One-step
- Substrate Reagent
- Stop Solution

6. Immunofluorescent Microscopy

Materials:

- Superfrost™ Plus Slides – VWR 631-0108
- BD Cytofix/Cytoperm Solution – BD Biosciences 554722
- Tris-Buffered Saline with 0.1% Tween-20 (TBST)
    - Tween-20 – Sigma P7949
- Blocking buffer with:
    - Donkey serum – Sigma D9663
    - Goat serum – Sigma G9023
    - Saponin – Fluka Biochemika 47036
- 4', 6'-Diamidino-2-Phenylindole, Dihydrochloride (DAPI) – Sigma D9564
- ProLong Gold anti-fade mountant – Life Technologies P36930

6.1 1X TBST

10X TBS stock was prepared by mixing 300ml 5M NaCl with 500ml 1M Tris-base adjusted to pH7.4 with HCl and 200ml deionised water. 1X TBST was prepared by diluting 100ml of 10X TBS stock in 900ml of deionised water. 1ml Tween-20 was added to 1L 1X TBS to give 0.1% TBST.

6.2 5% donkey and 5% goat serum blocking buffer

50ml blocking buffer was prepared by adding 50mg saponin to 47.5ml 1X TBS and addition of 2.5ml donkey or goat serum. 10ml aliquots were stored at -20°C. Cells that were co-stained

with both donkey anti-mouse IgG and goat anti-rabbit IgG secondary antibodies were blocked with 50µl 1:1 ratio of mixed 5% donkey and 5% goat serum blocking buffer.

6.3 Primary and secondary antibodies used in this study

Table D. Primary antibodies used in this study

Antibody	Clone	Isotype	Company (cat. No)	Dilution
RAGE	Polyclonal	Rabbit, IgG	Abcam ab37647	1:100
TLR9	26C593.2	Mouse, IgG	Abcam ab12121	1:100
MyD88	EPR590(N)	Rabbit, IgG	Abcam ab133739	1:100
NF-κB p65	F-6	Mouse, IgG1κ	Santa Cruz sc-8008	1:20
STAT3-P^{Y705}	D3A7	Rabbit, IgG	Cell Signalling Technology 9145	1:100

Table E. Secondary conjugated antibodies used in this study.

Antibody	Clone	Isotype	Fluorochrome	Company (cat. No)	Dilution
Rabbit IgG	Polyclonal	Goat, whole IgG	AF-488	Invitrogen A11034	1:100
Mouse IgG	Polyclonal	Donkey, whole IgG	AF-488	Invitrogen A21202	1:100
Mouse IgG	Polyclonal	Donkey, whole IgG	AF-546	Invitrogen A10036	1:100

6.4 DAPI

10mg DAPI was dissolved in 2ml DMSO to give 50mg/ml the first stock solution which was 1:10 diluted with DMSO to make the second stock solution (50µg/ml). Aliquots were stored at -20°C in the dark. For fluorescence microscopy, DAPI was diluted 1:1000 in TBST to give a working solution of 50ng/ml.

7. ImageStream X Mark II Flow Cytometry

Materials:

- BD Cytofix/Cytoperm Solution – BD Biosciences 554722
- Tris-Buffered Saline with 0.1% Tween-20 (TBST)
    - Tween-20 – Sigma P7949
- Blocking buffer with:
    - Donkey serum – Sigma D9663
    - Goat serum – Sigma G9023

- Saponin – Fluka Biochemika 47036

- 4', 6'-Diamidino-2-Phenylindole, Dihydrochloride (DAPI) – Sigma D9564

7.1 Primary and Secondary antibodies used in this study

Table F. Primary antibodies used in this study

Antibody	Clone	Isotype	Company (cat. No)	Dilution
RAGE	Polyclonal	Rabbit, IgG	Abcam ab37647	1:100
TLR9	26C593.2	Mouse, IgG	Abcam ab12121	1:50
MyD88	EPR590(N)	Rabbit, IgG	Abcam ab133739	1:100
NF-κB p65	F-6	Mouse, IgG1κ	Santa Cruz sc-8008	1:20
STAT3-P^{Y705}	D3A7	Rabbit, IgG	Cell Signalling Technology 9145	1:100

Table G. Secondary antibodies used in this study

Antibody	Clone	Isotype	Fluorochrome	Company (cat. No)	Dilution
Rabbit IgG	Polyclonal	Goat, whole IgG	AF-488	Invitrogen A11034	1:200
Rabbit IgG	Polyclonal	Goat, whole IgG	AF-647	A21244	1:200
Mouse IgG	Polyclonal	Donkey, whole IgG	AF-488	Invitrogen A21202	1:200
Mouse IgG	Polyclonal	Donkey, whole IgG	AF-647	Invitrogen A31571	1:200

8. Western Blotting

Materials:

- PBS – Sigma Aldrich D8537
- TBS – Trizma® Base - Sigma T1503
- Tween®-20 – Sigma P7949
- CelLytic M Cell Lysis reagent - Sigma C2978
- Protease inhibitor cocktail set II - Sigma P8340-1ML
- Phosphatase inhibitor cocktail set I – Sigma P2850
- Phosphatase inhibitor cocktail set II - Sigma P5726
- Bio-Rad Protein Assay Reagent Concentrate – Bio-Rad 500-0006
- Pierce™ Bovine Serum Albumin (BSA) Standard Ampules – Thermo Scientific 23209
- 20X MOPS Running Buffer – Invitrogen NP0001
- Transfer Buffer
- MagicMark™ XP Western standard – Thermo Fisher Scientific LC5602
- NuPage® LDS sample loading buffer 4X – Invitrogen NP0007

- NuPAGE® Reducing Agent 10X – Invitrogen NP0009
- NuPAGE® Antioxidant – Invitrogen NP0005
- Nu-PAGE® 4-12% Bis-Tris gel – Invitrogen NP0322
- PVDF membrane – EMD Millipore IPVH304FO
- Polyvinylpyrrolidone (PVP) – Sigma P5288
- FCS – Gibco Life Technologies 10500
- Sodium Azide – Sigma S8032
- SuperSignal™ West Pico PLUS Chemiluminescent Substrate – Thermo Scientific 1863098
- Restore PLUS® Western blot stripping buffer – Thermo Scientific 21059

8.1 Preparation of CelLytic M cell lysis buffer

Protease and phosphatase inhibitors were diluted 1:100 in CelLytic M cell lysis buffer prior to use to limit de-phosphorylation and protein degradation. Cell lysis buffer was kept on ice.

8.2 Preparation of Bio-Rad Protein Assay Dye Reagent

A 1X Bio-Rad protein assay dye working solution was prepared by diluting 40ml of reagent in 200ml of deionised water (1:5) and passed through filter paper to remove insoluble material. The working solution was kept in the dark at 4°C.

8.3 Bovine Serum Albumin (BSA) 0.5mg/ml stock solution

0.5mg/ml stock concentration of BSA was prepared by diluting 500µl of 2.0mg/ml Pierce™ BSA ampule in 1.5ml deionised water; 500µl aliquots were stored at -20°C.

8.4 1X MOPS Running Buffer

50ml of 20X MOPS running buffer was diluted in 950ml deionised water prior to use, to give a 1X working solution; MOPS concentrate was stored at 4°C.

8.5 Reducing LDS sample buffer and antioxidant 1X MOPS buffer

For reducing SDS-PAGE, NuPAGE® reducing agent was diluted 1:10 in LDS sample lysis buffer - 2µl in 18µl, respectively. 500µl NuPAGE® antioxidant was mixed with 200ml 1X MOPS buffer before pouring into the upper chamber.

8.6 Transfer Buffer

A 10X stock solution of transfer buffer was prepared by making 1L 0.25M Tris-base and 1.92M Glycine in deionised water. A working 1X transfer buffer solution was prepared by mixing

100ml 10X transfer buffer stock with 200ml of methanol and 700ml deionised water. 1X transfer buffer was stored at 4°C.

8.7 Polyvinylpyrolidine (PVP) blocking buffer and antibody diluent

5% PVP was prepared by dissolving 50g PVP in 1L 0.2% TBST and stored at 4°C. 0.5ml FBS was added to 10ml 5% PVP as the non-specific blocking reagent.

8.8 Antibodies used for Western blotting

Table H. Primary antibodies used in this study

Antibody	Clone	Isotype	Company (cat. No)	Dilution for probing
RAGE	Polyclonal	Rabbit, IgG	Abcam ab37647	1:3000
TLR9	26C593.2	Mouse, IgG	Abcam ab12121	1:3000
MyD88	EPR590(N)	Rabbit, IgG	Abcam ab133739	1:3000
HMGB1			Abcam	1:3000
NF-κB p65	F-6	Mouse, IgG1κ	Santa Cruz sc-8008	1:500
NF-κB-P-(P65)	93H1	Rabbit, IgG	Cell Signalling Technology 3033S	1:3000
STAT3-PY705	D3A7	Rabbit, IgG	Cell Signalling Technology 9145	1:3000
STAT3	Polyclonal	Rabbit, IgG	Cell Signalling Technology 12640S	1:3000
GAPDH	Polyclonal	Rabbit, IgG	Cell Signalling Technology 5174S	1:3000

Table I. Secondary antibodies used in this study

Antibody	Clone	Isotype	Company (cat. No)	Dilution for probing
Anti-rabbit IgG-HRP	Polyclonal	Goat, IgG	Cell Signalling Technology 7074S	1:3000
Anti-mouse IgG-HRP	Polyclonal	Horse, IgG	Cell Signalling Technology 7076S	1:3000

8.9 PVP with 10% sodium azide

10g of sodium azide was dissolved in 100ml deionised water to give a 10% azide stock solution. 100µl of 10% azide solution was added to 10ml PVP blocking buffer (1:100) for overnight primary antibody incubation.

8.10 Enhanced chemiluminescent (ECL) reagent preparation

500µl of SuperSignal West Pico PLUS Luminol/Enhancer Solution was mixed with 500 µl of SuperSignal West Pico PLUS Stable Peroxide Solution and left to equilibrate for 5 minutes at room temperature. Probed membranes were incubated with 1ml of 1:1 ECL solution for 5 minutes before exposure. Fresh ECL was used per blot.

9. Co-Immunoprecipitation (co-IP)

Materials:

- CelLytic M Cell Lysis Buffer with protease and phosphatase inhibitors – Sigma
- PBS – Sigma D8537
- Tween-20 – Sigma P7949
- Dynabeads™ Protein A
- DynaMag™-2 – Thermo Scientific 12321D
- NuPAGE® LDS Sample Buffer
- NuPAGE® Sample Reducing Agent
- Normal anti-mouse IgG – sc
- Mouse anti-TLR9 – Abcam ab12121

9.1 Phosphate Buffered Saline with 0.02% Tween-20 (PBST)

50ml PBS was mixed with 20µl Tween-20 to give 0.02% PBST for washing steps and Dynabed™-antibody incubation.

9.2 Co-IP Elution Buffer

18µl LDS sample buffer was mixed with 2µl 10X Reducing agent to make denaturing co-IP elution buffer; 20µl was used per sample. Antioxidant was included in SDS gel electrophoresis to ensure proteins were not oxidised as they migrate through the gel.

9.3 Antibodies used in this study

Table J. Primary antibodies used in this study

Antibody	Clone	Isotype	Company (cat. No)	Dilution
TLR9	26C593.2	Mouse, IgG	Abcam ab12121	5µg for immunoprecipitation 1:3000 for probing
IgG		Mouse, IgG	Sc-	5µg for immunoprecipitation
RAGE	Polyclonal	Rabbit, IgG	Abcam ab37647	1:3000
MyD88	EPR590(N)	Rabbit, IgG	Abcam ab133739	1:100
HMGB1	Polyclonal	Rabbit, IgG	Abcam ab18256	1:3000

Table K. Secondary antibodies used in this study

Antibody	Clone	Isotype	Company (cat. No)	Dilution for probing
Anti-rabbit IgG-HRP	Polyclonal	Goat, IgG	Cell Signalling Technology 7074S	1:3000
Anti-mouse IgG-HRP	Polyclonal	Horse, IgG	Cell Signalling Technology 7076S	1:3000

10. Mass Spectrometry

Materials:

- Pierce BCA Protein Assay Kit – Thermoscientific 23225
- Deoxyribonuclease I (DNAse I), from bovine pancreas – Sigma D4513
- Phosphatase inhibitors – Na_3VO_4, NaF
- Protease inhibitors – Pyrophosphate, β-glycerolphosphate
- Urea – Sigma 08884
- DTT – Sigma 000000010708984001
- IAM – Sigma I1149
- HEPES – Sigma H3375
- Glycolytic acid
- TiO2 beads – Merck 539722
- Glygen EMPTY spintips – Thermoscientific 84850
- LC-MS/MS instrumentation – Q Exactive Plus

10.1 Cell wash

50ml PBS and phosphatase inhibitors (1mM Na3VO4 (0.5ml of 100mM stock per 50 ml) and 1mM NaF (100µl of 0.5M stock per 50ml)).

10.2 Cell lysis buffer

20mM HEPES pH 8.0, 8M Urea, 1mM Na3VO4 (100µl of 100mM stock), 1mM NaF (20µl of 0.5M stock), 2.5mM pyrophosphate Na2H2P2O7 (100µl of 0.25M stock), 1mM β-glycerolphosphate (10µl of 1M stock).

10.3 HEPES buffer

20mM HEPES pH 8.0

11. Molecular Biology Techniques

Materials:

- Full-length RAGE plasmid – IBL international HM-310
- Endogenous-secreted RAGE plasmid – IBL international HM-311
- Subcloning efficiency DH5α competent cells – Invitrogen 18265-017
- QIAGEN plasmid purification midi kit – QIAGEN 12143
- FastDigest BamHI – ThermoScientific FD0054
- FastDigest SmaI – ThermoScientific FD0054

11.1 FL-RAGE and es-RAGE pcDNA3 plasmids

FL-RAGE and es-RAGE on a pcDNA3 backbone were sourced from HMGBiotech via IBL International. 20µg of dried plasmid DNA was reconstituted to 1.4µg/µl and 0.768µg/µl in RNase-free water for FL-RAGE and es-RAGE, respectively, and stored at -20°C. The pcDNA3 vector includes a CMV promoter for mammalian expression and genes for ampicillin bacterial resistance and neomycin selectable marker. FL-RAGE was inserted between EcoRI and XhoI restriction sites and es-RAGE was inserted between EcoRI and Xba restriction sites.

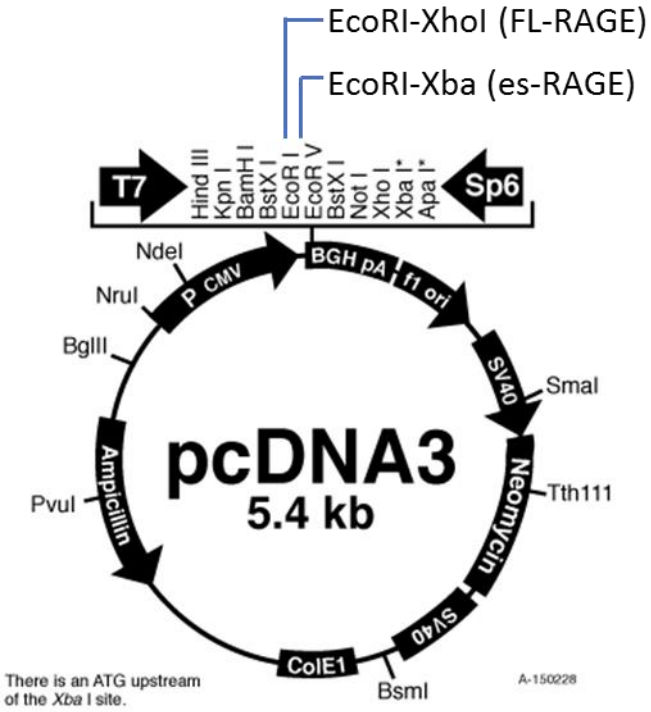

Appendix Figure 1. pcDNA3 plasmid backbone

11.2 Luria broth (LB) media

10g tryptone, 5g yeast extract and 10g NaCl was dissolved in 800ml of distilled water. The pH was adjusted to 7.0 with NaOH and the volume brought up to 1L with distilled water. LB media was sterilised by autoclaving.

11.3 Ampicillin agar plates

Bacteria are unable to digest agar, so growing antibiotic resistant bacteria on antibiotic containing agar gel allows isolation of single antibiotic resistant bacteria growing on top of the gel, compared to growth in solution such as LB media. 5g peptone, 10g peptone from casein, 10g NaCl, 12g agar-agar was dissolved in 1L sterile distilled water. Agar was sterilised by autoclaving and left to set before use. Upon use, agar was warmed in a 60°C water bath until molten and ampicillin added to a final concentration of 100µg/ml. Ampicillin-agar was poured into sterile 60mm x 15mm plates next to a working flame to ensure sterility and left to set. Plates were sealed and stored at 4°C until use.

11.4 Glycerol bacteria stock

1ml 100% glycerol was diluted to 50% with 1ml sterile distilled water. 500µl of 50% glycerol was mixed with 500µl of overnight bacterial culture in a 2ml cryovial; bacteria stocks were stored in -80°C.

11.5 Tris-EDTA (TE) buffer

1M Tris-HCl was prepared by adding 60.6g Tris-base to 500ml deionised water; Tris-base was adjusted to pH 8.0 with NaOH. 0.5M EDTA was prepared by adding 18.6g EDTA in deionised water; the pH was adjusted to 8.0 with NaOH. 500ml of TE buffer was prepared by adding 5ml 1M Tris-HCl (pH 8.0) and 1ml 0.5M EDTA (pH 8.0) to 494ml deionised water. TE buffer was sterile filtered through a 0.22µM filter and plasmid DNA reconstituted in 500µl sterile TE buffer inside a tissue culture hood. 50µl aliquots were stored in -20°C for long term storage.

11.6 Restriction digest map

BamHI and SmaI restriction enzymes were chosen based on enzyme availability and restriction sites in the pcDNA3 plasmid backbone and FL-RAGE and es-RAGE sequences. There is 1x BamHI and 1x SmaI cut site in the pcDNA3 plasmid vector. For the FL-RAGE plasmid, BamHI has 3 cut sites in total (2x in FL-RAGE sequence and 1x in pcDNA3 backbone) and SmaI has 2 cut sites in total (1x in FL-RAGE sequence and 1x pcDNA3 backbone). For es-RAGE plasmid, BamHI has 2 cut sites in total (1x in es-RAGE sequence and 1x in pcDNA3 backbone) and SmaI has 2 cut sites in total (1x es-RAGE sequence and 1x in pcDNA3 backbone).

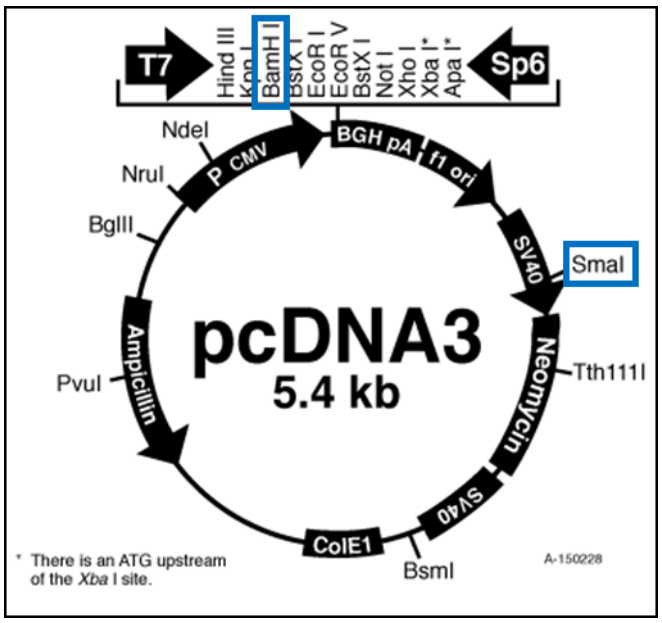

Appendix Figure 2. pcDNA3 plasmid backbone

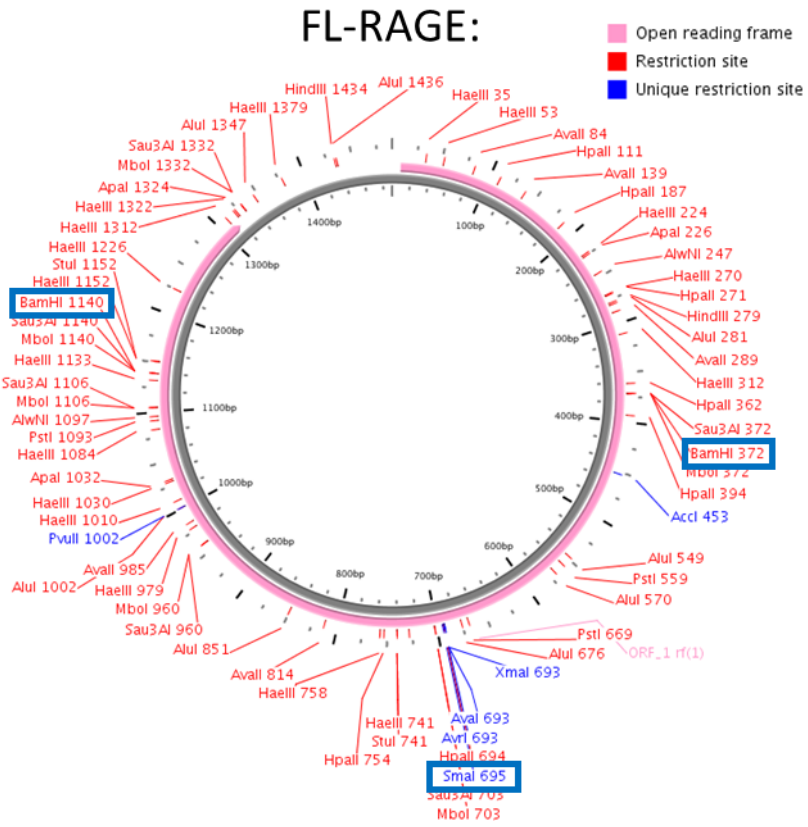

Appendix Figure 3. Full-length RAGE plasmid – IBL international HM-310

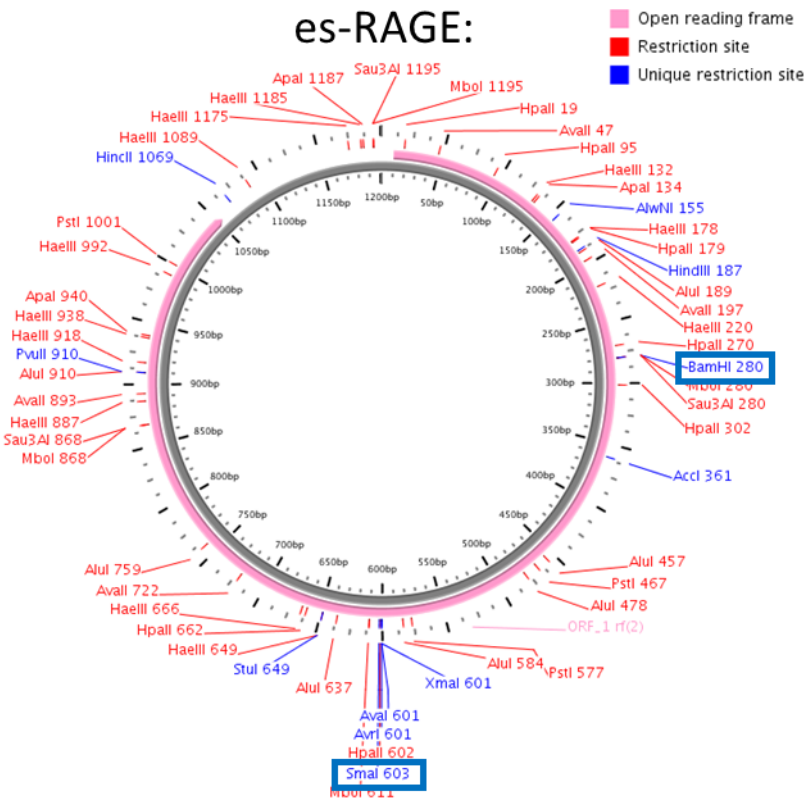

Appendix Figure 4. Endogenous-secreted RAGE plasmid – IBL international HM-311

11.7 Tris-borate-EDTA (TBE) buffer

10X TBE buffer was prepared by adding 108g Tris-base, 55g boric acid to 600ml deionised water. 40ml of 0.5M EDTA pH 8.0 (from Appendix I, 11.6) was added and the total volume brought up to 1L with deionised water. A working 1X TBE solution was prepared by mixing 100ml 10X TBE stock with 900ml deionised water.

11.8 JetPRIME reagent and DNA mix

5µg of plasmid DNA was mixed with 500µl of jetPRIME buffer and mixed. 10µl of JetPRIME reagent was added and the DNA-reagent mix was incubated for 10 minutes at room temperature.

12. Drug Preparation

Materials:

- Recombinant Human HMGB1 protein– R&D Systems 1690-HMB-050
- Polyclonal neutralising goat anti-RAGE IgG antibody – R&D Systems AF1145

- Class B CpG Oligonucleotide (ODN) – Invivogen 2006 (ODN 7909)
- Ionomycin – Sigma I0634
- GI254023X – Sigma SML0789

12.1 Preparation of HMGB1 200µg/ml stock solution (R&D Systems 1690-HMB-050)

50µg HMGB1 was diluted in 250µl sterile PBS to give a stock concentration of 200µg/ml and stored at -80°C in 5µl aliquots. 200ng/ml and 500ng/ml final concentrations were used in cell stimulations.

12.2 Preparation of rabbit anti-RAGE neutralising antibody (R&D Systems AF1145)

100µg of polyclonal goat anti-RAGE IgG was diluted in 100µl sterile PBS to give 1µg/ml stock concentration; 10µl aliquots were stored in -20°C. 4-12µg/ml can inhibit 50% RAGE in ELISAs, so a final concentration of 10µg/ml anti-RAGE was used *in vitro* for surface RAGE inhibition.

12.3 Preparation of Class B CpG ODN 500mM stock solution (Invivogen 2006 ODN 7909)

200µg ODN 2006 was resuspended in 52µl provided endotoxin-free water to give a stock concentration of 500µM. Aliquots were stored at -20°C. A working solution of 1µM was used for *in vitro* assays by adding 2µl/ml.

12.4 Preparation of ionomycin 1mM stock solution (Sigma I0634)

1mg of ionomycin (molecular weight = 747.08) was diluted in 700µl sterile DMSO to give 2mM stock concentration; aliquots were stored at -20°C. A working ionomycin concentration of 500nM was used for cell stimulations.

12.5 Preparation of GI254023X 10mM stock solution

5mg of GI254023X (molecular weight = 391.50) was diluted in 1277µl sterile DMSO to give 10mM stock concentration; stored at 4°C in the dark. Final GI254023X concentrations of 5µM, 10µM and 20µM were used to inhibit ADAM10 *in vitro*.

Appendix II

Chapter III TMAs

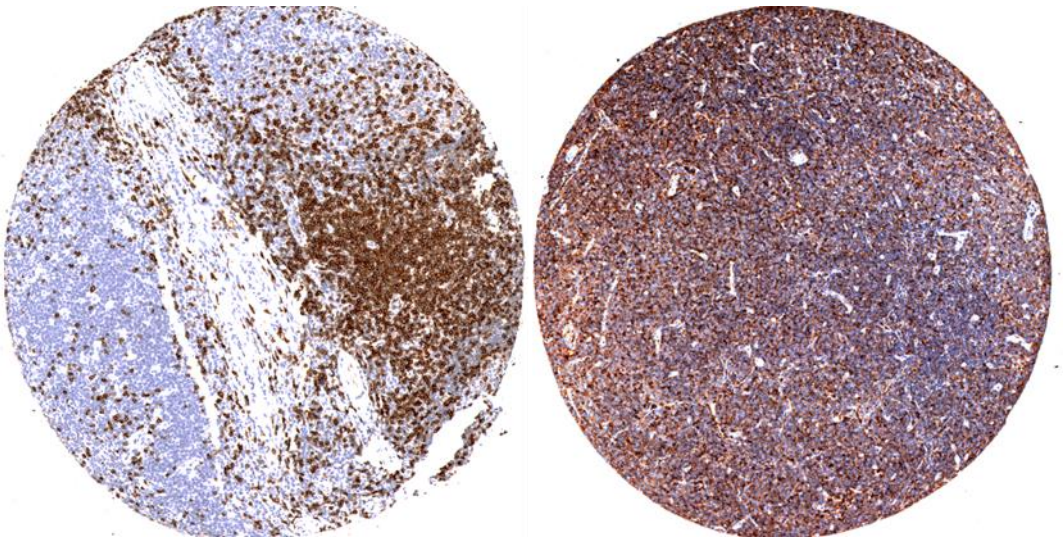

Appendix Figure 5. Representative images of immunohistochemical staining of CD5 in primary CLL LN TMAs
Representative images of CD5 staining in primary CLL LN tissue biopsies arrayed onto TMAs; 1mm^2 imaged LN cores are from 2 CLL patients. CD5 staining visualised in brown with DAB chromogen, and nuclei visualised in blue with haematoxylin staining. Areas high in brown CD5+ staining was selected for image analysis and ARIOL software image analysis training; i.e. right half of the first LN core and the whole of the second LN core.

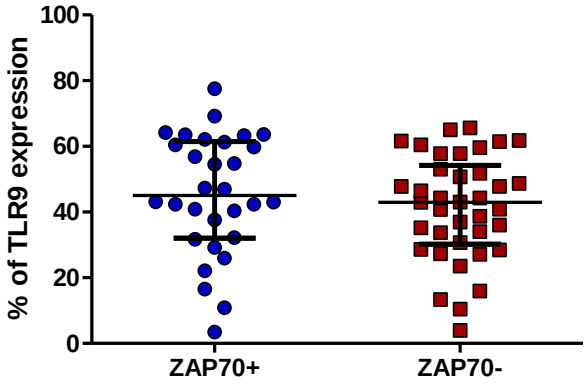

Appendix Figure 6. Comparison of CLL TLR9 whole LN core expression with ZAP70 positivity
Expression levels of CLL TLR9 stained by IHC were quantified using the ARIOL digital image analysis software (Figure 3-4). ZAP70 positive or negative expression levels were obtained from our clinical database and stained by IHC on the same CLL LN TMA. Statistical differences between ZAP70+/- % TLR9 expression levels was analysed by an unpaired Mann Whitney U test; data are presented as medians with interquartile range.

Table L. Clinical information of CLL patient samples used in IHC/CLL LN TMAs

Patient ID	Ki-67 %	RAGE %	TLR9 %	Survival (years)	Censored survival	Zap70 (tissue)	Age	Binet Stage
	0.83	0.83	36.92	3.58	0	1	42	
5393	1.25	2.63	30.73	2.41	1	1	62	B
5313	3.70	2.74	60.43	14.01	0	1	52	A
5496	2.40	3.20	27.15	2.63	1	1	55	B
9303	3.18	4.31	40.84	5.38	1	2	53	A
5907	1.14	4.88	13.38	10.18	1	1	51	B
9480	18.49	10.58	66.22	11.76	0		50	
	0.64	13.70	10.46	9.00	0	1	59	A
7799	3.99	13.71	40.36	7.32	1	2	66	A
5474	2.25	13.87	32.18	13.98	1	2	52	A
	2.45	16.13	34.08	1.17	1	1	73	
4380	1.33	16.55	28.48	7.41	1	1	69	A
10278	2.62	18.29	15.94	8.89	0	1	71	A
1970	1.15	18.53	10.85	4.60	1	2	62	
7075	1.22	19.02	33.67	3.16	1	1	63	
421	2.97	20.53	3.48	8.05	0	2	31	
7234	3.02	21.31	44.31	9.83	1	1	48	A
8236	7.66	21.46	50.67	4.79	1	1	57	
	2.81	21.77	47.20	6.00	0		59	
8369	7.87	22.44	47.81	5.96	1	1	63	A
5428	0.43	23.71	25.98	6.55	1	2	55	B
7105	6.23	23.83	38.75	11.41	0	1	63	A
8556	10.71	25.30	53.08	7.96	1	1	58	A
	2.67	25.96	43.84	12.00	0		79	A
5441	0.27	26.03	42.35	3.45	1	2	68	A
	0.77	26.08	16.56	5.00	1	2		
1934	0.61	26.08	20.45	24.70	0		52	A
7631	2.42	27.57	29.22	7.89	0	2	56	A
7161	3.05	28.50	44.33	7.21	1	1	80	A
	0.24	28.70	51.82	6.67	0	1	40	B
7987	8.48	31.62	43.01	3.21	1	2	63	B
8154	8.28	32.20	42.40	5.80	1	2	48	A
5959	5.00	32.42	36.01	15.09	0	1	46	A
5464	0.21	35.47	33.70	21.54	1		27	B
8137	12.82	35.64	37.64	5.77	1	2	69	A
7247	0.96	35.77	3.93	9.07	0	1	78	A
5471	0.48	38.43	43.08	5.08	1	2	64	A
7754	2.30	38.54	61.79	6.44	1	1	57	B
6744	5.89	39.63	48.74	12.09	0	1	38	A
7398	4.22	41.02	28.64	8.71	1	1	64	C
8591	12.60	42.92	65.62	2.05	1	1	36	A
10584	2.40	43.52	47.28	12.46	0	2	41	B
1380	0.67	43.82	46.48	10.60	1	1	58	
7770	11.69	45.21	75.27	8.48	1		48	A
7536	9.55	45.23	61.46	18.65	0	1	69	

8590	0.76	45.28	40.87	5.39	0	1	50	
8774	9.70	47.50	61.25	7.58	0	2	46	A
5478	2.18	48.34	25.81	9.10	1		57	B
7446	3.46	49.27	23.52	2.52	1	1	63	
5483	0.26	49.88	40.78	9.45	1	1	63	A
	1.64	51.21	57.76	9.25	1	1	55	
8314	10.92	51.30	60.50	3.46	1	2	50	A
7675	7.46	51.89	43.01	16.67	0	1	43	A
8368	7.42	52.70	63.31	11.26	1	2	57	A
6351	1.68	52.80	53.84	12.33	0		67	
	5.02	53.88	64.19	4.58	1	2	50	
7431	4.48	54.07	46.93	5.36	1	2	63	A
5390	1.46	54.57	35.24	7.87	1	1	68	B
4798	4.44	56.25	61.60	15.81	0	1	61	
8371	11.25	56.56	57.78	7.79	0	1	74	A
9095	6.99	56.62	69.66	4.21	0		59	
7921	4.96	57.85	42.93	9.16	1	1	43	A
1861	0.40	58.59	31.98	11.44	1		58	
8131	9.63	59.72	59.81	6.85	0	2	54	A
7124	5.61	60.49	31.71	4.91	1	2	55	
5426	11.99	60.57	69.19	18.22	0	2	44	
10583	9.15	62.75	60.84	11.52	0			
8315	3.82	63.50	54.81	8.20	1	2	57	B
7585	10.02	64.08	65.00	8.30	0	1	49	A
6760	17.91	65.50	47.75	0.87	1	1	66	C
7596	17.56	66.77	77.53	4.57	1	2	59	C
	1.01	68.82	27.31	7.58	0	1	61	
7903	21.97	73.32	63.54	4.45	1	2	76	
8155	11.33	74.48	75.98	6.52	1		76	
9935	9.33	75.65	57.93	8.34	0		61	
7510	12.42	77.31	62.13	6.58	1	2	56	B
	2.86	78.07	22.10	12.00	0	2	56	
7230	8.36	78.55	59.63	4.64	1	1	80	
7147	4.72	80.80	54.50	0.46	0	2	26	
8918	6.26	87.22	56.85	2.98	1	2	59	A
8779	17.85	91.98	90.62	3.14	1		68	C
9745	14.81	93.14	61.77	1.82	0		68	
5385	1.82	94.40	63.62	0.31	1	2	62	B
8375	13.66	98.13	46.19	6.25	0		45	A
10108	4.11	100.00	27.51	3.87	1		73	
7549	21.95	100.00	29.86	8.91	0		67	A
9402	4.73	100.00	35.37	3.12	0		72	
9601	27.10	100.00	39.08	5.12	0		31	
8321	37.49	100.00	46.59	2.93	1		45	B
6738	21.71	100.00	66.85	9.38	1		47	A
7262	22.78	100.00	71.82	0.60	0		71	

A

Descriptive Statistics

	Mean	Std. Deviation	N
Tissue	1.38	.494	29
Blood	1.31	.471	29

B

Correlations

		Tissue	Blood
Tissue	Pearson Correlation	1	.551**
	Sig. (2-tailed)		.002
	N	29	29
Blood	Pearson Correlation	.551**	1
	Sig. (2-tailed)	.002	
	N	29	29

**. Correlation is significant at the 0.01 level (2-tailed).

C

Correlations

			Tissue	Blood
Spearman's rho	Tissue	Correlation Coefficient	1.000	.551**
		Sig. (2-tailed)	.	.002
		N	29	29
	Blood	Correlation Coefficient	.551**	1.000
		Sig. (2-tailed)	.002	.
		N	29	29

**. Correlation is significant at the 0.01 level (2-tailed).

Appendix Figure 7. Evaluation of the association between LN tissue ZAP70 score and PB ZAP70 score
ZAP70 LN expression levels were determined by IHC and classified as positive if LN brown DAB ZAP70 staining was >20%; PB ZAP70 expression was determined in clinic by flow cytometry (A). Data for both ZAP70 LN and PB expression was extracted from our clinical database for the CLL TMAs. The correlation between LN ZAP70 and PB ZAP70 was assessed by Pearson's product-moment correlation method (B) and Spearman's rho correlation analysis (C). Data are presented as correlation coefficient, P-value and sample size (N); *P*<0.01**.

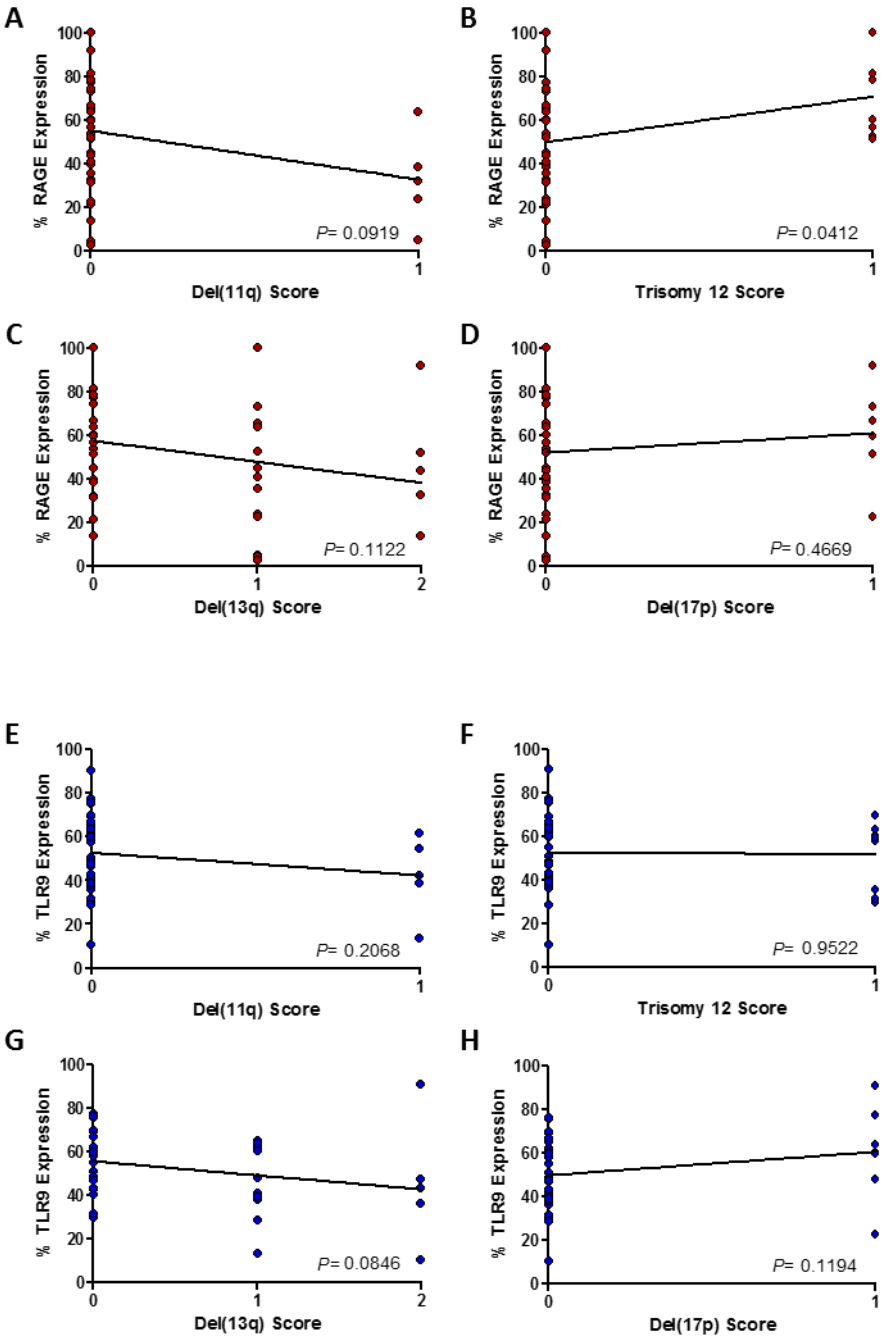

Appendix Figure 8. Evaluation of the association between RAGE and TLR9 and CLL cytogenetic abberations

CLL cytogenetic aberrations were compared to LN RAGE (A) and TLR9 (B) expression levels. Cytogenetic clinical data was extracted from our tissue bank clinical database and expression levels of RAGE and TLR9 were determined by IHC. Statistical differences were assessed by linear regression; $P<0.05$*.

Table M. RAGE, TLR9, Ki67, ZAP70 and age full backwards multivariate Cox regression analysis

Variables in the Equation

		B	SE	Wald	df	Sig.	Exp(B)	95.0% CI for Exp(B)	
								Lower	Upper
Step 1	RAGECAT			12.846	2	.002			
	RAGECAT(1)	-.392	.400	.964	1	.326	.675	.309	1.478
	RAGECAT(2)	2.429	.754	10.372	1	.001	11.344	2.587	49.734
	TLR9CAT			2.113	2	.348			
	TLR9CAT(1)	.300	.375	.640	1	.424	1.350	.648	2.813
	TLR9CAT(2)	.934	.652	2.055	1	.152	2.545	.710	9.127
	Ki67CAT			6.697	2	.035			
	Ki67CAT(1)	-.633	.427	2.199	1	.138	.531	.230	1.226
	Ki67CAT(2)	.975	.612	2.541	1	.111	2.652	.799	8.797
	ZAP70	.582	.360	2.619	1	.106	1.790	.884	3.623
	AGECat	.866	.353	6.017	1	.014	2.378	1.190	4.750
Step 2	RAGECAT			12.465	2	.002			
	RAGECAT(1)	-.112	.336	.112	1	.738	.894	.463	1.726
	RAGECAT(2)	2.497	.736	11.521	1	.001	12.140	2.872	51.321
	Ki67CAT			7.951	2	.019			
	Ki67CAT(1)	-.425	.400	1.127	1	.288	.654	.299	1.432
	Ki67CAT(2)	1.270	.529	5.750	1	.016	3.559	1.261	10.047
	ZAP70	.612	.365	2.814	1	.093	1.845	.902	3.772
	AGECat	.726	.343	4.473	1	.034	2.067	1.055	4.050

Note: Multivariate Cox regression analysis with backward selection was used to analyze multiple categorical variables. CAT: low expression, CAT(1): media expression; and CAT(2) High expression.

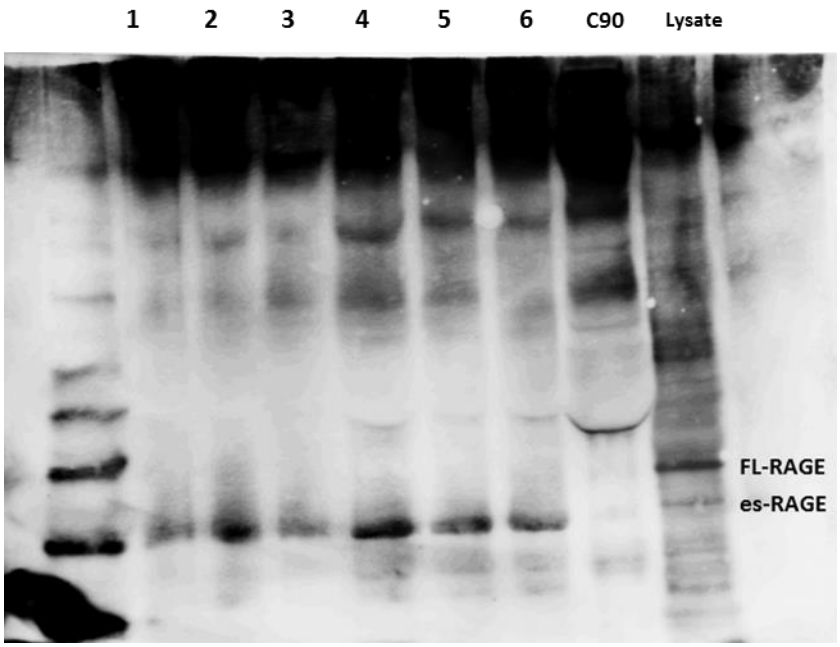

Appendix Figure 9. Western blot analysis of extracellular sRAGE isoforms in CLL patient plasma
Extracellular RAGE protein mass was assessed in 40µg of plasma protein from 6 CLL patients with high sRAGE (lanes 1-6) and compared with healthy control patient plasma (C90) and CLL patient (5959) whole cell lysate. Whole western blot is presented. FL-RAGE = Full-length RAGE, and es-RAGE = alternatively spliced endogenous secreted RAGE isoform whole cell lysate expression labelled in figure.

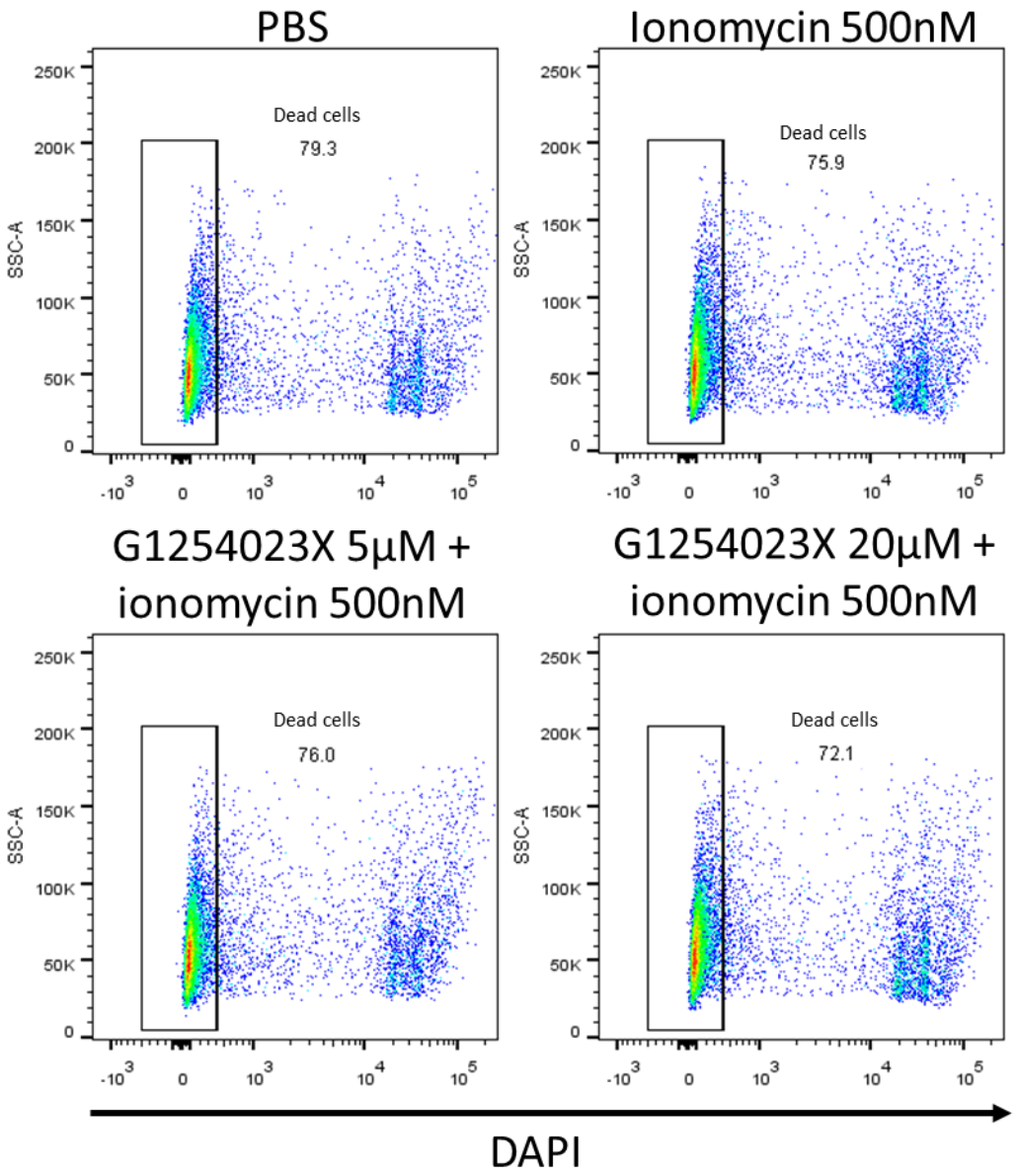

Appendix Figure 10. Evaluation of live and dead transfected HEK293 cell line post RAGE shedding by flow cytometry

RAGE shedding in FL-RAGE transfected HEK293 cells was measured following ADAM10 stimulation with 500nM ionomycin for 1-hour or ADAM10 inhibition with GI254023X 5µM, 10µM and 20µM for 1-hour prior to addition of 500nM ionomycin. Cell death in response to these treatments was assessed by DAPI staining for cells treated for 1 hours with PBS, 500nM ionomycin, 1-hour pre-treatment with GI254023X 5µM and 20µM with another hour of ionomycin treatment. DAPI is able to bind to DNA in dead cells with permeable cell membranes so can distinguish live cells with intact cell membranes from dead cells.

Table N. Significantly abundant phosphopeptides (log2 fold change ≥1 and *P*<0.05) following 15 minutes and 2 hours HMGB1 treatment in each patient compared to PBS baseline

8231		6799	
HMGB1 alone		HMGB1 alone	
15 minutes	2 hours	15 minutes	2 hours
K2C1_HUMAN	K1C13_HUMAN	YTHD2_HUMAN	ZN318_HUMAN
MPP10_HUMAN	UBP24_HUMAN	SAFB1_HUMAN	DNMBP_HUMAN
VIME_HUMAN	HP1B3_HUMAN	TRI33_HUMAN	ARHGB_HUMAN
FUBP1_HUMAN	H90B4_HUMAN	ZBT22_HUMAN	RPR1B_HUMAN
F122A_HUMAN	SAFB1_HUMAN	KANL1_HUMAN	SFR15_HUMAN
NCF1B_HUMAN	COX5A_HUMAN	ZN281_HUMAN	TBB8_HUMAN
RSMB_HUMAN	ATPG_HUMAN	SP4_HUMAN	SFR15_HUMAN
RAB6A_HUMAN	RBG1L_HUMAN	TFPT_HUMAN	UBE2O_HUMAN
RAB1A_HUMAN	FUBP1_HUMAN	CDK13_HUMAN	PI4KA_HUMAN
RB33B_HUMAN	RSMB_HUMAN	BORG4_HUMAN	TBB8_HUMAN
RAB15_HUMAN	G6PI_HUMAN	MFAP1_HUMAN	TBB4B_HUMAN
S12A6_HUMAN	GNAI2_HUMAN	AKP13_HUMAN	ZNT4_HUMAN
MARCS_HUMAN	SVIL_HUMAN	RBM25_HUMAN	TCOF_HUMAN
HNRL1_HUMAN	IL16_HUMAN	PSME2_HUMAN	NACC1_HUMAN
EF1D_HUMAN	RBBP4_HUMAN	HNRPU_HUMAN	PERQ2_HUMAN
SAFB2_HUMAN	MDHC_HUMAN	TCPB_HUMAN	ROA0_HUMAN
SRSF9_HUMAN	IFIX_HUMAN	CCD43_HUMAN	NUP53_HUMAN
LEUK_HUMAN	MBD3_HUMAN	KS6A1_HUMAN	SUN2_HUMAN
ZC3HD_HUMAN	CHAP1_HUMAN	TPR_HUMAN	ZEB2_HUMAN
USF1_HUMAN	RS11_HUMAN	SP140_HUMAN	NUMA1_HUMAN
TLK2_HUMAN	SMC3_HUMAN		PDLI2_HUMAN
TPD52_HUMAN	S10A8_HUMAN		BMPR2_HUMAN
PSIP1_HUMAN	TBB8_HUMAN		PTN14_HUMAN
TP53B_HUMAN	H2A1A_HUMAN		PTN14_HUMAN
LC7L2_HUMAN	ICAM5_HUMAN		PKCB1_HUMAN
IL2RG_HUMAN	PRDX2_HUMAN		RD23A_HUMAN
KLDC4_HUMAN	MIF_HUMAN		VEZF1_HUMAN
TPD54_HUMAN	DDX5_HUMAN		PKCB1_HUMAN
CAND1_HUMAN	GNA12_HUMAN		NCOR2_HUMAN
TB10C_HUMAN	HP1B3_HUMAN		PSA5_HUMAN
TR150_HUMAN	TCPZ_HUMAN		RBP56_HUMAN
SP100_HUMAN	CU129_HUMAN		SHIP1_HUMAN
	XPO2_HUMAN		KHDR1_HUMAN
	H2A1B_HUMAN		ACTY_HUMAN
	RS25_HUMAN		FOCAD_HUMAN
	UBC9_HUMAN		RBP56_HUMAN
	HNRL2_HUMAN		TRAK1_HUMAN
	TCPQ_HUMAN		MED31_HUMAN
	H2AV_HUMAN		AGK_HUMAN
	RAB28_HUMAN		MA7D1_HUMAN
	ILEU_HUMAN		MYPT1_HUMAN
	H15_HUMAN		AHNK_HUMAN
	RL11_HUMAN		KCY_HUMAN

API5_HUMAN	TLE1_HUMAN
1433S_HUMAN	VRK3_HUMAN
BCR_HUMAN	FIS1_HUMAN
SRSF1_HUMAN	FA65B_HUMAN
PPIA_HUMAN	SAC1_HUMAN
ERP29_HUMAN	PEG10_HUMAN
TRIP4_HUMAN	SYNE3_HUMAN
K1614_HUMAN	ZEP2_HUMAN
RPKL1_HUMAN	ZFAN5_HUMAN
ARPC4_HUMAN	MCAF1_HUMAN
DBLOH_HUMAN	MYO9B_HUMAN
HNRPU_HUMAN	CAC1A_HUMAN
ATPB_HUMAN	
ENOB_HUMAN	
HNRDL_HUMAN	
G3P_HUMAN	
DDI2_HUMAN	
DDI2_HUMAN	
BCR_HUMAN	
RLA0L_HUMAN	
EF1A1_HUMAN	
TRY1_HUMAN	
FA98B_HUMAN	
APT_HUMAN	
KI26B_HUMAN	
PKHJ1_HUMAN	
H12_HUMAN	
HMGA1_HUMAN	
FBLL1_HUMAN	
HNRH1_HUMAN	
H2B1B_HUMAN	
CH10_HUMAN	
MRE11_HUMAN	
RAN_HUMAN	
HNRPD_HUMAN	
HNRPM_HUMAN	
SRS10_HUMAN	
HNRPC_HUMAN	
NUCKS_HUMAN	
MRE11_HUMAN	
SRRM2_HUMAN	
PROF1_HUMAN	
LOX12_HUMAN	
DDX17_HUMAN	
HNRPK_HUMAN	
RPRD2_HUMAN	
RPRD2_HUMAN	
TR150_HUMAN	
ADT3_HUMAN	
SAFB1_HUMAN	

TM109_HUMAN	
HNRPC_HUMAN	
NUCKS_HUMAN	
TBA4A_HUMAN	
UTP18_HUMAN	
BCLF1_HUMAN	
ENPL_HUMAN	
HNRPD_HUMAN	
CXCR4_HUMAN	
EVPLL_HUMAN	
KPCB_HUMAN	
MCM3_HUMAN	
HNRPC_HUMAN	
GBG1_HUMAN	
ATPA_HUMAN	
CX7A2_HUMAN	
TCP4_HUMAN	
VPS4B_HUMAN	
H31T_HUMAN	
SSRP1_HUMAN	
SSRP1_HUMAN	
MINK1_HUMAN	
GDIR2_HUMAN	
RBMX_HUMAN	
MECP2_HUMAN	
COX5B_HUMAN	
HNRL2_HUMAN	
API5_HUMAN	
SRSF6_HUMAN	
CROCC_HUMAN	
COTL1_HUMAN	
TPM1_HUMAN	

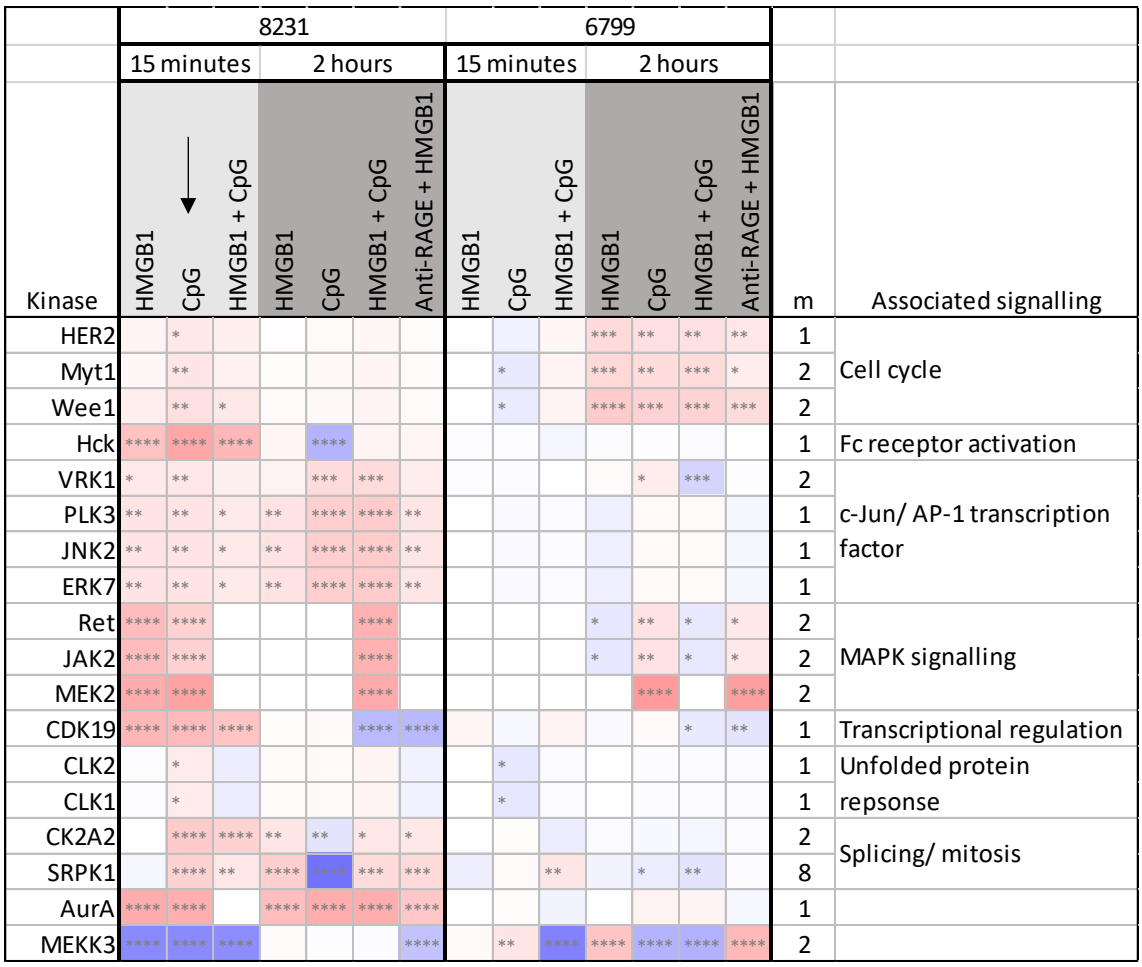

Appendix Figure 11. Heat map showing the enrichment of substrate groups for the different kinases calculated by KSEA algorithm, with significant abundance following CpG treatment for 15 minutes for patient 8231

Cell samples were treated, processed and phosphopeptides quantified by LC/MS-MS as previously described in Figure 5 10. Enrichment of substrate groups was calculated by the KSEA algorithm and divided by the abundance of phosphopeptides in the PBS treated sample. Heat map colours correspond to the coloured enrichment key in Figure 5 10 and indicates -5 to +5-fold enrichment compared to PBS treated sample. Statistical significance of these changes was calculated by Student's t test compared to PBS treated samples; P<0.05*, P<0.01**, P<0.001***, P<0.0001****. m, number of substrates in the indicated kinase substrate group. KSEA results were filtered based on significantly abundant substrate groups for patient 8231 following CpG-B class for 15 minutes (column indicated by arrow).

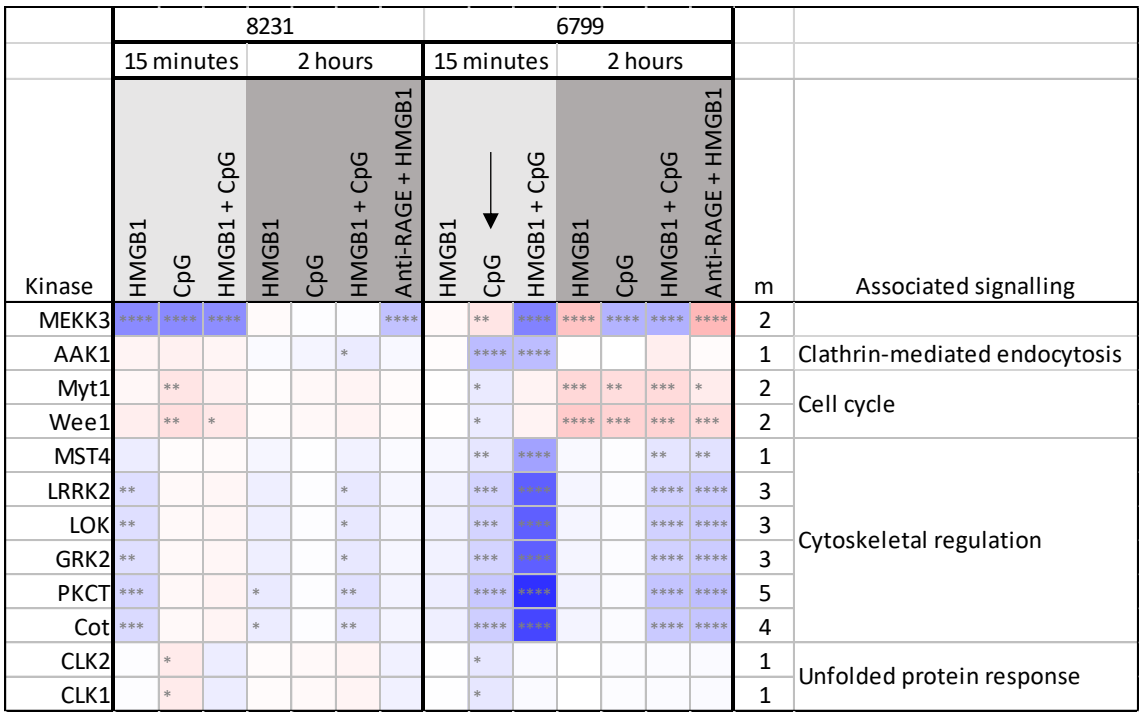

Appendix Figure 12. Heat map showing the enrichment of substrate groups for the different kinases calculated by KSEA algorithm, with significant abundance following CpG treatment for 15 minutes for patient 6799

Cell samples were treated, processed and phosphopeptides quantified by LC/MS-MS as previously described in Figure 5 10. Enrichment of substrate groups was calculated by the KSEA algorithm and divided by the abundance of phosphopeptides in the PBS treated sample. Heat map colours correspond to the coloured enrichment key in Figure 5 10 and indicates -5 to +5-fold enrichment compared to PBS treated sample. Statistical significance of these changes was calculated by Student's t test compared to PBS treated samples; P<0.05*, P<0.01**, P<0.001***, P<0.0001****. m, number of substrates in the indicated kinase substrate group. KSEA results were filtered based on significantly abundant substrate groups for patient 6799 following CpG-B class for 15 minutes (column indicated by arrow).

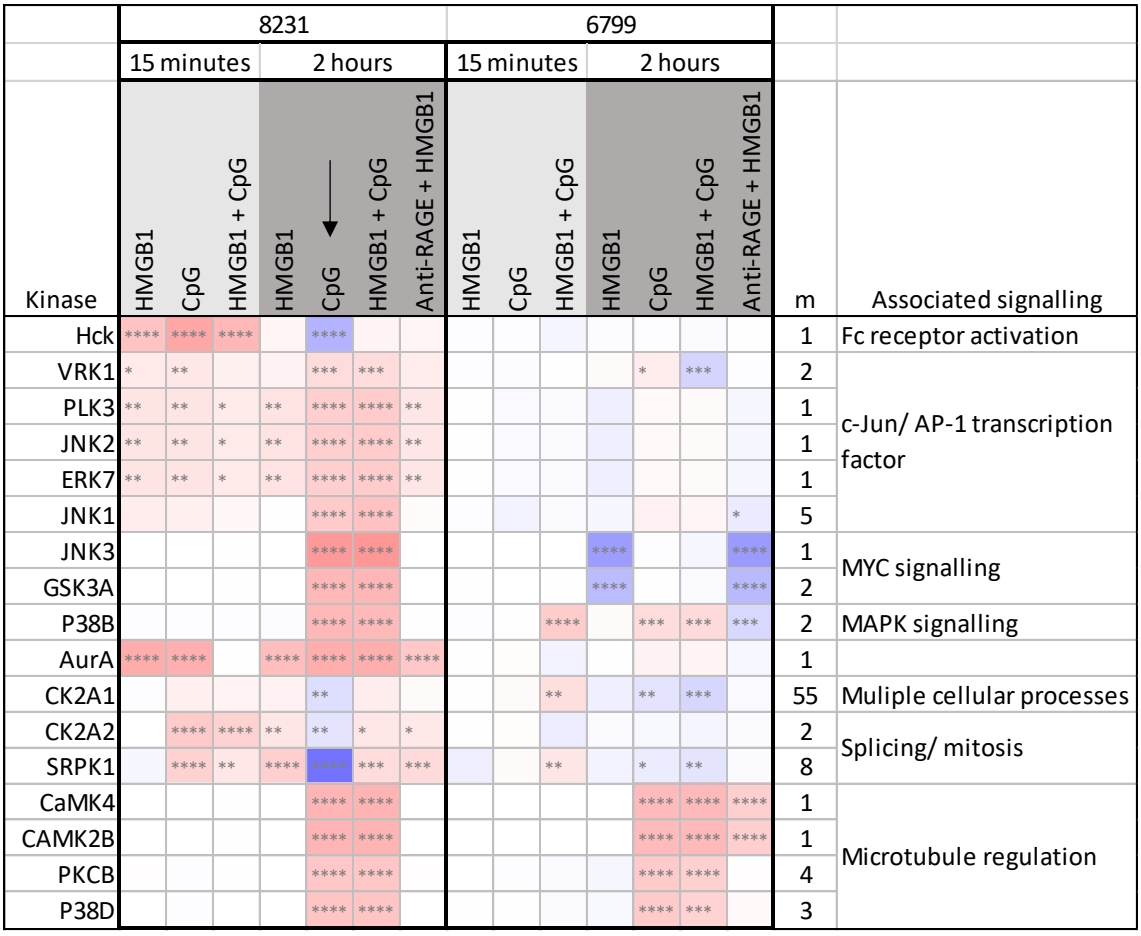

Appendix Figure 13. Heat map showing the enrichment of substrate groups for the different kinases calculated by KSEA algorithm, with significant abundance following CpG treatment for 2 hours for patient 8231

Cell samples were treated, processed and phosphopeptides quantified by LC/MS-MS as previously described in Figure 5 10. Enrichment of substrate groups was calculated by the KSEA algorithm and divided by the abundance of phosphopeptides in the PBS treated sample. Heat map colours correspond to the coloured enrichment key in Figure 5 10 and indicates -5 to +5-fold enrichment compared to PBS treated sample. Statistical significance of these changes was calculated by Student's t test compared to PBS treated samples; P<0.05*, P<0.01**, P<0.001***, P<0.0001****. m, number of substrates in the indicated kinase substrate group. KSEA results were filtered based on significantly abundant substrate groups for patient 8231 following CpG-B class for 2 hours (column indicated by arrow).

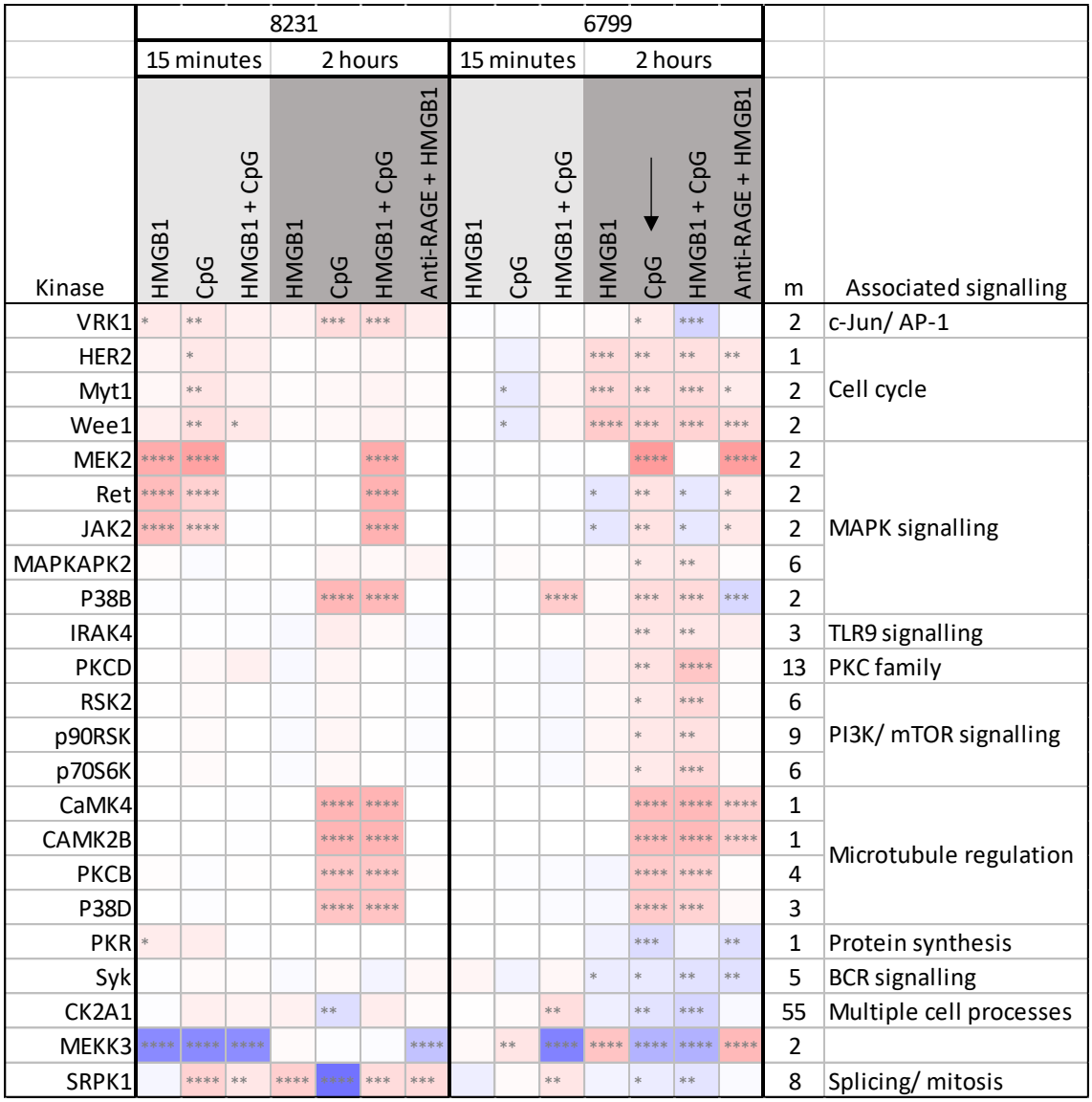

Appendix Figure 14. Heat map showing the enrichment of substrate groups for the different kinases calculated by KSEA algorithm, with significant abundance following CpG treatment for 2 hours for patient 6799

Cell samples were treated, processed and phosphopeptides quantified by LC/MS-MS as previously described in Figure 5 10. Enrichment of substrate groups was calculated by the KSEA algorithm and divided by the abundance of phosphopeptides in the PBS treated sample. Heat map colours correspond to the coloured enrichment key in Figure 5-10 and indicates -5 to +5-fold enrichment compared to PBS treated sample. Statistical significance of these changes was calculated by Student's t test compared to PBS treated samples; P<0.05*, P<0.01**, P<0.001***, P<0.0001****. m, number of substrates in the indicated kinase substrate group. KSEA results were filtered based on significantly abundant substrate groups for patient 6799 following CpG-B class for 2 hours (column indicated by arrow).

Table O. Significantly abundant phosphopeptides (log2 fold change ≥1 and *P*<0.05) following 2 hours HMGB1 treatment with or without 30 minutes pre-RAGE blockade in each patient compared to PBS baseline

8231		6799	
HMGB1 alone	Anti-RAGE and HMGB1	HMGB1 alone	Anti-RAGE and HMGB1
2 hours		2 hours	
K1C13_HUMAN	KIF1A_HUMAN	ZN318_HUMAN	SFR15_HUMAN
UBP24_HUMAN	ABHGB_HUMAN	DNMBP_HUMAN	DNMBP_HUMAN
HP1B3_HUMAN	MOV10_HUMAN	ARHGB_HUMAN	RPR1B_HUMAN
H90B4_HUMAN	ATPG_HUMAN	RPR1B_HUMAN	ARHGB_HUMAN
SAFB1_HUMAN	G6PI_HUMAN	SFR15_HUMAN	SMC5_HUMAN
COX5A_HUMAN	FUBP1_HUMAN	TBB8_HUMAN	CHTOP_HUMAN
ATPG_HUMAN	COBL1_HUMAN	SFR15_HUMAN	CHTOP_HUMAN
RBG1L_HUMAN	PA2G4_HUMAN	UBE2O_HUMAN	PERQ2_HUMAN
FUBP1_HUMAN	ZBT21_HUMAN	PI4KA_HUMAN	TB10C_HUMAN
RSMB_HUMAN	SELH_HUMAN	TBB8_HUMAN	KS6A4_HUMAN
G6PI_HUMAN	RBBP4_HUMAN	TBB4B_HUMAN	DNMBP_HUMAN
GNAI2_HUMAN	IL16_HUMAN	ZNT4_HUMAN	NEK9_HUMAN
SVIL_HUMAN	GNAI2_HUMAN	TCOF_HUMAN	FBX42_HUMAN
IL16_HUMAN	RHG30_HUMAN	NACC1_HUMAN	TB182_HUMAN
RBBP4_HUMAN	LSP1_HUMAN	PERQ2_HUMAN	AGO2_HUMAN
MDHC_HUMAN	TR150_HUMAN	ROA0_HUMAN	UN93B_HUMAN
IFIX_HUMAN	RBG1L_HUMAN	NUP53_HUMAN	CCD12_HUMAN
MBD3_HUMAN	RSMB_HUMAN	SUN2_HUMAN	PIGR_HUMAN
CHAP1_HUMAN	KPB2_HUMAN	ZEB2_HUMAN	LAIR1_HUMAN
RS11_HUMAN	NUCL_HUMAN	NUMA1_HUMAN	RL27_HUMAN
SMC3_HUMAN	TCPQ_HUMAN	PDLI2_HUMAN	HCFC1_HUMAN
S10A8_HUMAN	ILEU_HUMAN	BMPR2_HUMAN	ZNT4_HUMAN
TBB8_HUMAN	HP1B3_HUMAN	PTN14_HUMAN	SVIL_HUMAN
H2A1A_HUMAN	DDX5_HUMAN	PTN14_HUMAN	PTN12_HUMAN
ICAM5_HUMAN	ACADM_HUMAN	PKCB1_HUMAN	PTN12_HUMAN
PRDX2_HUMAN	IPP2_HUMAN	RD23A_HUMAN	UBXN6_HUMAN
MIF_HUMAN	UBC9_HUMAN	VEZF1_HUMAN	SSH2_HUMAN
DDX5_HUMAN	RLA0L_HUMAN	PKCB1_HUMAN	RBM15_HUMAN
GNA12_HUMAN	ERP29_HUMAN	NCOR2_HUMAN	CAP1_HUMAN
HP1B3_HUMAN	APT_HUMAN	PSA5_HUMAN	PAIRB_HUMAN
TCPZ_HUMAN	ARPC4_HUMAN	RBP56_HUMAN	BIN2_HUMAN
CU129_HUMAN	EVPLL_HUMAN	SHIP1_HUMAN	CCD86_HUMAN
XPO2_HUMAN	GBG1_HUMAN	KHDR1_HUMAN	ERN1_HUMAN
H2A1B_HUMAN	TBB8_HUMAN	ACTY_HUMAN	FR1L5_HUMAN
RS25_HUMAN	PRDX2_HUMAN	FOCAD_HUMAN	CHD2_HUMAN
UBC9_HUMAN	FBLL1_HUMAN	RBP56_HUMAN	VRK3_HUMAN
HNRL2_HUMAN	RL11_HUMAN	TRAK1_HUMAN	KHDR1_HUMAN
TCPQ_HUMAN	RS25_HUMAN	MED31_HUMAN	SRSF2_HUMAN
H2AV_HUMAN	GNA12_HUMAN	AGK_HUMAN	GTF2I_HUMAN
RAB28_HUMAN	ATPB_HUMAN	MA7D1_HUMAN	SRSF2_HUMAN

ILEU_HUMAN	HNRPC_HUMAN	MYPT1_HUMAN	H12_HUMAN
H15_HUMAN	COR1A_HUMAN	AHNK_HUMAN	RRP12_HUMAN
RL11_HUMAN	ADT3_HUMAN	KCY_HUMAN	SRRM2_HUMAN
API5_HUMAN	HNRDL_HUMAN	TLE1_HUMAN	SRRM2_HUMAN
1433S_HUMAN	DDX17_HUMAN	VRK3_HUMAN	MYPT1_HUMAN
BCR_HUMAN	GDIR2_HUMAN	FIS1_HUMAN	SCML4_HUMAN
SRSF1_HUMAN	CROCC_HUMAN	FA65B_HUMAN	SSF1_HUMAN
PPIA_HUMAN	H2A1B_HUMAN	SAC1_HUMAN	DYH2_HUMAN
ERP29_HUMAN	TM109_HUMAN	PEG10_HUMAN	CENPA_HUMAN
TRIP4_HUMAN	TBB3_HUMAN	SYNE3_HUMAN	DNLI3_HUMAN
K1614_HUMAN	HNRPC_HUMAN	ZEP2_HUMAN	RL1D1_HUMAN
RPKL1_HUMAN	HNRPD_HUMAN	ZFAN5_HUMAN	NOLC1_HUMAN
ARPC4_HUMAN	ENOB_HUMAN	MCAF1_HUMAN	TPD52_HUMAN
DBLOH_HUMAN	EF1A1_HUMAN	MYO9B_HUMAN	DNLI3_HUMAN
HNRPU_HUMAN	COTL1_HUMAN	CAC1A_HUMAN	DDX17_HUMAN
ATPB_HUMAN	HNRH1_HUMAN		ZN318_HUMAN
ENOB_HUMAN	MIF_HUMAN		WIZ_HUMAN
HNRDL_HUMAN	1433S_HUMAN		NUTM1_HUMAN
G3P_HUMAN	RAN_HUMAN		VRK3_HUMAN
DDI2_HUMAN	ATPA_HUMAN		LIPB2_HUMAN
DDI2_HUMAN	RAB28_HUMAN		LIPB2_HUMAN
BCR_HUMAN	G3P_HUMAN		RHG04_HUMAN
RLA0L_HUMAN	XIRP1_HUMAN		RHG04_HUMAN
EF1A1_HUMAN	CU129_HUMAN		RL28_HUMAN
TRY1_HUMAN	XPO2_HUMAN		FUBP3_HUMAN
FA98B_HUMAN	PROF1_HUMAN		FUBP3_HUMAN
APT_HUMAN	H2B1B_HUMAN		IRS1_HUMAN
KI26B_HUMAN	K1614_HUMAN		IFIX_HUMAN
PKHJ1_HUMAN	RPKL1_HUMAN		PKCB1_HUMAN
H12_HUMAN	H15_HUMAN		SCAFB_HUMAN
HMGA1_HUMAN	ICAM5_HUMAN		SCAFB_HUMAN
FBLL1_HUMAN	PPIA_HUMAN		ZYX_HUMAN
HNRH1_HUMAN	BCR_HUMAN		H31T_HUMAN
H2B1B_HUMAN	SRSF1_HUMAN		K1551_HUMAN
CH10_HUMAN	BCR_HUMAN		SCIMP_HUMAN
MRE11_HUMAN	RPRD2_HUMAN		H2AY_HUMAN
RAN_HUMAN	RPRD2_HUMAN		IF16_HUMAN
HNRPD_HUMAN	KI26B_HUMAN		PAN3_HUMAN
HNRPM_HUMAN	PKHJ1_HUMAN		CENPA_HUMAN
SRS10_HUMAN	HNRPC_HUMAN		ARHGI_HUMAN
HNRPC_HUMAN	TR150_HUMAN		LMO7_HUMAN
NUCKS_HUMAN	SRS10_HUMAN		ELK3_HUMAN
MRE11_HUMAN	NUCKS_HUMAN		ANKL2_HUMAN
SRRM2_HUMAN	PRP4B_HUMAN		SRRM2_HUMAN
PROF1_HUMAN	T3JAM_HUMAN		SUN2_HUMAN
LOX12_HUMAN	BCLF1_HUMAN		C2C2L_HUMAN
DDX17_HUMAN	H12_HUMAN		EHBP1_HUMAN
HNRPK_HUMAN	H2A1A_HUMAN		CENPA_HUMAN
RPRD2_HUMAN	SRRM2_HUMAN		RGPA1_HUMAN
RPRD2_HUMAN	RBM25_HUMAN		P2RX7_HUMAN

TR150_HUMAN	HDAC1_HUMAN	TALDO_HUMAN
ADT3_HUMAN	NUCL_HUMAN	TBCD1_HUMAN
SAFB1_HUMAN	TRIP4_HUMAN	Z280D_HUMAN
TM109_HUMAN	H2AV_HUMAN	SC61B_HUMAN
HNRPC_HUMAN	SAFB1_HUMAN	MYO9B_HUMAN
NUCKS_HUMAN	LOX12_HUMAN	IF2M_HUMAN
TBA4A_HUMAN	HMGN1_HUMAN	PRAME_HUMAN
UTP18_HUMAN	SRSF7_HUMAN	MARK3_HUMAN
BCLF1_HUMAN	UTP18_HUMAN	MARK3_HUMAN
ENPL_HUMAN	SRSF7_HUMAN	MET16_HUMAN
HNRPD_HUMAN	MATR3_HUMAN	IF16_HUMAN
CXCR4_HUMAN	RBMX2_HUMAN	SRRM2_HUMAN
EVPLL_HUMAN	ZRAB2_HUMAN	BAZ1B_HUMAN
KPCB_HUMAN	SON_HUMAN	XRN2_HUMAN
MCM3_HUMAN	HMGA1_HUMAN	TFIP8_HUMAN
HNRPC_HUMAN	K1C13_HUMAN	PEA15_HUMAN
GBG1_HUMAN	COX5A_HUMAN	SC61B_HUMAN
ATPA_HUMAN		NCF1B_HUMAN
CX7A2_HUMAN		NCF1B_HUMAN
TCP4_HUMAN		BIN2_HUMAN
VPS4B_HUMAN		YBOX1_HUMAN
H31T_HUMAN		SRRM2_HUMAN
SSRP1_HUMAN		HMHA1_HUMAN
SSRP1_HUMAN		NOP2_HUMAN
MINK1_HUMAN		SLTM_HUMAN
GDIR2_HUMAN		EMAL3_HUMAN
RBMX_HUMAN		PCBP1_HUMAN
MECP2_HUMAN		SLTM_HUMAN
COX5B_HUMAN		SLTM_HUMAN
HNRL2_HUMAN		AHDC1_HUMAN
API5_HUMAN		AHDC1_HUMAN
SRSF6_HUMAN		AHDC1_HUMAN
CROCC_HUMAN		WIZ_HUMAN
COTL1_HUMAN		XRN2_HUMAN
TPM1_HUMAN		P4K2A_HUMAN
		ZN329_HUMAN
		MYH16_HUMAN
		RL7L_HUMAN
		RIF1_HUMAN
		RAI1_HUMAN
		NUTM1_HUMAN
		P4K2A_HUMAN
		ING3_HUMAN
		PKHA6_HUMAN
		MAGI3_HUMAN
		SEM3G_HUMAN
		MYO5C_HUMAN
		AN32E_HUMAN
		NUP53_HUMAN
		NUCKS_HUMAN

	XRN2_HUMAN
	XRN2_HUMAN
	STIM2_HUMAN
	H2AY_HUMAN
	MADD_HUMAN
	YBOX1_HUMAN
	TFEB_HUMAN
	SLTM_HUMAN
	ZGRF1_HUMAN
	OSB11_HUMAN
	RBP56_HUMAN
	ARI5B_HUMAN

Table P. Clinical information of CLL patient samples used *in vitro*

Patient ID	S100 (pg/ml)	HMGB1 (ng/ml)	sRAGE (pg/ml)	Cytogenetic description	Binet stage	ZAP70 (inhouse)	Time to first treatment (months)	Date of first treatment	First treatment	First response	Date of relapse
10450	88.4	72.7	0.0	TRISOMY 12	B	Y					
8553	0.0	381.8	27.6	11Q AND 13Q	A	Y	41	29/01/2013	LENALIDOMIDE	STABLE DISEASE	
8921	0.0	78.9	1.5	17P DEL	A	Y	23	23/01/2012	CAMPATH	PARTIAL REMISSION	
9095	0.0	16.5	25.5	TRISOMY 12			43	26/08/2014	FLUD+CYCLO+RITUX		
9887	0.0	16.0	52.2		A	N					
7921	0.0	8.1	35.1		A	Y	36	15/06/2005	CB	PARTIAL REMISSION	15/03/2006
9956	0.0	79.3	90.3	NORMAL	A						
5959	0.0	30.1	91.5	DEL (13Q)	A						
6158	0.0	63.6	89.3	NOT DONE	A	N	116	15/06/2000	CB	PARTIAL REMISSION	18/12/2003
8320	0.0	145.0	141.2			N	0	15/06/2003	FLUDARABINE	COMPLETE REMISSION	15/09/2007
9361	0.0	185.6	103.1			Y	24	15/06/2008	FLUD. CYCLO + RITUX		15/12/2011
8232	0.0	37.2	34.1		A						
9024	79.0	92.4	7.8	17P DEL, 11Q DEL	C	N	2	07/02/2011	CB	TREATMENT DEATH	
8560	0.0	71.8	0.0	13Q-, 17P-	A	N					
7549	126.0	328.2	36.6	TRISOMY 12	A	Y	80	15/10/2012	LENALIDOMIDE	PROGRESSION	
7362	0.0	191.5	0.0	DEL13Q, TRISOMY 12	B	N	1	15/01/2006	FLUDARABINE & CYCLO	PARTIAL REMISSION	07/01/2014

8009	237.0	394.1	101.9	DEL (13Q)	A	N					
9746	68.2	133.9	133.4		C	Y	416	05/02/2013	CB - RANDOMISED (CELGENE-008)	PARTIAL REMISSION	22/04/2015
9401	0.0	16.3	24.1	13Q DEL	A	Y					
9491	3.6	33.6	25.0	17P DEL	C	Y					
9885	0.0	139.8	0.0			Y	0	15/06/2010	FLUD. CYCLO + RITUX	GOOD PARTIAL RESPONSE	15/03/2012
T-2488	0.0	193.3	108.7	TRISOMY 12	A	Y	39	01/09/2011	FLUD. CYCLO + RITUX		
9853	0.0	79.6	38.8	13Q DEL	A	N	25	18/02/2015	FLUD. CYCLO + RITUX		
5313	0.0	80.7	56.7		A	Y	3	10/04/2000	FMD	PARTIAL REMISSION	10/01/2006
9528	0.0	28.3	29.2	13Q DEL	A	Y					
7893	0.0	42.1	81.1	DEL (13Q)	A	Y	39	15/09/2003	CB	PARTIAL REMISSION	29/01/2013
9480	0.0	123.2	0.0			Y	24	15/06/2005	CB	PARTIAL REMISSION	15/02/2007
10686	0.0	18.1	114.5		A	Y					
9685	0.0	15.4	72.2	TRISOMY 12	A	Y					
8692	0.0	47.9	144.2			Y					
10687	0.0	205.9	136.4	11Q22	A	Y					
7358	79.9	58.1	66.8	DEL (13Q)	A	N	57	15/02/2005	CB	PARTIAL REMISSION	17/10/2006
8357	0.0	17.7	0.0		A	N					
7581	0.0	126.6	137.8	DEL (13Q)	A	N	128	15/06/2015	TREATED ELSEWHERE		
9070	0.0	119.9	92.2	13Q DEL	A	Y	32	15/02/2010	FLUD. CYCLO + RITUX		

T-2490	0.0	48.6	2.6	11Q AND 13Q	C	Y	1	23/09/2011	CB + RITUX	PARTIAL REMISSION	
8231	0.0	244.9	25.7	DEL (13Q)	A	Y					
8550	0.0	53.9	124.2	NORMAL	A	Y	53	15/03/2013	FLUD. CYCLO + RITUX	COMPLETE REMISSION	
6794	0.0	26.1	65.9	13Q DEL	A	Y					
T-2555	0.0	13.0	49.1		STAGE IV	Y					
9601	0.0	96.9	37.8	13Q DEL		Y	44	16/10/2012	ARCTIC:FCR-PO	COMPLETE REMISSION	
7888	0.0	12.4	117.1	DEL (13Q)	A	N	97	01/10/2014	FLUDARABINE & CYCLO	COMPLETE REMISSION	
6799	12.3	48.8	61.3	DEL (13Q)	A	N					
10688	0.0	41.1	30.6		A	N					
5928	0.0	91.5	70.3	13Q DEL	A	Y	153	25/02/2015	BENDAMUSTINE+RITUX		
T-1985	0.0	78.9	0.0		A (C IN 2013 STILL AT PRE-TREATMENT	N					
10278	0.0	50.7	101.2		A	Y	115	12/01/2016	GALACTIC STUDY		